



HAL
open science

Optimization of cell-based therapy using an injectable hydrogel after stroke: MRI and histological study

Ligia Simoes Braga Boisserand

► To cite this version:

Ligia Simoes Braga Boisserand. Optimization of cell-based therapy using an injectable hydrogel after stroke: MRI and histological study. Human health and pathology. Université Grenoble Alpes, 2016. English. NNT : 2016GREAV038 . tel-01685406

HAL Id: tel-01685406

<https://theses.hal.science/tel-01685406>

Submitted on 16 Jan 2018

HAL is a multi-disciplinary open access archive for the deposit and dissemination of scientific research documents, whether they are published or not. The documents may come from teaching and research institutions in France or abroad, or from public or private research centers.

L'archive ouverte pluridisciplinaire **HAL**, est destinée au dépôt et à la diffusion de documents scientifiques de niveau recherche, publiés ou non, émanant des établissements d'enseignement et de recherche français ou étrangers, des laboratoires publics ou privés.

THÈSE

Pour obtenir le grade de

**DOCTEUR DE LA COMMUNAUTÉ UNIVERSITÉ GRENOBLE
ALPES**

Spécialité : **Neurosciences - Neurobiologie**

Arrêté ministériel : 25 mai 2016

Présentée par

Ligia SIMOES BRAGA BOISSERAND

Thèse dirigée par **Olivier DETANTE** et **Claire ROME**

préparée au sein du **Grenoble Institut des Neurosciences – ISERM U1216**
dans l'**École Doctorale de Chimie et Sciences du Vivant**

Optimisation de la thérapie par cellules souches par l'application d'un hydrogel injectable après un accident vasculaire cérébral: une étude histologique et par IRM

Thèse soutenue publiquement le **28 novembre 2016**, devant le
jury composé de :

Dr. Marlène WIART

Directeur de recherche, Inserm U1060 (Examineur) Président du jury

Pr. Omar TOUZANI

Professeur des Universités, UMR ISTCT 6301 (Rapporteur)

Dr. Isabelle LOUBINOUX

Directeur de recherche, UMR 825 Inserm (Rapporteur)

Dr. Walid RACHIDI

Vice-Doyen Recherche, Directeur Adjoint de l'UFRPharm (Examineur)

Dr. Claire ROME

Maitre de conférences, Inserm U 1216 (Co-encadrant de thèse)

Dr. Olivier DETANTE

MCU-PH, Inserm U 1216 – UGA/CEA/CHU (Directeur de thèse)



ACKNOWLEDGMENT

Firstly, I would like to express my sincere gratitude to my advisor Dr. Olivier Detante for the continuous support of my Ph.D. studies and the related research, for his patience, motivation, and positivity. His guidance conducted me with clearance through research and the writing of this thesis. Thank you.

Furthermore, I express my acknowledgment to the CAPES Foundation, Ministry of Education of Brazil, for the financial support of my PhD.

I also express my gratitude to my co-advisor Dr. Claire Rome for the stimulating discussions and support.

In addition to that, I give thanks to Dr. Chantal Remy, for the scientific support, for the patience, scientific rigor, great knowledge, generosity, and humanity. Chantal, you are my mentor and an example for me.

My sincere thanks also go to Dr. Emmanuel Barbier who provided an opportunity to join their team as PhD student, and who also gave access to the laboratory and research facilities.

Without this precious support, it would not be possible to conduct this research.

I salute my fellow labmates, especially Dr. Benjamin Lemasson and Nora Collomb for helping me with the experiments. But also the other colleagues for the stimulating discussions in the break room.

Moreover, I thank my friends in the following institution Emmanuelle Bellot, Lydiane Hirschler and Ivy Uszynski and Jérémie Papassin for the support and the good moments.

I also express my deepest gratitude to my family which I love so much: my parents Selma and Galileu and to my brothers Juliano, Tiago and sister Jordana for supporting me despite the distance and in my life in general. Words cannot describe how grateful I am to my mother and father for all of the sacrifices they have made on my behalf.

Last but not least, I thank all my friends and relatives who supported me in the writing, and incited me to strive towards my goals. To conclude, I express my profound gratitude to my beloved husband Alexis Boisserand, for

correcting all my documents in French and for attempting all presentations that I have prepared, with patience and support during these three years.

Résumé en français

Contexte général

L'accident vasculaire cérébral (AVC) touche environ 6 millions de personnes dans l'Union Européenne, avec 1.1 million de nouveaux cas chaque année. Le coût total de l'AVC a été estimé à environ 64,1 milliards d'€ en 2010 en raison du coût élevé des soins à long terme (Gustavsson et al. 2011).

A l'heure actuelle, la seule thérapie disponible pour l'AVC d'origine ischémique est la reperfusion par thrombolyse (Alteplase) et par thrombectomie. Cette thérapie est cependant limitée à une fenêtre thérapeutique étroite (6 heures). La thérapie de reperfusion à phase aigüe est conditionnée à une détection et prise en charge très précoce, pour cette raison, moins de 10% des patients en bénéficient.

Au-delà des premières heures d'occlusion, aucun traitement efficace en dehors de la rééducation n'est disponible, soulignant l'importance de la recherche des traitements favorisant la récupération.

L'application des nouvelles techniques d'imagerie cérébrale comme l'imagerie par résonance magnétique (IRM) peut être de grande utilité dans la compréhension des mécanismes de l'AVC et dans l'identification des candidats potentiels à la reperfusion ainsi que pour évaluer de manière non invasive les effets des nouvelles thérapies.

Au delà de la phase aigüe, le réel besoin de disposer des thérapies avec une fenêtre thérapeutique plus étendue s'impose. La thérapie cellulaire semble prometteuse dans le traitement de l'AVC. De nombreuses études précliniques suggèrent que l'injection de cellules souches permet une réduction du handicap post-AVC grâce à des mécanismes de neuroprotection et de stimulation de la réorganisation cérébrale (Gutiérrez-Fernández et al., 2013; Sinden and Muir, 2012). Malgré ces résultats positifs, des aspects comme la faible migration des cellules vers le site de la lésion quand les cellules sont administrées de manière

systémique et l'importante mort cellulaire quand les cellules sont administrées dans la cavité de l'infarctus restent encore à améliorer (Detante et al., 2009; Lappalainen et al., 2008).

Des nouvelles stratégies thérapeutiques basées sur l'utilisation de biomatériaux (hydrogel) dans le système nerveux central sont actuellement en développement afin d'améliorer les effets de la greffe cellulaire. Les hydrogels peuvent être produits avec des composants de la matrice extracellulaire comme le collagène et l'acide hyaluronique pour fournir un microenvironnement favorisant la survie cellulaire (Aguado et al., 2012).

L'objectif général de la présente thèse a été de tester un biomatériau hydrogel (à base d'acide hyaluronique) avec pour but d'améliorer les effets de la thérapie cellulaire dans un modèle d'AVC ischémique par occlusion de l'artère cérébrale moyenne (oACM). Pour cela nous avons d'abord testé la biocompatibilité du biomatériau hydrogel (HyStem™-HP, Sigma-Aldrich) et son potentiel à fournir une protection cellulaire à long terme dans le tissu cérébral sain. En outre, nous avons évalué le potentiel d'une technique d'IRM développée au sein de notre équipe qui mesure la saturation locale en oxygène (StO₂) (Christen et al., 2011) dans la détection du cœur ischémique et pour la prédiction de la nécrose finale.

Résultats de la première étude

La première étude réalisée concerne l'évaluation à la phase aigüe de l'ischémie cérébrale par IRM multiparamétrique. Des paramètres hémodynamiques, vasculaires, StO₂ et les altérations en diffusion ont été évalués au cours des deux premières heures de MCAo. Le potentiel de la cartographie du StO₂ à prédire la nécrose finale a lui aussi été évalué en comparaison à l'imagerie par diffusion.

Notre étude multiparamétrique par IRM a mis en évidence (en utilisant un seuil de 40% de StO₂) une importante hétérogénéité à la phase aigüe de l'ischémie dans la zone d'altération en diffusion. Cette zone est considérée comme celle correspondant au cœur ischémique (non

recupérable). Cette hétérogénéité détectée est liée à la présence de zones avec différents degrés de sévérité au sein de la zone de diffusion diminuée. Nos résultats ont mis en évidence le potentiel de la cartographie StO₂ à détecter de façon précise le cœur ischémique sans l'inclusion des régions potentiellement récupérables à la phase aigüe. La cartographie StO₂ par IRM est une méthode qui prend en compte les valeurs de StO₂ dans chaque voxel et qui peut ainsi détecter de façon plus précise la gravité de l'ischémie.

Notre étude multiparamétrique a mis en évidence que la zone détectée par StO₂ comme non récupérable correspond aussi à la zone avec les valeurs les plus faibles dans la cartographie des paramètres hémodynamiques et microvasculaires. Ces différences n'ont pas été détectables par la cartographie de diffusion. Lors de notre suivi, nos résultats ont démontré que l'imagerie par diffusion surestime la nécrose finale, contrairement à la cartographie d'oxygénation (StO₂).

Résultats de la deuxième étude

Lors de notre deuxième étude, nous avons évalué la biocompatibilité d'un hydrogel à base d'acide hyaluronique (HyStemTM-HP, Sigma-Aldrich) chez le rat, dans le cerveau sain. En plus, nous avons évalué le potentiel de l'IRM à observer *in vivo* le devenir du gel (biodégradation) après l'administration intracérébrale de 10 μ L d'hydrogel HyStemTM-HP. Cette évaluation a été réalisée à l'aide d'un suivi IRM pendant 4 semaines en utilisant 2 séquences IRM pour détecter l'hydrogel : une séquence anatomique pondérée en T2 et une séquence en diffusion. Les rats ont été sacrifiés à des différents temps pour réaliser des analyses histologiques (détection du gel) et par immunofluorescence (détection de la réponse locale à l'administration de l'hydrogel (microglie et astrocytes)).

Les résultats préliminaires de cette étude pilote ont montré que l'hydrogel HyStemTM-HP peut être détecté par IRM de diffusion de manière fiable grâce à sa composition riche en eau.

Les résultats du suivi IRM sont encourageants concernant la longue durée de présence de l'hydrogel dans le tissu cérébral du rat jusqu'à 28 jours après l'administration intracérébrale. L'analyse immunohistologique a détecté une activation des cellules microgliales (Iba1+) et des astrocytes (GFAP+) en bordure du gel. Une analyse supplémentaire avec un nombre élevé de rats serait nécessaire pour quantifier le taux de dégradation de l'hydrogel HyStem™-HP. Cependant, certains signaux de dégradation (rétraction) ont été détectés à partir du 14^{ème} jour.

Résultats de la troisième étude

Au cours de la troisième étude, nous avons étudié les effets de la combinaison de l'hydrogel HyStem™-HP avec des cellules souches mésenchymateuses humaines (CSMh). Nous avons évalué les effets de la greffe intracérébrale sur la survie cellulaire, et le remodelage cérébral après l'oACM. Nous avons également évalué à l'aide d'un suivi comportemental (sensori-moteur) la récupération fonctionnelle. En outre, nous nous sommes aussi intéressés à suivre in vivo la lésion ischémique et sa récupération à l'aide d'un suivi par IRM.

Nous n'avons pas mis en évidence de différence quant à la taille de la lésion (évaluée par IRM) en réponse aux différentes thérapies.

L'hydrogel HyStem™-HP est bien toléré, et la survie des CSMh a été augmentée dans le groupe ayant reçu la combinaison hydrogel+CSMh.

La combinaison hydrogel+CSMh a aussi induit une augmentation des marqueurs vasculaires (RECA1) et (COL-IV) 21 jours après l'administration. L'angiogenèse est un des principaux éléments du remodelage post-AVC, car la formation des nouveaux vaisseaux est nécessaire à la migration des facteurs de croissance et des cellules progénitrices dans la zone péri-lésionnelle. Nous n'avons pas détecté de différences concernant l'activation microgliale,

astrocytaire ou la survie neuronale. En revanche, le groupe hydrogel+CSMh n'a pas présenté d'augmentation de l'astrogliose ni de l'activation microgliale après l'ischémie.

Malgré ces effets positifs concernant la survie des CSMh et l'augmentation des marqueurs vasculaires, ni la combinaison hydrogel+CSMh, ni le traitement avec des CSMh seules n'ont induit une récupération fonctionnelle dans notre étude.

Des nouvelles stratégies pour améliorer la thérapie cellulaire doivent être étudiées. Des études précliniques sont encore nécessaires pour tester des approches thérapeutiques innovantes et optimiser les approches actuellement en cours dans les essais cliniques.

Summary

1	Introduction	14
1.1	Stroke	14
1.1.1	Definition	14
1.1.2	Epidemiology	15
1.1.3	Pathophysiology	16
1.1.4	Anatomy of arterial cerebral circulation	16
1.1.5	Neurovascular Unit	18
1.1.6	Regulation of brain perfusion	20
1.1.7	Hemodynamic alterations in acute cerebral ischemia.....	21
1.1.8	Mechanisms of brain cell death	25
1.2	Endogenous mechanisms of neuroprotection and brain remodeling...	33
1.2.1	Endogenous neuroprotection	33
1.2.2	Endogenous brain remodeling.....	34
1.2.3	Stroke treatments.....	44
1.3	Mesenchymal stem cells therapy	50
1.3.1	MSCs mechanisms	50
1.3.2	Protective mechanism	51
1.3.3	Brain remodeling	52
1.3.4	Current status of clinical research.....	55
2	Problems	58
3	Objectives	59
4	General methodology	61
4.1.1	General anesthesia and analgesia.....	61
4.1.2	Model of transient ischemic stroke.....	62

4.1.3	MRI Methods	64
4.1.4	Human Mesenchymal Stem cells preparation.....	69
4.1.5	Stereotaxic intracerebral administration	70
4.1.6	Samples extraction (brain).....	70
4.1.7	Histological analysis	71
5	Part I: MRI Evaluation of stroke at acute phase.....	75
	Study 1: Multiparametric MRI analyses post stroke	76
5.1	Conclusion	89
6	Part II: Optimization of cell therapy post-stroke with a biomaterial hydrogel	90
	A. Review of literature	92
	Study 2: HyStem™-HP Hydrogel a study of in vivo biocompatibility	107
6.1.1	Introduction.....	107
6.1.2	General methodology	108
6.1.3	Results	111
6.1.4	Discussion	115
6.1.5	Conclusion	116
	Study 3 : Hyaluronic acid hydrogel combined with mesenchymal stem cell therapy after ischemic stroke.....	117
6.1.6	Adittional results.....	148
6.1.7	Discussion (additional MRI results)	153
6.1.8	Conclusions (part II)	154
7	Conclusions and perspectives	155
8	Scientific production	161
9	References	162
10	Appendix.....	181

List of abbreviations

ACA: anterior carotid artery

ADC: apparent diffusion coefficient

ADC: apparent diffusion coefficient

AIF: apoptotic induction factor

AMPA: α -amino-3-hydroxy-5-methyl-4-isoxazolepropionic acid

ANG: angiotensin

ART: adhesive removal test

ATP: adenosine triphosphate

BBB: blood brain barrier

BCL-2: B-cell lymphoma 2

BDNF: brain-derived neurotrophic factors

BL: basal lamina

BM: bone marrow

BMMNCs: bone marrow mononuclear cells

BrdU: bromodeoxyuridine

BV: blood vessel

BVf: blood volume fraction

CBF: cerebral blood flow

CBV: cerebral blood volume

CCA: Common carotid artery

CMRO₂: cerebral metabolic rate of O₂

CNS: central nervous system

COX-2: cyclooxygenase-2

CPP: Cerebral perfusion pressure

CT: computerized tomography

CVT: Cerebral venous thrombosis

CXCR4: chemokine receptor 4

DCX: doublecortin

ECA: external carotid artery

ECM: extracellular matrix
ECs: Endothelial cells
eNOS : endothelial NOS
EPCs: endothelial progenitor cells
ER: endoplasmic reticulum
E-selectin
EU: European Union
FGF: fibroblast growth factor
GABA: γ -aminobutyric acid
GCSF: granulocyte-colony stimulating factor
GDNF: glial--derived neurotrophic factors
GEFC: gradient echo flow compensated
GF: growth factors
GFAP: glial fibrillary acid
GFP: green fluorescent protein
GluR2: glutamate receptor (subunit 2)
GM: gray matter
h:human
HA: hyaluronic acid
HSC: Hematopoietic stem cells HSP: heat-shock protein
IA: intra-arterial
ICA: internal carotid artery
ICAM-1: intercellular adhesion molecule
ICP: intracranial pressure
IGF1: insulin-like growth factor
IL: interleukin
iNOS: inducible NOS type II
IP3: inositol tri-phosphate
iPS: induced pluripotent cells
IV: intravenous

LV: lateral ventricle

MAP: mean arterial blood pressure

MCA: middle cerebral artery

MCAo: middle cerebral artery occlusion

MMP: matrix metalloprotease

MNC: mononuclear cells

mNSS: modified neurological severity score

mqBOLD: multiparametric quantitative blood oxygenation level-dependent

MRI: Magnetic Resonance Imaging

MSC: Mesenchymal stromal/stem cells

MTT: mean transit time

NADPH: Nicotinamide adenine dinucleotide phosphate

NGF: nerve growth factor

NIHSS: National Institute of Healthy Stroke Scale

NMDA: N-methyl-D-aspartate receptor

nNOS : neuronal NOS type I

NO: nitric oxide

NOS : Nitric Oxyde synthases

NPCs: neural progenitor cells

NSCs: neural stem cells

NVU: neurovascular unit

O₂ EF: O₂ extraction fraction

OA: occipital artery

PBS: phosphate buffer saline

PCA: posterior cerebral artery

pCASL: pseudo-continuous arterial spin labeling

PDGF: Platelet-derived growth factor

PEGDA: polyethylene glycol diacrylate

PET: positron emission tomography

PPA: pterygopalatine artery

RMS: rostral migratory stream

rTPA: recombinant tissue plasminogen activator

SC: stem cell

SDF-1: stromal derived factor-1

SGZ: subgranular zone

SVZ: subventricular zone

T₂W: T₂-weighted

TE: echo time

TGF β : transforming growth factor β

TNF α : tumor necrosis factor

TNF α : tumoral necrosis factor

TR: repetition time

UCBCs: umbilical cord blood cells

VCAM-1: vascular cell adhesion molecule

VEGF: vascular endothelial growth factor

VEGFR: VEGF receptor 1 and 2

VP: mean venous pressure

VSI: vessel size index

WM: white matter

1 INTRODUCTION

1.1 STROKE

1.1.1 Definition

Brain stroke is classically characterized as neurological deficit attributed to an acute focal injury by a vascular cause (Sacco et al., 2013). The term stroke should be used to include central nervous system (CNS) infarction (brain, spinal cord or retinal cells) (Sacco et al., 2013), but here I will discuss exclusively brain stroke. A recent consensus of American Heart Association and American stroke association was published consisting in an actual definition for stroke to include the recent advances in sciences and technology including brain imaging (Sacco et al., 2013).

Stroke diagnosis should be based on pathological, imaging or other evidence objective of cerebral focal ischemic injury in a defined vascular distribution (Sacco et al., 2013) or clinical evidence of cerebral injury based on symptoms persisting ≥ 24 h or until death and others etiology excluded (Sacco et al., 2013). Cerebrovascular disorders include four conditions: ischemic stroke, intracerebral hemorrhage, subarachnoid hemorrhage and cerebral venous thrombosis.

1.1.1.1 Ischemic stroke

Ischemic stroke could be transient (Transient ischemic attack) (Albers et al., 2002) or a brain infarction. This second one is characterized by an episode of neurological dysfunction caused by cellular death due to an interruption of the blood supply to a brain artery or territory. Brain ischemia is the most frequent type of stroke 80% and is the subject of my thesis.

1.1.1.2 Intracerebral Hemorrhage

Intracerebral hemorrhage (ICH) is a bursting of an artery in brain parenchyma representing 15% of all cases of stroke (Qureshi et al., 2009). It consists of a focal collection of blood within the brain parenchyma or ventricular system that is not caused by trauma, resulting in rapidly developing of clinical signs (Sacco et al., 2013).

1.1.1.3 Subarachnoid hemorrhage

Correspond to a bleeding into the subarachnoid space resulting in a rapidly developing of clinical signs or headache (Sacco et al., 2013). Frequently associated with an aneurism rupture, representing less than 5% of stroke cases (Bederson et al., 2009).

1.1.1.4 Cerebral venous thrombosis

Cerebral venous thrombosis (CVT) consists in an **occlusion** of a cerebral venous structure which could lead to venous infarction and/or hemorrhage (Sacco et al., 2013). Usually in veins or sinus (Ferro and Canhão, 2014). CVT is a rare form of stroke, constituting 0.5%-1.0% of all cerebral strokes (Pizzi et al.)

1.1.2 Epidemiology

The present work concerns arterial ischemic stroke. However available epidemiological data presents general rates of stroke including different subtypes.

In a relevant study, Valery Feigin and colleagues (Feigin et al., 2014) report a global estimation of stroke incidence, prevalence, mortality disability-adjusted life-years (DALYs) (Feigin et al., 2014). In 2010, the reported number of people with first stroke worldwide was 16.9 million, stroke survivors 33 million, stroke-related deaths 5.9 million, and DALYs lost 102 million. An increase of 68%, 84%, 26%, and 12%, respectively, in comparison with 1990, and probably will continue to rise in the coming years (Feigin et al., 2014; Giroud et al., 2014). In the European Union (EU) stroke affects approximately 6 million people, with 1.1 million new cases every year. The total cost of disorders of the brain was estimated at 798 billion € in 2010, of that 64.1 billion € is due to stroke mainly because of long-term special care and rehabilitation (Gustavsson et al., 2011). Stroke burden is expected to increase due to the aging of the population and diabetes, which is reaching an epidemic level.

1.1.3 Pathophysiology

Such as defined above, ischemic stroke is a cerebrovascular disease due to an abrupt interruption of blood flow leading to a dysfunction and ultimate the death of the highly organized complex cells that forms the cerebral tissue.

Before presenting the pathophysiological events that lead to cerebral ischemia, some important concepts will be introduced including the anatomical organization of blood vessels that irrigate the brain, the cells which form the neurovascular unit and the brain perfusion regulation.

1.1.4 Anatomy of arterial cerebral circulation

Brain vasculature can be divided into two networks, the anterior of which originates from the two internal carotid arteries that supply anterior and middle cerebral arteries while the posterior (vertebro-basilar) system originates from the two vertebral arteries that merge to form the basilar artery supplying the brainstem, cerebellar and posterior cerebral arteries (Figure 1). Several small perforating arteries feed deep brain territories. The circle of Willis allows anastomosis between anterior and posterior systems via posterior communicating arteries and between both hemispheres via the anterior communicating artery. In addition to other anastomotic networks, such as leptomeningeal arteries or internal/external carotid anastomosis, the circle of Willis can provide physiological protection by preventing ischemia in case of one artery occlusion (Jung et al., 2013) Unfortunately, this auxiliary feature is often insufficient due to considerable variation among individuals, their age and associated vascular risk factors including altered white matter from chronic small-vessel disease, vasoreactivity and post-stroke recovery (Miyamoto et al., 2013).

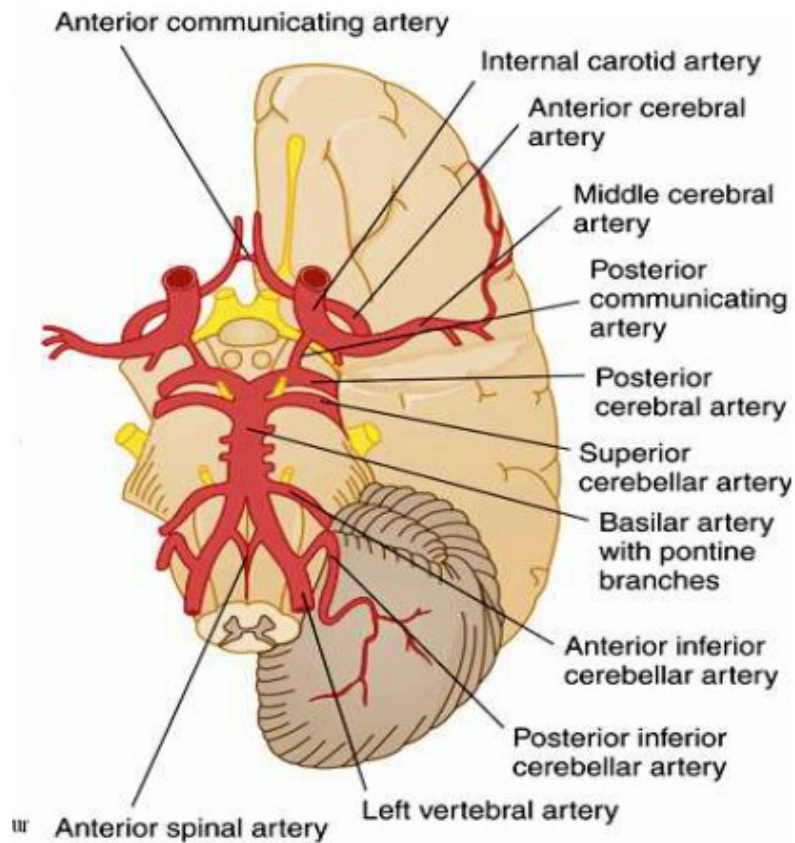


Figure 1 : Anatomy of arterial vascularization in human brain. From de Border et al. 2006

Rats present a brain vasculature analogous to humans, the anatomic distribution of the anterior carotid artery (ACA) (Figure 2), posterior cerebral artery (PCA) and middle cerebral artery (MCA) in rats is similar to that in humans (Longa et al., 1989). Some notable differences such as the absence of anterior communicant artery and the direct connection between PCA and intracranial portion of internal carotid artery (ICA) are present. However, the blood supply of rat thalamus and basal ganglia is similar to humans (Longa et al., 1989). Rat brain present similar anatomy and physiology to the human brain, for this reason (and for ethical and economics reasons), rat is the most common animal model used in stroke studies (Durukan and Tatlisumak, 2007).

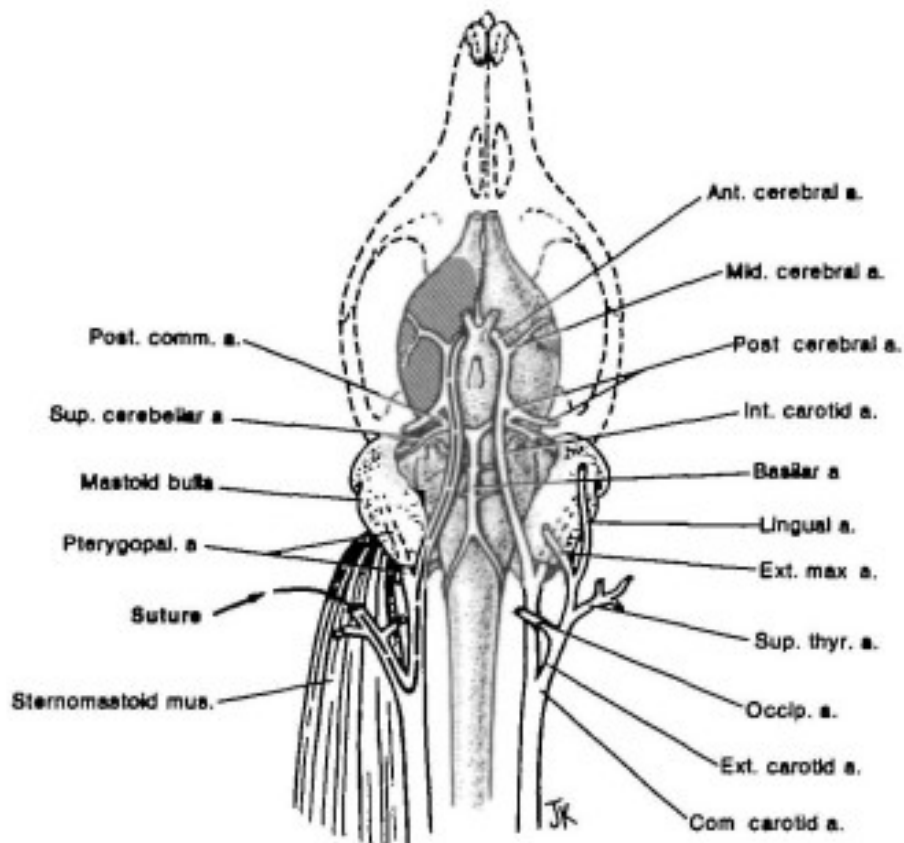


Figure 2 : Arterial vascularization in rat brain from Longa et al. 1989 (Longa et al., 1989)

1.1.5 Neurovascular Unit

The complexity of cerebral ischemia pathophysiology is not only due to the loss of highly specialized cells but also because it involves the dysfunction of cerebral vasculature and parenchymal cells which are organized in “neurovascular units”.

The concept of the neurovascular unit (NVU) arose from long-known and studied phenomenon of coupling between neuronal activity (energy demand) and local blood flow (energy supply) (Stanimirovic and Friedman, 2012).

The NVU is a functional and structurally interdependent multi-cellular complex comprised of endothelial cells, the basal lamina, pericytes, astrocytes, and neurons (Stanimirovic and Friedman, 2012; del Zoppo, 2010) (Figure 3). As a conceptual construct, the NVU emphasizes the importance of cell–cell signaling between all cells in neural, glial, and vascular compartments (Lok et al., 2007, 2015).

Endothelial cells (ECs) play a very important role in brain function including the control of vascular tone, release of trophic factors and by integrating a highly selective barrier. These cells produce vasoactive factors such as nitric oxide (vasodilatation) or thromboxane (vasoconstriction) (Duchemin et al., 2012; Kis et al., 1999). Tight junction proteins such as claudin and occludin, existing in endothelial cells are the most important proteins modulating the integrity of blood-brain barrier (BBB) (Strazielle and Ghersi-Egea, 2013).

Astrocytes contribute for numerous functions on CNS in healthy conditions including release of growth factors, uptake of neurotransmitters, regulation of blood flow, participating in synapse function and integrating the BBB (Sofroniew and Vinters, 2009). Astrocytic cells are strategically localized to act as relay cells in neurovascular communication. They communicate with synapses and thus can be stimulated by neuronal activity, whereas end foot processes are ideally situated around the blood vessels and can control vessel diameter (Attwell et al., 2010).

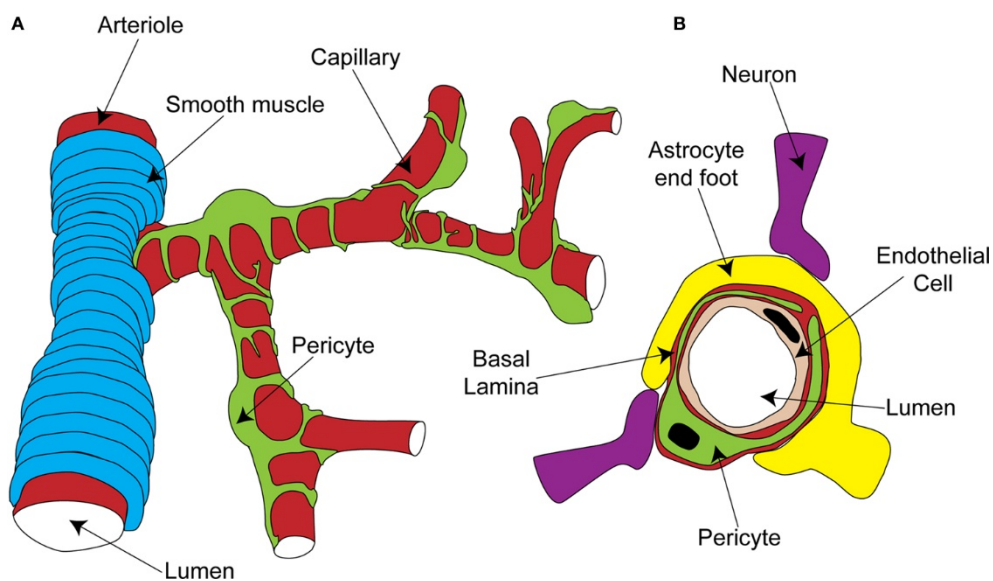


Figure 3 : Cellular components of Neurovascular unit from Hamilton (Hamilton et al., 2010)

Pericytes are small cells located on the external side of the vessel. They are separated from the parenchyma by the basal lamina, a thin layer of which also interposes between the pericyte and endothelial cells (Hamilton et al., 2010). Pericytes play a crucial role in a range of functions including

angiogenesis, endothelial cell regulation, vessel stabilization and maintenance of the BBB (Hamilton et al., 2010; Lai and Kuo, 2005).

Microglial cells integrate indirectly the NVU, these cells are implicated in inflammatory response and their role is discussed deeper bellow (brain inflammation topic).

Neurons are highly dependent on glucose and oxygen and can detect a very small variation in these molecules. Neuronal cells are strategically localized near microvessels. Additionally, they have an intimate anatomical and chemical relationship with NVU cells. When necessary, a neuron communicates with the vessels through the astrocytes influencing the blood supply to the area surrounding it (Muio et al., 2014).

NVU is a vital structure in the brain homeostasis by regulating the cerebral blood flow (CBF), BBB permeability, neurotransmitter inactivation and angiogenic/ neurogenic coupling (Zlokovic, 2008).

1.1.6 Regulation of brain perfusion

The Cerebral perfusion pressure (CPP) depends on mean arterial blood pressure (MAP), mean venous pressure (VP) and intracranial pressure (ICP): $CPP=MAP-(VP+ICP)$ in which VP is usually negligible. For CPPs between 60 and 150-170 mmHg, the CBF is autoregulated at 50 mL/100g/min (i.e. 750 mL/min, 20% of cardiac output) by arteriole and capillary vasodilatation corresponding to the hemodynamic or vascular reserve. CPP range of CBF autoregulation can be shifted towards higher values in the case of chronic arterial hypertension. Additionally, CBF depends on the arterial pressure of CO₂ and O₂, increasing during hypercapnia or hypoxia by microvessel vasodilatation, on blood viscosity, hematocrit, and on neuronal activity. CBF is around 80 mL/100g/min in gray matter and 20 mL/100g/min in white matter. The neurovascular coupling allows an increase of tissue oxygenation by CBF regional increase, so called “functional hyperemia”, in response to local neuronal activity. This would especially be triggered by transient local changes of temperature and glial cell pH. Moreover, brain activity induces expression of vasoactive mediators, such as K⁺, acetylcholine, γ -aminobutyric acid (GABA), catecholamines, neuropeptides, and neurotransmitters such as glutamate that stimulate the production of vasodilator agents such as nitric oxide (NO) and cyclooxygenase-2 (COX2)

(Iadecola, 2004). Neurovascular coupling involves the entire neurovascular unit, which includes neurons, astrocytes, endothelial cells, pericytes, basal membrane and extracellular matrix (ECM). For example, astrocyte edema plays a key role in CBF regulation during neuronal activation via transmembrane aquaporin-4 permeability (Igarashi et al., 2013).

1.1.7 Hemodynamic alterations in acute cerebral ischemia

Cerebral ischemia is the consequence of interrupted blood flow through a cerebral artery mainly due to proximal artery or cardiac emboli (Figure 4). It can be defined as a focal CPP decrease below the cerebral blood flow (CBF) autoregulation threshold that leads to a lack of oxygen and nutrient supply, neuronal anoxic depolarization, and necrosis. Acute ischemia is a rapid and dynamic process in time and space from “electrophysiological silence” of still viable neurons responsible for neurological deficit (penumbra area under moderate ischemia) to irreversible necrosis (infarct core). These separate classes of severity can be distinguished from each other using Magnetic Resonance Imaging (MRI) or computerized tomography (CT)-scan during the initial imaging following stroke onset. The cell death is driven by several mechanisms such as Ca^{2+} , Na^+/K^+ ion homeostasis, excitotoxicity, depolarization, oxidative stress, and inflammation (Hossmann 2009; Deb, Sharma et al. 2010).

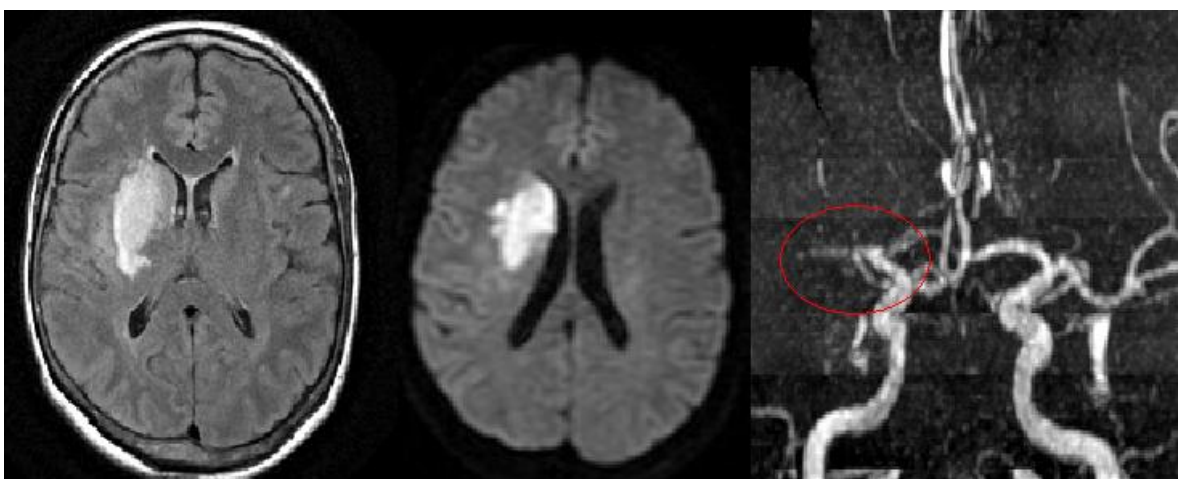


Figure 4: Detection of cerebral ischemia by MRI. Cerebral infarction in the middle cerebral artery (MCA) territory detected by an axial T₂ FLAIR (image left), axial diffusion imaging

(middle) and angiography “time of flight” demonstrates occlusion of the distal MCA trunk (red circle). (Velayudhan et al., 2016).

These are not limited to neurons but involve all brain cells including astrocytes, endothelial cells, oligodendrocytes, microglia and extracellular matrix (ECM), i.e. all components that define the “glio-neurovascular unit” (Moskowitz, Lo et al. 2010; Dirnagl 2012; Xing, Arai et al. 2012; Zhang, Badaut et al. 2012).

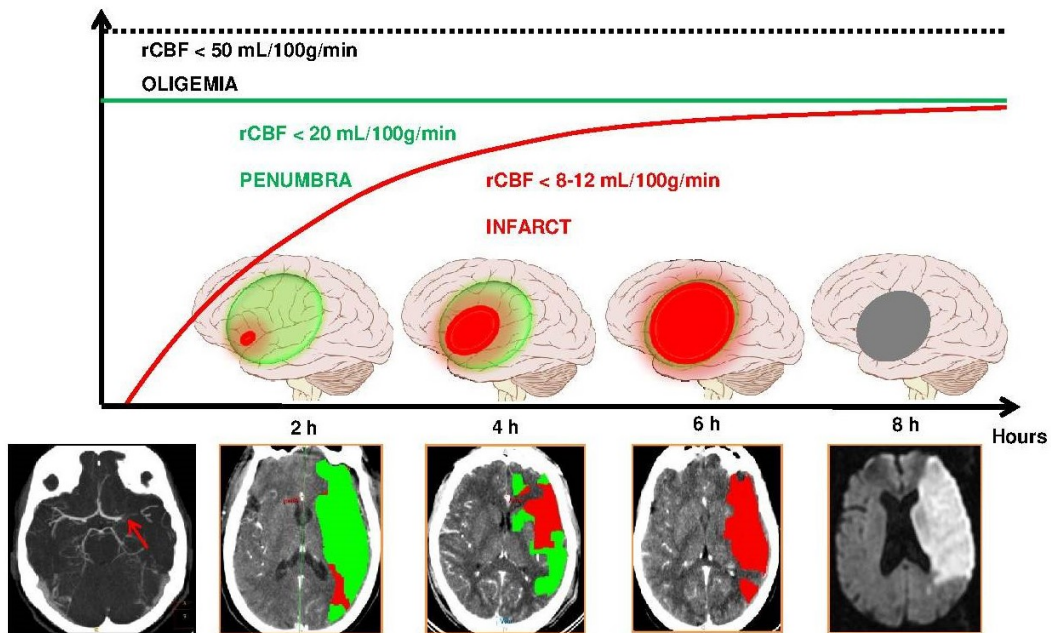


Figure 5: Evolution of brain ischemia at acute phase. The ischemic “core” (infarct in red) progress including the penumbra (in green) in the infarcted zone. This evolution is variable (from some minutes to hours) depending on individual differences such as collateral circulation. In clinical practices the values of regional cerebral blood flow rCBF give an estimation of infarct (very low CBF <12mL/100g/min) or penumbra (low CBF 12-20mL/100g/min) (Adapted from Detante et al. 2014).

1.1.7.1 From penumbra to infarction

Cerebral ischemia is defined as CPP decrease under the CBF autoregulation threshold. Subsequent CBF decrease below 20 mL/100g/min (for CPP < 30 mmHg) leads to insufficient O₂ and energy (adenosine triphosphate, ATP) supply. Ischemia is a dynamic process evolving in time and space and rapidly conducting to irreversible brain infarct (Figure 5). CBF decrease (50 to 20 mL/100g/min) initially induces an oligemia area with O₂ consumption maintenance at a cerebral metabolic rate of O₂ (CMRO₂) of 3 mL/100g/min as a result of an O₂ extraction fraction (O₂ EF) increase from 40% to 90%, which corresponds to the O₂ extraction reserve (

Figure 6). Subsequently, compensatory mechanisms become insufficient, and a decrease in CBF below 20 mL/100g/min leads to ischemia with two characteristic spatial regions (Figure 5, 6).

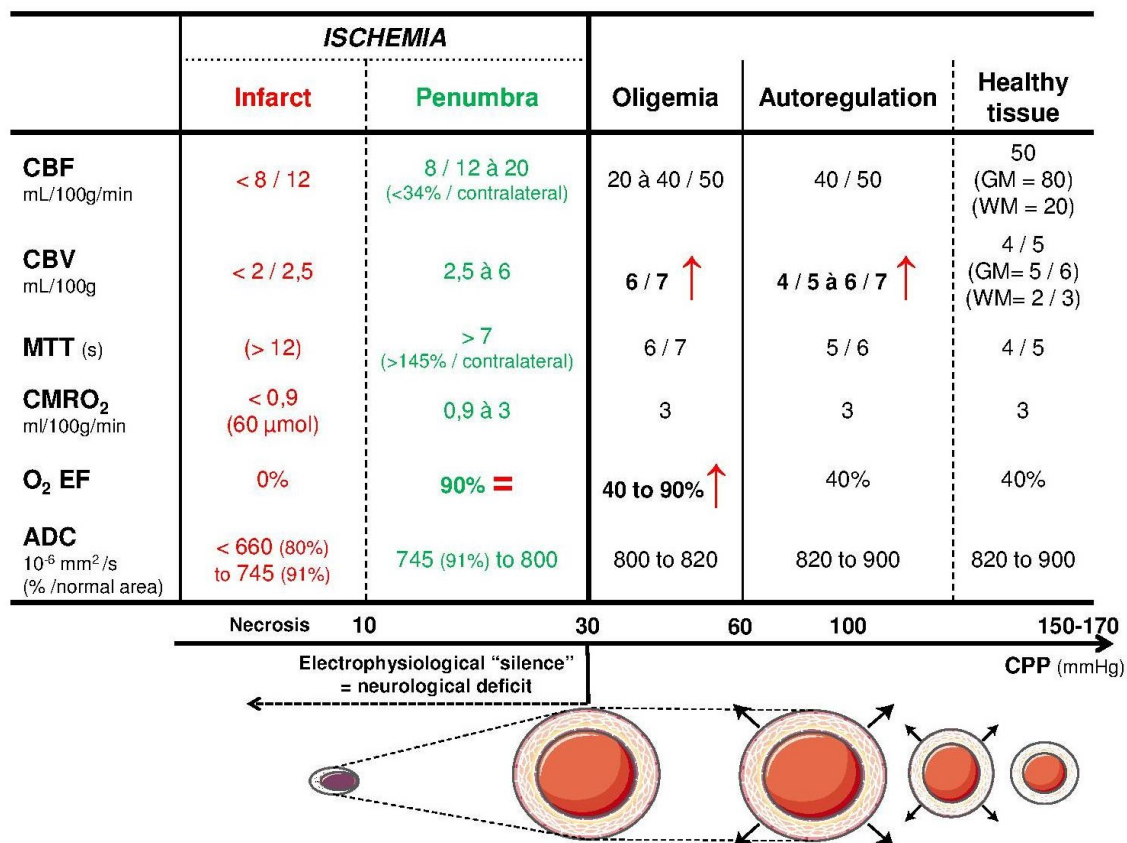


Figure 6 : Hemodynamic alterations in the different brain regions in acute ischemic stroke. Indicative values in each zone of cerebral blood flow (CBF), cerebral blood volume (CBV),

mean transit time (MTT), cerebral metabolic rate (CMRO₂), oxygen extraction fraction (O₂ EF), apparent diffusion coefficient (ADC) and cerebral perfusion pressure (CPP). Some values vary in gray matter (GM) and white matter (WM). (Adapted from Detante et al. 2014)

The first region is the ischemic penumbra in which sufficient oxygenation (CMRO₂ < 3 mL/100g/min) maintains cell viability but not neuronal activity, an electrophysiological “silence” that induces neurological deficit (Heiss, 2012; del Zoppo, 2010). The second region is the ischemic core (i.e. infarct) in which severe decreases in CBF (< 8 mL/100g/min), cerebral blood volume (CBV < 2-2,5 ml/100g) and oxygenation (CMRO₂ < 0,9 mL/100g/min; local O₂ saturation < 40% (Kurth et al., 2002) result in an irreversible brain lesion (Figure 6).

1.1.7.2 Imaging of acute cerebral ischemia

Hemodynamic and oxygenation standards to identify these different ischemic domains have been defined for nuclear imaging: single-photon emission computed tomography, positron emission tomography (¹⁵O₂ or ¹⁸F-fluoromisonidazole PET) (Baron, 1999), and inhaled-Xenon CT-scan. Neuronal damage corresponding to the infarct area has been well described by PET using a radioligand of benzodiazepine receptors (¹¹C-Flumazenil). The two ischemic domains can now be distinguished using easily available imaging techniques such as diffusion/perfusion MRI and perfusion CT-scan (Jensen-Kondering and Baron, 2012) (Kidwell et al., 2013). Diffusion MRI permits good visualization of severe cell edema in the infarct area which appears as a dramatic decrease in apparent diffusion coefficient. However, the early diffusion hyposignal that is observed at a CBF value of 41 mL/100g/min after 30min of ischemia might overestimate the infarct area size and include a part of the penumbra (Rosso et al., 2009). Usually, penumbra assessment is carried out using perfusion imaging for comparison with diffusion MRI in order to identify any discrepancy in the assessment of the infarct core boundary with the larger surrounding hemodynamic abnormalities (Albers et al., 2006) or cerebral blood volume (CBV)/ mean transit time (MTT) CT-scan mismatch (Wintermark, Flanders et al. 2006). Penumbra can also be estimated using the “radio-clinical” mismatch between a small acute

infarct seen by diffusion MRI and severe clinical deficit due to the electric silence of neurons in the penumbra area. MRI is currently being explored for its potential to allow direct oxygen brain mapping by measuring CMRO₂ and local oxygen saturation (Christen et al., 2011; Jensen-Kondering and Baron, 2012). All of these imaging techniques can be adapted for arterial imaging such as angio-CT scan or angio-MRI to discriminate the restored vessels from the persistently occluded. Thus, the combined assessment of viable penumbra tissue with mapping of arterial status enables prediction of acute ischemia duration, guiding decisions made during initial care, such as the extension of the time window for reperfusion therapies (Campbell et al., 2014).

1.1.8 Mechanisms of brain cell death

Brain is particularly vulnerable to a deficit in O₂ or glucose supply because of its high energy consumption, nearly exclusive aerobic glucose metabolism and the absence of any *in situ* reserve. Neurons are more vulnerable to ischemia than glial or endothelial cells, and the salvageable penumbra may be affected by a selective neuronal loss, as opposed to pan necrosis (Baron et al., 2014).

Mechanisms leading to cell death by necrosis or apoptosis are numerous (Xing et al., 2012) (Figure 7).

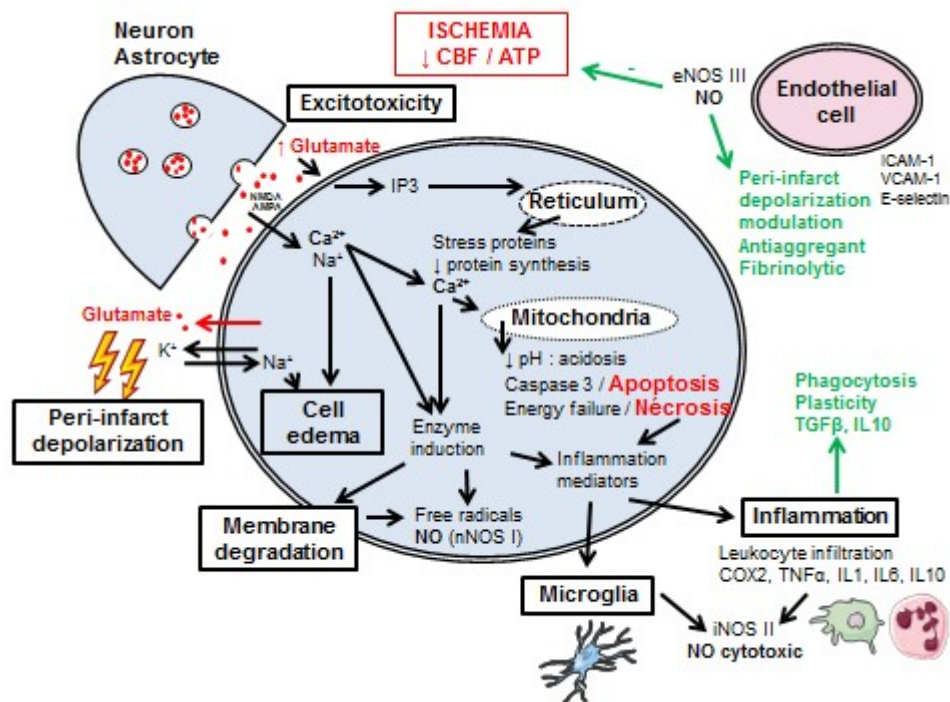


Figure 7: Mechanisms leading to cellular death in ischemia. AMPA : α -amino-3-hydroxy-5-methyl-4-isoxazolepropionic acid ; ATP : adenosine tri-phosphate ; COX2 : cyclooxygenase 2; CBF : cerebral blood flow; IL : interleukin ; IP3 : inositol triphosphate ; NMDA : N-methyl-D-aspartate receptor ; NOS : Nitric Oxide synthases (nNOS : neuronal NOS type I ; iNOS : inducible NOS type II ; eNOS : endothelial NOS type III) ; TGF β : transforming growth factor β ; TNF α : tumoral necrosis factor, ICAM-1: intercellular adhesion molecule; VCAM-1: vascular cell adhesion molecule ; E-selectin. (Adapted from Detante et al. 2014)

Not all deleterious phenomena occur simultaneously. According to cerebral ischemia severity and duration, there is a sequence of disorders corresponding to the “metabolic” penumbra area (salvageable tissue) and infarct area (irreversible necrosis) (Hossmann, 2008).

1.1.8.1 Toxicity of intracytoplasmic calcium increase

Physiologically, Ca²⁺ enters a neuron via voltage-dependent channels, kainate and glutamate receptors channels: N-methyl-D-aspartate (NMDA), α -amino-3-hydroxy-5-methyl-4-isoxazole propionate

(AMPA). Maintaining the Ca^{2+} intra/extra-cellular gradient (1/10,000) requires energy-consuming processes: 1. Storage into cytoplasmic proteins, endoplasmic reticulum (ER) and mitochondria; 2. Release into extracellular space via $\text{Na}^+/\text{Ca}^{2+}$ transporter and Ca^{2+} -ATPase pump. During cerebral ischemia, the disruption of supplied energy induces a dramatic increase of intracytoplasmic Ca^{2+} (Cross et al., 2010). This is aggravated by the increase in extracellular glutamate which acts on ionotropic receptors, accelerating Ca^{2+} release from ER.

Intracytoplasmic Ca^{2+} provokes a series of deleterious consequences such as mitochondria dysfunction (energy deficit, free radical synthesis), neuronal NO synthase (nNOS type I) activation (cytotoxic NO generation), enzyme activation (endonucleases, phospholipases, kinases, proteases), and ER dysfunction (protein synthesis inhibition).

1.1.8.2 Glutamate and excitotoxicity

Cerebral ischemia quickly leads to the release of inhibitory (GABA) and excitatory (glutamate) neurotransmitters from neurons and astrocytes, as well as reuptake dysfunction (Malarkey and Parpura, 2008).

Glutamate synaptic exocytose is notably due to the overexpression of synaptic neuronal protein SNAP25 (synaptosomal-associated protein 25) and to the dysfunction of astrocyte Ca^{2+} -dependent release by the SNAR complex (Soluble N-éthylmaleimide-sensitive-factor Attachment protein Receptor) which includes synaptobrevin-2, syntaxin-1, SNAP23 and synaptotagmin-4. In addition, glutamate storage failure occurs in astrocytes via H^+ ATPase vacuolar protein (V-ATPase) and vesicular glutamate transporters (VGLUT) dysfunction (Deb et al., 2010). Glutamate acts on NMDA, AMPA and kainate receptors and induces deleterious Na^+ and Ca^{2+} intracellular inflow. Additionally, glutamate metabotropic receptor activation leads to RE stress via the G protein – phospholipase C – inositol triphosphate transduction pathway. Glutamate and extracellular K^+ increases also contribute to the spread of peri-infarct depolarization.

GABA role is less understood during ischemia. However, alteration of the inhibitory GABA neurotransmission would play an important role in peri-infarct hypoexcitability, Cl^- gradient,

intracellular Ca^{2+} increase, or reactive oxygen species generation, and thus could be an interesting therapeutic target (Schwartz-Bloom and Sah, 2001).

1.1.8.3 Peri-infarct depolarization and spreading depression

Within the infarct core, there is an irreversible anoxic depolarization. In the peri-infarct area, extracellular K^+ increases via Na^+/K^+ -ATPase pump dysfunction. This K^+ increase, coupled to glutamate, leads to an intense peri-infarct depolarization of neuronal and glial membranes. Depolarization slowly spreads into adjacent cortex (2 to 9 mm/min), is called “spreading depression” and is characterized by neuronal swelling and distortion of dendritic spines (Dreier, 2011). Depolarization can alter the basal membrane integrity of the BBB via matrix MMP9 activation (Gursoy-Ozdemir et al., 2004). Depolarization moreover causes a spreading ischemia that propagates in the penumbra area (Strong et al., 2007) notably due to endothelial NOS (eNOS type III) blocking with extracellular NO decrease. Spreading depolarizations were observed in human stroke and can be associated with both unfavorable and protective hemodynamic responses (Woitzik et al., 2013).

1.1.8.4 Cell edema (cytotoxic edema)

During cerebral ischemia, the loss of ionic gradient (Na^+/Cl^- inflow via Na^+/K^+ -ATPase pump and AMPA receptors) and lactate intracellular accumulation followed by passive water influx due to an increase in intracellular osmolarity lead to early cell edema. This affects all the neural cells and quickly leads to their necrosis. The swelling of astrocytes and endothelial cells aggravates local hypoperfusion by microvessel compression.

Cell edema occurs within the first minutes of ischemia and mainly corresponds to the infarct area with some limited extension into the penumbra. Diffusion MRI permits visualization of cell edema size by the dramatic decrease in the apparent diffusion coefficient caused by the extracellular space restriction, correlating with the final lesion and functional prognosis (Baird et al., 2001; Rosso et al., 2009).

1.1.8.5 Blood-brain barrier permeability and vasogenic edema

BBB is composed of endothelial cells, basal membrane, astrocyte end-feet, and contractile pericytes. After cerebral ischemia, BBB permeability increases from the first hour (Huang et al., 2013a) and continuing for several weeks (Strbian et al., 2008). BBB breakdown is caused by microvascular endothelial cell dysfunction (Huang et al., 2013b) such as endothelin receptor alteration, activation of Na⁺/K⁺-ATPase endothelial pumps due to increased extracellular K⁺, vasodilator NO synthesis, and by basal membrane destruction notably by matrix metalloprotease MMP2 and MMP9 overexpressed 1 and 3 hours after ischemia. Tissue edema occurs within few hours as a result of osmotic gradient and is worsened by protein (albumin) extravasation between 12h to 2 days post-ischemia, leading to a delayed brain vasogenic edema as well as ICP increase. Intracranial hypertension can subsequently aggravate hypoperfusion and cause distant damage by compression and brain herniation.

BBB leakage also plays a key role in post-stroke inflammation by enhancing leukocyte infiltration to brain parenchyma. This infiltration also increases BBB permeability via neutrophil MMP9 expression notably during hemorrhagic transformation after cerebral ischemia (Rosell et al., 2008).

1.1.8.6 Oxidative stress: nitric oxide (NO) and free radicals

Cerebral ischemia, particularly if followed by reperfusion, quickly results in activation of several neuronal and vascular enzymes responsible for generating free radicals such as superoxide dismutase, catalase, and glutathione peroxidase. Protective anti-oxidant systems, such as α -tocopherols (vitamin E) and vitamin C, are usually too slow to prevent oxidative damage (Dalkara and Moskowitz, 1994; Moskowitz et al., 2010). Intracytoplasmic Ca²⁺ increase enhances superoxide ion production through cyclooxygenase COX2 expression, NADPH oxidase (NOX) activation (Nayernia et al., 2014) by protein kinase C, and NO produced by neuronal NOS (nNOS type I) (Brennan et al., 2009). NO, which is also produced by inducible (i.e. immunologic) NOS (iNOS type II), interacts with superoxide anion, also generated by depolarized mitochondria, to form peroxynitrite.

Free radicals interact with all cell components leading to a high cytotoxicity. Additionally, they induce free fatty acid (such as arachidonic acid) release (Adibhatla and Hatcher, 2009) and mitochondrial

malfunction. Free radicals also cause ER stress, poly-ADP ribose polymerase (PARP) activation, DNA fragmentation, and pericyte constriction (Yemisci et al., 2009).

In parallel, NO produced by endothelial NOS (eNOS type III) has beneficial effects during ischemia such as vasodilation, anti aggregation, fibrinolysis, and modulation of peri-infarct depolarizations (Petzold et al., 2008).

1.1.8.7 Acidosis and glycolysis

Glucose is the near-exclusive energy source of the brain and plays a role in many brain disorders (Mergenthaler et al., 2013). Spontaneous hyperglycemia is frequent during the acute phase of cerebral ischemia (30-40% of cases) and is correlated to poor prognosis via aggravation of ischemia and reperfusion injuries (Kruyt et al., 2010) particularly during intravenous (IV) thrombolysis with an enhancement of superoxide ion production (Won et al., 2011).

During ischemia, glucose consumption at first increases and is characterized by a high glucose / O₂ consumption (CMRO₂) ratio. This metabolic “decoupling” is identifiable by PET and marks the initiation of anaerobic glycolysis. Afterward, the glucose consumption decreases (for a CBF < 25 mL/100g/min) and acidosis occurs due to lactic acid accumulation. This acidosis activates acid-sensing Ca²⁺ channels and contributes to intracellular Ca²⁺ overload. It also induces ER stress with a protein synthesis loss and caspase 12 activation that leads to apoptosis of astrocytes in the peri-infarct area (Aoyama et al., 2005).

However, acidosis also acts as a neuroprotective during ischemia by blocking NMDA receptors (anti-excitotoxic effect) and by anti-apoptotic effect (Fan et al., 2014).

1.1.8.8 Necrosis and apoptosis

Cell death by necrosis quickly occurs in the infarct core. It immediately follows cell edema and membrane injuries that lead to cell disintegration. Necrotic fragments are cytotoxic and proinflammatory, and so aggravate the ischemic lesion. Interestingly, cell death is not limited to

infarct core. Distant from this one characterized by pannecrosis, a selective neuronal loss can occur in salvaged penumbra area which hampers recovery (Baron et al., 2014). Programmed cell death by apoptosis begins a few hours after cerebral ischemia as inflammation progresses. Apoptosis is a consequence of complex mechanisms requiring energy supply (Hengartner, 2000) and thus occurs mainly in the penumbra. It is characterized by cell condensation and fragmentation that forms phagocytatable apoptotic bodies. Cerebral ischemia induces direct damages of mitochondria membrane, and expression of proapoptotic genes such as Trp53 (p53), Bax, Bid, Bad, Bag, JNK, c-jun, cdk5, p38, but also anti-apoptotic genes such as Bcl2, Bcl-XL, Iap. Bad and Bax, which are modulated by Bcl2 and Bcl-XL. These factors enhance, via an intrinsic pathway, cytochrome C and apoptotic induction factor (AIF) release from mitochondria (Joza, Susin et al. 2001). Cytochrome C can also be released from mitochondria via an extrinsic pathway, by Fas receptor stimulation (CD95) on neuron and glial cell surfaces, stimulated by the Fas ligand (FasL) on neurons, microglia, cytotoxic T lymphocytes and natural killers cells (NK). Fas-FasL interaction induces formation of the death-inducing signal complex (DISC) and activation of caspase 8 and pro-apoptotic factor Bid. Additionally, cerebral ischemia leads to TNF-related apoptosis ligand (TRAIL) expression from astrocytes and microglia. Cytochrome C with apoptotic peptidase activating factor 1 (APAF 1) and procaspase 9 constitute the apoptosome that activates caspase 9 and other proapoptotic caspases such as 1 and 3 in few hours.

1.1.8.9 Brain inflammation and stroke-induced systemic immunodepression

After cerebral ischemia, many inflammatory processes are ambivalent, with both deleterious consequences and/or beneficial effects such as neuroprotection and remodeling. Inflammation concerns not only the brain tissue but also innate and adaptive systemic immunity (Iadecola and Anrather, 2011) with reciprocal crosstalk taking place between them (Dirnagl and Schwab, 2009; Kamel and Iadecola, 2012). Inflammatory processes begin after few minutes of ischemia and persist for years contributing to post-stroke atrophy and dementia.

In brain tissue, microglia cells represent 5-20% of glial cells and are analogous to resident phagocytes involved in survey and plasticity (Hanisch and Kettenmann, 2007; Ziv et al., 2006). From the first few minutes of ischemia, microglial cells are activated by extracellular ATP increases and a loss of neuronal contact, and proliferate over the course of weeks, particularly in the penumbra. Two types of activated microglia can be distinguished: 1) “inflammatory” microglia (M1) releasing inflammation mediators such as interleukin IL1 β , tumor necrosis factor (TNF α), but also NO, free radicals, prostanoids, and enzymes such as cathepsin, MMP9; and 2) “anti-inflammatory” microglia (M2) releasing anti-inflammatory cytokines such as transforming growth factor (TGF β) and neurotrophic factors such as glia- or brain-derived neurotrophic factors (GDNF, BDNF), fibroblast growth factor (FGF β), insulin-like growth factor (IGF1), and vascular endothelial growth factor (VEGF) (Xing et al., 2012). Microglia scavenges the infarct by phagocytosis of dead cell fragments and apoptotic bodies.

Astrocytes are also involved in post-stroke inflammation producing proinflammatory cytokines and MMP9 but also neuroprotective factors such as VEGF, TGF β 1 and erythropoietin. In neurons, post-ischemia disorders lead to complement activation, transcription factor synthesis such as nuclear factor (NF κ B), hypoxia inducible factor (HIF1), STAT3, and proinflammatory gene activation such as platelet activation factor, TNF α , IL1, IL6, IL8, IL10, monocyte chemoattractant protein 1 (MCP1). On the endothelial cell surface, intercellular and vascular adhesion molecules (ICAM1, VCAM1), P- and E-selectin expression contribute to post-ischemia neutrophil migration and infiltration (maximum at 2-3 days post-ischemia). Neutrophils aggravate microvessel occlusion and release proteases such as MMP9 (Allen et al., 2012), proinflammatory molecules, and cytotoxic NO from iNOS II activation. Neutrophils are accompanied by mastocytes, monocytes/macrophages and dendritic cell infiltration, which strengthen cytokine production and phagocytosis. Interestingly, perivascular macrophages can exhibit similar phenotypes M1/M2 as microglia.

The effect of lymphocytes and delayed adaptive immunity against cerebral antigens remains controversial (Iadecola and Anrather, 2011) as leukocyte infiltration chronology after ischemia (Gelderblom et al., 2009; Möller et al., 2014). Although T4 and T8 lymphocytes seem to play a deleterious pro-inflammatory role by infiltrating ischemic tissue, other lymphocyte subtypes such as

T-helpers (Th) and T-regulators (Treg) could provide immunomodulatory and neurotrophic effects via IL10 and TGF β 1 release.

Beyond the brain tissue, cerebral ischemia induces a severe systemic immunodepression with lymphopenia and high levels of IL6, IL10 and cortisol (Klehmet et al., 2009) notably due to spleen and liver disturbances via their noradrenergic innervations (Wong et al., 2011). This stroke-induced immunodepression syndrome could be protective for brain lesion but leads to frequent severe systemic infections mainly urinary tract infection and pneumonia that worsen mortality and prognosis.

1.2 ENDOGENOUS MECHANISMS OF NEUROPROTECTION AND BRAIN

REMODELING

It is reported in clinical and experimental settings that brain functions usually undergo some degree of spontaneous improvement post-acute phase (Kwakkel and Kollen, 2013; Seevinck et al., 2010). This phenomenon is probably due to endogenous mechanism of protection and healing. Some of the major mechanisms of brain protection and remodeling are discussed below.

1.2.1 Endogenous neuroprotection

Beyond initial tissue reperfusion by artery recanalization or anastomosis, different endogenous protections occur in parallel of the deleterious processes (Dirnagl et al., 2003).

Alterations concerning brain perfusion are detected in the acute phase of stroke. A vasodilation of adjacent areas of ischemia is reported such as compensatory mechanisms to brain ischemia.

Some minutes after stroke onset, many mechanisms of protection such as impairment of inhibitory neurotransmission (Redecker et al., 2002) or anti-inflammatory cytokines (Klehmet et al., 2009) are activated. Post-stroke up regulation or down regulation of hundreds of genes associated with either survival or cell death is reported (Prasad et al., 2012).

Although endogenous neuroprotection often remains insufficient (or too slow) to avoid all cerebral ischemia damages, it gives perspectives to develop treatments enhancing its benefit.

1.2.2 Endogenous brain remodeling

Ischemic stroke presents a highly complex cascade of mechanisms implicated in its physiopathology. Furthermore, the endogenous restorative process following initial ischemic damage involves a brain remapping to compensate damaged networks (Winship and Murphy, 2009) that include angiogenesis, reorganization of contralateral brain hemisphere and axonal sprouting (Murphy and Corbett, 2009).

1.2.2.1 Angiogenesis

Angiogenesis is defined as a biological process involving the formation of new blood vessels from pre-existing vessels. It is a multi-step biological process including proliferation and sprouting of endothelial cells, formation of tube-like vascular structures branching and anastomosis (Risau, 1997). In physiological conditions, angiogenesis is restricted in adult brains, most vasculature is quiescent, with only 0.01% of endothelial cells undergoing division (Carmeliet and Jain, 2000). Studies from human and experimental stroke indicate that neovascularization is present in the adult brains in response to cerebral ischemia (Hayashi et al., 2003; Krupinski et al., 1994; Yin et al., 2015).

Inflammation and hypoxia are one the major pathological trigger for angiogenesis in non-neoplastic diseases (Carmeliet and Jain, 2000). Hypoxia activates hypoxia-inducible transcription factors (HIFs), which function as master switches to induce expression of several angiogenic factors (Semenza, 1998).

-Vascular endothelial growth factor (VEGF), is the most important mitogen in the process of angiogenesis (Beck and Plate, 2009). The binding of VEGF to its receptors on the surface of endothelial cells activates intracellular tyrosine kinases, triggering multiple downstream signals that promote angiogenesis (Beck and Plate, 2009). The angiogenic effects of VEGF are primarily mediated

by binding to specific VEGF receptors: VEGFR-1 and VEGFR-2. **VEGFR-1** is a key receptor in developmental angiogenesis is selectively expressed in distinct vascular beds (Hicklin and Ellis, 2005).

VEGFR-2 is expressed on almost all endothelial cells mediates the majority of the downstream angiogenic effects of VEGF, including microvascular permeability, endothelial cell proliferation, invasion, migration and survival (Hicklin and Ellis, 2005).

Analysis of VEGFR following brain ischemia revealed an induction of both receptors in vessels of the infarct brain (Moisan et al., 2014). Induction of VEGFR-1 and 2 expressions started 48 h after the insult in vessels at the border of the infarction and strong expression levels persisted up to 7 days (Kovács et al., 1996; Marti et al., 2000).

This initial process of angiogenesis contributes to BBB leakage (Durukan et al., 2009). However, this process seems essential for endogenous mechanism of recovery. A recent experimental study demonstrated that the administration of Pifithrin- α a specific p53 inhibitor (p53 is transcription factor described as an important regulator of apoptosis and VEGF) 24 hours after stroke induce VEGF expression and improves the recovery (Zhang et al., 2016).

-Platelet-derived growth factor (PDGF) is another growth factor implicated in angiogenesis. PDGF-B and its receptor PDGFR are essentials during embryonic development for the recruitment of pericytes to brain capillaries (Lindahl et al., 1997). Post-stroke analysis in human brain samples showed an expression of PDGF-B and its receptor on microvessel endothelial cells (Krupinski et al., 1997)

-Fibroblast growth factors (FGFs) family are known to play a crucial role in the regulation of a plethora of developmental processes, in both the embryonic and adult stages of life (Hallinan et al., 2016). Both acidic FGF (FGF-1) and basic FGF (FGF-2) are expressed after brain ischemia. The expression of FGF-1 by neurons and macrophages is detected 24 hours after the insult, is increased until about 14 days after ischemia , but decreased gradually and was undetectable after more than 30 days (Hara et al., 1994). Following cerebral ischemia, enhanced levels of FGF-2 were observed in neurons in the penumbra after 1 day. Besides FGF-2 is also expressed by macrophages, endothelial

cells and reactive astrocytes in the first 2 weeks following vessel occlusion (Beck and Plate, 2009; Chen et al., 1994). FGF-2 is necessary for endothelial cells proliferation (Slevin et al., 2006), but inhibits differentiation by maintaining PDGFR (PDGF receptor)- α on the cell surface (McKinnon et al., 1990).

-**TGF- β** signaling has a context-dependent inducing pro or anti-angiogenic effects. TGF- β play a role in vessel maturation evidenced by studies demonstrating that the loss of TGF- β receptors ALK-1 and TGFR-1 results in arteriovenous malformation known as hereditary hemorrhagic telangiectasia.

-**Angiopoietin** family in humans is composed of three ligands, ANG-1, ANG-2 and ANG-4 and two receptors TIE-1 and TIE-2. Healthy vessels are equipped with mechanism of stability while remaining able to respond to angiogenic stimuli (Carmeliet and Jain, 2000). Ang-1 maintain endothelial cells quiescence through TIE-2 activation (Saharinen et al., 2008). Ang-2 is a antagonist of Ang-1+TIE2 signaling, stimulating mural cells detachment, increase of vascular permeability and endothelial cells sprouting (Augustin et al., 2009). Ang-4 and TIE-1 actions are not well elucidated.

-The ECM forms a physical link between vascular cells and their surround tissues. Endothelial cells possess mechanism to interact with ECM and alter the matrix, for example through proteases activation. Distinct proteases such as **MMPs** modulate angiogenesis by different mechanisms, including proteolytic remodeling of basement membrane and release of VEGF and FGF (Carmeliet and Jain, 2011)*. The alteration of ECM proteins composition facilitates EC migration and tube formation.

*Most of the actual knowledge about adult angiogenesis come from the research for therapeutic anti-angiogenic approaches for cancer diseases. Dr Carmeliet revised this mechanism in an elegant review of literature (Carmeliet and Jain, 2011). The cited study was of great help for my understanding of angiogenic process.

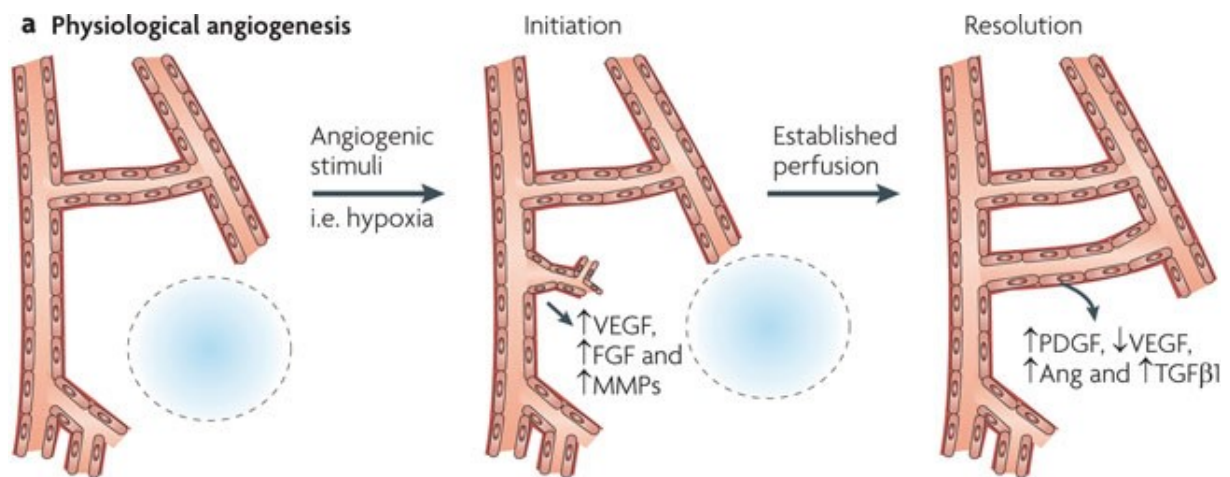


Figure 8. Schematic illustration of angiogenic process induced by ischemia, from Chung et al. 2010 (Chung et al., 2010) Vascular endothelium growth factor, VEGF; Fibroblast growth factor, FGF; Matrix metalloproteinases, MMPs; Angiopoietin, Ang and transforming growth factor beta 1, TGF- β 1.

- **Steps of angiogenesis.** Blood vessels are equipped with O_2 alteration sensors which allow vessels re-adjust their shape through vasodilatation or vasoconstriction optimizing blood flow. Angiogenesis initiates with vasodilatation mediated by Nitric oxide (NO), a mediator of relaxation of blood vessels. In response to angiogenic signals mediated by Ang-2, pericytes liberate themselves from basement membrane by proteolytic degradation mediated by MMPs. Vascular permeability increases in response to VEGF facilitating endothelial cells migration.

Endothelial cells migrate onto ECM surface and proteases cells liberate angiogenic molecules stored in ECM such as VEGF and FGF and remodel ECM into an angio-competent milieu (Carmeliet and Jain, 2011). With the aim to avoid massive endothelial cell moving towards the angiogenic signals, one of endothelial cells called tip cell becomes selected to lead the vessel tip (Verdegem et al., 2014). Endothelial cells proliferate in response to VEGF, migrate following tip cells signals to form a tube and became responsive to others factors such as Ang-1 and TGF- β .

For a properly function of blood vessels, they must be mature and covered by mural cells, PDGF family, angiopoietins and TGF- β contributes to this process (Jain, 2003) (Figure 8).

Angiogenesis naturally occurs following cerebral ischemia, this process is principally detected in lesion boundary and seems to be crucial for regenerative process such as neurogenesis and synaptogenesis. Angiogenic process can be amplified by various experimental treatment strategies as discussed below.

1.2.2.2 Neurogenesis

Another important mechanism related to brain endogenous remodeling is neurogenesis.

Neurogenesis is a process by which neurons are generated from progenitor cells such as neural stem cells. This process occurs during embryogenesis and also continuously in adult mammalian brain (Reynolds and Weiss, 1992; Taupin and Gage, 2002).

Important advances in neurogenesis research are achieved owing the introduction of bromodeoxyuridine (BrdU) (Kuhn et al., 1996). With this discovery, it was possible to demonstrate the long-life continuous neurogenesis in almost all mammals, including humans (Eriksson et al., 1998).

The production of new neurons in adult brain take place in specific areas called neurogenic niches (Eriksson et al., 1998). Under normal conditions adult neurogenesis is restricted to hippocampus in subgranular zone (SGZ) of dentate gyrus where new dentate granule cells are generated (Figure 9), and in the subventricular zone (SVZ) (Figure 10) of lateral ventricles where new neurons are generated and migrate through the rostral migratory stream (RMS) to the olfactory bulb to become interneurons (Gage, 2000). Neurogenesis in other adult CNS regions is very limited under physiological conditions but could be induced in pathological conditions such as stroke (Ming and Song, 2011).

Adult neurogenesis is regulated by many physiological stimuli such as physical exercise (van Praag et al., 1999) and enriched environment (Kempermann et al., 1997) improving proliferation and new neuron survival. In contrast, aging leads to a significant reduction in cell proliferation (Rossi et al., 2008)

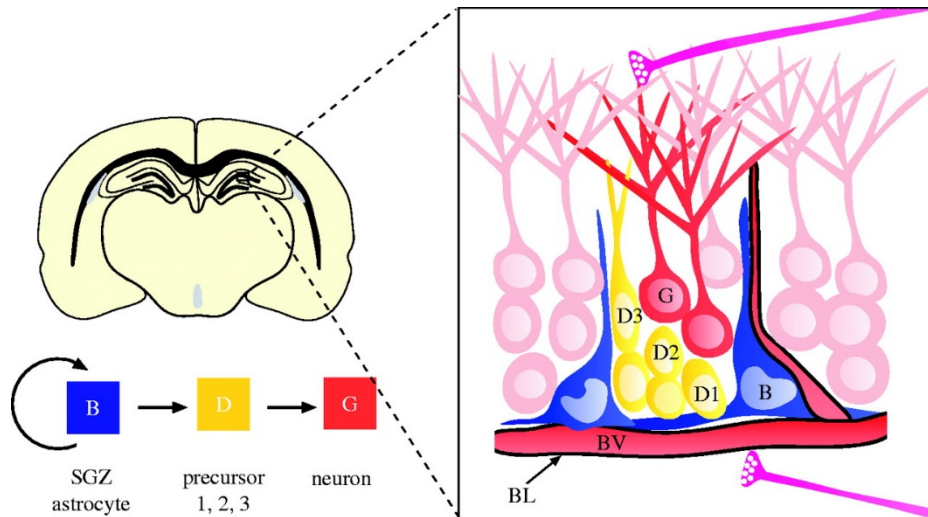


Figure 9. Neurogenic niche Subgranular zone (SGZ) from (Riquelme et al., 2008). Illustrative image of frontal section of rat brain underlying the adult neurogenic niche on SGZ of hippocampus. Astrocytes (B, blue) generate intermediate precursors (D, yellow), which are progressively differentiated (type D1→type D2→type D3), until becoming mature granule neurons (G, red).

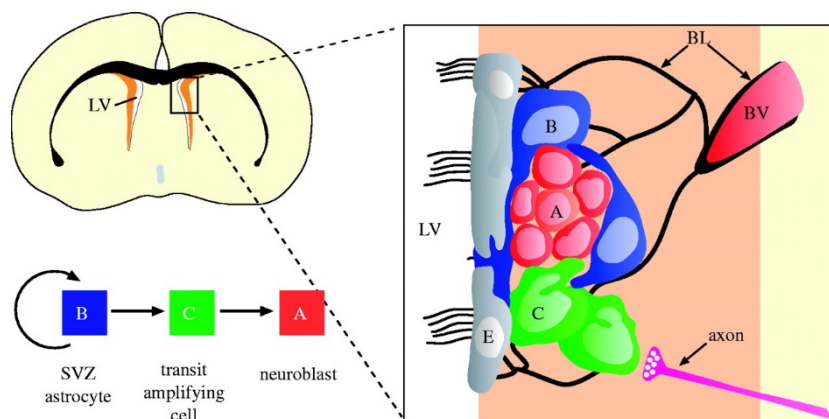


Figure 10. Neurogenic niche Subventricular zone (SVZ) from (Riquelme et al., 2008). Illustrative image of frontal section of rat brain underlying the adult neurogenic niche SVZ (orange) adjacent to lateral ventricle (LV) on striatum. Astrocytes (B, blue) generate migrating neuroblasts (A, red), designates to olfactory bulb via transit amplifying cell (c, green), multi-ciliated ependymal cells (E, gray) basal lamina (BL, black), blood vessels (BV).

- **Post stroke-induced neurogenesis**

Ischemia-induced neurogenesis occurs in the neurogenic niches SGZ and SVZ but also in non-neurogenic areas in the intact brain (Lindvall and Kokaia, 2015).

Evidence suggests that stroke induces neurogenesis in cerebral areas where neurons are not normally formed such as striatum (Figure 11). Cells expressing BrdU, given intraperitoneally after stroke and markers of immature neurons (DCX) and mature neurons (NeuN and DARPP-32) were detected in damaged striatum (Parent et al., 2002). The occurrence of neurogenesis in the cerebral cortex is less well established (Lindvall and Kokaia, 2015). However, new cells expressing markers of neuroblasts or mature neurons were detected in ischemia-damaged cerebral cortex (Zhang et al., 2006a).

These immature neurons can also be originating from SVZ. Kreuzberg and colleagues (Kreuzberg et al., 2010) in a study using transgenic mice, in which neuroblasts originating in SVZ expressed green fluorescent protein (GFP), reported that neural progenitors migrated toward the cortical infarct after middle cerebral artery occlusion (MCAo). In a similar study, neuroblasts DCX⁺/BrdU⁺ migrating along the corpus callosum to peri-infarct cortex were detected 2 weeks after an ischemic lesion in mice (Osman et al., 2011)

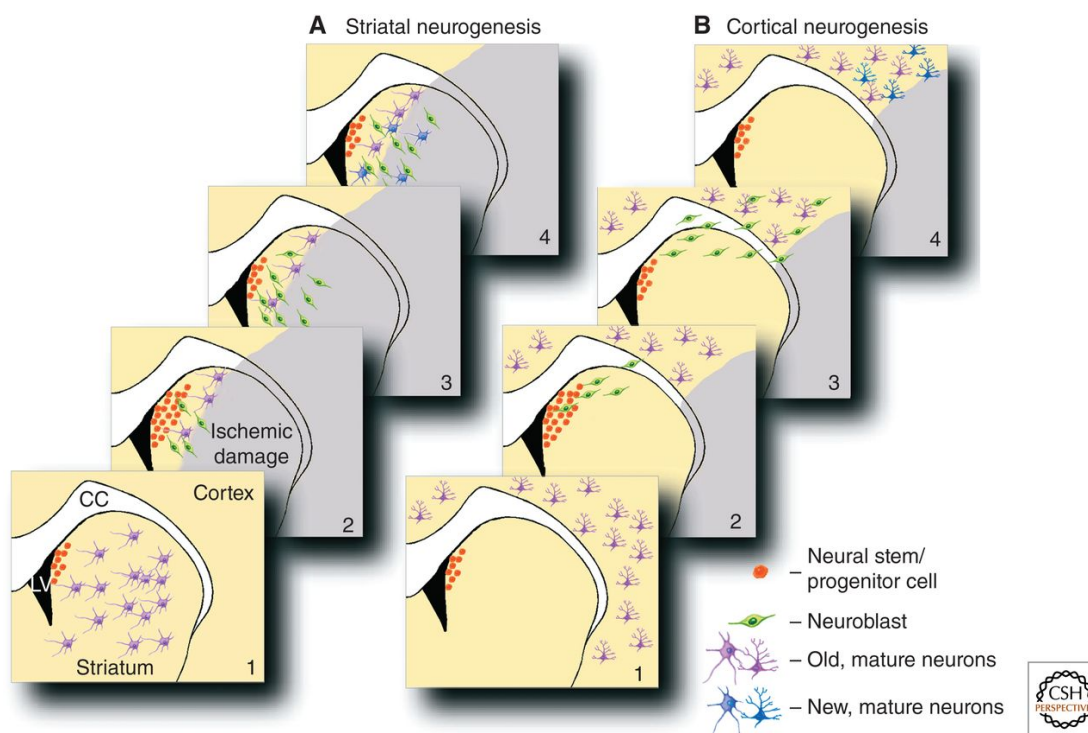


Figure 11 : Schematic representation of stroke-induced neurogenesis on striatum and cortex, from Lindvall et al 2015. Corpus Callosum (CC) (Lindvall and Kokaia, 2015).

- Steps of neurogenesis

The SVZ has been reported as the main source of neuroblasts generated after stroke which migrate towards the damaged area in rodents (Lindvall and Kokaia, 2015). For this reason, we decide to focus on the steps of neurogenesis in SVZ that are different from which detected in SGZ.

Proliferation The first step of neurogenic process is proliferation. Ischemia triggers a transient alteration in SVZ cell division, from asymmetric to symmetric, expanding the pool of progenitor cells. Apparently, stroke promotes an increase in the proportion of dividing cells in the SVZ and reduces their cell-cycle length (Zhang et al., 2006b). Other cellular types such as ependymal cells proliferation are induced by ischemia. In a rat stroke study, Zhang et al (Zhang et al., 2007) reported that ependymal cells lining the lateral ventricle wall were transformed into radial glia cells and were surrounded by type-C (progenitors) and type-A (neuroblasts) cells in SVZ. Several molecules and mechanisms are implicated in neural stem progenitor cells (NPCs) regulation. The Notch signaling pathway is implicated in this regulation (Carlén et al., 2009; Wang et al., 2009).

Survival: About 80% of new neurons die during the first two weeks after their formation (Arvidsson et al., 2002). Caspases are probably involved in this neuronal loss and administration of caspase inhibitors improve the survival of neuroblasts (Thored et al., 2006). Inflammation seems also having a role in stroke induced-neurogenesis. Microglial cells produce important factors which contribute to the maintenance of neurogenic response such as insulin-like growth factor-1 (IGF-1) (Thored et al., 2009).

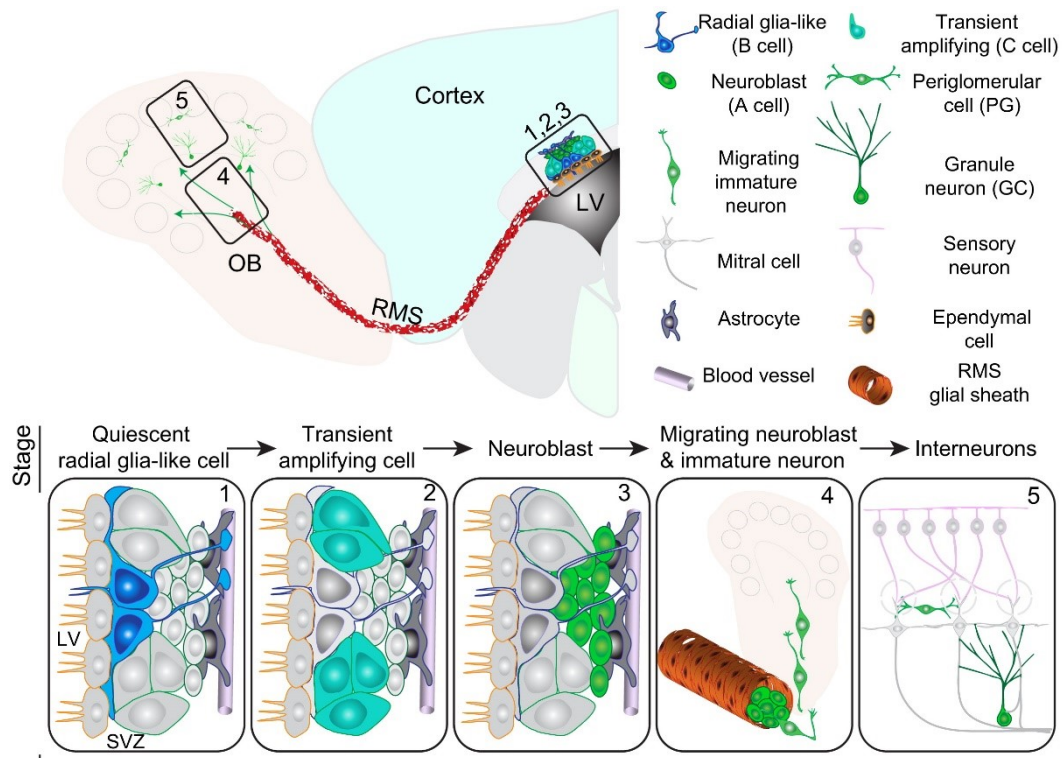


Figure 12: Steps of adult neurogenesis in adult Subventricular zone (SVZ), from Ming and Song 2011. Lateral ventricle (LV), olfactory bulb (OB), Rostral migratory system (RMS).

Migration: In physiological conditions, neuroblasts form a chain, the rostral migratory system (RMS) and migrate towards the olfactory bulb through a tube formed by astrocytes (Lois et al., 1996). Once reaching the core of bulb olfactory, immature neurons migrate radially towards glomeruli where they differentiate into different subtypes of interneurons (Ming and Song, 2011) (Figure 12).

Post-stroke studies suggest that neuroblasts from SVZ are recruited to damaged area. The molecular mechanisms involved in guiding the new neurons to the damaged zone are only partly understood (Lindvall and Kokaia, 2015).

Radial glia is distributed in both SVZ and striatum after stroke and probably guides migrating neuroblasts (Zhang et al., 2007). Blood vessels are also involved in this process, neuroblasts were located in large number in physical proximity to endothelial cells in the peri-infarct cortex in the presence of vascular remodeling (angiogenesis) (Thored et al., 2007). Vascular cells play a role in migration and survival of neuroblasts.

The better-established mechanism of regulation of neuroblasts migration is the chemokine stromal derived factor-1 (SDF-1) and its receptor CXCR4. SDF-1/CXCR4 signaling regulates the direct migration of new striatal neurons towards lesion (Robin et al., 2006). Post-stroke SDF-1 is expressed by reactive astrocytes, activated microglia and endothelial cells. CXCR4 is expressed on neural progenitors and neuroblasts (Robin et al., 2006).

Differentiation and integration: Proliferating neuroblasts that migrate into damaged area following stroke are able to differentiate into a variety of functional mature neuronal cells. The functional integration of newly generated neurons was evidenced by the presence of abundant pre-synaptic vesicles and by the presence of new synapses with neighboring cells (Yamashita et al., 2006). Similarly, neurons BrdU⁺/NeuN⁺ were detected in the ipsilateral striatum 12 weeks after MCAo (Sun et al., 2012). Additionally, precursor subtypes display significant plasticity in their lineage choice, neuroblasts DCX⁺ were converted to an oligodendrocyte fate upon demyelination of corpus callosum (Jablonska et al., 2010).

1.2.2.3 Brain plasticity

Some degree of functional improvement after stroke is experienced by humans and observed in experimental models of stroke (Kwakkel and Kollen, 2013; Seevinck et al., 2010). This is induced by an important aspect of brain recovery, the brain plasticity.

Brain connectivity studies of motor networks using resting state MRI in humans demonstrated that brain plasticity after stroke involves the connection of survival cells with neural network including brain regions adjacent to the lesion and/ or to contralateral hemisphere (Thiel and Vahdat, 2015).

After stroke, cortical remapping is both activity-dependent and based on competition (Murphy and Corbett, 2009). For this reason, therapeutic approaches such as rehabilitation (in patients) (Koganemaru et al., 2015) or motor training (in rats) (Mestriner et al., 2011) improve brain plasticity and results in functional recovery.

Brain plasticity refers to the ability of brain to adapt to the new condition and create new engrams. Naturally, the plasticity benefits from brain remodeling through new vessels formation, growth factors release and newborn cells induction. This process includes the formation of new synapses and sprouting of axons.

Cortical modifications were detected in peri-infarct area including an increase in neurofilaments and axonal outgrowth (Ueno et al., 2012). These modifications were associated to Akt activation-dependent. This result was confirmed *in vitro* when cortical neurons were submitted to oxygen glucose deprivation an increase in axonal outgrowth and in the levels of phosphorylated neurofilaments proteins was detected via Akt activation. When inhibited pharmacologically by an Akt antagonist the effects were suppressed. (Ueno et al., 2012).

To have a substantial impact on the recovery after stroke, the mechanisms of self-repair including neurogenesis, angiogenesis, and cortical remapping need to be enhanced, for example, by increasing the survival and differentiation of the generated neuroblasts and by improving the functionality of the new vessels. Alternative therapies to improve endogenous brain recovery and to restore the lost function for patients have been developed.

1.2.3 Stroke treatments

Ischemic stroke presents a complex and dynamic cascade of mechanisms implicated in its physiopathology. These mechanisms are time-dependent and therapeutic strategies focusing on selective mechanism depends on of their respective therapeutic windows (Figure 13).

Additionally to reperfusion therapies, (currently the only treatment approved in clinical application), some clinical approaches are recommended by American heart association and American Stroke association (AHA/ASA) guidelines, which includes: aspirin within 48h, decompressive craniotomy for large strokes, and management in stroke care units for intensive care and rehabilitation (Jauch et al., 2013).

Many strategies of treatment were developed focusing on isolated mechanism and have failed in translating for clinical settings (Dirnagl and Endres 2014). Here we will discuss briefly some therapeutic strategies tested in ischemic stroke.

1.2.3.1 Restoring Circulation

Currently in clinical settings, the only approved pharmacological therapy at acute phase is the reperfusion by administration of recombinant tissue plasminogen activator (tPA). This treatment focuses on restoration of blood flow to penumbra tissue. Intravenous administration of tPA improves stroke outcome when the treatment is administrated in the first 4.5h after stroke onset (Hacke et al., 2008) with a possible extension to 6h such as demonstrated in a recent clinical trial (Wang et al., 2015).

Endovascular interventions of mechanical or chemical clot removal are also currently employed in clinics and have shown benefit within the acute therapeutic window (Berkhemer et al., 2015) Given the variety of strokes and patients differences in brain vasculature, selecting the correct patients may be critical for the success of these therapies (Liebeskind et al., 2014).

A rapid and efficient brain imaging to detect lesion extension and gravity is relevant for clinical decisions (Albers et al., 2006; Davis and Donnan, 2014). Unfortunately, a vast majority of stroke patients are not able to receive the acute treatments because of the short therapeutic window (George and Steinberg, 2015), for this reason, therapies targeting later time windows are also needed.

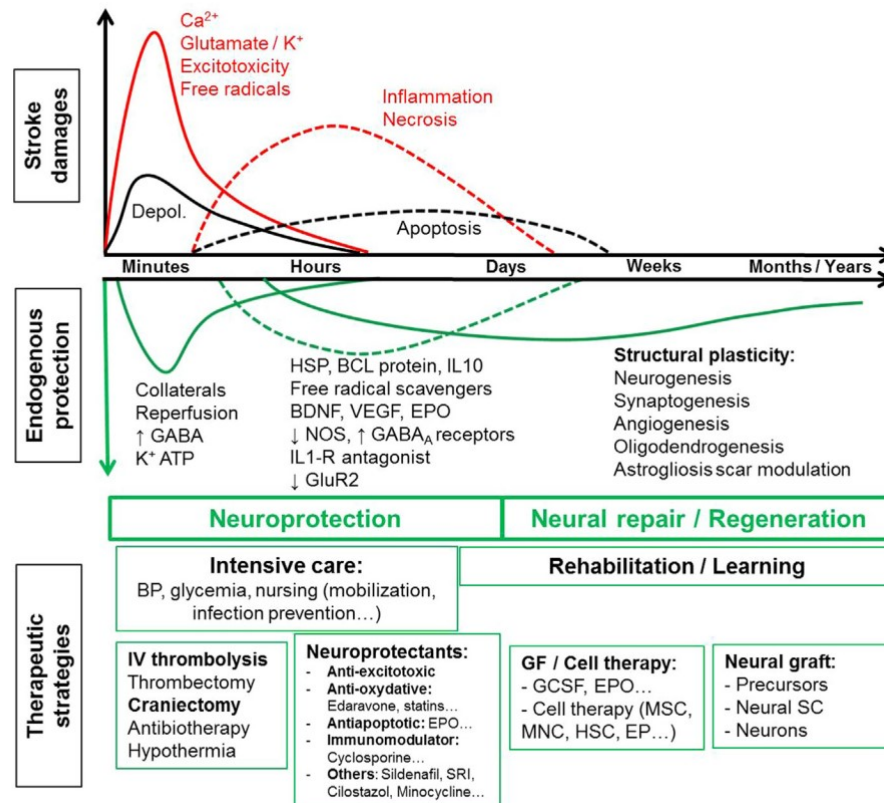


Figure 13 Time course of stroke and associated therapeutic time windows from Detante et al. (Detante et al., 2014). BCL:B-cell lymphoma protein; BDNF: brain-derived neurotrophic factor; BP: blood pressure; Depol.: peri-infarct depolarization; EP:endothelial progenitors (CD34+); EPO: erythropoietin; GCSF: granulocyte-colony stimulating factor; GF: growth factors; GluR2: glutamate receptor (subunit 2); HSC: Hematopoietic stem cells (CD34+); HSP: heat-shock protein; IL: interleukin; IP3: inositol tri-phosphate; IV: intravenous; MNC:mononuclear cells; MSC:Mesenchymal stromal/stem cells; NOS: NO synthase; SRI: serotonin reuptake inhibitors; VEGF: vascular endothelial growth factor.

1.2.3.2 Neuroprotection

In the acute and sub-acute phase of stroke, many strategies of neuroprotection have been studied, these therapeutic approaches focus on the mechanism implicated in the ischemic lesion.

- Mild brain hypothermia (33°C) is the gold standard for acute neuroprotection in rodent stroke models (Zhao et al., 2007), and provides good results in clinics by improving neurological outcomes in patients with global cerebral ischemia (secondary to cardiac arrest) (Bernard et al., 2002). Hypothermia induces a reduction in mitochondrial dysfunction (Gong et al., 2012) and attenuates oxidative stress and apoptosis. Therapeutic hypothermia has demonstrated beneficial effects by

limiting glutamate toxicity (Li et al., 2014), modulating neuroinflammatory response (Matsui et al., 2012) and by its hemodynamic effect (reduction of blood flow pace) demonstrated in a model of traumatic brain injury reducing brain edema (Li et al., 2014).

- Inflammatory mechanisms are also considered as an important target for stroke therapy. Numerous cellular and molecular mechanisms are activated after ischemic stroke participating in inflammatory response. Several pre-clinical and clinical studies have investigated the effects of immunomodulation on neuroprotection (Veltkamp and Gill, 2016). Minocycline, an anti-inflammatory drug has protective effects in animal models of stroke through a variety of mechanisms, including anti-inflammatory effects, reduction of microglial activation and inhibition of apoptosis (Lampf et al., 2007). Many immunomodulatory drugs have been tested in stroke therapy, but their action is also limited to acute and sub-acute phase.

-Another neuroprotective drug that demonstrated beneficial effects is fluoxetine. This drug is a known anti-depressive drug, acting as a selective serotonin reuptake inhibitor (SSRI). Fluoxetine has been found to stimulate the cAMP-responsive element binding protein (CREB), to increase the production of brain-derived neurotrophic factor (BDNF) and, neurotrophic peptide S100 β , and to enhance glycogenolysis in astrocytes. These mechanisms suggest that fluoxetine may also have a potential for the treatment of a number of neurological disorders (Mostert et al., 2008). In a recent pre-clinical study, fluoxetine increased neurogenesis but does not improve functional outcome (Sun et al., 2015).

1.2.3.3 Cell-based therapy

Another promising alternative in stroke treatment is the cell-based therapy. Stem cells are multipotent or pluripotent cells with the capacity for self-renewal and differentiation.

A distinct advantage of cell-based therapy is their unique ability to respond dynamically to complex and highly variable environments such as this found in post-stroke (Sullivan et al., 2015).

Transplanted cells are an example of plastic biological products because they can adapt to different local conditions in the damaged brain while not being limited to a unique target (Detante et al., 2014).

The efficacy of cell-based therapies is no longer based on a tissue replacement paradigm. Stem cells

can act on a wide range of neuroprotective and brain repair process including immunomodulation, neuronal, glial and vascular remodeling (Detante et al., 2014).

Endogenous stem cell induction

Endogenous therapeutic strategies focus on increasing proliferation, migration, and survival of neuroblasts and of endothelial progenitor cells (EPCs) (Arvidsson et al., 2002; Griese et al., 2003; Yamashita et al., 2006).

Such as discussed above, NPCs are produced along adult life in specific neurogenic niches and in other brain regions in the presence of ischemic stroke (Lindvall and Kokaia, 2015; Parent et al., 2002). Endothelial progenitor cells (EPCs) are also available in adult brain from peripheral circulation and participate in vascular remodeling in the presence of angiogenic stimuli such as ischemia (Griese et al., 2003).

These endogenous mechanisms are not enough to improve significantly the disabilities induced by stroke. Some strategies have been tested to improve post-stroke endogenous neurogenesis including the use of extrinsic growth factors and specific molecules such as statins (Chen et al., 2003; Cho et al., 2015), erythropoietin (Gonzalez et al., 2013) and fluoxetine (Sun et al., 2015).

These therapeutic strategies effectively improved neurogenesis and angiogenesis but not necessarily improved behavioral outcome (Sun et al., 2015).

Exogenous stem cells administration

Exogenous stem cells treatment refers to their delivery to the brain via blood stream or direct transplantation. Many types of stem cells have been evaluated for their therapeutic potentials in the treatment of ischemic stroke including embryonic (ESCs), neural (NSCs), induced pluripotent cells (iPS) and mesenchymal stem cells (MSCs) (Honmou et al., 2012; Lam et al., 2014; Tae-Hoon and Yoon-Seok, 2012).

Stem Cells can be obtained from a variety of cell sources including embryonic or fetal, adult or *in-vitro* cell culture.

Embryonic stem cells have unlimited self-renewal capacity and are pluripotent cells. These cells are derived from the inner mass of blastocyst-stage embryos (Thomson et al., 1998) and have the potential to differentiate in any cell type of the organism. Their potential to differentiate in neuronal cells was demonstrated *in vitro* using mouse ESCs (Bain et al., 1995). ESCs beneficial effects were detected *in vivo* after MCAo in rats with effective improvements in infarct size and behavioral recovery (Tae-Hoon and Yoon-Seok, 2012). However, ethical controversy severely limits the clinical application of ESCs (Tang et al., 2015).

The discovery of induced pluripotent stem cells (iPS) broke a paradigm in cell differentiation and won a Nobel price (Takahashi and Yamanaka, 2006). The ability to transform *in vitro* fibroblast into pluripotent stem cells using cell reprogramming by introducing four factors (Oct3/4, Sox2, c-Myc, and Klf4) passed many of the concerns of ESCs therapy like ethical questions (George and Steinberg, 2015). iPS cells from adult human fibroblast can migrate to lesion site and improve brain lesion and sensory-motor function (Jiang et al., 2011). One concern with iPS is the cellular immunogenicity, teratoma formation is reported after iPS administration (Yamashita et al., 2011; Zhao et al., 2011).

Exogenous NSCs can be obtained from ESCs, iPS cells, bone-marrow and adipose-derived MSC, fetal and adult nervous system (Garzón-Muvdi and Quiñones-Hinojosa, 2010). These cells could proliferate *in vitro* when stimulated by various growth factors and differentiate into neurons, astrocytes, oligodendrocytes (Chu et al., 2004; Hao et al., 2014; Jablonska et al., 2010). Despite these encouraging results, cell replacement therapies using NSCs or NPSCs are also affected by cellular loss, or poor differentiation and require immunosuppressant treatments.

Adult stem cells have been studied for their paracrine and trophic support in post-stroke research (Seo and Cho, 2012). Adult stem cells can be obtained from a variety of tissues such as bone marrow (Wexler et al., 2003), adipose tissue (Zuk, 2002), peripheral blood (Koerner et al., 2006), dental pulp (Pierdomenico et al., 2005) and others (Liu et al., 2016). Stromal/stem cells isolated from adipose tissue, bone marrow, umbilical cord are widely investigated in experimental studies and cell therapy trials (Detante et al., 2014). MSCs are the cellular type used in the present work and for this reason, the current state of MSC therapy in pre-clinical and clinical setting is discussed in a separate chapter.

The development of efficient therapies is crucial for improving stroke recovery. Strategies with an ample spectrum of brain protection and repair such as cell-based therapy could be a good candidate for this mission.

Many questions remain in stem cells therapy such as the best administration route, dose, therapeutic window, poor migration to lesion site and cell survival. In the present work, we test an alternative to optimize at least one of these issues (poor cell survival) with the aim to improve functional outcomes.

1.3 MESENCHYMAL STEM CELLS THERAPY

Mesenchymal Stem Cells (MSCs) are multipotent non-hematopoietic progenitor cells, with the capacity to differentiate into several distinct mesenchymal lineages (Caplan, 2009). MSCs have been demonstrated to differentiate into bone tissue, cartilage, adipocytes (Je et al., 1991; Qian et al., 2010; Solchaga et al., 2011). Additionally, controversial data suggest that MSCs may give rise to myogenic cells including cardiomyocytes, endothelial cells and even neural cells of non-mesodermal origin (Cao et al., 2005; Makino et al., 1999; Takeda and Xu, 2015). MSCs can be easily obtained from a variety of tissues including bone marrow where these cells were initially identified, muscle, adipose tissue, human amniotic fluid, placenta, umbilical cord blood, and veins as well as in several fetal tissues (Malgieri et al., 2010).

The International Society for Cellular Therapy Committee proposes minimal criteria to define MSCs :1) MSCs must be plastic-adherent when maintained in standard culture conditions; 2) MSCs must express CD105, CD73 and CD90 and lack expression of CD45, CD34, CD14 or CD11b, CD79a or CD19 and HLA-DR surface molecules; 3) MSCs must differentiate to osteoblasts, adipocytes and chondroblasts *in vitro*.

1.3.1 MSCs mechanisms

MSCs have emerged as an excellent candidate in cell-based therapies for a variety of diseases because of their easy access, good bio-preservation, and, in human trials, they have shown no adverse

reactions to allogenic versus autologous MSC transplants (Díez-Tejedor et al., 2014; Malgieri et al., 2010; Taguchi et al., 2015).

Despite their potential for differentiation, the controversial replacement theory does not explain the beneficial effects of MSC therapy. The mechanism related to MSCs induced-repair include paracrine/juxtacrine effects of growth factors and cytokines produced by the cells, extracellular matrix reorganization and immunosuppressive effects (Di Nicola, 2002) (Figure 14).

Experimental clinical and pre-clinical studies started to elucidate the utility of MSCs based therapy to prevent or repair brain injuries such as stroke. I will discuss briefly the main therapeutic mechanisms associated to MSCs.

1.3.2 Protective mechanism

When administrated systemically (by intravenous or intra-arterial way) or locally (intracerebral), MSCs migrate to the lesion site, influenced by inflammatory local mediators (Merino et al., 2011). The interaction between stromal cell-derived factor-1 α (SDF-1 α) and its cognate receptor CXC chemokine receptor 4 (CXCR4) is crucial for homing and migration of multiple stem cell types (Merino et al., 2011).

In an *in vitro* study, MSCs demonstrated immunomodulatory properties through inhibition of cytotoxic T-lymphocytes (Le Blanc, 2003). This effect was tested in the treatment of an experimental encephalomyelitis model (Zappia et al., 2005). MSCs administrated 1 day after induction of a global ischemia improved neurologic function and prevented cell death on hippocampus through modulation of inflammatory and immune responses (Ohtaki et al., 2008).

Similarly in a recent study MSCs therapy was able to reduce levels of caspase 3 (pro-apoptotic), increase B-cell lymphoma 2 (BCL-2) levels resulting in a reduction of apoptosis and increase of functional recovery (Feng et al., 2016). These neuroprotective and immunomodulatory effects were observed when MSCs were transplanted in the acute phase, around 24 hours after the injury.

Another mechanism associated to MSCs therapy is protection against brain degeneration. MSCs promoted increase in functional outcomes following brain ischemia via the inhibition of three

inhibitors of myelin regeneration: Nogo-A, oligodendrocyte myelin glycoprotein (OMgp) and myelin-associated glycoprotein (MAG) (Feng et al., 2016)

1.3.3 Brain remodeling

Transplanted MSCs improve host repair and tissue remodeling primarily through trophic factors support in response to injury cues, including angiogenic, synaptogenic and neurogenic factors (Castillo-Melendez et al., 2013; Seo and Cho, 2012). This response seems to be mediated by direct and indirect actions (Castillo-Melendez et al., 2013). MSCs secrete soluble (cytokines growth factors) and insoluble (extracellular matrix proteins) factors through paracrine signalization (Castillo-Melendez et al., 2013).

A principal aspect of post-stroke regeneration is the angiogenesis and vascular remodeling. Moisan et al. demonstrated an increase in angiogenic factors Ang1 and TGF β 1 at day 16 induced by MSCs enhancing the stabilization of newborn vessels and resulting in functional improvement (Moisan et al., 2016).

In another recent study, MSCs therapy was associated to rehabilitation (treadmill training) post permanent MCAo resulting in a reduction of lesion volume, synaptogenesis and functional improvement (Sasaki et al., 2016).

Astrocytes play a variety of crucial functions in healthy brain (Sofroniew and Vinters, 2009). Astrocytic response to brain injury and cerebral remodeling are also important. MSCs mediated protection of astrocytes against oxygen-glucose deprivation *in vitro* reducing apoptosis, increasing metabolic activity and reducing glial fibrillary acid (GFAP) overexpression (Huang et al., 2015). These results were mediated by paracrine factors secreted by MSCs (reducing p38 MAPK and JNK signaling) (Huang et al., 2015).

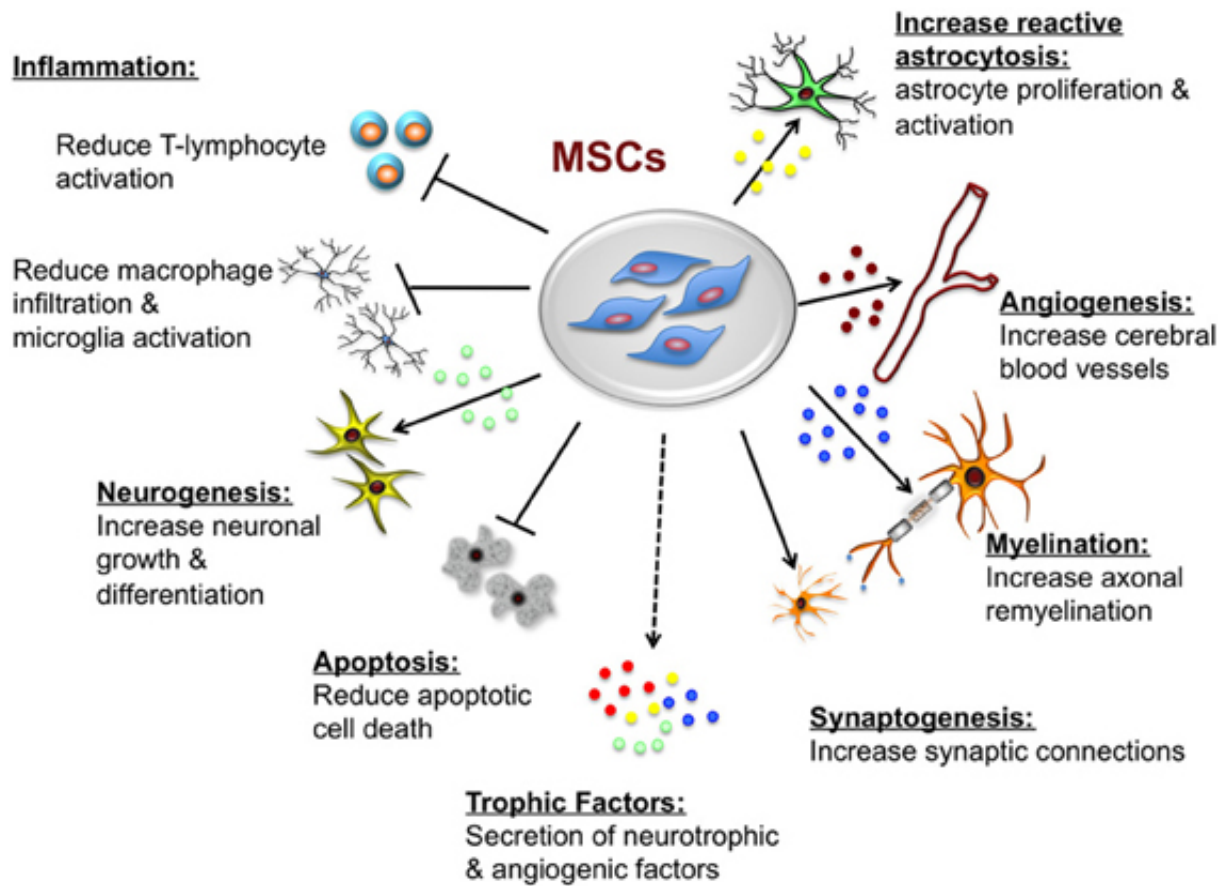


Figure 14: Mesenchymal Stem Cells (MSC) therapeutics mechanism, from Castillo-Melendez et al., 2013 (Castillo-Melendez et al., 2013)

In an *in vivo* study, MSCs induced stabilization of BBB through regulation of astrocytes filaments around the vessels reverting the elevation of VEGF and eNOS (Park et al., 2015). The reduction of this factors related with vessel permeability induced by MSCs treatment reduced neutrophil infiltration and enhanced survival of dopaminergic neurons (Park et al., 2015).

Other studies demonstrated the role of MSCs in the release of neurogenic growth factors including BDNF, VEGF, GDNF, nerve growth factor (NGF), IGF-1, SDF-1 and others factors stimulating endogenous neurogenesis (Drago et al., 2013; Salgado et al., 2015).

Nevertheless, an interesting role was recently described in a trauma brain injury model in rats, (Tajiri et al., 2013), MSCs seem to play an integral role in recruiting cells from the neurogenic niches to injured area within the cortex (Duncan et al., 2015). This conduit for endogenous cells is a “biobridge” located between the cortex lesioned and the SVZ neurogenic niche and was visualized using

immunohistochemistry and laser capture assay. This guided migration is facilitated by the ability of MSCs to alter the expression of MMPs (Sullivan et al., 2015) (Figure 15)

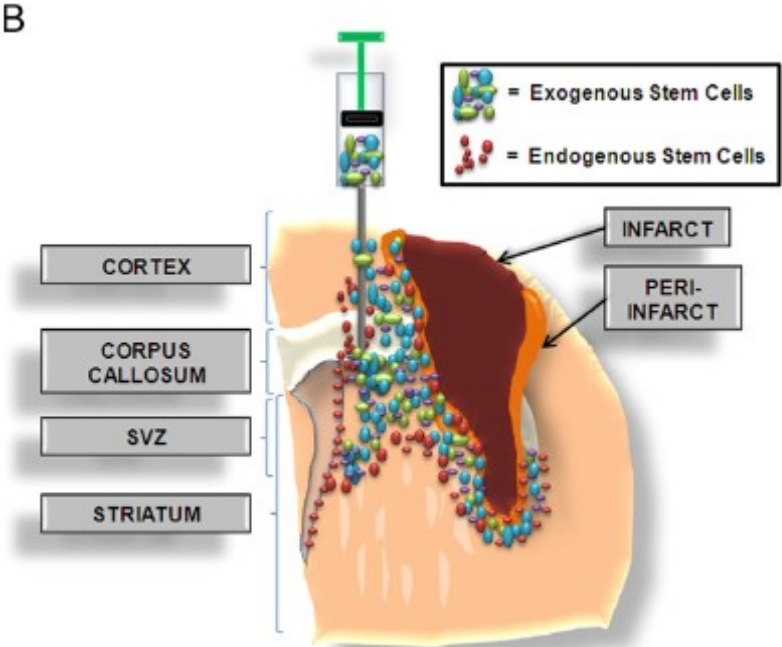


Figure 15: Illustration of the “Biobridge” from Duncan et al. 2015 (Duncan et al., 2015). Endogenous stem cells (SC) from the subventricular zone (SVZ) guiding exogenous SC migration to peri-infarct zone.

1.3.4 Current status of clinical research

Until 2014, seventeen clinical trials have been published such as reviewed by Detante et al (Detante et al., 2014). Recently four additional studies were published reporting their clinical results (Banerjee et al., 2014; Diez-Tejedor et al., 2014; Steinberg et al., 2016; Taguchi et al., 2015).

The cell source most commonly used in these studies was bone marrow from autologous or allogenic donor. Bone marrow mononuclear cells (BMMNCs) were the cellular type the most used, followed by MSCs (Detante et al., 2014). Phase I/II clinical studies provide results about feasibility and safety in humans with no teratoma formation (Bhasin et al., 2013), but with some adverse events related and modest functional outcomes, maybe by the difficulty to estimate the effects due to the number of patients studied.

For example, Taguchi et al. demonstrated positive results concerning functional recovery evaluated by National Institute of Healthy Stroke Scale (NIHSS) in a phase 1/2 study (n=12 stroke patients), using IV injection of autologous (BMMNC) (Taguchi et al., 2015). However, one patient presented a recurrent stroke one day after transplantation (Taguchi et al., 2015).

In another study, bone marrow derived MSCs genetically modified to express Notch-1 (SB623 cells) were intracerebrally administrated in chronic stroke patients (n=18) (Steinberg et al., 2016). In this study patients also experienced functional improvement evaluated by multiple functional scales (Steinberg et al., 2016). Adverse events related to surgery were reported.

Currently, over 40 studies with known status are recorded at clinicaltrials.gov website involving “stroke” and “Stem cell” therapy in adults. Among these studies, twenty studies are with status active, most then recruiting patients, see Table 1: Active clinical trials.

New strategies to optimize stem cell therapy such as modified cells or a biomaterial co-administrated with the stem cells have been evaluated in pre clinical studies (Kim et al., 2015; Liang et al., 2013).

The ultimate goal in pre-clinical research is to produce knowledge and tools to progress in clinics.

A Chinese study, opening in April 29, 2016 (ClinicalTrials.gov Identifier: NCT02767817) using an injectable collagen scaffold combined with MSCs is currently recruiting patients with traumatic brain

injury. The use of biomaterials in brain tissue is still recent and in developing field and more pre-clinical studies are needed.

Table 1: Active clinical trials.

Clinical trial ID	Study type	Cell type	Nbr	Timing of delivery	Route	Status	Country/Principal Investigator/ Sponsor
NCT01832428	Ph1/2-NR-OL	BMACS	50	chronic	IT	recruiting	India/ Sachin Jamadar
NCT02290483	Ph1-NR-OL	BMMNC	76	1-7days	IA	recruiting	Spain/Francisco Moniche
NCT02117635	Ph2-R-OL	CTX0E03 NSC	21	2-3 months	IC	recruiting	UK/ReNeuron Limited
NCT01151124	Ph1-NR-OL	CTX0E03 NSC	12	6-60 months	IC	active, not recruiting	UK/ReNeuron Limited
NCT00875654	Ph2-R-OL	MSC	30	<6 weeks	IV	active, concluded	Grenoble/Olivier Detante
NCT01297413	Ph1/2-NR-OL	MSC	35	>6 months	IV	active, not recruiting	USA/ Lev Verkh (Stemmedica Cell Technologies, Inc)
NCT01678534	Ph1/2-R-DB	MSC	40	<14 days	IV	active, not recruiting	Spain/Exuperio Diez-Tejedor
NCT01922908	Ph1/2-R-DB	MSC	48	3-10 days	IV	active, not yet recruiting	USA/Sean Savitz
NCT01468064	Ph1/2-R-DB	MSC and EPCS	20	>7 days	IV	recruiting	China/Zhenzhou Chen
NCT01287936	Ph1/2-NR-OL	SB623	18	6-36 months	IC	active, Preliminary data	USA/ Gary K Steinberg (Steinberg et al., 2016)
NCT02397018	Ph1	UCBCs	10	<9 days	IV	active, not recruiting	USA/Joanne Kurtzberg
NCT01461720	Ph2	MSC	50	2weeks-2 months	IV	recruiting	Malaysia/ Norlinah Mohamed Ibrahim
NCT02564328	Ph1/R/SB	BM MSC	40	6-60 months	IV	recruiting	China/Xiaodan Jiang
NCT02605707	Ph1/2-R-SB	EPCs	30	6-60 months	IV	recruiting	China/ Zhen-Zhou Chen
NCT02849613	Ph2/3	ADSC	400	1-4 days	IV	recruiting	European/ Detante, Diez-Tejedor,(Grenoble hospital)
NCT01714167	Ph1/NR/OL	BMMSC	30	3-60 months	IC	recruiting	China/ Qichuan Zhuge
NCT02813512	Ph1/NR/OL	ADSC	3	>6 months	IC	active, not yet recruiting	Taiwan/ China B Hospital
NCT02378974	Ph1/2-R-DB	CDMSC	18	<7days	IV	recruiting	Republic of Korea/CHABiotech CO
NCT02448641	Ph2/DB	SB623	156	6-60 months	IC	recruiting	USA/ Gary Steinberg (SanBBio Inc)
NCT02580019	Ph2/R/OL	MSC	2	3months	IV	recruiting	China/ Duan Lian

Clinical trials identifiant (ID); phase (Ph)1/2; non randomized (NR); randomized (R); Double Blind (DB); Single Blind (SB);open label (OL); bone marrow (BM), adipose cells (ADCs); mesenchymal stem cell (MSC), neurural SC (NSC) endothelial progenitor cells (EPCs), umbilical cord blood cells (UCBCs), Modified Stromal Cells (SB623).

2 PROBLEMS

Stroke affects approximately 6 million people in the European Union, with 1.1 million new cases every year. The total cost of stroke was about €64.1 billion in 2010 because of long-term special care and rehabilitation (Gustavsson et al., 2011).

Current treatment options are limited to intravenous (IV) thrombolysis by Alteplase within 4.5h-6h, thrombectomy, aspirin within 48h, decompressive craniectomy for large strokes, and management in stroke care units for intensive care and rehabilitation (Sarraj and Grotta, 2014).

A rapid diagnostic is crucial to save brain tissue. The role of brain imaging techniques has expanded substantially to identify candidates for endovascular therapy. Recent advances in brain imaging offer new tools to characterize the ischemic lesion. These new techniques may improve the detection of salvageable zones and increase the number of patients who could benefit from acute therapy.

Beyond the first hours (acute phase) of stroke, effective therapies are urgently needed. Cell-based restorative therapies have emerged as an attractive candidate for the treatment of stroke (Gutiérrez-Fernández et al., 2013; Sinden and Muir, 2012). The mechanisms induced by stem cells therapy involve activation of brain repair and enhancement of spontaneous functional recovery. Despite the promising results in post-stroke brain regeneration, in experimental studies (Feng et al., 2016; Gutiérrez-Fernández et al., 2013), some limitations remain challenging for translational research. A low rate of cell survival when these cells are administrated within lesion cavity (intracerebral administration) and poor migration to lesion site (systemic administration) are reported (Detante et al., 2009; Lappalainen et al., 2008). Therapeutic strategies, such as bioengineered scaffolds (Hydrogel) have been developed to improve the efficacy of stem cell therapy. Hydrogels can mimic physiological environment, protect stem cells and improve cell viability (Aguado et al., 2012). Pre-clinical studies using biomaterials associated to stem cells in a complete organism to investigate their fate and effects are still necessary.

3 OBJECTIVES

Regarding the unsolved problems presented concerning cell-based therapy and the necessity of consistent results in pre-clinic research to translate these to clinics, in the present study a therapeutic strategy to improve cell-based therapy post a model of ischemic stroke induced by middle cerebral artery occlusion (MCAo) in rats was investigated.

The main objective of the present thesis was: **to test a biomaterial Hyaluronic acid (HA) based hydrogel with the aim to improve outcomes of cell therapy in ischemic stroke.** On this context, a commercial hydrogel HyStemTM-HP (Sigma) was used co-administrated with clinical grade human MSC from bone marrow.

Clearly, the application of non-invasive techniques such as Magnetic Resonance Imaging (MRI) allows an *in vivo* monitoring of cell therapy effects. The use of *in vivo* evaluations would significantly improve the predictive value of preclinical models. In this context, we performed MRI evaluations in the different experiments:

1. The first study of the present thesis consists in an acute phase evaluation of ischemic stroke using multiparametric MRI. The general aim was **to assess the mapping of brain oxygenation with MRI in acute experimental stroke to detect the ischemic core and to assess its potential to predict the final necrosis.** Accessorily we used a multiparametric MRI study to evaluate the hemodynamics, vascular, and diffusion alterations during the first 2 hours of MCAo.
2. In the second study, we assessed the *in vivo* biocompatibility of the HA hydrogel. The goal of this pilot study was: **to evaluate the host immune response and the fate of HyStemTM-HP hydrogel in healthy brain.** Accessorily we evaluated the hydrogel detection by MRI diffusion *in vivo* to evaluate degradation rate of hydrogel. Preliminary studies using similar HA-based hydrogel have evaluated the effects of hydrogel in cell culture and post stroke (Liang et al., 2013; Zhong et al., 2010), but the host brain response to HyStemTM-HP hydrogel and *in vivo* evaluation of hydrogel biodegradation in healthy brain as far as we know was not yet demonstrated.

3. In the third and last study, the effects of the combination HA-hydrogel+MSC were evaluated. The general aim of this study was **to evaluate the effects of the combination hydrogel+hMSC on cell survival, brain remodeling and functional recovery after experimental stroke.**

4 GENERAL METHODOLOGY

The general methodology described here concerns the common techniques used in different experiments.

Specific aspects of each study will be described in the correspondent chapter.

All experimental procedures used in this thesis are in accordance with French and European laws.

All procedures and animal care were in accordance with French government guidelines and were performed under permit from the French Ministry of Agriculture. Each experimental protocol was approved by the “Grenoble – Institute of Neuroscience” local ethics committee for animal care and use (agreement number 004) and French Ministry of the Research.

In the reported studies a total of 205 rats, Sprague-Dawley (Charles River, France and Janvier, France) young adult male (7 weeks) were used.

4.1.1 General anesthesia and analgesia

All experimental procedures with a potential risk of pain or discomfort for the animals (stroke model by MCAo, IC or IV injections), or requiring immobility (MRI acquisition) were performed under general anesthesia. Anesthesia was induced by inhalation of a gas mixture of 5% isoflurane (IsoFlo, Abbot Laboratories Ltd, Berkshire, UK) in medical air in an induction box and was maintained through a facial mask between 1.0-2.5% of isoflurane in a mix of 30% of oxygen and 70% of air along the surgical procedures and MRI acquisition.

For surgical procedures, additionally to Isoflurane anesthesia, the rats received a local subcutaneous injection of 0.1 mL Lurocaine (Vétoquinol, Magny-Vernois, France) as local anesthesia. Additionally, in the first three days after MCAo, rats received 250 mg/kg of Paracetamol (Sanofi-Aventis®, France) by oral route.

4.1.2 Model of transient ischemic stroke

Focal transient ischemic stroke was induced by occlusion of the middle cerebral artery (MCA) during 90 minutes with an intraluminal suture (Longa et al., 1989). The model of reversible regional cerebral ischemia in rats without craniotomy is commonly used in our team (Barbier et al., 2005; Detante et al., 2009, 2012; Moisan et al., 2014). This model described by Longa et al (Longa et al., 1989), consists in advancing an intraluminal suture from the internal carotid artery (ICA) to occlude the origin of the MCA (Longa et al., 1989) (Figure 16).

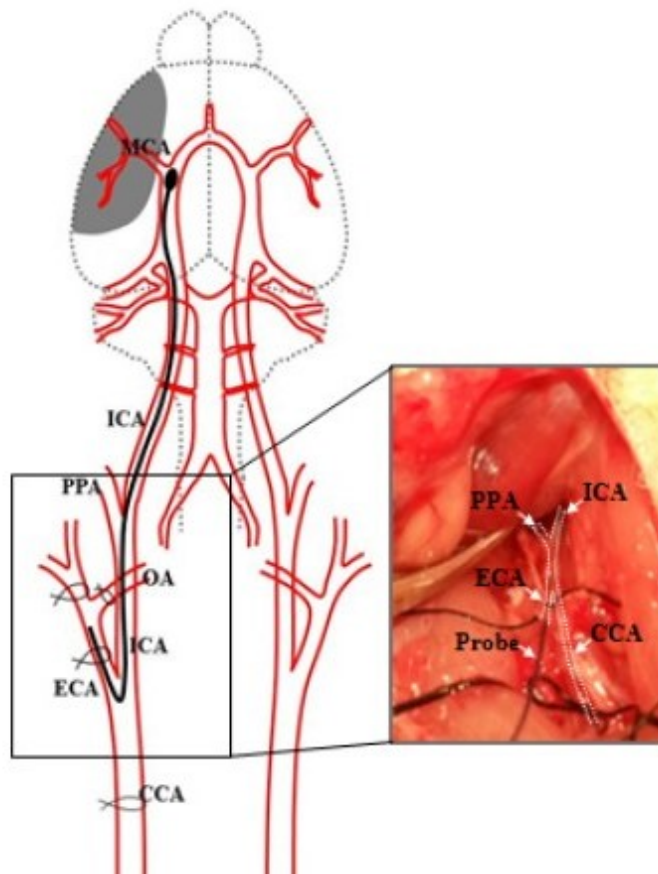


Figure 16: Schema of filament-induced MCAo from Lee et al., 2014 (Lee et al., 2014) Common carotid artery (CCA), external carotid artery (ECA), internal carotid artery (ICA), occipital artery (OA), pterygopalatine artery (PPA) and middle cerebral artery (MCA) occluded by the filament.

Under a surgical microscope, a middle line incision was performed in the ventral aspect of neck. A surgical retractor was positioned between sternohyoid and sternomastoid muscles, to expose the right carotid bifurcation. Occipital artery (OA) branch of external carotid artery (ECA) was then isolated and coagulated. Next, the superior thyroid and ascending pharyngeal arteries were dissected and coagulated. The ECA was dissected further distally and coagulated. The ICA was isolated and separated from the adjacent vagus nerve. A silk suture was tied loosely around the mobilized ECA stump. Microvascular clips were placed across the CCA and the ICA to avoid bleeding (Wang-Fischer et al., 2009). The monofilament (silicon rubber-coated monofilaments: 0.37mm or 0.39mm in diameter, Docol, Sharon, MA, USA) was introduced in the ECA and advanced from the ECA to the ICA lumen until 9 mm after skull base. The silk suture around the ECA stump was tightened around the intraluminal monofilament suture to prevent bleeding, and the microvascular clips were removed.

The incision was sutured and the filament was left in place for 90 minutes. After wake-up, rats were tested to certify neurological deficit. Afterward, rats were re-anesthetized and monofilament was retracted allowing a reperfusion (Wang-Fischer et al., 2009).

A silicon rubber-coated monofilament with a diameter of 0.37 mm (403723PK10-TL40) was used in rats weighing between 280-300g, and a 0.39 mm was used in the animals weighing 300-330g in accord with manufacturer recommendations. (Figure 17)

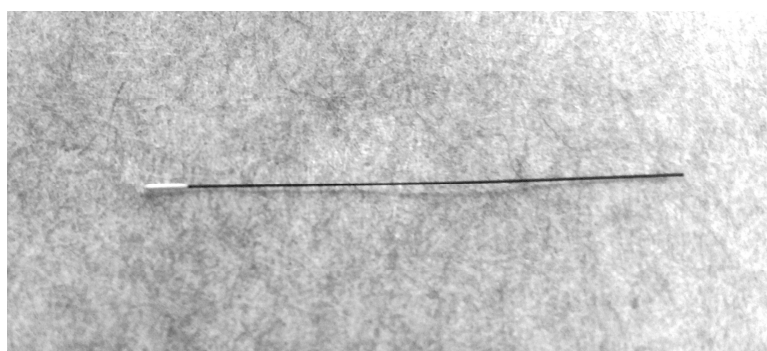


Figure 17: Monofilament in silicon rubber-coated.

Sham rats were submitted to the same procedures of anesthesia and surgery, without occlusion of MCA, presenting no deficits.

During the surgical procedures, body temperature was monitored and maintained around $36.5^{\circ}\text{C} \pm 0.5$ with help of an animal temperature control system that consists of a heating pad, a rectal thermometer probe, and a control box.

4.1.3 MRI Methods

MRI is widely applied for stroke diagnosis in clinical and experimental settings. MRI is a non-invasive method that allows an *in vivo* follow-up. In the present study, MRI was an important tool used to evaluate rat brain (ischemic lesion or hydrogel) in all experiments. All MRI data were acquired using a 4.7T magnet (Bruker Biospec®, Germany) (IRMaGe facility, Grenoble, France).

Physiological parameters were monitored during MRI acquisition, including body temperature that was maintained at 37°C with help of a warming system. Breath rate was maintained constant (45-60 breath per minute) by modulating of inhaled anesthesia.

For the experiences which have need of contrast agent administration, a catheter connected to an extension (200 μL of volume) containing physiological serum was inserted in tail vein for contrast agent administration during MRI acquisition.

After securing the animal in a cradle using tooth and ear bars to restrict head movement, a volume coil for excitation and a surface coil for detection were used. The slice orientation was identical for all MRI sequences. The MRI scans used and the time point in which the rats were evaluated for the different studies is described in each chapter.

4.1.3.1 MRI protocol

A variate number of MRI scans were used depending on of the study objective. A complete protocol experimental is presented below.

- A Tri-pilot scan for positioning verification spin-echo weighted in T_1 .
- A T_2 -weighted (T_2W) spin-echo scan repetition time (TR)/echo time (TE) = 7000/50 ms, 31 slices with a voxel size = $234 \times 234 \times 800 \mu\text{m}$.

This scan was used to obtain anatomic images of the lesion and to evaluate lesion size.

- Apparent diffusion coefficient (ADC) map was obtained from a diffusion-weighted, spin-echo, single-shot echo-planar imaging (EPI) (TR/TE = 2250/33 ms, 8 averages, 9 slices, voxel size = $234 \times 234 \times 800 \mu\text{m}$). This scan was applied 4 times, once without diffusion weighting and 3 times with diffusion weighting ($b = 800 \text{ s/mm}^2$) in three orthogonal directions.

Cerebral blood flow map was calculated using the follow sequences:

- A pseudo-continuous arterial spin labelling (pCASL) gradient echo flow compensated (GEFC) (TR= 225ms, 1 spin echoes, TE=5ms, 2 averages, labelling duration = 200 ms, post-labelling delay = 0 ms, one slice and voxel size=125 x 125 x 800 μm)
- Pseudo-continuous arterial spin labeling (pCASL) with an EPI readout (spin-echo EPI, TR/TE = 3600/21 ms, labeling duration = 3 s, post-labelling delay = 400 ms, 50 label/control pairs, 5 slices with voxel size = $234 \times 234 \times 800 \mu\text{m}$).
- A T_1 map was obtained using an inversion-recovery sequence (TR/TE = 8000/33 ms; 15 inversion times: 35–7000; five slices; voxel size = $234 \times 234 \times 800 \mu\text{m}$).

Brain tissue oxygen saturation (StO_2) map was calculated using the follow scans:

- A T_2 map was obtained using a multi-spin-echo sequence (26 echoes; TR/TE = 2000/12–312 ms; 5 slices; voxel size = $234 \times 234 \times 800 \mu\text{m}$).

- A high-resolution T_2^* map was obtained from a 3D multiple gradient echo sequence (15 echoes; TR/TE = 100/4–67 ms; 26 slices; voxel size = $117 \times 117 \times 200 \mu\text{m}$).
- A multiple gradient echo sequence (16 gradient echoes; TR/TE = 4000/3–56 ms, and one spin-echo TE = 60 ms; 5 slices, voxel size = $234 \times 234 \times 800 \mu\text{m}$) was performed before, and 1 min, after an IV injection of ultrasmall superparamagnetic iron oxide nanoparticles (USPIO) contrast agent (P904, 200 μmol of iron/kg, Guerbet S.A., Aulnay-Sous-Bois, France) flushed with 250 μL of saline.

These sequences were used also to calculate the maps ΔR_2^* to obtain the blood volume fraction (BVf) and vessel size index (VSI) map (Figure 18) (Troprès et al., 2001, 2004).

4.1.3.2 Contrast agent

MRI paramagnetic contrast agents allow a complementary assessment of vascular flow, tissue perfusion and BBB integrity (Dijkhuizen and Nicolay, 2003). Longitudinal (T_1) and transverse (T_2) relaxation times are reduced in the presence of contrast agents on the tissue surrounding these labeled cells, thereby generating localized hyperintense or hypointense areas on T_1 - or T_2 (*) weighted MRI images respectively (Deddens et al., 2012). The paramagnetic contrast agent used in two studies presented in this thesis was the P904 (Guerbet Laboratories, Paris, France). P904 is composed by Ultrasmall Superparamagnetic Iron Oxide (USPIO) particles. USPIO offers the advantages of not being immediately removed from the circulation by the reticulo endothelial system (RES), due to their small size ($< 20 \text{ nm}$) presenting a longer blood half-life and wider biodistribution. The blood half-life for 200 μM of Iron/Kg is of 4.5h in rats allowing a long MRI acquisition.

USPIOs generate a static magnetic field inhomogeneity around the vessels affecting spin echo and gradient echo transverse relaxation rates (R_2 and R_2^* , respectively) in a different way (Seevinck et al., 2010). Changes in the transverse relaxation rate R_2 (i.e. ΔR_2), as a result of the application of an intravascular susceptibility contrast agent, are predominantly sensitive to small vessels ($< 10 \mu\text{m}$), while

changes in the transverse relaxation rate R_2^* (i.e. ΔR_2^*) are sensitive to vessels of all sizes (Seevinck et al., 2010).

4.1.3.3 MRI data processing

ADC map was generated with Paravision 5.1 software (Bruker, Germany) computed as the mean of the ADCs measured in the 3 principal directions of the gradient system.

For all other maps, data were processed with software developed in our team using in Matlab 2013 (MathWorks, Natick, MA, USA). This software was used to generate maps and to create the regions of interest (ROI).

VSI and **BVf** maps were derived from the change of T_2 and T_2^* induced by injection of iron oxide particles as previously described (Troprès et al., 2001).

Vessel density (Density) was derived from the ratio of the changes in transverse relaxation rates, using the equations (13) to (15) described in Troprès et al (Troprès et al., 2015)

A quantitative **CBF** map was computed with the equations described in Alsop et al. using both the pCASL sequence and the T_1 map (Alsop et al., 2015).

A **StO₂** map was computed using the T_2 map, map and BVf map as previously described (Christen et al., 2011).

All MRI maps were generated with a spatial resolution of $(234 \times 234 \times 800 \mu\text{m})$. To avoid a long acquisition, all parametric maps had 5 slices which are placed in the center of the lesion. Except for ADC maps (9 slices).

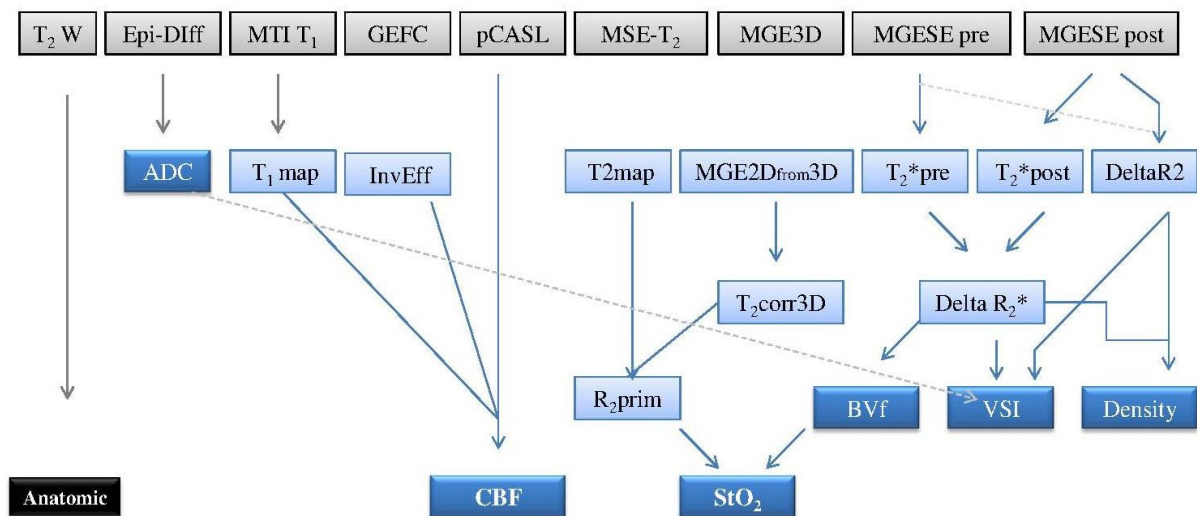


Figure 18: Illustration of MRI scan acquired (in gray), intermediate maps (in clear blue) and final maps in blue.

Anatomical and ADC maps were used in all studies of the present manuscript for ischemic lesion or hydrogel detection.

Different regions of interest (ROI) were created to evaluate rat brain *in vivo*; the ROIs are described in the corresponding study chapter.

Diffusion-weighted images use the diffusion of water molecules in the tissue to generate contrast in MR images (Shen et al., 2003). ADC map is a numerical measure of diffusion allows the quantification of diffusion of water molecules, detecting alteration such as cellular edema.

CBF and BVf imaging allows analyzing the hemodynamic alterations in the blood flow present in ischemic stroke.

Beyond measuring these two parameters, the capacity of MRI to characterize microvascular architecture, and thereby producing maps of microvessel density and microvessel caliber, using a contrast agent was demonstrated (Troprès et al., 2015)

A microvascular analysis was employed at acute phase of stroke to describe the alteration in using **VSI and Vessel density** (Density)

Additionally, StO₂ map, developed in our team was used in the study 1 to evaluate in a voxelwise basis, the brain tissue oxygen saturation. This multiparametric evaluation can be of great value in the evaluation of lesion gravity and post-stroke recovery.

4.1.4 Human Mesenchymal Stem cells preparation

Clinical grade hMSCs were provided by the clinical biology institute of Grenoble hospital (*Institut de Biologie et Pathologie – CHU Grenoble, and Cell Therapy and Engineering Unit, EFS St -Ismier*). Human MSCs were isolated from bone marrow aspirate from 4 healthy donors who gave consent, the same cells used in a clinical trial realized in our center (ISIS, NCT00875654). Culture procedures were conducted according to previously described methods by Moriscot et al (Moriscot et al., 2005).

hMSCs were selected from bone aspirate by plastic adhesion in accord with procedure adopted for the clinical study. Plastic-adherent cells were seeded within plastic flask at a density of 5×10^4 cells/cm². Fresh complete medium Minimum essential medium alpha (MEM α), supplemented with 100 μ g/mL penicillin, 100 μ g/mL streptomycin (Invitrogen), 2 mmol/L L-glutamine (Invitrogen, France), and 10% fetal calf serum (Invitrogen, France), incubated at 37°C in a humidified atmosphere containing 5% CO₂ (Moriscot et al., 2005).

The first phase of expansion (passage 0, P0) was pursued until obtained a colony forming efficiency superior to 80%, the medium was replaced twice a week. Upon reaching near confluence, cells were detached with a solution of 0.25% trypsin and 1 mmol/L EDTA (Invitrogen, France) for 2–3 minutes at 37°C and plated at 1,000 cells/cm² until obtaining a new confluence superior to 80%. The hMSCs used in our study were harvested after two or three passages.

The cells were delivered by clinical biology institute of Grenoble hospital in a cell culture flask in the administration day. The cells were harvested from plastic using trypsin, were the centrifuged and counted.

For the groups treated with cells, 10^5 hMSC were diluted in phosphate buffer saline (PBS) to obtain a volume total of $10\mu\text{L}$, or with the compounds of HyStemTM-HP hydrogel obtaining $10\mu\text{L}$ of an hMSC-Hydrogel solution.

4.1.5 Stereotaxic intracerebral administration

The administration route of hMSC and hydrogel administration was the intracerebral (IC) route.

The IC administration procedure was carried out such as described below:

After being anesthetized, scalp skin was shaved and scrubbed with alcohol and chlorhexidine surgical scrub. The animal was fixed in rat stereotaxic instrument in the skull flat position. Starting slightly behind the eyes, a midline sagittal incision about 1.5 cm long was made. Using the *bregma* as reference a hole was drilled in the skull above the right striatum to allow the penetration of a 26-gauge Hamilton syringe. Vehicle solution (PBS), hMSC and hydrogel were administrated in striatum, the follow stereotaxic coordinates were used: *bregma* 0; medial-lateral, ± 3.5 mm; dorsal-ventral, -5.5 mm (Paxinos and Watson, 1982). In specific cases, stereotaxic coordinates were adapted to lesion size and localization to specifically target cortical or striatal lesions observed by MRI. The IC administration was performed with help of infusion pump with a rate of $2\mu\text{L}/\text{min}$ and the needle was withdrawn 5 min after the end of administration.

4.1.6 Samples extraction (brain)

At the end of each experience, brain samples were collected for histological analysis.

For this, the animals were euthanized with a lethal dose of anesthetic pentobarbital (Doléthol – Vétoquinol, France). Brain samples were removed from skull, frozen at -40 °C and stored at -80 °C. Frozen brains were cut with a cryostat (thickness, $20\mu\text{m}$) at -20 °C. Coronal slices were generated per animal around the zone of lesion for ischemic rats, in the zone correspondent for Sham groups or around the injection site for hydrogel experiment.

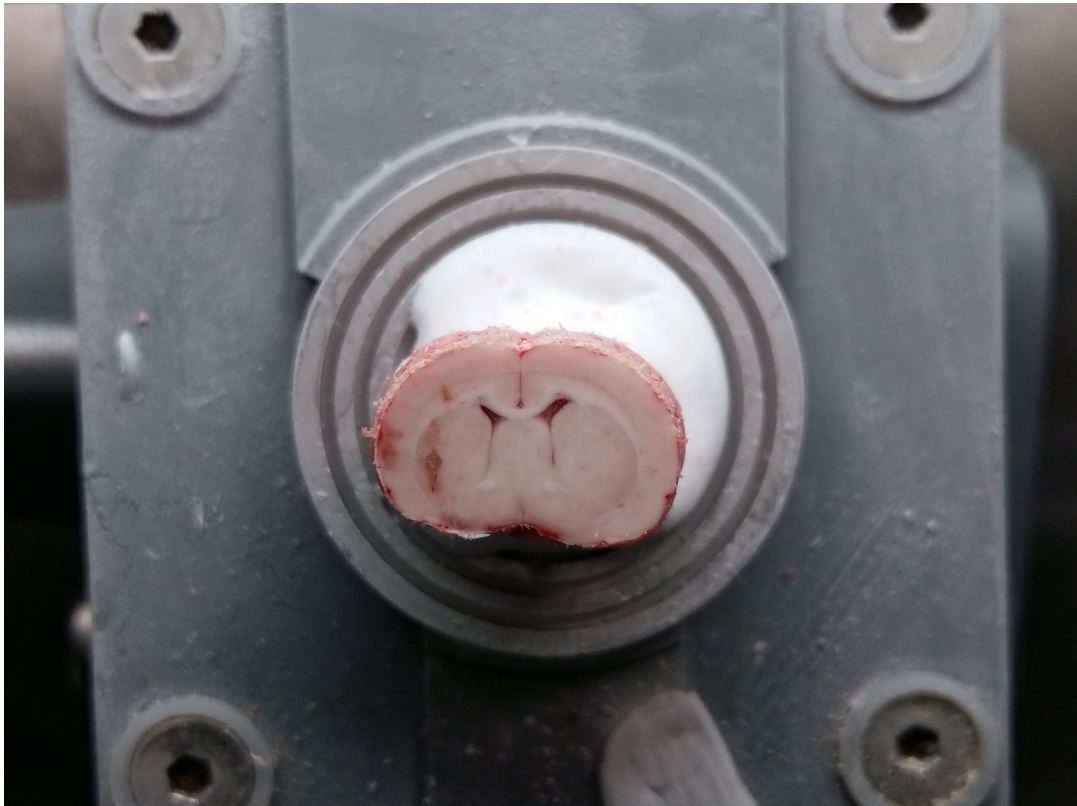


Figure 19: Illustrative image of a brain sample in cryostat.

4.1.7 Histological analysis

4.1.7.1 Hematoxylin- Erythrosine staining

Hematoxylin- Erythrosine staining is a classical histological technique which in brain studies allows the detection of different structures and to detect ischemic lesion.

Hematoxylin has a deep blue-purple color and stains nucleic acids by a complex, incompletely understood reaction. Eosin is pink and stains proteins nonspecifically. After place the microscope slides in a glass support, staining were realized by slide immersion in different baths: fixation in acetone (2 min),

hematoxylin stain (4 min), HCl 1% (30 s), 0.2% ammonia water (45 s), rinse the slide in distilled water, erythrosine stain (1 min), rinse the slide in distilled water, dehydrate through 95% alcohol (3 passage), toluene (3 passage). Samples were mounted with based mounting medium (Pertex, Histolab®, Gothenburg)

Microscope slices dried overnight and were digitized at a resolution of 2400 dot per inch using a photo scanner (Perfection 4870; Epson, Long Beach, CA).

4.1.7.2 Cresyl Violet

Another classic histological staining with cresyl violet acetate was used to detect hydrogel.

After place the microscope slides in a glass support, staining was realized by slide immersion in different baths. Sections of brain containing hydrogel implants were fixed in methanol/acetone, rinse in distilled water, stained with 0.1% cresyl violet (5min), (Waldeck GmbH, Munster, Germany), rinse in distilled water, dehydrated through a 50%,70%, 95%, and 100% alcohol series (1 passage for each), post-fixed in Xylene and finally mounted with a mounting medium (Pertex, Histolab®,Gothenburg).

4.1.7.3 Immunohistology

Immunofluorescence technique was used in the experiments 3 and 4 to detect and evaluate the response of host brain cells to ischemia, hydrogel administration, and hMSC or hMSC-hydrogel treatment.

For this, parallel series of sections from each animal were thawed at room temperature, fixed with ExcellPlus (American Mastertech, Lodi –USA), washed with PBS Tween 0.1% (Sigma-Aldrich, France), incubated in 3% of the bovine serum albumin and 0.2% PBS-Triton for 40 min prior to overnight incubation with primary antibodies (Table 2) at 4 °C. Sections were washed 3 times in PBS-Tween 0.1% (Sigma) followed by incubation with the appropriate secondary antibody (1:200, Alexa Fluor 488/546/568, Invitrogen) for 2 hours at room temperature. Omission of the primary antibody provided a

negative control to account for unspecific binding of the secondary antibody. Sections were rinsed 3 times in PBS-Tween 0.1% before application of Vectashield with DAPI (Vector Labs) and coverslips. Images were obtained using epifluorescence microscopy (Nikon Eclipse E600, Tokyo, Japan) and a CCD camera (Olympus, Rungis, France).

Table 2 : Primary antibodies

Antibody	Host	Manufacturer	Dilution	Mark
HuNu	Mouse	Milipore -MAB1281	1:200	Human cells
GFAP	Rabbit	Dako -Z0334	1:500	Astrocytes
Iba1	Rabbit	Abcam -ab108539	1:500	Microglia/macrophage
NeuN	Mouse	Chemicon-MAB337	1:100	Mature neurons
RECA	Mouse	BioRad- MCA970R	1:200	Endothelial cells
COL-IV	Goat	Southerbiotec- 1340-01	1:1000	Blood vessels collagen type IV

The primary antibodies used to bound: human nucleus (anti-HuNu), glial fibrillary acid protein (anti-GFAP), anti-Ionized calcium binding adaptor molecule 1 (anti-Iba1), anti-Neuronal Nuclei (anti-NeuN), anti endothelial cells RECA1 and anti-collagen type IV (anti-COL-IV).

4.1.7.4 Data analysis

Images were obtained using a epifluorescence microscopy (Nikon Eclipse E600, Tokyo, Japan) and a CCD camera (Olympus XC30, Rungis, France).

Brain images were acquired in the medial border zone of the lesion or the hydrogel injection site, or in the correspondent zone of striatum for sham groups.

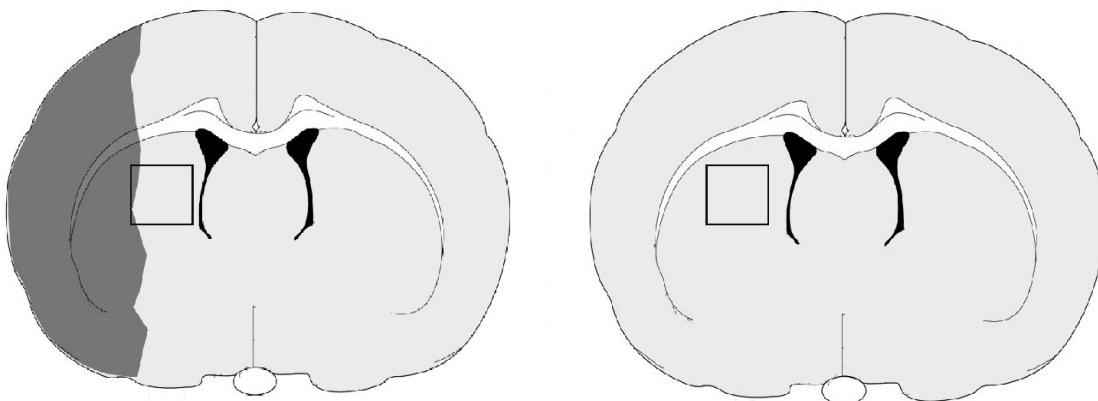


Figure 20 : Illustrative images of brain regions selected for immunofluorescence quantification

The total area occupied by astrocytes (GFAP+), microglia/macrophages (Iba1+), blood vessels (RECA and COL-4+), neurons mature (NeuN+) were determined using Image J (National Institutes of Health, USA). Images containing the ROI (lesion boundary and the corresponding zone on striatum at sham rats) were turned into (8-bit) gray scale. A mask of each brain section image was then created using an auto-threshold tool from Image J with the aim to correct background and unequal illumination (shading correction) (Centenaro et al., 2011). The same threshold mask was applied for all animals for each cellular type evaluate. All lightning conditions and magnifications were held constant. The total percentage (%) area occupied by each cell (including soma and process) was measured.

5 PART I: MRI EVALUATION OF STROKE AT ACUTE PHASE

The present work was developed in the team “Neuroimaging and Brain Perfusion” team (Grenoble Institute of Neurosciences). MRI methods are developed with the purpose of advancing the understanding of pathologies such as stroke, traumatic brain injury and brain tumors (Christen et al., 2011, 2014, Troprès et al., 2001, 2015) .

At acute phase of stroke, the rapidly hemodynamic modifications result in a lesion in part reversible if treated within a therapeutic window (see Introduction). The real relevance of imaging on this phase is widely recognized and even the World Health Organization (WHO) changed recently their definition of stroke to include brain imaging in the text.

A MRI technique to detect brain oxygenation using a multiparametric quantitative blood oxygenation level-dependent (mqBOLD) approach was developed in our team. The first study of the present thesis (chapter 1) consists in the application of this technique to detect ischemic areas at acute phase and for evaluating the potential of this technique to predict necrosis.

*A master 1 student co-supervised by me realized a retrospective study evaluating MRI diffusion in the prediction of mortality (appendix 1) using rats that died within the first 24 hours in this experiment.

STUDY 1: MULTIPARAMETRIC MRI ANALYSES POST STROKE

The present work was published in the Journal of cerebral blood flow and metabolism.

Context of the study

Ischemic stroke is an important health issue due to their high rate of disability and mortality.

During the acute phase, the rapid hemodynamic modifications results in a lesion in part reversible if treated within a therapeutic window (under 4.5h-6h). Brain imaging presents relevance in acute phase by allowing the identification of the lesion “type” (ischemic or hemorrhagic), localization and severity. Magnetic resonance imaging (MRI) is a non-invasive and highly versatile imaging modality widely applied both in experimental stroke models and in the clinics. Advanced neuroimaging techniques which allow mapping microvascular and metabolic alterations can be helpful to understanding of pathophysiological process of ischemia. The present study consists of an acute phase evaluation of ischemic stroke using multiparametric MRI, including microvascular, hemodynamic and diffusion imaging. The objective was to assess the mapping of brain tissue oxygen saturation (StO₂) with MRI (developed in our team (Christen et al., 2011)) in acute experimental stroke to detect the ischemic core and to assess its potential to predict the final necrosis.

Principal results

Our study demonstrates the potential of StO₂ MRI to more accurately detect the ischemic core without the inclusion of any reversible ischemic damage. The region detected by StO₂ such non-salvageable (core) was also the zone presenting the lower values of microvascular and hemodynamic parameters.

We compared the prediction of final necrosis by StO₂ MRI method with the classic predictor of ischemic core by MRI, the diffusion imaging. Our follow-up study indicates that apparent diffusion coefficient imaging overestimated the final necrosis while StO₂ imaging did not.

Multiparametric magnetic resonance imaging including oxygenation mapping of experimental ischaemic stroke

Ligia Simões Braga Boisserand^{1,2,3}, Benjamin Lemasson^{1,2},
Lydiane Hirschler^{1,2,4}, Anaïck Moisan^{1,2,5}, Violaine Hubert¹,
Emmanuel L Barbier^{1,2}, Chantal Rémy^{1,2} and
Olivier Detante^{1,2,6}

Abstract

Recent advances in MRI methodology, such as microvascular and brain oxygenation (StO₂) imaging, may prove useful in obtaining information about the severity of the acute stroke. We assessed the potential of StO₂ to detect the ischaemic core in the acute phase compared to apparent diffusion coefficient and to predict the final necrosis. Sprague-Dawley rats (n = 38) were imaged during acute stroke (D0) and 21 days after (D21). A multiparametric MRI protocol was performed at 4.7T to characterize brain damage within three region of interest: 'LesionD0' (diffusion), 'Mismatch' representing penumbra (perfusion/diffusion) and 'Hypoxia' (voxels < 40% of StO₂ within the region of interest LesionD0). Voxel-based analysis of stroke revealed heterogeneity of the region of interest LesionD0, which included voxels with different degrees of oxygenation decrease. This finding was supported by a dramatic decrease of vascular and perfusion parameters within the region of interest hypoxia. This zone presented the lowest values of almost all parameters analysed, indicating a higher severity. Our study demonstrates the potential of StO₂ magnetic resonance imaging to more accurately detect the ischaemic core without the inclusion of any reversible ischaemic damage. Our follow-up study indicates that apparent diffusion coefficient imaging overestimated the final necrosis while StO₂ imaging did not.

Keywords

mqBOLD, magnetic resonance imaging, oxygenation, penumbra, stroke

Received 13 January 2016; Revised 1 July 2016; Accepted 4 July 2016

Introduction

Stroke is a major public health issue due to the socio-economic burden of stroke-induced disability.¹ Ischaemic stroke is the most common subtype of stroke (accounting for around 80% of all stroke cases), resulting from an arterial occlusion that dramatically decreases local brain perfusion. Cerebral ischaemia is a complex and dynamic process that spans from hyperacute to acute, subacute and chronic phases. When diagnosed quickly, ischaemic stroke can be treated by thrombolysis, using recombinant tissue plasminogen activator (rtPA).² Mechanical thrombectomy via an endovascular route can be performed either as an alternative to thrombolysis to reduce the risk of brain haemorrhage³ or in association with rtPA.⁴ Patients can benefit from thrombolysis up to 6 h after ischaemic

stroke onset.⁵ However, evidence suggests that time alone is not sufficient to optimally select patients for thrombolysis. Neuroimaging can play an influential role in refining treatment decisions by correctly

¹Univ. Grenoble Alpes, Grenoble Institut des Neurosciences, Grenoble, France

²Inserm, U1216, Grenoble, France

³CAPES Foundation, Ministry of Education of Brazil, Brasilia, Brazil

⁴Bruker Biospin, Ettlingen, Germany

⁵Cell Therapy and Engineering Unit, EFS Rhône Alpes, Saint Ismier, France

⁶CHU Grenoble Alpes, Grenoble, France

Corresponding author:

Emmanuel L Barbier, GIN – U1216, Chemin Fortuné Ferrini, 38700 La Tronche, France.

Email: emmanuel.barbier@univ-grenoble-alpes.fr

distinguishing between salvageable tissue and the central irreversible core.⁶

Indeed, two distinct regions can be detected during the acute phase of stroke: an ischaemic core that is severely and irreversibly damaged, and a zone of 'penumbra' defined as an ischaemic tissue that is functionally impaired and at risk of infarction but has the potential to be salvaged.^{7,8} Currently, the standard imaging technique to identify the penumbra is positron emission tomography (PET)¹⁵O₂.⁹ However, the use of PET imaging in acute stroke remains limited in clinical practice by its high cost, relative invasiveness and limited availability. A more widely available alternative is perfusion-weighted imaging (PWI)/diffusion-weighted imaging (DWI) mismatch MRI. Using MRI, the ischaemic core is detected as the zone of water diffusion abnormality, while the penumbra area is indirectly detected as the mismatch between the zone of perfusion deficit and the zone of diffusion abnormality. Recently, it has been observed that an area of diffusion alteration that shows a modest apparent diffusion decrease could be salvaged with timely reperfusion.¹⁰ Different degrees of severity within the apparent diffusion coefficient (ADC) lesion were detected using PWI (mean transit time).¹¹ A pilot clinical study using ¹⁸F-MISO PET also reported the presence of extensive penumbra in each patient (n = 3), which included the zone of abnormality identified by DWI.⁹ This suggested that ADC may not be the best biomarker for an ischaemic core or predictor of the final lesion.

Recent advances in brain imaging techniques offer new tools to characterize the ischaemic lesion. Currently, it is possible to map microvascular parameters such as vessel size index (VSI),¹² vessel density (VD)^{13,14} and brain tissue oxygen saturation (StO₂) in a voxelwise basis, using a multiparametric quantitative blood oxygenation level-dependent (mqBOLD) approach.^{15,16}

Changes in infarct progression may be better detected with voxel-based methods than with methods using volumetric mismatches.¹⁷ In this way, these new parameters might allow a more accurate identification of salvageable areas and the core (irreversible damage) within the ADC lesion. Based on previous studies,^{16,18} a drop in StO₂ below 40% of control levels predicts irreversible damage. However, it is not yet known how ADC and StO₂ compare in the context of acute stroke. The specific goals of this study were (1) to investigate the sensitivity of StO₂ to detect an acute stroke lesion (compared to ADC); (2) to assess the distribution of hypoxic zones within the ADC lesion, and their impact on haemodynamic parameters; and (3) to assess the potential of combined StO₂ and ADC to predict the final necrosis (three weeks after stroke onset).

To address these goals, we used a multiparametric MRI protocol, which combined standard diffusion/

perfusion maps with the acquisition of novel MRI parameters (VSI, VD and StO₂). We examined these MRI parameters within four regions of interest (ROI): the lesion detected on ADC (ROI LesionD0), the zone of mismatch CBF (cerebral blood flow)/ADC (ROI Mismatch), the zone with a StO₂ below 40% within the ADC lesion (ROI Hypoxia) and the contralateral tissue (ROI Contra).

Materials and methods

All procedures and animal care were in accordance with French government guidelines and were performed under permit numbers 380820 and A3851610008 (for experimental and animal care facilities) from the French Ministry of Agriculture. The study design was approved by the 'Grenoble Institute of Neuroscience' local ethics committee for animal care and use (agreement number 004). This study is in compliance with the ARRIVE guidelines (Animal Research: Reporting in Vivo Experiments).¹⁹ Male Sprague Dawley rats (n = 38; 294 ± 93 g; age = 7 weeks) were obtained from Charles River (France), and housed in groups of 3–4 in Plexiglas cages under standard laboratory conditions (12 h light/dark cycle with lights off at 7:00 p.m. and at a controlled temperature of 22 ± 2 °C). Water and standard laboratory chow were provided ad libitum. Figure 1(a) shows the full experimental protocol.

Animal preparation

For all experimental procedures with a potential risk of pain or discomfort for the animals, anaesthesia was induced by inhalation of a gas mixture of 5% isoflurane (IsoFlo, Abbot Laboratories Ltd, Berkshire, UK) in medical air through a facial mask and maintained between 1.0 and 2.5% of isoflurane during the surgical procedures and MRI acquisition. Body temperature was monitored by a rectal probe and maintained at 37 ± 0.5 °C via a heating blanket. The tail vein was equipped with a catheter to deliver the contrast agent.

Middle cerebral artery occlusion surgery

Focal brain ischaemia was induced by middle cerebral artery occlusion (MCAo) using the intraluminal filament technique.²⁰ The incision site was shaved, cleaned and injected subcutaneously with 2 mg/kg 0.05% Bupivacaine (Pfizer, France). Briefly, the right carotid arterial tree was isolated. A monofilament (silicon rubber-coated monofilaments: 0.37 mm in diameter, Doccol, Sharon, MA, USA) was advanced from the lumen of the external carotid artery into the internal carotid artery to occlude the right MCA at its origin. The external carotid artery was ligated, the occipital

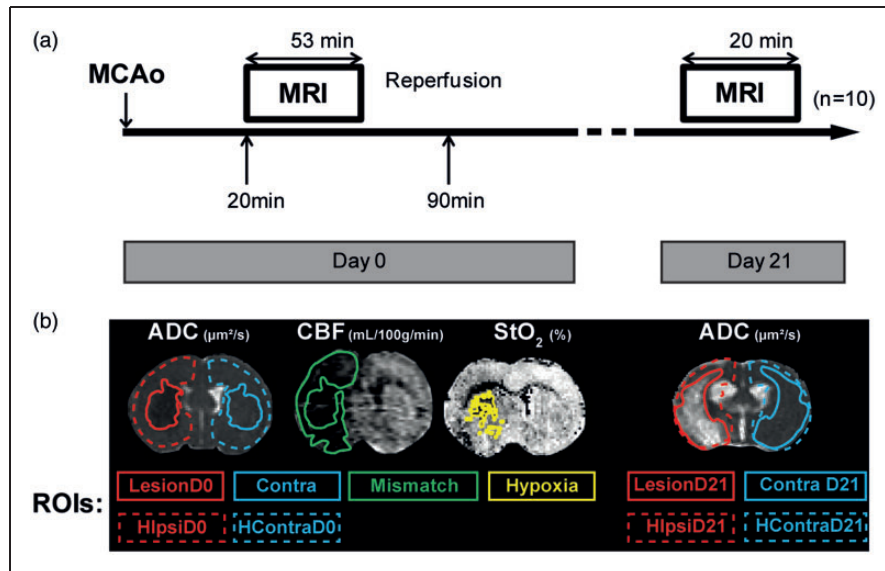


Figure 1. (a) Experimental protocol. Ischaemic stroke induction by Middle Cerebral Artery occlusion (MCAo). MRI protocol acquisition started 20 min after MCAo, lasting for 53 min at day 0. Reperfusion took place 90 min after MCAo. MRI acquisition was repeated 21 days after (duration 20 min); finally the animals were euthanized for histological analyses; $n = 10$ rats. (b) Representative image of regions of interest (ROIs) delineated on the ADC (apparent diffusion coefficient) map: ROIs measured at day 0: LesionD0, ContraD0, hemisphere (H) ipsilateral (ipsi) HipsiD0 and HContraD0. ROIs measured at day 21: LesionD21, ContraD21, HipsiD21 and HContraD21. ROI Mismatch was delineated on the CBF (cerebral blood flow) map; ROI Hypoxia was delineated on the StO₂ (brain tissue oxygen saturation) map.

artery branch of the external carotid artery and superior thyroid artery were isolated and electro-cauterized. After 20 min of MCAo, the MRI session began. At the end of the MRI session, the filament was retracted to allow reperfusion. Therefore, ischaemia lasted around 100 min (Figure 1(a)).

Magnetic resonance imaging protocol

MRI was performed at day 0 (multiparametric protocol, duration: 53 min) and at day 21 (anatomical and diffusion sequences, duration: 20 min).

All MRI data were acquired using a 4.7T magnet (Bruker Biospec[®], Germany) (MRI facility IRMaGe, Grenoble, France). After securing the animal in a cradle using tooth and ear bars to restrict head movement, a volume coil for excitation and a surface coil for detection were used. The slice orientation was identical for all MRI sequences. During each MRI session, physiological variables were continuously monitored.

The multiparametric MRI protocol was as follows. After a pilot sequence to ensure the correct rat position, anatomical T₂-weighted (T₂W) images were acquired using a spin-echo sequence (repetition time (TR)/echo time (TE) = 7000/50 ms, 31 slices with a voxel size = 234 × 234 × 800 μm). ADC was mapped using diffusion-weighted, spin-echo, single-shot echo-planar imaging (EPI) (TR/TE = 2250/33 ms, eight averages, nine slices, voxel size = 234 × 234 × 800 μm). This

sequence was applied four times, once without diffusion weighting and three times with diffusion weighting ($b = 800 \text{ s/mm}^2$) in three orthogonal directions. CBF was determined using pseudo continuous arterial spin labelling (pCASL) with an EPI readout (spin-echo EPI, TR/TE = 3600/21 ms, labelling duration = 3 s, post-labelling delay = 400 ms, 50 label/control pairs, five slices with voxel size = 234 × 234 × 800 μm). Note that the use of a fixed 400 ms post-labelling delay may not account for all arterial delays that occur during experimental ischaemic stroke. In practice, this approach may underestimate the absolute CBF values in the lesion territory. A T₁ map was obtained using an inversion-recovery sequence (TR/TE = 8000/33 ms; 15 inversion times: 35–7000; five slices; voxel size = 234 × 234 × 800 μm). A T₂ map was obtained using a multi-spin-echo sequence (26 echoes; TR/TE = 2000/12–312 ms; five slices; voxel size = 234 × 234 × 800 μm). A high resolution T₂* map was obtained from a 3D multiple-gradient echo sequence (15 echoes; TR/TE = 100/4–67 ms; 26 slices; voxel size = 117 × 117 × 200 μm). A blood volume fraction (BVf) map was obtained using a steady-state approach.¹² A multiple-gradient echo sequence (16 gradient echoes; TR/TE = 4000/3–56 ms, and one spin-echo TE = 60 ms; five slices, voxel size = 234 × 234 × 800 μm) was performed before, and 1 min, after an intravenous injection of ultrasmall superparamagnetic iron oxide nanoparticles (USPIO) contrast agent (P904, 200 μmol of iron/kg, Guerbet

S.A., Aulnay-sous-bois, France) flushed with 250 μ l of saline.

At day 21, the MRI protocol was composed of the same anatomical and ADC sequences.

Histology

After euthanasia at day 21, brains were quickly removed, frozen in -40°C isopentane, and stored at -80°C until processing. Coronal cryosections (20 μ m thick) were cut along the entire lesion at -20°C on a cryotome (Leica, Nanterre, France).

Haematoxylin–erythrosine (HE) staining was performed according to the manufacturer's instructions on the slice with the largest lesion area to assess the final necrosis ($n = 10$).

MRI data processing

MRI data were processed using homemade software developed in Matlab 2013 (MathWorks, Natick, MA, USA). This software allows map calculation and the creation of ROIs.

ADC maps were generated with Paravision 5.1 software (Bruker, Germany) computed as the mean of the ADCs measured in the three principal directions of the gradient system. VSI and BVf maps were derived from the change of T_2 and T_2^* induced by injection of iron oxide particles as previously described.¹² VD was derived from the ratio of the changes in transverse relaxation rates, using the equations (13) to (15) described in Troprès et al.¹³ A quantitative CBF map was computed with the equations described in Alsop et al. using both the pCASL sequence and the T_1 map.²¹ A StO_2 map was computed using the T_2 map, T_2^* map and BVf map as previously described.¹⁵ The spatial resolution of all MRI maps was set to that of the lowest acquired ($234 \times 234 \times 800 \mu\text{m}$). Except for ADC maps (nine slices), all parametric maps had five slices placed in the centre of the lesion because of technical limitations.

MRI data analysis

At day 0, four ROIs were delineated to evaluate the alterations of the MRI parameters following ischaemia (Figure 1(b)). The ROI LesionD0 was obtained by contouring the zone with abnormal diffusion on the ADC map (over nine slices). The ROI Contra was the 'mirror' of the ROI LesionD0 in the contralateral hemisphere. The ROI Mismatch was defined as the difference between the low-CBF ROI manually delineated (over five slices) on the CBF map and the ROI LesionD0. To delineate the low-CBF ROI, we searched for anatomically relevant areas (i.e. excluding

ventricles) that exhibited a sharp CBF decrease (about 20%). The ROI Hypoxia was automatically defined as the voxels with a StO_2 value below 40% and located within the ROI LesionD0 (over five slices). The StO_2 threshold of 40% was chosen on the basis of a previous study demonstrating that a value below 40% is not sufficient for cell survival.¹⁸ These four ROIs were transferred to each parametric map.

In addition, two ROIs, ROI HIpsiD0 (9 slices) and ROI HContraD0 (9 slices), were defined by delineating hemispheres on $T_2\text{W}$ images and excluding ventricles and corpus callosum. The volume of each hemisphere was estimated by multiplying the number of voxels in the ROI by the voxel volume ($234 \times 234 \times 800 \mu\text{m}^3$). At day 21, the lesion volume (LesionD21) was estimated by delineating regions of hyperintensity on the ADC map of the nine slices (approximately between the coordinates $+2.20$ and 4.0 mm from bregma) and the ROI ContraD21 was the 'mirror' of LesionD21. The volume of each hemisphere (HIpsiD21 and HContraD21) was measured as described above.

The volume occupied by the ROI Hypoxia in the ipsilateral hemisphere was compared to that detected three weeks after, the ROI LesionD21. Finally, we compared the in vivo (MRI) and ex vivo (histological analysis) detection of the final necrosis at day 21.

The comparison between the volume of the lesion detected on the StO_2 map at day 0 and the final lesion at day 21 was performed using five slices, because the StO_2 maps had only five slices (cf. MRI data processing section of 'Materials and Methods'). For ADC-based measurements, nine slices were used. Hemisphere volumes were evaluated at day 0 and day 21 to detect brain oedema or shrinkage. Lesion volume was also evaluated at both time points to assess the ADC lesion fate.

Histological data analysis

After HE staining, the slices were digitized at a resolution of 2400 dot per inch using a photo scanner (Perfection 4870; Epson, Long Beach, CA) with back-lighting. Brain images were imported into the Matlab environment (using homemade software), converted to black and white and then warped (elastic registration) to ensure matching of the histological regions and the anatomical points detected by MRI $T_2\text{W}$ (one slice). Briefly, a simple 2D elastic registration was done in three steps using built-in Matlab functions (MathWorks, Natick, MA, USA): (1) manually selecting control point pairs that correspond to the same anatomical structure between the HE staining and the MRI anatomical image (Matlab function called *cpselect*), (2) infer the spatial transformation from control point pairs using a piecewise linear transformation

(Matlab function called cp2tform) and (3) transform the HE image according to the 2D spatial transformation returned by the cp2tform function (Matlab function called imtransform). The ROI NecrosisD21 was defined by delineating the zone of HE alteration.

Statistical analysis

We tested the normality of our data distribution using the Shapiro–Wilk test. Comparisons of ROI areas, volumes and parameter values at day 0 were analysed with Student’s paired t-test if the distribution was normal or by Wilcoxon Signed-rank test otherwise. The Spearman correlation coefficient was used for the correlation analysis of MRI at day 0 and day 21 and the Pearson correlation coefficient was used for the correlation of MRI D21 and histological analysis. Statistical significance was set to $p < 0.05$. Statistical analysis was conducted with statistical software package SPSS 21.0 (IBM, Armonk, USA). Data are presented as mean \pm Standard Error of Mean (SEM) for MRI data or mean \pm standard deviation (SD) for physiological data.

Results

Four animals were excluded for not presenting an ischaemic lesion ($n = 2$) or because of problems with the contrast agent administration ($n = 2$). We also lost 22 rats spontaneously due to stroke, and two because of deteriorating health, leaving 10 rats in our follow-up study. The mean occlusion time was 101 ± 15 min. Physiological variables (day 0 and day 21) were monitored and maintained within physiological limits (Table 1). We found higher heart (HR, $p = 0.04$) and breathing rates (BR, $p = 0.01$) at day 0 than at day 21.

The HIpsi and HContra had similar volumes, at both time points (at day 0: 375.3 ± 3.8 and 364.9 ± 6.8 mm³, $p = 0.17$; at day 21: 365.0 ± 5.7 and 363.0 ± 5.7 mm³, $p = 0.97$, respectively). Comparisons between HIpsiD0 versus HIpsiD21 $p = 0.10$; and

HContraD0 versus HContraD21 $p = 0.88$, evaluated by a paired analysis Wilcoxon Signed-rank test) (Figure 2(a) and (b)).

Mortality

Rats spontaneously died due to the severity of ischaemia ($n = 22$) or were euthanized due to deteriorating health ($n = 2$). The criteria for euthanasia were based on clinical examination and assessment of the rat’s level of pain, distress or significant weight loss (20% from preoperative body weight). Rats were euthanized by an intra-cardiac injection of pentobarbital 200 mg/kg (Dolethal, Vétquinol Inc, France) under deep anaesthesia by isoflurane (IsoFlo, Abbot Laboratories Ltd, Berkshire, UK).

Effect of ischaemia on MRI parameters during the acute phase

Table 2 and Figure 3 summarize the values of each MRI parameter within each ROI at day 0 ($n = 10$). Comparisons between these parameters were based on estimates obtained from five slices, with the exception of ADC (nine slices), and were performed by a paired analysis (Student’s paired t-test for a normal distribution or Wilcoxon Signed-rank test otherwise).

ADC. As expected, a decreased ADC was observed in the MCA territory following MCAo. The ROIs LesionD0 and Hypoxia showed a similar ADC decrease ($p = 0.14$). The mean ADC within the ROI Mismatch was similar to that of the ROI Contra ($p = 0.22$) (Figure 3(b)).

Perfusion. The CBF in the ROI Hypoxia was lower than that of the ROI Mismatch ($p = 0.001$) or LesionD0 ($p = 0.01$) (Figure 3(c)). BVf, measured with a steady-state approach, confirmed a reduced perfusion in the ipsilateral ROIs, with the greatest reduction observed in the ROI Hypoxia, followed by LesionD0 and Mismatch ($p = 0.04$ for the comparison between Hypoxia and the LesionD0 and $p < 0.01$ for comparisons between the other groups) (Figure 3(d)).

VSI and VD. Figure 3(e) and (f) shows the average VSI and VD, respectively, across all rats and for each ROI. MCAo induced alterations in the apparent microvascular architecture: the three ipsilateral ROIs exhibited larger VSI and lower VD than in the ROI Contra. Moreover, the ROI LesionD0 had higher VSI values than the Mismatch ($p = 0.05$) and Hypoxia ($p = 0.02$) ROIs. VD in ROI Hypoxia was lower than that of ROI Mismatch ($p < 0.01$) but similar to that of ROI LesionD0 ($p = 0.37$).

Table 1. Physiological data.

	Day 0 (mean \pm SD)	Day 21 (mean \pm SD)
SaO ₂ (%)	95.55 \pm 4.06	98 \pm 1.35
HR (bpm)	392.19 \pm 20.5*	334.5 \pm 38.9
BR (brpm)	64.07 \pm 9.3*	51.5 \pm 6.97

bpm: beats per minute; BR: breathing rate; brpm: breaths per minute; HR: heart rate; SaO₂: saturation of oxygen. Physiological variables during magnetic resonance imaging acquisition. Data are expressed as mean \pm standard deviation (SD), $n = 10$. * Significant difference detected by paired Student’s t-test $p < 0.05$.

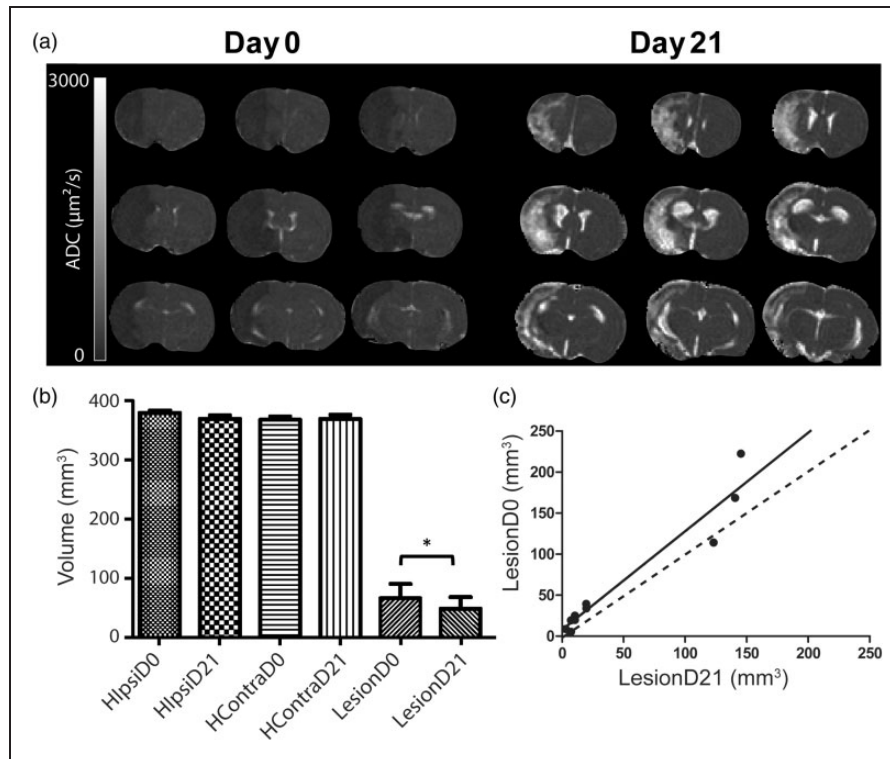


Figure 2. (a) Evolution of the apparent diffusion coefficient (ADC) map of a rat brain from one animal during middle cerebral artery occlusion at day 0 (D0) and 21 days after (D21). (b) Volume of the cerebral hemispheres: Ipsilateral (Hlpsi) and contralateral to the lesion (HContra) at D0 and D21, and volume of the altered zone detected by diffusion MRI during middle cerebral artery occlusion. Region of interest (ROI) LesionD0 at day 0 and at D21 (LesionD21) over the nine slices of ADC map. *Difference between the MR diffusion alteration volume at D0 and D21 detected by Wilcoxon Signed-Rank test ($p = 0.02$). (c) Correlation between the volumes of ROI Lesion at day 0 and day 21 $r^2 = 0.93$, $p < 0.001$, $y = 1.202x + 7.435$ ($n = 10$).

Table 2. Magnetic resonance imaging parameter values in each region of interest.

MRI parameters	Regions of interest (mean \pm SEM)			
	Contra	LesionD0	Mismatch	Hypoxia
ADC ($\mu\text{m}^2/\text{s}$)	763 \pm 15.6	576.7 \pm 16.3	742 \pm 7.5	563 \pm 16.1 [#]
CBF (ml/100 g/min)	153 \pm 4.6	46 \pm 5.1	61 \pm 5.2	31 \pm 2.0[#]
BVf (%)	4 \pm .1	2 \pm .1	3 \pm .1	2 \pm .1[#]
VSI (μm)	7 \pm .6	10 \pm .9	8 \pm .7	9 \pm .8
VD (mm^{-2})	289 \pm 39.9	147 \pm 40.8	230 \pm 41.4	139 \pm 51.1 [#]
StO ₂ (%)	70 \pm 1.5	47 \pm 1.4	60 \pm 2.2	22 \pm .6[#]

ADC: apparent diffusion coefficient; BVf: blood volume fraction; CBF: cerebral blood flow; MRI: magnetic resonance imaging; StO₂: brain tissue oxygen saturation; VD: vessel density; VSI: vessel size index. Significant differences detected by paired Student's t-test comparison (for ADC, CBF, BVf, VSI and StO₂ maps) or by Wilcoxon Signed-rank (for VD map). In bold, ROIs different from LesionD0; [#]from ROI Mismatch. For all MRI parameters evaluated, the ROIs Mismatch, LesionD0 and Hypoxia were different from ROI Contra, except for the ROI Mismatch in ADC. Data are expressed as mean and standard error of the mean (SEM) $p < 0.05$.

StO₂. Figure 3(g) shows the mean StO₂ values in the different ROIs. The three ipsilateral ROIs exhibited lower StO₂ values than the ROI Contra (StO₂ = 70.2%, $p < 0.01$). As expected, the lowest

values of StO₂ were found in the ROI Hypoxia when compared to the ROI LesionD0 (22.3% versus 46.7%, respectively, $p = 0.01$) or to the Mismatch ROI (22.3% versus 59.8%, $p = 0.01$).

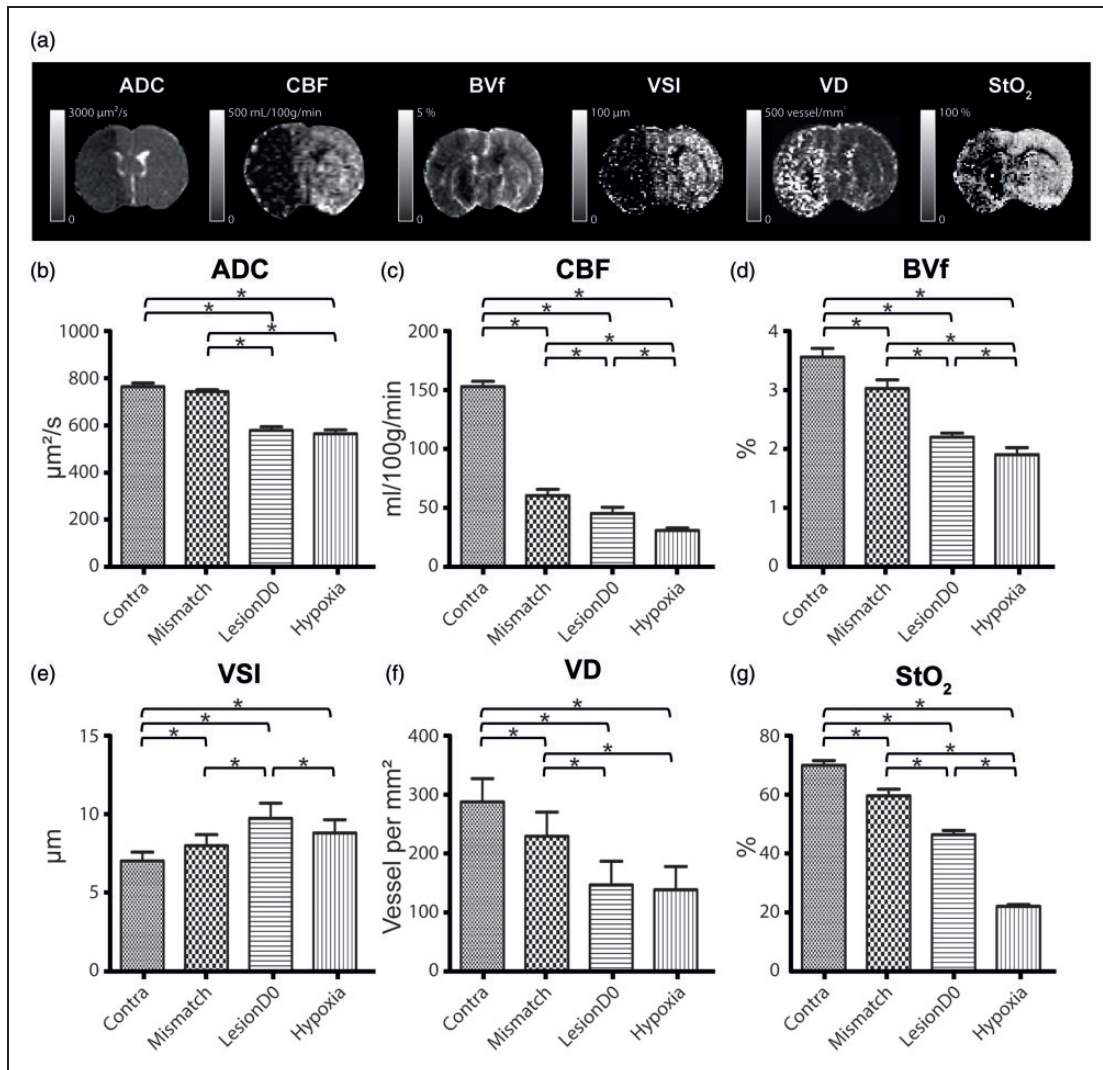


Figure 3. (a) Representative images of multiparametric MRI post-ischaemic stroke. Six MRI parameters were mapped: apparent diffusion coefficient (ADC), cerebral blood flow (CBF), blood volume fraction (BVf), vessel size index (VSI), vessel density (VD) and brain tissue oxygen saturation (StO_2). The grey scale bar represents the range of values of each map. Comparison of values of each MRI parameter: (b) ADC, (c) CBF, (d) BVf, (e) VSI, (f) VD and (g) StO_2 within each region of interest (Contra, Mismatch, LesionD0 and Hypoxia) at day 0. *Significant difference detected by paired Student's t-test comparison (for ADC, CBF, BVf, VSI and StO_2 maps) or by Wilcoxon Signed-rank (for VD map) $p < 0.05$, $n = 10$.

Evolution of the ischaemic lesion three weeks after stroke

A paired test showed that the volume of altered ADC (over nine slices, $n = 10$ rats) was lower at day 21 (ROI LesionD21: $48.6 \pm 19.2 \text{ mm}^3$) than at day 0 (ROI LesionD0: $65.8 \pm 24 \text{ mm}^3$, $p = 0.02$) (Figure 2(b)). A good correlation was detected between the two time points ($r^2 = 0.93$, $y = 1.202x + 7.435$, $p < 0.01$). At day 21, the ADC values reported in the ROIs LesionD21 and Contra (ADC map) were 1743.7 ± 134.6 and $756.2 \pm 10 \mu\text{m}^2/\text{s}$, respectively.

Moreover, we compared the volume of ROI Hypoxia detected by MRI at day 0 using the ADC and StO_2 maps with the final lesion detected on the ADC map at day 21. We observed no significant difference in the volume of ROI Hypoxia ($24.29 \pm 9.57 \text{ mm}^3$; five slices) and the lesion volume detected at day 21 in the ROI LesionD21 ($34.66 \pm 12.87 \text{ mm}^3$; five slices; $p = 0.64$) (Figure 4). A good correlation was detected between the volume of the ROI Hypoxia and the ROI LesionD21 ($r^2 = 0.68$, $p < 0.01$) (Figure 4(b) and (c)).

To check the accuracy of the lesion detection by MRI in the chronic phase, we assessed the

correlation between lesions detected in vivo by MRI (ROI LesionD21) and ex vivo by histological staining (ROI Necrosis). We found a good correlation between the in vivo and ex vivo detection of necrotic area ($r^2=0.85$; $p<0.01$) (Figure 5). Altogether, these results suggest that there is a good agreement between the volume of ROI Hypoxia, measured during the acute phase of the stroke, and the chronic lesion volume.

Discussion

The aims of this study were to investigate the sensitivity of StO_2 to detect hypoxic areas during the acute phase of ischaemic stroke compared to ADC and to assess its potential in predicting the final necrosis. During the acute phase of stroke, both ADC and StO_2 detected a lesion. The results obtained with multiparametric MRI show that the lesion may be divided into three zones with different degrees of severity: the ROIs Mismatch (CBF/ADC mismatch), LesionD0 (the ADC lesion) and Hypoxia (as a part of the ADC lesion). After three weeks, the final lesion volume was smaller than that of the initial ischaemic core defined on the ADC map. StO_2 and ADC were equivalent in predicting the final necrosis.

Contralateral hemisphere

Most of the parameter values assessed in the contralateral hemisphere are in agreement with previous reports for ADC,²² BVf, VD,²³ CBF,²⁴ and StO_2 .^{16,25} Contralateral VSI values appear to be slightly higher than those previously reported in literature ($7.0 \pm 0.6 \mu m$ versus $4.5 \pm 0.8 \mu m$).^{26,27} This result might be explained, as previously reported, by long-term changes in myogenic reactivity of MCAs in both ischaemic and non-ischaemic hemispheres.²⁸

Penumbra

In this study, the ‘mismatch’ area (ROI Mismatch), usually considered to be a salvageable zone, exhibited the least severe alterations among the three ipsilateral ROIs. Note that this penumbra, being observed around 60 min after stroke onset was evolving more slowly than just after stroke onset. We observed an important reduction in CBF (61.0 ± 5.2 ml/100 g/min) compared to the contralateral hemisphere (153.0 ± 4.6 ml/100 g/min), but with values compatible with cell survival,²⁹ and no alteration of ADC. For all other parameters (BVf, VD, StO_2), a slight reduction was observed, compared to the contralateral hemisphere, except for VSI whose values were slightly higher ($7.0 \pm 0.6 \mu m$ versus $8.1 \pm 0.7 \mu m$).

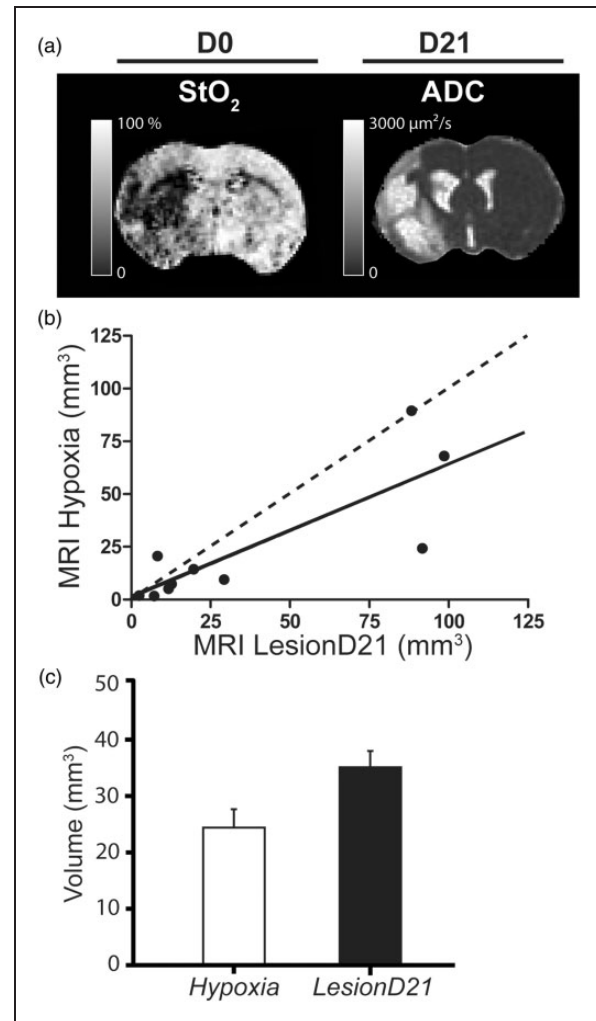


Figure 4. (a) Volume of Lesion at day 0 and at day 21. Representative images of the MRI maps at day 0 (D0) (StO_2 , brain tissue oxygen saturation map) and at day 21 (ADC D21). (b) Comparison of the volume of the ROI Hypoxia and LesionD21 over five slices expressed in mean and the standard error of mean (SEM). No significant differences were detected between the volume occupied by the ROI LesionD21 (34.66 ± 12.87 mm³) and ROI Hypoxia (24.29 ± 9.57 mm³) ($p = 0.05$). (c) Correlation between the volume of ROI Hypoxia versus LesionD21; the correlation coefficient was $r^2 = 0.67$, $p = 0.005$, $y = 0.63x + 0.98$ ($n = 10$).

Ischaemic core

Quantitative measures of ADC in previous studies revealed that during ischaemia, ADC declines before energy metabolism fails.³⁰ These results suggest that a reduced ADC area may overestimate the size of the infarct core. In the present study, the ROI LesionD0 (i.e. the ADC abnormality) exhibited lower values of ADC, CBF, BVf, VD and StO_2 than the contralateral hemisphere and the mismatch area. Conversely, VSI

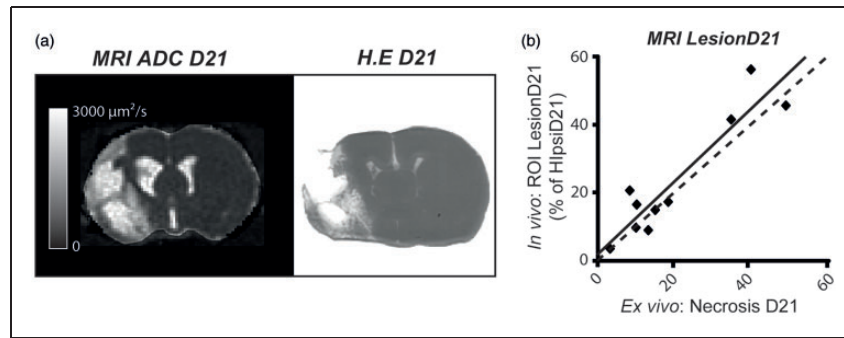


Figure 5. Quantitative correlation between in vivo and ex vivo evaluation. (a) Representative images of apparent diffusion coefficient (ADC) at day 21 (used to define ROI LesionD21) and haematoxylin erythroline (HE) staining (used to define ROI NecrosisD21). (b) Correlation between the size of ROI LesionD21 and ROI NecrosisD21. Dashed line represents identity; solid line represents the identity line. Pearson coefficient correlation was $r^2 = 0.85$, $p = 0.001$, $y = 1.04x + 2.31$ ($n = 10$).

was higher in the initial diffusion lesion (LesionD0 ROI) than in the mismatch area and contralateral hemisphere. Regarding both the ischaemic core and the penumbra, the increase in VSI, combined with a decrease in BVf and VD, could result from a decrease in the number of perfused vessels. Indeed, it is unlikely that microvessels have disappeared 1 h after MCAo. It is more likely that MCAo and oedema prevent blood flow in some vessels, which become inaccessible to contrast agent (USPIO), resulting in an apparent reduction in VD. The increase in VSI suggests that these non-perfused vessels are the smallest in diameter. Alternatively, the increase in VSI could arise from vasodilation of the remaining perfused vessels or to a combination of both phenomena. The balance between the reduction in VD and the increase in VSI yields a reduction in CBV.

The ROI Hypoxia was defined as the pixels located within the diffusion lesion (ROI LesionD0) with a StO_2 below 40%. This segmentation yielded the same hypoxic area as that estimated by pimonidazole ex vivo.¹⁶

This threshold was chosen based on a study using near-infrared spectroscopy.¹⁸ In the study, the authors demonstrated that a lactate increase is detected at an oxygen saturation of 44%, minor electroencephalography alterations appear at 42% and the adenosine triphosphate decreases at 33%.¹⁸ In a previous study by our team, a comparison between hypoxic zones detected in vivo by MRI (threshold of 40% of StO_2) and by histological analysis with pimonidazole was performed.¹⁶ Pimonidazole is a bioreductive hypoxic marker that is activated in an oxygen-dependent manner and is covalently bound to thiol-containing proteins in hypoxic cells.³¹ This binding is reported in viable hypoxic cells but not in necrotic cells. The redox-dependent process is progressively inhibited at increasing oxygen tensions and involves the cell-specific action of cellular nitroreductases.³² A good correlation was

previously reported between StO_2 MRI and pimonidazole-positive hypoxic cells 2 h after ischaemia onset.¹⁶

The values of the MRI parameters within the hypoxic zone (ROI Hypoxia), located by construction within the diffusion lesion (ROI LesionD0), were in general much lower than those of the two other ipsilateral regions, except for ADC and VD, where the ROI Hypoxia values were similar to LesionD0. The mean value of CBF in the ROI Hypoxia ($31.0 \pm 1.4 \text{ ml}/100 \text{ g}/\text{min}$) was no longer compatible with cell survival.²⁹ StO_2 fell to $22.0 \pm 0.6\%$; in the ROI LesionD0 it was $47.0 \pm 1.4\%$. BVf was also reduced (from 2.2 ± 0.7 to $1.9 \pm 0.1\%$) but to a lesser extent. Note that we could not find a BVf or a CBF threshold that could yield the same Hypoxia area as that detected with the 40% StO_2 threshold.

Altogether, our results demonstrate that StO_2 is a discriminant parameter to detect the most severe ischaemic areas within the zone of ADC decrease. In this way, our data confirmed our hypothesis that the zone of ADC decrease is heterogeneous, based on our vascular and oxygenation results.

In the present study, the reperfusion was performed after the MRI acquisition, and we therefore investigated hypoperfused areas. It should be noted that if the artery had already been recanalized at the time of scanning, the blood vessel StO_2 concentration would have been high even in zones of already dead tissue. In such cases, StO_2 values would not represent brain tissue oxygenation. The morphology and function of cerebral capillaries undergo profound changes during cerebral ischaemia. Capillary constrictions regulated by pericytes could block the blood supply; this could explain the occasional absence of tissue reperfusion even after the large-vessel recanalization. This result corresponds to the well-described no-reflow phenomenon.³³ This neurovascular dysfunction involves the formation of reactive species of oxygen at the level of

the vascular endothelium and affects the local oxygen delivery.³³

In clinical settings, a spontaneous reperfusion could be a limitation for the detection of an ischaemic core using a low StO₂ threshold. Abnormally high StO₂ and normal CBF values could also be a marker of already dead tissue.

Evolution of the ischaemic lesion

The final lesion volume was estimated from the area of increased ADC (LesionD21: $1743.7 \pm 134.6 \mu\text{m}^2/\text{s}$ versus ContraD21: $756.2 \pm 10 \mu\text{m}^2/\text{s}$). This increase in ADC, in line with a previous study,³⁴ is a consequence of cell death and subsequent cavitation of brain tissue being filled by liquid and cell debris. The final lesion volume (48.5 mm^3) was smaller than the initial volume (65.8 mm^3). In accordance with previous reports,³⁵ this suggests that an altered ADC during the acute phase does not necessarily yield a lesion. In addition, some morphological changes were detected at day 21 such as brain shrinkage and enlargement of ventricles (Figure 3(a)). Brain shrinkage, a process commonly associated with stroke, occurs not only in the perilesional zone but also in contralateral hemisphere.³⁶ Additional processes, such as axonal degeneration, are involved in shrinkage, and result in expansion of the lesion to include remote regions connected to the affected area.^{36,37}

The ischaemic lesion has a complex and dynamic physiopathology process, and even after reperfusion the lesion can continue to change. One limitation of our study is that our estimation of the hypoxic zone (ROI Hypoxia based on the StO₂ map) did not take into account neighbouring voxels. Indeed a recent study, which considered each voxel independently, showed that the distribution of intensities surrounding a voxel at the early ischaemic stages may capture the dynamic of the lesion growth and be predictive of tissue outcome.^{6,38}

There was a good correlation between the volume of the MRI lesion detected at day 0, 1 h after stroke onset, by StO₂ map (ROI Hypoxia) or by ADC (ROI LesionD0), and the volume measured at day 21 (ROI LesionD21), which corresponded to that of Necrosis D21, estimated post-mortem. Due to the above-mentioned morphological changes that occur between day 0 and day 21, we were not able to conduct a pixel-by-pixel analysis to determine whether each voxel of the StO₂ lesion evolved towards necrosis. Nevertheless, we observed that LesionD0 tended to overestimate the volume of LesionD21, while Hypoxia tended to underestimate it. Further studies are needed, including MRI maps obtained at several time points between 30 and 90 min after a stroke for the acute phase, and obtained one or two days after a stroke for the late phase, to

assess the fate of low StO₂ voxels within the ADC lesion and determine whether StO₂ MRI is a better predictor of the final infarct than ADC alone.

Study limitations

The primary limitation of our study is the mortality rate. We lost around 60% of animals, including the animals euthanized due to deteriorating health. Our model of ischaemic stroke promotes a massive lesion that includes the fronto-parietal cortex and striatum. In our experience, a short occlusion time promotes smaller and more heterogeneous lesions. To avoid this heterogeneity, we used a minimum occlusion time of 90 min. This resulted in a high number of large homogeneous lesions but also in a higher mortality. The mortality in this case can be linked to complications that are common in large stroke, such as cerebral oedema and haemorrhagic transformation. The majority of rats died after the filament retraction. The actual American Heart Association/American Stroke Association guidelines recommend not reperfusing patients with severe stroke.³⁹ Note that our study, like all stroke studies, is biased towards small stroke lesions: indeed, as reported in the 'Results' section, rats with large lesions died early.

A second point is that a voxel-based evaluation of the lesion progression over time is inherently challenging. First, because it requires the exact same placement of the rats in the magnet, and second because of the occurrence of brain shrinkage and/or ventricle enlargement. Overall, the registration quality was not sufficient to allow voxel-by-voxel analysis. However, the co-localization was visually inspected and we observed a coherent evolution of infarction.

An additional limitation is that here we use manual contouring for the diffusion map. The zone of ADC abnormality could be also detected using thresholds to detect the voxels with the most severe decrease of ADC. This method of detection has previously been used in a clinical study of patients with persistent arterial occlusion.³⁵

In the present study, we focused on StO₂ mapping for core discrimination but other parameters such as BVf or CBF could be used to estimate stroke severity within the zone of ADC decrease. For this, perfusion thresholds should be used to detect the voxels corresponding to the irreversibly damaged zones. Engelhorn et al. evaluated the absolute CBF using radioactive-labelled microspheres.²⁹ They demonstrated that the baseline CBF (before MCAo) is variable by region, for example between the parietal ($0.88 \pm 0.26 \text{ ml/g/min}$) and temporal cortex ($0.74 \pm 0.24 \text{ ml/g/min}$). In addition, this difference is increased in ischaemic conditions, dropping to $0.51 \pm 0.21 \text{ ml/g/min}$ in the parietal

cortex and 0.20 ± 0.15 ml/g/min in the temporal cortex.²⁹ Thirty minutes after MCAo, the absolute CBF in viable areas was 0.39 ± 0.15 ml/g/min, while in hypoxic brain tissue the CBF average was 0.30 ± 0.09 ml/g/min.²⁹ Hypoxic zones detected by the StO₂ (<40%) mapping could be compared with those detected by perfusion using a threshold. Wu et al. reported that the use of automated threshold techniques by MR-based algorithms combining PWI and DWI was more sensitive to the detection of salvageable areas (penumbra) than diffusion alone.¹⁷ A limitation of our study is that we have not performed the analysis based on perfusion. Brain oxygenation is linked to perfusion (BVF), and perfusion could provide a similar core discrimination to StO₂.

Summary

The voxel-based analysis performed using the StO₂ map reveals heterogeneity within the ischaemic zone in the acute phase. Diffusion imaging is commonly employed during the acute phase of ischaemic stroke to detect the ischaemic core. We report that the zone of ADC decrease includes voxels with different degrees of severity, as confirmed by the multiparametric analysis including CBF, BVf, VSI and StO₂. This study therefore provides evidence of the utility of a multiparametric analysis including StO₂ mapping to more accurately analyse the severity and heterogeneity of brain focal ischaemia. Our follow-up study indicated that both ADC and StO₂ MRI maps were able to predict the final necrosis. However, the lesion volume detected by ADC mapping decreased significantly three weeks after stroke. This could indicate that salvageable tissue is included within the initial diffusion lesion.

Few microvascular MRI studies concerning stroke have been conducted.¹³ As far as we know, this is the first study assessing the VSI and VD during the acute phase in a model of ischaemic stroke.

Currently, the most common methods of analysis of CT and MRI images in clinical settings are volumetric based, and until voxel-based analysis becomes available, perfusion–diffusion mismatch is useful in clinical settings.⁴⁰ Overall, a multiparametric approach appears to be promising in depicting the severity of a stroke, but such an approach still requires further validation and simplification of data analysis. For clinics, the use of this MRI methodology to identify heterogeneous acute stroke could be useful to better select the optimal candidates for recanalization procedures.

Funding

The author(s) disclosed receipt of the following financial support for the research, authorship, and/or publication of this article: IRMaGe was partly funded by the French programme

‘Investissement d’Avenir’ run by the ‘Agence Nationale pour la Recherche’; grant ‘Infrastructure d’avenir en Biologie Santé’ – ANR-11-INBS-0006. We also acknowledge the CAPES Foundation, Ministry of Education of Brazil, for the financial support of our PhD student.

Acknowledgements

The authors gratefully acknowledge the excellent technical support of the MRI Facility of Grenoble (IRMaGe).

Declaration of conflicting interests

The author(s) declared no potential conflicts of interest with respect to the research, authorship, and/or publication of this article.

Authors’ contribution

LSBB has participated in all steps of this study including study design, experiments, MRI acquisition, histology, data processing and analysis, interpretation of the data and writing of the paper; BL performed the experiments, analysed the MRI data, interpreted the data and wrote the paper; LH performed the MRI acquisition; ELB, AM, OD and VH designed the study; CR and ELB interpreted the data and wrote and revised the paper.

References

1. Feigin VL, Forouzanfar MH, Krishnamurthi R, et al. Global and regional burden of stroke during 1990–2010: findings from the Global Burden of Disease Study 2010. *Lancet* 2014; 383: 245–254.
2. Kwiatkowski TG, Libman RB, Frankel M, et al. Effects of tissue plasminogen activator for acute ischemic stroke at one year. *N Engl J Med* 1999; 340: 1781–1787.
3. Smith WS, Sung G, Starkman S, et al. Safety and efficacy of mechanical embolectomy in acute ischemic stroke results of the MERCI trial. *Stroke* 2005; 36: 1432–1438.
4. Campbell BCV, Donnan GA, Lees KR, et al. Endovascular stent thrombectomy: the new standard of care for large vessel ischaemic stroke. *Lancet Neurol* 2015; 14: 846–854.
5. Wang H, Chen M, Wang F, et al. Comparison of therapeutic effect of recombinant tissue plasminogen activator by treatment time after onset of acute ischemic stroke. *Sci Rep* 2015; 5: 11743.
6. Scalzo F, Nour M and Liebeskind DS. Data science of stroke imaging and enlightenment of the penumbra. *Stroke* 2015; 6: 8.
7. Donnan GA and Davis SM. Neuroimaging, the ischaemic penumbra, and selection of patients for acute stroke therapy. *Lancet Neurol* 2002; 1: 417–425.
8. Astrup J, Siesjö BK and Symon L. Thresholds in cerebral ischemia - the ischemic penumbra. *Stroke J Cereb Circ* 1981; 12: 723–725.
9. Alawneh JA, Moustafa RR, Marrapu ST, et al. Diffusion and perfusion correlates of the 18F-MISO PET lesion in acute stroke: pilot study. *Eur J Nucl Med Mol Imaging* 2013; 41: 736–744.

10. Kidwell CS, Saver JL, Mattiello J, et al. Thrombolytic reversal of acute human cerebral ischemic injury shown by diffusion/perfusion magnetic resonance imaging. *Ann Neurol* 2000; 47: 462–469.
11. Carrera E, Jones PS, Alawneh JA, et al. Predicting infarction within the diffusion-weighted imaging lesion: does the mean transit time have added value? *Stroke J Cereb Circ* 2011; 42: 1602–1607.
12. Troprès I, Grimault S, Vaeth A, et al. Vessel size imaging. *Magn Reson Med* 2001; 45: 397–408.
13. Troprès I, Pannetier N, Grand S, et al. Imaging the microvessel caliber and density: principles and applications of microvascular MRI. *Magn Reson Med* 2015; 73: 325–341.
14. Wu EX, Tang H and Jensen JH. High-resolution MR imaging of mouse brain microvasculature using the relaxation rate shift index Q. *NMR Biomed* 2004; 17: 507–512.
15. Christen T, Lemasson B, Pannetier N, et al. Evaluation of a quantitative blood oxygenation level-dependent (qBOLD) approach to map local blood oxygen saturation. *NMR Biomed* 2011; 24: 393–403.
16. Christen T, Bouzat P, Pannetier N, et al. Tissue oxygen saturation mapping with magnetic resonance imaging. *J Cereb Blood Flow Metab* 2014; 34: 1550–1557.
17. Wu O, Christensen S, Hjort N, et al. Characterizing physiological heterogeneity of infarction risk in acute human ischaemic stroke using MRI. *Brain J Neurol* 2006; 129: 2384–2393.
18. Kurth CD, Levy WJ and McCann J. Near-infrared spectroscopy cerebral oxygen saturation thresholds for hypoxia-ischemia in piglets. *J Cereb Blood Flow Metab* 2002; 22: 335–341.
19. Kilkeny C, Browne W, Cuthill IC, et al. Animal research: reporting in vivo experiments—the ARRIVE guidelines. *J Cereb Blood Flow Metab* 2011; 31: 991–993.
20. Longa EZ, Weinstein PR, Carlson S, et al. Reversible middle cerebral artery occlusion without craniectomy in rats. *Stroke J Cereb Circ* 1989; 20: 84–91.
21. Alsop DC, Detre JA, Golay X, et al. Recommended implementation of arterial spin-labeled perfusion MRI for clinical applications: a consensus of the ISMRM perfusion study group and the European consortium for ASL in dementia. *Magn Reson Med* 2015; 73: 102–116.
22. Shen Q, Meng X, Fisher M, et al. Pixel-by-pixel spatio-temporal progression of focal ischemia derived using quantitative perfusion and diffusion imaging. *J Cereb Blood Flow Metab* 2003; 23: 1479–1488.
23. Lemasson B, Valable S, Farion R, et al. In vivo imaging of vessel diameter, size, and density: a comparative study between MRI and histology. *Magn Reson Med* 2013; 69: 18–26.
24. Coquery N, Francois O, Lemasson B, et al. Microvascular MRI and unsupervised clustering yields histology-resembling images in two rat models of glioma. *J Cereb Blood Flow Metab* 2014; 34: 1354–1362.
25. Lemasson B, Christen T, Serduc R, et al. Evaluation of the relationship between MR estimates of blood oxygen saturation and hypoxia: effect of an antiangiogenic treatment on a gliosarcoma model. *Radiology* 2012; 265: 743–752.
26. Troprès I, Lamalle L, Farion R, et al. Vessel size imaging using low intravascular contrast agent concentrations. *Magn Reson Mater Phys Biol Med* 2004; 17: 313–316.
27. Valable S, Lemasson B, Farion R, et al. Assessment of blood volume, vessel size, and the expression of angiogenic factors in two rat glioma models: a longitudinal in vivo and ex vivo study. *NMR Biomed* 2008; 21: 1043–1056.
28. Winters A, Taylor JC, Ren M, et al. Transient focal cerebral ischemia induces long-term cerebral vasculature dysfunction in a rodent experimental stroke model. *Transl Stroke Res* 2012; 3: 279–285.
29. Engelhorn T, Doerfler A, Forsting M, et al. Does a relative perfusion measure predict cerebral infarct size? *Am J Neuroradiol* 2005; 26: 2218–2223.
30. Ramos-Cabrer P, Campos F, Sobrino T, et al. Targeting the ischemic penumbra. *Stroke J Cereb Circ* 2011; 42: S7–11.
31. Varia MA, Calkins-Adams DP, Rinker LH, et al. Pimonidazole: a novel hypoxia marker for complementary study of tumor hypoxia and cell proliferation in cervical carcinoma. *Gynecol Oncol* 1998; 71: 270–277.
32. Bergeron M, Evans SM, Sharp FR, et al. Detection of hypoxic cells with the 2-nitroimidazole, EF5, correlates with early redox changes in rat brain after perinatal hypoxia-ischemia. *Neuroscience* 1999; 89: 1357–1366.
33. Østergaard L, Jespersen SN, Mouridsen K, et al. The role of the cerebral capillaries in acute ischemic stroke: the extended penumbra model. *J Cereb Blood Flow Metab* 2013; 33: 635–648.
34. Foley LM, Hitchens TK, Barbe B, et al. Quantitative temporal profiles of penumbra and infarction during permanent middle cerebral artery occlusion in rats. *Transl Stroke Res* 2010; 1: 220–229.
35. Oppenheim C, Samson Y, Manaï R, et al. Prediction of malignant middle cerebral artery infarction by diffusion-weighted imaging. *Stroke* 2000; 31: 2175–2181.
36. Seghier ML, Ramsden S, Lim L, et al. Gradual lesion expansion and brain shrinkage years after stroke. *Stroke J Cereb Circ* 2014; 45: 877–879.
37. Kraemer M, Schormann T, Hagemann G, et al. Delayed shrinkage of the brain after ischemic stroke: preliminary observations with voxel-guided morphometry. *J Neuroimaging* 2004; 14: 265–272.
38. Scalzo F, Hao Q, Alger JR, et al. Regional prediction of tissue fate in acute ischemic stroke. *Ann Biomed Eng* 2012; 40: 2177–2187.
39. Jauch EC, Saver JL, Adams HP, et al. Guidelines for the early management of patients with acute ischemic stroke a guideline for healthcare professionals from the American Heart Association/American Stroke Association. *Stroke* 2013; 44: 870–947.
40. Albers GW, Thijs VN, Wechsler L, et al. Magnetic resonance imaging profiles predict clinical response to early reperfusion: the diffusion and perfusion imaging evaluation for understanding stroke evolution (DEFUSE) study. *Ann Neurol* 2006; 60: 508–517.

5.1 CONCLUSION

In the present study, we evaluated the alterations in acute phase of stroke detected by multiparametric MRI (including diffusion, vascular, hemodynamic and brain tissue oxygenation mapping) and the potential of StO₂ mapping in predict final necrosis in a model of ischemic stroke in rats.

Our multiparametric MRI evaluation demonstrated a high heterogeneity at acute phase within the zone of ADC decreased. This heterogeneity is related to the presence different degrees of severity (voxels presenting a StO₂ <40%) inside of region the ROI Lesion. Voxels-wise approaches such as StO₂ mapping are more precise in detect this heterogeneity by considering the values of each voxel. Both ADC and StO₂ MRI maps were able to predict the final necrosis. However, the lesion volume detected by ADC mapping decreased significantly three weeks after stroke. This could be an indication that salvageable tissue was included within the initial diffusion lesion.

6 PART II: OPTIMIZATION OF CELL THERAPY POST-STROKE WITH A BIOMATERIAL HYDROGEL

Context of study:

With the publication of the firsts clinical results concerning stem cell therapy (safety, good tolerance but modest functional results), pre-clinical researchers have focused their efforts to optimize cell therapy outcomes (by modifying SCs, dose or route optimization...).

In the present study, we decided to test a way to optimize cell survival in intracerebral administration. A recent meta-analysis of pre-clinical studies demonstrated that MSCs in post-stroke therapy was associated with improvement of neurological function and intracerebral route was associated with the greatest improvement (Vu et al., 2014).

Infarct cavity is an ideal place to cell transplantation because it is a compartmentalized zone of loose tissue directly adjacent to peri-infarct region, the site of greatest remodeling after stroke, and it can accept a considerable volume of injection (Carmichael, 2006; Zhong et al., 2010). Nevertheless, cell transplantation within infarct cavity presents a limitation, most transplanted cells die because infarct cavity is a non-hospitable environment (Baeten and Akassoglou, 2011).

The use of materials specially developed for use inside human body started during the 1960s and 1970s, becoming the basis for the field of biomaterials. Most recently, the third generation of materials has been designed to stimulate a cellular response at the level of molecular biology (Hench and Polak, 2002) and can be used in central nervous system.

Third-generation of biomaterials that involve the molecular tailoring of microenvironments to achieve specific cellular responses (such as stimulation of cell survival, proliferation, and differentiation) has shown great promise for SC scaffolding. Biomaterial application to optimize stem cells effects in post-stroke therapy was evaluated in the present work.

This chapter is introduced by a review of literature about the application of different kinds of biomaterials tested in experimental stroke including their compounds, mechanical and physical properties. Followed by the results of my experiments using a hyaluronan-based HyStemTM-HP Hydrogel in healthy tissue (study II) and after an ischemic stroke induced by middle cerebral artery occlusion (MCAo) (study III).

Principal results:

The preliminary results presented here in our pilot study put in evidence that HyStemTM-HP hydrogel can be detected by MRI. Diffusion MRI seems to a good method to detect hydrogel due to the high water content of the hydrogel. Additionally, our preliminary results were encouraging concerning long-lasting of hydrogel in rat brain tissue for until 28 days. An increase of host brain response evidenced by Iba1 and GFAP activation was detected. Additional analysis using a higher number of rats is required to quantify degradation rate of HyStemTM-HP hydrogel. Nevertheless, some signals of degradation were detected from 14th day to the end of experiment 28th day HyStemTM-HP. In our post-stroke experiment, the hydrogel application was well-tolerated and effectively improved MSC survival. Post-stroke angiogenesis, one of the main components of post-stroke remodeling was also improved by the combination HyStemTM-HP+hMSC. Unfortunately, the improvement in cell survival and vascular density were not able to improve behavioral outcomes. Further optimization of biomaterials and their combination with cells are warranted to improve their effects after stroke.

A. REVIEW OF LITERATURE

*The present article integrated a special issue published in the journal **Stem Cells International** in May 2016, where I reviewed the main compounds, characteristics, advantages and therapeutic effects of biomaterials administration in experimental post-stroke cell therapy.*

Among others, the application of hyaluronan-based biomaterials (the main hydrogel compound used in my experiments) and the advantages of an injectable hydrogel are discussed in this review paper.

Review Article

Biomaterial Applications in Cell-Based Therapy in Experimental Stroke

Ligia S. B. Boisserand,^{1,2,3} Tomonobu Kodama,⁴ Jérémie Papassin,^{1,2,5} Rachel Auzely,⁶ Anaïck Moisan,⁷ Claire Rome,^{1,2} and Olivier Detante^{1,2,4,5}

¹Inserm, U1216, BP 170, 38042 Grenoble Cedex 9, France

²Grenoble Institut des Neurosciences (GIN), Université Grenoble Alpes, 38000 Grenoble, France

³CAPES Foundation, Ministry of Education of Brazil, 70040-020 Brasília, DF, Brazil

⁴Institute for Frontier Medical Sciences, Department of Reparative Materials, Kyoto University, Kyoto 606-8507, Japan

⁵CHU Grenoble Alpes, Stroke Unit, Department of Neurology, CS 10217, 38043 Grenoble, France

⁶CERMAV, CNRS, CERMAV, Université Grenoble Alpes, 38000 Grenoble, France

⁷Cell Therapy and Engineering Unit, EFS Rhône Alpes, 464 route de Lancey, 38330 Saint-Ismier, France

Correspondence should be addressed to Claire Rome; claire.rome@ujf-grenoble.fr

Received 18 December 2015; Revised 11 March 2016; Accepted 4 April 2016

Academic Editor: Paulo Henrique Rosado de Castro

Copyright © 2016 Ligia S. B. Boisserand et al. This is an open access article distributed under the Creative Commons Attribution License, which permits unrestricted use, distribution, and reproduction in any medium, provided the original work is properly cited.

Stroke is an important health issue corresponding to the second cause of mortality and first cause of severe disability with no effective treatments after the first hours of onset. Regenerative approaches such as cell therapy provide an increase in endogenous brain structural plasticity but they are not enough to promote a complete recovery. Tissue engineering has recently aroused a major interesting development of biomaterials for use into the central nervous system. Many biomaterials have been engineered based on natural compounds, synthetic compounds, or a mix of both with the aim of providing polymers with specific properties. The mechanical properties of biomaterials can be exquisitely regulated forming polymers with different stiffness, modifiable physical state that polymerizes *in situ*, or small particles encapsulating cells or growth factors. The choice of biomaterial compounds should be adapted for the different applications, structure target, and delay of administration. Biocompatibilities with embedded cells and with the host tissue and biodegradation rate must be considerate. In this paper, we review the different applications of biomaterials combined with cell therapy in ischemic stroke and we explore specific features such as choice of biomaterial compounds and physical and mechanical properties concerning the recent studies in experimental stroke.

1. Introduction

The stroke is a major public health issue in the world due to aging populations and the socioeconomic burden of neurovascular disorders. It corresponds to the one of the leading causes of death and severe disability in adults worldwide. Ischemic stroke is the most common type of stroke corresponding to 85% of all strokes [1]. Pathophysiology of ischemic stroke involves a complex and dynamic process which is not limited to neurons but involves all brain cells and extracellular matrix (ECM) in a “glioneurovascular niche” that interacts with the peripheral immune system. Stroke patients could benefit from reperfusion therapies up to 6 h

after ischemic stroke onset [2]. After these first hours, there is no effective treatment available besides rehabilitation [3].

Development of innovating therapies using stem cells or trophic factors can enhance brain remodeling; this process is crucial and success requires a pathophysiological viewpoint [4]. These approaches also have the advantage of action over an extended therapeutic time-window after stroke and thereby might be effective in more patients than those helped by current acute strategies such as thrombolysis and thrombectomy. Cell-based therapy has been proposed as a potential source of new cells to replace lost cells due to central nervous system injury, as well as a source of trophic molecules to minimize damage and promote recovery [5, 6].

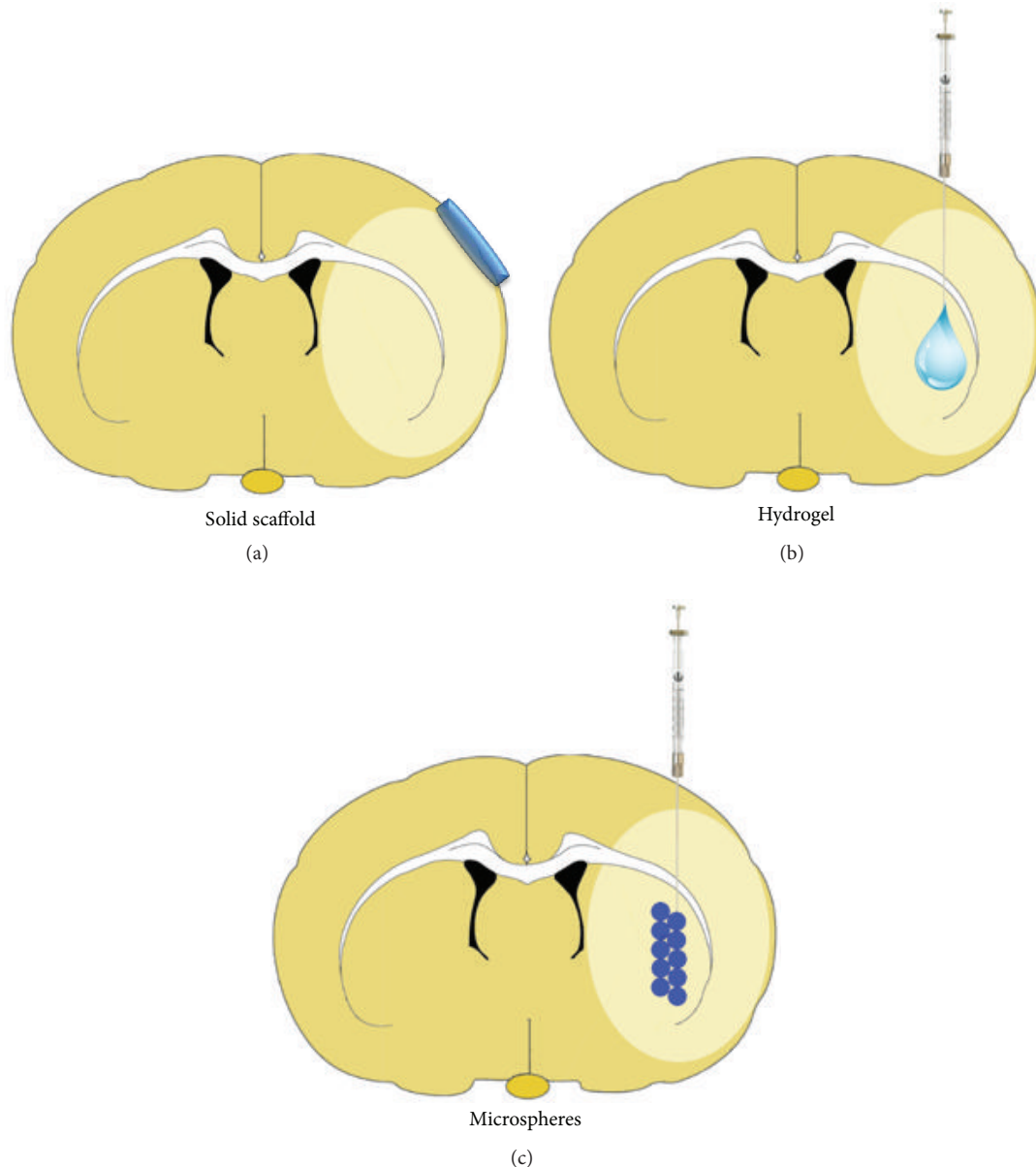


FIGURE 1: Schematic illustration of different biomaterial applications on ischemic brain. (a) Solid brain scaffolds for surface application and gradual liberation of cells, drugs, or growth factors. (b) Injectable hydrogel, in liquid phase with an *in situ* gelation. (c) Microspheres for gradual intracerebral delivery.

Stem/progenitor cell transplantation improves recovery after stroke in rodent models [7]. Nevertheless, there are two main limits concerning clinical translation in cell transplantation in stroke [8].

Firstly, when the stem/progenitor cells are systemically administered, this requires the administration of a high number of cells and only a few amounts of cells achieve the brain [9]. An alternative way is the intracerebral (IC) administration of cells directly into the brain parenchyma and/or into the lesion cavity [10] (Figure 1). This location is a compartmentalized area of lost tissue that has undergone necrosis and can allow a large volume injection, and it is

directly adjacent to peri-infarct zone [11], site of greatest neuroplasticity after stroke [12].

The second point concerning cell administration is the important cell death observed after IC graft. After stroke, within the infarct cavity, a very important loss of ECM in addition to neuronal and glial cell loss is noted. This cavity is filled by extracellular fluid and proteins from leakage of plasma proteins [13]. This damaged area is a hostile environment for cell transplantations resulting in a severe loss of grafted cells [14, 15].

Recent advances in tissue engineering have produced applications that may provide solutions to the problem of

transplanted cell death and damage associated with the transplant [11]. Biopolymer hydrogels have been projected to promote cell survival and engraftment (Figure 1).

Currently, biomaterials researchers are seeking to optimize injectable hydrogels by combining cell seeding with the incorporation of growth factors or tracers. The use of biomaterials to improve benefit of cell therapy after stroke must be carefully investigated in experimental studies prior to transferring this promising procedure to clinical trials.

In this paper, we aim to review the different applications of biomaterials after ischemic brain lesion and to explore specific features such as the choice of biomaterial compounds, physical and mechanical properties, biocompatibilities, and degradation regarding recent studies in experimental stroke (Table 1).

Stem Cell in Stroke Repair. The benefits of exogenous cell-based strategies include their potential to rescue damaged brain tissue by simultaneously promoting endogenous neuroprotection and neural repair (including neurogenesis, angiogenesis, oligodendroglialogenesis, axonal sprouting, and synaptogenesis) [6]. Additionally, these cells could act in synergy with endogenous stem cells. The different cell sources and types were recently reviewed by Jendelová et al. [16].

Currently, we distinguish two main strategies of cell therapy: (1) a paracrine trophic support using “peripheral” stem or stromal cells and (2) a direct neural replacement using neural stem/progenitor cells or mature cells such as neurons. The route, dose, and timing for cell transplantation after stroke are still debated, depending on the chosen cell product and the expected therapeutic effect.

Direct replacement of injured neurons (“homotopic” repair) has been suggested after neural stem cells (NSC) IC administration [17] or intra-arterial (IA) injection [18]. These results were demonstrated by using induced pluripotent stem cells (iPSC) derived neurons [19], bone marrow stromal cells (BMSCs) [20], or embryonic stem cells (ESC) derived mesenchymal stem cells (MSC) injections [21]. However, only a few grafted cells can be expected to express neuronal markers, and long-term graft survival is relatively poor [22–26]. Moreover, despite possible integration of grafted NSCs [27–29] into the host circuitry, functional recovery occurs, too early to be caused by newly formed neurons and synapses.

The effects of cell therapies on poststroke vasculogenesis and angiogenesis seem to be crucial. IC injection of endothelial cells can improve vasculogenesis linked to neurogenesis via vascular endothelial growth factor (VEGF) release mechanisms [30]. Proangiogenic effects were also observed early after MSC injection contributing to VEGF-induced angiogenesis [31], after injection of NSC [32, 33], endothelial progenitor (EP) [34], or cord-blood mononuclear cells CD34+ [35]. Moreover, EP, MSC, or NSC can also facilitate protection or restoration of the blood-brain barrier after stroke [33, 36, 37].

Another important effect of cell therapy is enhancement of glial remodeling and limitations in anterograde degeneration [38–40]. For example, intravenous (IV) injection of MSC has beneficial effects on both poststroke glial remodeling and axonal remyelination [41]. It also increases glial cell-derived

neurotrophic factor (GDNF) levels, creating a hospitable environment for neural repair and neuroblast migration from the subventricular zone (SVZ) [42].

Additionally, cell therapies can limit host cell death through antiapoptotic and immunomodulatory mechanisms. Although MSCs are known to attenuate microglia and leukocyte inflammatory responses after stroke [43–45], some immunomodulatory properties were also observed for cord-blood cells [46] or NSC [47, 48], which can both influence splenic inflammatory responses after stroke [49].

2. Biomaterials as Cell Scaffold to Enhance Cell Graft

An important cell death is reported after IC graft into the damaged area [14, 15]. The use of “carrier” scaffolds is particularly relevant for injections into the stroke cavity at a chronic stage, avoiding a deleterious injection into the adjacent brain tissue where important recovery processes may be underway.

Enhancing the graft survival after IC injection is the common aim of several ongoing experimental strategies. Advances in regenerative medicine are increasingly providing new opportunities to repair damaged tissue by using biomaterials to enhance cell graft. Biomaterials are materials specially developed for use in tissues with the minimum of biological response to the foreign body. Furthermore, biomaterial seems to improve graft cell survival, proliferation, migration, and differentiation, protecting grafted cells from immune response and thus improving cell therapy effects.

A study using matrix gel scaffolding associated with human ESC neuronal precursor cells (NPCs) administrated 3 weeks after an experimental ischemic stroke in rats demonstrated beneficial effects induced by biomaterial coadministration. The effects include cell survival and neuronal differentiation, reduction of infarct volume, and improvement of functional outcome [50].

Biomaterials improve cell survival even if these cells are administrated in the intact brain adjacent to the lesion. A study using a thermoreversible gelation polymer (TGP) as scaffold in MSCs transplantation demonstrated that the association of MSC-TGP significantly improved cell survival [51]. The fate of transplanted MSC was examined 8 weeks after transplantation with immunohistochemistry. The majority of cells were positive for both NeuN and MAP2 [51].

Zhong et al. tested the effects of a Hyaluronan-Heparin-Collagen based hydrogel in cell protection *in vitro* [11]. Stem cell survival was tested under conditions of growth factor and nutritional support and under conditions of stress induced by growth factor and nutrition withdrawal to mimic the initial transplant state. In stem cell cultures with nutrient and growth factor support, the hydrogel modestly but significantly increased survival. In stem cell cultures without such support, the hydrogel substantially increased the survival [11]. Furthermore, they demonstrated that this hydrogel was able to improve the survival of NPCs into the brain cavity after stroke. Additionally, the authors reported a reduction of inflammatory cells infiltration into the graft.

TABLE 1: Examples of biomaterials applications in experimental stroke.

Cells/growth factors	Species/stroke model	Biomaterial	Outcomes	References
hRecombinant osteopontin	Rats tMCAO	Gelatin type A microspheres	↓ of infarct volume neurological deficits	Jin et al. 2014 [122]
rBMSCs	Rats pMCAO	N-Isopropyl- acrylamide polymer sheets	Improvement of motor function	Ito et al. 2014 [87]
Pegylated EGF and EPO	Mice focal ischemia endothelin-1	PEG microparticles PLGA nanoparticles dispersed in a (HAMC) hydrogel	↓ of inflammation, ↓ of infarct volume	Wang et al. 2013 [99]
hNSC	Rats tMCAO	VEGF-PLGA microparticles	Neovascularization, angiogenesis	Bible et al. 2012 [123]
iPS-NPCs	Mice cortical photothrombotic	HA, acrylate	↑ of differentiation to neuroblast	Lam et al. 2014 [95]
hNSC	Rats tMCAO	Xenogeneic (ECM) bioscaffold	Formation of <i>de novo</i> tissue	Bible et al. 2012 [121]
ONO-1301	Rats tMCAO	Subcutaneous (PLGA) microspheres	Neuroprotection and ↓ side effects compared to OA	Hazekawa et al. 2012 [81]
HMGB1	Rats tMCAO	Gelatin microspheres	↓ infarct volume	Jin et al. 2011 [124]
EGF	Mice focal ischemia endothelin-1	PEG microparticles dispersed in a (HAMC) hydrogel	↑ neural stem/progenitor cells	Cooke et al. 2011 [125]
NSC	Rats tMCAO	Collagen type I matrix	↑ synapses and functional recovery	Yu et al. 2010 [57]
hVEGF	Rats tMCAO	Alginate hydrogel	↓ infarct volume ↓ functional deficits	Emerich et al. 2010 [55]

MCAO p or t, permanent or transient middle cerebral artery occlusion; BMSCs, bone marrow stromal cells; EGF, epidermal growth factor; EPO, erythropoietin; SC, stem cells; PEG, polyethylene glycol; HAMC, hyaluronan methylcellulose; h, human; NSC, neural stem cells; VEGF, vascular endothelial growth factor; iPS, induced pluripotent stem; HA, hyaluronic acid; NPCs, neural pluripotent cells; PLGA, poly lactic-co-glycolic acid; OA, oral administration; HMGB1, high-mobility group box 1 protein; ECM, extracellular matrix.

Active microglia/macrophages infiltrating the cell engraftment were significantly decreased with hydrogel [11].

Such as described below (see “Interest of Biomaterials in Cell Therapies”), the inflammatory response is an important step of healing process. Nevertheless, it is recognized that a reduced inflammatory response can result in a more favorable outcome.

Biomaterials alone are able to modulate the inflammatory response. In a cortical brain damage model, a three percent HA gel was coated onto the lesion for the experimental groups and normal saline solutions for the control groups. The results from immunohistological analysis put in evidence a significant reduction of the number of GFAP⁺ cells [52].

The ultimate goal of stroke treatment is the functional recovery. Identifying behavioral deficits in animal models of stroke is essential for potential translational applications [53]. As we noted, regenerative approaches such as cell therapy and administration of trophic factors provide an increase in endogenous brain structural plasticity and motor remapping after ischemia [54]. The use of biomaterials may enhance these functional effects. Emerich et al. have demonstrated that alginate hydrogel used as implant for sustained release of VEGF promotes functional and structural protection from ischemic damage after transient ischemia [55]. The group treated with VEGF-Hydrogel had an important decrease (about 80%) in lesion volume evaluated by

2,3,5-triphenyltetrazolium chloride (TTC) staining. Behavioral analysis using motor asymmetry and neurologic scores demonstrated that recovery is improved by the association of hydrogel-VEGF compared to VEGF alone [55]. Similarly, Guan et al. demonstrated that human MSCs transplanted with collagen scaffolds in a model of brain injury present better outcomes compared to MSC alone [56]. Collagen scaffolds increased the retention of MSC in the lesion site and limited its distribution at the transplanted region resulting in better functional recovery during 4 weeks after transplantation [56]. Another study assessed the combination of NSC and collagen type-I administrated 24 hours after stroke and showed an improvement of the structural and functional recovery [57]. In this study, rats were submitted to a transient ischemia and received a graft of a brain scaffold of collagen type-I seeded with NSC. The evaluation by microscopy showed that, 30 days after transplantation, NSC-collagen group presented new synapses and better functional recovery, while at this time point collagen has been completely degraded [57].

2.1. Interest of Biomaterials in Cell Therapies. Some minutes after blood flow interruption and energetic deprivation, a cascade of cellular and molecular mechanisms are activated resulting in cell death.

Inflammation is initiated by necrosis and tissue injury through the recognition of damage associated molecular

patterns [58]. The process of activation of inflammatory response is currently incompletely understood [59]. Inflammation subserves a number of biological functions and can have both positive and negative consequences [60]. This process is necessary to remove necrotic and apoptotic cells and cleaved extracellular matrix molecules and to initiate angiogenesis and tissue repair [61]. However, exacerbates and chronic inflammation lead to the formation of inhospitable environment for regeneration and cell grafting, resulting in further cell death.

The ischemic lesion promotes changes in extracellular environment such as ECM. The ECM is a three-dimensional, noncellular structure composed of collagens, elastin, proteoglycans (including hyaluronan), and noncollagenous glycoproteins [62] in healthy conditions. ECM macromolecules are bioactive and modulate cellular events such as adhesion, migration, proliferation, differentiation, and survival [63]. During brain ischemia, the basement membranes of blood-brain barrier are degraded and new ECM proteins are deposited in brain parenchyma, either by secretion from activated glia or by leakage of plasma proteins, such as fibrinogen [64]. The significance and consequences of these changes may vary with the time point after injury [13].

Remodeling and repair of brain parenchyma are influenced by ECM composition. Stroke induces alterations in ECM such as increase of proteoglycans [65], inhibition of neurite outgrowth by astrocytic activation [66], and upregulation of matrix-metalloproteinases (MMPs) [62]. These mechanisms can contribute negatively to endogenous remodeling and to the host response to cell therapy.

To enhance structural and functional recovery after stroke, biomaterials protecting grafted cells and/or supporting repair processes such as ECM substitute are currently in development and could be a promising neurorestorative approach.

3. Biomaterials Components

Biomaterials are based on natural or on synthetic compounds used alone or in mixtures, providing a polymer with different properties [67]. The choice of biomaterial is of importance because it can influence biomaterial effectiveness and the response of host tissue. Natural polymers such as hyaluronan, chitosan, and collagen are advantageous because they have already been used in clinical applications as injectable hydrogels such as lubricants, wound sealants, viscosupplements, or filling agents in esthetic medicine [68, 69].

On the other hand, synthetic hydrogels can be engineered to more accurately mimic the physical and mechanical characteristics of ECM [70]. The advantage of synthetic biomaterials is the ability to tightly control the polymerization, degradation, and biocompatibility of hydrogel. Synthetic hydrogels are better chemically defined and in most cases are biologically inert, reducing potential immune reaction into the brain [70]. In this section, we explore some components used in recent studies in experimental stroke.

3.1. Chitosan. Biomaterial can be produced from chitosan, a natural polysaccharide produced by deacetylation of chitin

from crustacean shells [71]. Chitosan-based biomaterials have been used in different applications such as corneal wound healing [72], peripheral nerve injury [73], and mechanical brain injury [74]. In a recent study, chitosan hydrogel coadministered with ESC-derived endothelial cells showed a positive effect by presenting a high cell survival and minimal cytotoxicity *in vitro* [75]. When this chitosan-based hydrogel encapsulating mixed adult and endothelial cells and containing VEGF was implanted into a mouse model of hindlimb ischemia, it induced neovascularization through vasculogenesis and angiogenesis. It also led to recovery of blood flow in ischemic hindlimbs [75]. Ding et al. have demonstrated a most pronounced neuroprotective effect mediated by acetyl-11-keto- β -boswellic acid (AKBA) loaded in O-carboxymethyl chitosan nanoparticles (NPs) when compared to the AKBA only in a rat model of ischemic stroke [76]. The combination AKBA+NPs promoted a functional improvement by reducing infarct volume and apoptosis [76]. However, chitosan-based biomaterials present some disadvantages such as a fast biodegradation *in situ*. Additionally, the compatibility of chitosan with physiological medium depends on the preparation method. Residual proteins could indeed cause allergic reactions [71].

3.2. Hyaluronic Acid (HA). Another promising material is HA, an abundant glycosaminoglycan in the brain ECM [13, 62, 63]. HA is a linear polymer composed of the repeating disaccharide unit of D-glucuronic acid and N-acetyl-D-glucosamine. This polysaccharide plays a key role in many biological processes such as stabilizing the ECM, regulating cell adhesion and motility, and mediating cell proliferation and differentiation [77]. Liang et al. reported an increase in engrafted cells' survival and proliferation of three different cell lines (C17.2 cells, human neural progenitor cells (ReNcells), and human glial-restricted precursors) into a HA-gelatin-polyethylene glycol diacrylate (PEGDA) gel, although a mild inflammatory response towards the implanted hydrogel was observed [8]. As an example, we report here that the same HA hydrogel can be used for MSC transplantation after experimental stroke (Figure 2).

3.3. Poly(Lactic-co-glycolic Acid) (PLGA). PLGA is one of most commonly used biodegradable synthetic polymers for three-dimensional (3D) scaffolds in tissue engineering [78]. The advantage of synthetic polymers is a high control of degradation rate and mechanical properties [79]. PLGA is biocompatible and has been investigated to increase cell survival. NSCs grafted into PLGA slices of 2 mm depth were viable after 14 days of culture [80]. PLGA can be used to produce microspheres for a gradual delivery of cells or drugs [81–83]. Bible et al. optimized the conditions for cell attachment in order to preserve the MHP36 cell line properties in PLGA microspheres [84]. In this experiment, 100–200 μm PLGA microparticles that were modified with poly(allylamine) via plasma polymerization of allylamine and further coated with plasma-derived fibronectin were administered into the lesion cavity (two weeks after stroke). They demonstrated a primitive *de novo* tissue

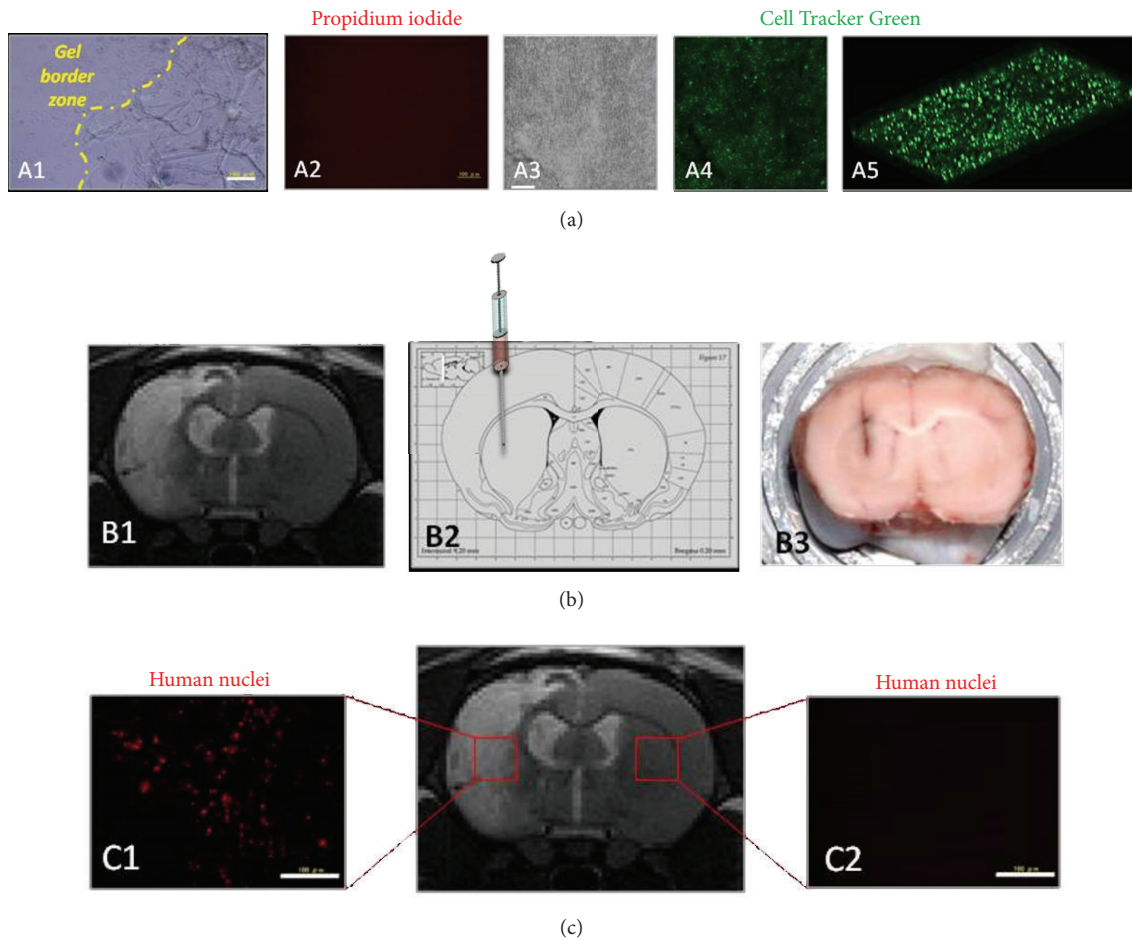


FIGURE 2: Different experimental steps for intracerebral graft of cell-biomaterial after stroke. Scale bar = 100 μm . (a) *In vitro* biocompatibility: after mixing human mesenchymal stem cells (MSC) within hyaluronic acid (HA) hydrogel (Hystem HP, Sigma: hyaluronan+polyethylene glycol diacrylate), MSC survived into the gel during several days in culture (A1) without cell death (A2, propidium iodide cell dead assay). Cell survival and spreading into the HA gel were assessed in one-week culture (A3) using confocal microscopy and confocal microscopy stacks and viable cell labelling (A4 and A5, Cell Tracker Green CMFDA, Life). (b) Intracerebral transplantation: one week after experimental ischemic stroke in rat, magnetic resonance imaging was used to determine the injection site into the stroke cavity near plastic areas surrounding the lesion (B1). Coordinates for stereotactic injection were defined using anatomic atlas (Watson-Paxinos) (B2). By histology, the stereotactic tract can be macroscopically observed (B3, cryostat section). (c) *In vivo* biocompatibility and effects: *ex vivo* brain immunohistology demonstrated cell survival into the graft site such as human MSC identification in stroke lesion (C1, human-specific monoclonal antibody to nuclear antigen, MAB1281, 1/1,000, Chemicon) without cell migration in contralateral hemisphere (C2). Additional experiments must be done to assess long-term cell differentiations and host integration, hydrogel biodegradation, local inflammatory response, and behavior recovery effects.

formation within 7 days [84]. Another interesting study using PLGA microspheres showed that a single subcutaneous administration of ONO-1301 (a long-acting prostacyclin agonist) in PLGA microspheres was able to improve poststroke recovery, edema, and infarct volume in rats [81].

There are some concerns that PLGA degrades into acidic by-products within the brain that may exacerbate inflammation and secondary damage after brain injuries [79]. The less explored poly- ϵ -caprolactone (PCL) polymers might be a safer alternative. PCL induced a lower inflammatory response than PLGA, as demonstrated by lower activated macrophages and glial fibrillary acidic protein (GFAP) expression [85].

4. Mechanical and Physical Properties

Biomaterials can be produced using various types of polymerization and take on distinct forms such as solid scaffolds, hydrogels, or micro/nanoparticles. The choice of biomaterial stiffness depends on the administration site target (brain surface or parenchyma), delay of release intended (gradual or immediate), and the therapeutic goal (Figure 1).

Solid scaffolds require surgery to implant and thus are more suitable for surface application [86, 87]. *In situ* gelling hydrogels and particles can typically be delivered in a minimally invasive manner using a syringe without the need of open surgery [58]. Hydrogel micro/nanoparticles are also suited for protein, gene, and drug delivery [76, 88,

89]. Hydrogels can be used to graft cells and to provide a microenvironment that can be tuned, promoting cell survival and improving function [8, 11, 57] (Figure 1).

4.1. Brain Scaffolds. In a recent study, Hwang et al. used a model of corticectomy to monitor in a noninvasive way by bioluminescence the behavior of stem cells embedded within poly-L-lactic acid (PLLA) scaffold [86]. Human NSCs expressing enhanced firefly luciferase were implanted into the ablated area with or without a PLLA scaffold. They have demonstrated that NSC survived over 14 days compared with 8 days for the nonencapsulated cells [86]. The mechanical strength or stiffness of a hydrogel is named compressive modulus measured in kPa. Solid scaffolds can be projected to present compressive moduli that stimulate cell survival and proliferation [90].

4.2. Injectable Hydrogels. Hydrogels are 3D cross-linked networks of water-soluble polymers [91]. Hydrogel polymers can absorb a high water content up to 99%, due to their hydrophilic nature [70], and can be engineered in a variety of physical forms, including a liquid state for *in situ* cross-linking [8]. They have excellent nutrient and oxygen permeability, allowing cell survival in the scaffold [92]. The most important advantage of this kind of biomaterial is that hydrogels form *in situ* [79], allowing an administration with a minimal invasiveness by injection [8, 11, 68]. The cross-linking process can be induced by temperature [93], pH [94], or addition of a synthetic cross-linker such as PEGDA for HA hydrogel. Besides, hydrogels possess elastic properties that are similar to those of brain tissue. Hydrogels injected in liquid phase usually present low compressive moduli after polymerization, which promotes a stem cell differentiation toward neural lineages [90].

Lam et al. assessed the effect of cell therapy by administering neural progenitor cells derived from iPSC (iPSC-NPC) into the infarct cavity of mice submitted to a cortical photothrombotic stroke. iPSC-NPCs were encapsulated in a HA hydrogel matrix or in PBS [95]. The combination (hydrogel + iPSC-NPC) was able to promote differentiation of the neural progenitor cells to neuroblasts. Despite this good result, it did not increase cell survival one week after transplantation [95]. The hydrogels used in this study were synthesized to contain the adhesion peptide and were cross-linked with either matrix-metalloproteinase (MMP) degradable peptides or non-MMP degradable peptides. The hydrogel was specifically engineered to have a compressive modulus of ~3 kPa because that is the approximate stiffness of the brain [96]. In a recent study, Massensini et al. assessed rheological properties and gelation at body temperature of a biological hydrogel produced from porcine urinary bladder ECM [97]. They performed an efficient MRI-guided injection with drainage of fluid from the cavity to assess *in situ* hydrogel formation and ECM retention at different concentrations. The concentrations superior than 3 mg/mL polymerized within stroke cavity, whereas lower concentrations remained in liquid phase permeating the peri-infarct area.

A downside to hydrogels is that cell migration and outgrowth are often poor due to its weak mechanical structure [79]. Moreover, biodegradation rate is hard to control [98] and must be carefully investigated in the future (see Section 5).

4.3. Microencapsulation. Biomaterials can also be used to encapsulate molecules, cells, cell aggregates, or drugs with the aim of promoting a gradual liberation [88, 99] or graft protection. Molecules or cells encapsulation can be automated to provide a large number of implantable “active” capsules. This could be an alternative to intracerebroventricular injection through the catheter/osmotic minipump systems. This strategy provides a gradual release and a sufficient penetration of growth factors in brain tissue [99]. Nakaguchi et al. have demonstrated an increase in the endogenous neurogenesis in the SVZ of adult mice induced by IC administration of growth factors: insulin-like growth factor 1 and hepatocyte growth factor encapsulated into gelatin hydrogel microspheres [100]. For NSC grafting, Skop et al. optimized multifunctional and biocompatible chitosan-based films and microspheres. Heparin was covalently cross-linked to the chitosan scaffolds which bound fibroblast growth factor-2 (FGF-2) and sustain survival and growth of NSC [101].

4.4. Neural Networks as Potential Strategy. In general way, cell replacement strategies do not take account of the complexity of the brain. Indeed, the cerebral abilities are linked to highly complex connections established between specialized neuroanatomical regions. Replacing lost neurons and extracellular environment does not warrant the restoration of this complex network of axonal tracts. Focusing on this question, alternative biomaterials have been developed with the aim to restore long-distance axonal connections. Replacing lost neurons and extracellular environment does not warrant the restoration of this complex network of axonal tracts. Focusing on this question, alternative biomaterials have been developed with the aim of restoring long-distance axonal connections.

A recent strategy in neural tissue engineering involves the development and application of “living scaffolds,” which are defined as constructs with a controlled, often heterogeneous, and anisotropic 3D cell architecture and biomaterial composition [102]. This living cellular-biomaterial scaffold presents a new form to implant biomaterials and cells. These living scaffolds are able to orientate, give support to, and aid regenerating cells and/or processes (e.g., axons), mimicking crucial aspects of developmental path finding [102]. The cells constitute the “living” component of scaffolds.

A very interesting study of Struzyna et al. [103] using microtissue engineering neural networks for reconstituting the architecture of axonal tracts demonstrates that this approach is effective in promoting survival at least one month and additionally they detected neurite penetration and synapse formation [103]. In this referred study, the microtube was constructed based on an agarose hydrogel and the interior containing extracellular matrix proteins and cerebral cortical neurons and was implanted in healthy rat

brain. This very encouraging result presents a great potential for neuroregenerative therapy and may ultimately facilitate functional recovery if it could be transposed/overlapped in stroke models in the future.

5. Biomaterials Degradation

Many materials formulated for tissue engineering and/or the release of therapeutics are designed to be biodegradable (or bioresorbable) to reduce the complications of tissue scarring and glia tumor formation from permanent implants [70]. Thus, it is necessary to determine the biodegradability of materials *in vitro* and *in vivo* [104]. Independent of their composition (cross-linking reagents and the functional group of HA derivatives), HA hydrogels have variable degradation rate. By example, in Hahn et al., the authors demonstrated that HA hydrogels prepared with three different cross-linking reagents have variable degradation test results [105]. Indeed, adipic acid dihydrazide grafted HA (HA-ADH), methacrylated HA (HA-MA), thiolated HA (HA-SH) were compared and according to *in vitro* degradation tests, HA-SH hydrogel was degraded very fast, compared to HA-ADH and HA-MA hydrogels and HA-ADH hydrogel was degraded slightly faster than HA-MA hydrogel. Moreover, when HA-MA hydrogels and HA-SH hydrogels are implanted in the back of rats, HA-SH hydrogel was *in vivo* degraded completely only in 2 weeks, whereas HA-MA hydrogels were degraded only partially even in 29 days. There was no adverse effect during the *in vivo* tests.

6. Biocompatibilities with Therapeutic Cells and Host Tissue

Brain is mostly isolated from the periphery by the blood-barrier. It has a similar but slightly different response to tissue damage and foreign materials [70]. The use of biomaterials, such as hydrogels, as neural cell delivery devices is becoming more common in areas of research such as stroke, traumatic brain injury, and spinal cord injury.

When reviewing the available research, there is some ambiguity in the type of materials used and results are often at odds. Hydrogels must be designed to be biocompatible with the implanted cells [106] and with the tissue environment. *In vitro* cultures of embedded cells to assess cell compatibility and functionality must be done prior to *in vivo* graft (Figure 1). 3D cultures can be useful to precise cell location and cell distribution into a gel.

In vivo, a wide variety of synthetic polymers have been shown to be biocompatible in the body, such as polyesters and acrylates [107–110]. Natural polymers, such as poly(amino acids) and HA, have been modified to form biocompatible hydrogels. Polymeric hydrogels placed into a fimbria-fornix lesion cavity promote fiber (re)growth in morphological study in the rat [111–114]. This biocompatibility refers to the histocompatibility of an implanted hydrogel and the local and systemic response of the host which includes the inflammatory and immune reaction of the brain [70]. Implanted biomaterials promote a foreign body response. This inflammatory response presents a variable level which varies depending on the material choice and the site of

implantation [115]. After implantation, a biomaterial acquires a layer of host proteins that is associated with the surface chemistry of material [58].

Brain tissue engineering in the postinjury brain represents a promising option for cell replacement and rescue, providing a cell scaffold for transplanted or resident cells. But a number of natural biomaterials have intrinsic anti-inflammatory properties, including HA and chitosan [116]. Thus, they are suitable as carriers for anti-inflammatory therapeutics. However, synthetic materials are also capable of acting in an anti-inflammatory way. Zhong et al. have demonstrated a beneficial effect of a hyaluronan-heparin-collagen hydrogel by promoting the survival of ES-NPCs and by reducing inflammatory infiltration of the graft with the hydrogel transplant [11]. However, further optimization of hydrogel compositions is warranted to avoid possible inflammatory responses such as those observed in immunocompetent mouse brain 2 weeks after IC injection of a HA hydrogel preseeded with human NSCs or glial precursors [8]. Indeed, HA degradation is facilitated in inflammation and injury by the production of reactive oxygen and nitrogen species [77, 117]. HA is degraded *in vivo* by hyaluronidases (HAases) into shorter fragments. However, the extent of HA degradation that occurs under pathological conditions may be greatly enhanced.

7. Imaging of Biomaterials Engraftment

Clinical studies can benefit from noninvasive methods to assess brain stroke. Experimental studies also have used noninvasive imaging techniques to monitor grafted cells distribution and their effects on brain tissue [118]. Several imaging techniques such as MRI [31], positron emission tomography (PET) [119], and nuclear imaging [9] have been used to track transplanted cells *in vivo*. Imaging modalities with precise anatomical information like MRI can be used to evaluate the lesion size and extension and to precisely guide biomaterial administration. Furthermore, recent advances using multiparametric MRI enable longitudinal monitoring of vascular remodeling [7, 120] and brain function by using functional MRI.

Bible et al., for example, have demonstrated that NSCs coadministered with ECM bioscaffold produced from porcine brain and urinary bladder promote the formation of *de novo* tissue in the lesion cavity and repair processes after ischemic stroke evaluated by MRI [121]. Noninvasive imaging by MRI was used to guide the administration of biomaterials in a similar study [97].

Noninvasive evaluations are a powerful tool for determining the efficacy of the combination biomaterials with cell therapy, allowing a validation of biomaterial application by a correlation of *in vivo* images and histological findings (Figure 3).

8. Conclusion

The use of biomaterials for stroke therapy provides a promising avenue for cell transplantation, especially in the brain where the regenerative properties can be limited.

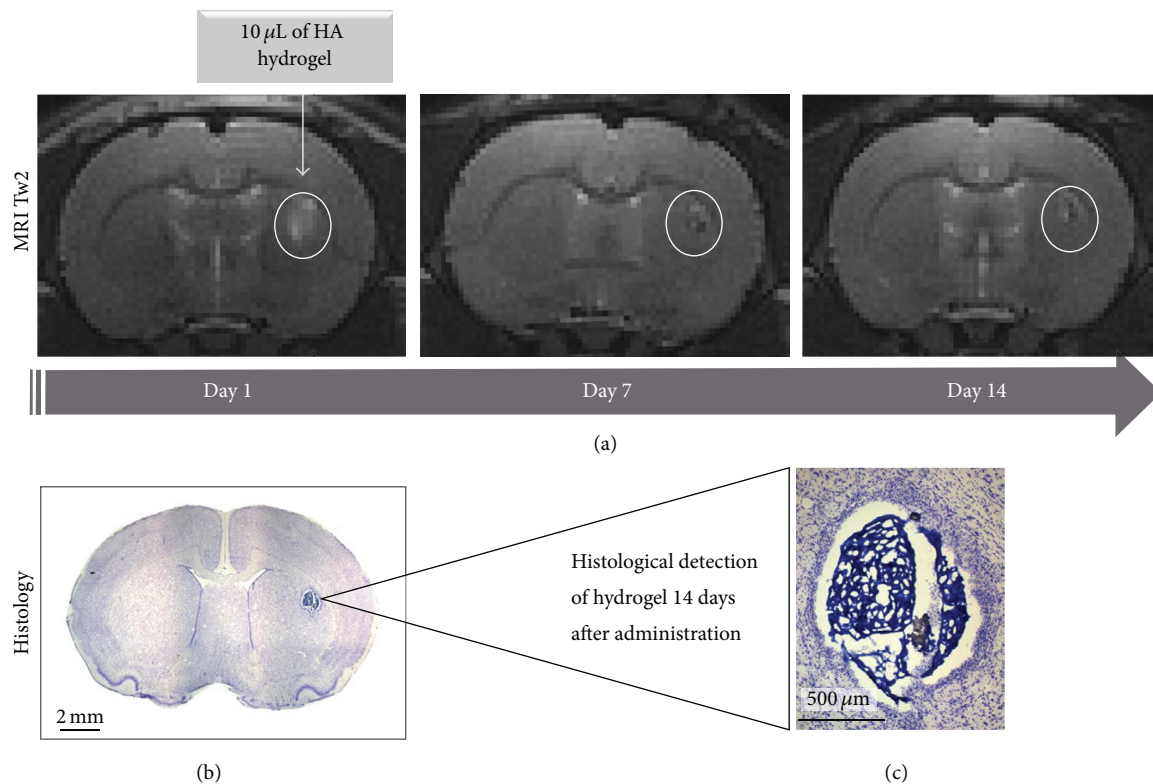


FIGURE 3: Representative images of *in vivo* and *ex vivo* detection of hyaluronan-acid (HA) hydrogel. (a) Magnetic Resonance Imaging (MRI) weighed in T₂, hydrogel detected at different time points (days one, seven, and fourteen after administration). (b) Cresyl violet staining of HA hydrogel acquired two weeks after administration, noted in ($\times 2$) (b) and (c) ($\times 10$) magnification. These images demonstrate efficient local gel formation instead of liquid diffusion which would be due to a delayed polymerization after infusion and the *in vivo* stability of HA hydrogel.

However, the choice of biomaterial compounds and properties must be adapted, according to biocompatibilities with embedded cells and host tissue and to biodegradation rate. Thus, collaborations between bioengineering researchers and neuroscientists are required to validate and optimize preclinical experiments. Purification of biomaterials is imperative for safe use in humans. Therefore, it requires rigorous tests of cytotoxicity. Important aspects such as reproducibility, correlation with behavioral outcomes, and a long-term assessment of biomaterials degradation should be considered before clinical translation.

Hydrogels could be used to enhance cell transplantation benefit in patients by stereotactic injection of liquid hydrogel with *in situ* polymerization, or by surgical graft of stiffer cell-biomaterial layers, for example, during a hemicraniectomy for large stroke or during subsequent reparative cranioplasty. An appropriate follow-up with a noninvasive brain imaging to track hydrogel degradation and brain remodeling is strongly indicated.

Abbreviations

ADH: Adipic acid dihydrazide
 AKBA: Acetyl-11-keto- β boswellic acid
 BBB: Blood-brain barrier
 BMSC: Bone marrow stromal cells
 CCL-2: Chemokine ligand 2

ECM: Extracellular matrix
 EGF: Epidermal growth factor
 EP: Endothelial progenitor
 EPO: Erythropoietin
 ESC: Embryonic stem cells
 FGF-2: Fibroblast growth factor type 2
 GDNF: Glial cell-derived neurotrophic factor
 GFAP: Glial fibrillary acidic protein
 h: Human
 HA: Hyaluronic acid
 HAMC: Hyaluronan methylcellulose
 HGF: Hepatocyte growth factor
 HMGB1: High-mobility group box 1 protein
 HMW: High molecular weight
 IA: Intra-arterial
 IC: Intracerebral
 IGF1: Insulin-like growth factor 1
 IL-12: Interleukin-12
 iNOS: Inducible nitric oxide synthase
 iPSC: Induced pluripotent stem cells
 IV: Intravenous
 kPa: Kilopascals
 LMW: Low molecular weight
 MA: Methacrylated
 MCAo: Middle cerebral artery occlusion
 MIP-1 α : Macrophage inflammatory protein

MSC: Mesenchymal stem cells
 NPC: Neural progenitor cell
 NSC: Neural stem cells
 PBS: Phosphate buffered saline
 PEG: Polyethylene glycol
 PEGDA: Polyethylene glycol diacrylate
 PLC: Poly- ϵ -caprolactone
 PLD: Poly-D-lysine
 PLLA: Poly-L-lactic acid
 SC: Stem cells
 SH: Thiolated
 SVZ: Subventricular zone
 TNF- α : Tumoral necrosis factor
 TTC: 2,3,5-Triphenyltetrazolium chloride
 VEGF: Vascular endothelial growth factor.

Competing Interests

The authors declare that they have no competing interests.

References

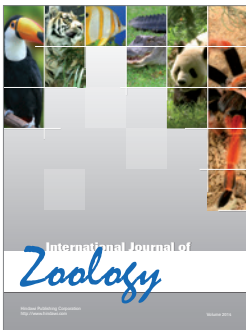
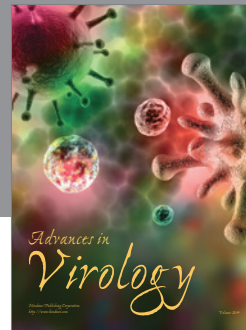
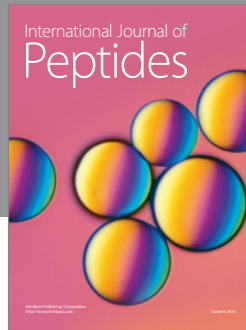
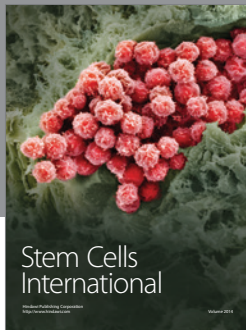
- [1] C. C. Beal, "Gender and stroke symptoms: a review of the current literature," *The Journal of Neuroscience Nursing*, vol. 42, no. 2, pp. 80–87, 2010.
- [2] H.-R. Wang, M. Chen, F.-L. Wang et al., "Comparison of therapeutic effect of recombinant tissue plasminogen activator by treatment time after onset of acute ischemic stroke," *Scientific Reports*, vol. 5, Article ID 11743, 2015.
- [3] P. W. Duncan, R. Zorowitz, B. Bates et al., "Management of adult stroke rehabilitation care: a clinical practice guideline," *Stroke*, vol. 36, no. 9, pp. e100–e143, 2005.
- [4] O. Detante, A. Jaillard, A. Moisan et al., "Biotherapies in stroke," *Revue Neurologique*, vol. 170, no. 12, pp. 779–798, 2014.
- [5] L. Pellegrini, Y. Bennis, B. Guillet, L. Velly, N. Bruder, and P. Pisano, "La thérapie cellulaire de l'accident vasculaire cérébral ischémique: du mythe à la réalité," *Revue Neurologique*, vol. 169, no. 4, pp. 291–306, 2013.
- [6] M. Castillo-Melendez, T. Yawno, G. Jenkin, and S. L. Miller, "Stem cell therapy to protect and repair the developing brain: a review of mechanisms of action of cord blood and amnion epithelial derived cells," *Frontiers in Neuroscience*, vol. 7, article 194, 2013.
- [7] A. Moisan, I. M. Favre, C. Rome et al., "Microvascular plasticity after experimental stroke: a molecular and MRI study," *Cerebrovascular Diseases*, vol. 38, no. 5, pp. 344–353, 2014.
- [8] Y. Liang, P. Walczak, and J. W. M. Bulte, "The survival of engrafted neural stem cells within hyaluronic acid hydrogels," *Biomaterials*, vol. 34, no. 22, pp. 5521–5529, 2013.
- [9] O. Detante, A. Moisan, J. Dimastromatteo et al., "Intravenous administration of mTc^{99m}-HMPAO-labeled human mesenchymal stem cells after stroke: in vivo imaging and biodistribution," *Cell Transplantation*, vol. 18, no. 12, pp. 1369–1379, 2009.
- [10] Y. Wu, J. Wu, R. Ju, Z. Chen, and Q. Xu, "Comparison of intracerebral transplantation effects of different stem cells on rodent stroke models," *Cell Biochemistry and Function*, vol. 33, no. 4, pp. 174–182, 2015.
- [11] J. Zhong, A. Chan, L. Morad, H. I. Kornblum, G. Fan, and S. T. Carmichael, "Hydrogel matrix to support stem cell survival after brain transplantation in stroke," *Neurorehabilitation and Neural Repair*, vol. 24, no. 7, pp. 636–644, 2010.
- [12] S. T. Carmichael, "Cellular and molecular mechanisms of neural repair after stroke: making waves," *Annals of Neurology*, vol. 59, no. 5, pp. 735–742, 2006.
- [13] K. M. Baeten and K. Akassoglou, "Extracellular matrix and matrix receptors in blood-brain barrier formation and stroke," *Developmental Neurobiology*, vol. 71, no. 11, pp. 1018–1039, 2011.
- [14] T. Bliss, R. Guzman, M. Daadi, and G. K. Steinberg, "Cell transplantation therapy for stroke," *Stroke*, vol. 38, no. 2, pp. 817–826, 2007.
- [15] A. Bakshi, C. A. Keck, V. S. Koshkin et al., "Caspase-mediated cell death predominates following engraftment of neural progenitor cells into traumatically injured rat brain," *Brain Research*, vol. 1065, no. 1-2, pp. 8–19, 2005.
- [16] P. Jendelová, Š. Kubinová, I. Sandvig, S. Erceg, A. Sandvig, and E. Syková, "Current developments in cell- and biomaterial-based approaches for stroke repair," *Expert Opinion on Biological Therapy*, vol. 16, no. 1, pp. 43–56, 2015.
- [17] S. Kelly, T. M. Bliss, A. K. Shah et al., "Transplanted human fetal neural stem cells survive, migrate, and differentiate in ischemic rat cerebral cortex," *Proceedings of the National Academy of Sciences of the United States of America*, vol. 101, no. 32, pp. 11839–11844, 2004.
- [18] S. Rosenblum, N. Wang, T. N. Smith et al., "Timing of intra-arterial neural stem cell transplantation after hypoxia-ischemia influences cell engraftment, survival, and differentiation," *Stroke*, vol. 43, no. 6, pp. 1624–1631, 2012.
- [19] D. Tornero, S. Wattananit, M. Grønning Madsen et al., "Human induced pluripotent stem cell-derived cortical neurons integrate in stroke-injured cortex and improve functional recovery," *Brain*, vol. 136, no. 12, pp. 3561–3577, 2013.
- [20] B. J. Crain, S. D. Tran, and E. Mezey, "Transplanted human bone marrow cells generate new brain cells," *Journal of the Neurological Sciences*, vol. 233, no. 1-2, pp. 121–123, 2005.
- [21] Y.-P. Liu, H. Seçkin, Y. Zci, Z. W. Du, Y.-P. Yan, and M. K. Başkaya, "Neuroprotective effects of mesenchymal stem cells derived from human embryonic stem cells in transient focal cerebral ischemia in rats," *Journal of Cerebral Blood Flow and Metabolism*, vol. 29, no. 4, pp. 780–791, 2009.
- [22] J. Chen, Y. Li, L. Wang et al., "Therapeutic benefit of intravenous administration of bone marrow stromal cells after cerebral ischemia in rats," *Stroke*, vol. 32, no. 4, pp. 1005–1011, 2001.
- [23] D. Lu, P. R. Sanberg, A. Mahmood et al., "Intravenous administration of human umbilical cord blood reduces neurological deficit in the rat after traumatic brain injury," *Cell Transplantation*, vol. 11, no. 3, pp. 275–281, 2002.
- [24] L. H. Shen, Y. Li, J. Chen et al., "One-year follow-up after bone marrow stromal cell treatment in middle-aged female rats with stroke," *Stroke*, vol. 38, no. 7, pp. 2150–2156, 2007.
- [25] L. H. Shen, Y. Li, J. Chen et al., "Therapeutic benefit of bone marrow stromal cells administered 1 month after stroke," *Journal of Cerebral Blood Flow and Metabolism*, vol. 27, no. 1, pp. 6–13, 2007.
- [26] P. Ramos-Cabrer, C. Justicia, D. Wiedermann, and M. Hoehn, "Stem cell mediation of functional recovery after stroke in the rat," *PLoS ONE*, vol. 5, no. 9, Article ID e12779, 11 pages, 2010.
- [27] U. Englund, A. Björklund, K. Victorin, O. Lindvall, and M. Kokaia, "Grafted neural stem cells develop into functional pyramidal neurons and integrate into host cortical circuitry," *Proceedings of the National Academy of Sciences of the United States of America*, vol. 99, no. 26, pp. 17089–17094, 2002.

- [28] S. Ishibashi, M. Sakaguchi, T. Kuroiwa et al., "Human neural stem/progenitor cells, expanded in long-term neurosphere culture, promote functional recovery after focal ischemia in Mongolian gerbils," *Journal of Neuroscience Research*, vol. 78, no. 2, pp. 215–223, 2004.
- [29] M. M. Daadi, S. H. Lee, A. Arac et al., "Functional engraftment of the medial ganglionic eminence cells in experimental stroke model," *Cell Transplantation*, vol. 18, no. 7, pp. 815–826, 2009.
- [30] H. Ishikawa, N. Tajiri, K. Shinozuka et al., "Vasculogenesis in experimental stroke after human cerebral endothelial cell transplantation," *Stroke*, vol. 44, no. 12, pp. 3473–3481, 2013.
- [31] A. Moisan, N. Pannetier, E. Grillon et al., "Intracerebral injection of human mesenchymal stem cells impacts cerebral microvasculature after experimental stroke: MRI study," *NMR in Biomedicine*, vol. 25, no. 12, pp. 1340–1348, 2012.
- [32] T. Roitbak, L. Li, and L. A. Cunningham, "Neural stem/progenitor cells promote endothelial cell morphogenesis and protect endothelial cells against ischemia via HIF-1 α -regulated VEGF signaling," *Journal of Cerebral Blood Flow and Metabolism*, vol. 28, no. 9, pp. 1530–1542, 2008.
- [33] N. Horie, M. P. Pereira, K. Niizuma et al., "Transplanted stem cell-secreted vascular endothelial growth factor effects poststroke recovery, inflammation, and vascular repair," *Stem Cells*, vol. 29, no. 2, pp. 274–285, 2011.
- [34] A. Rosell, A. Morancho, M. Navarro-Sobrinho et al., "Factors secreted by endothelial progenitor cells enhance neurorepair responses after cerebral ischemia in mice," *PLoS ONE*, vol. 8, no. 9, Article ID e73244, 2013.
- [35] A. Taguchi, T. Soma, H. Tanaka et al., "Administration of CD34+ cells after stroke enhances neurogenesis via angiogenesis in a mouse model," *The Journal of Clinical Investigation*, vol. 114, no. 3, pp. 330–338, 2004.
- [36] C. V. Borlongan, J. G. Lind, O. Dillon-Carter et al., "Bone marrow grafts restore cerebral blood flow and blood brain barrier in stroke rats," *Brain Research*, vol. 1010, no. 1–2, pp. 108–116, 2004.
- [37] K. Shinozuka, T. Dailey, N. Tajiri, H. Ishikawa, Y. Kaneko, and C. Borlongan, "Stem cell transplantation for neuroprotection in stroke," *Brain Sciences*, vol. 3, no. 1, pp. 239–261, 2013.
- [38] Q. Gao, Y. Li, and M. Chopp, "Bone marrow stromal cells increase astrocyte survival via upregulation of phosphoinositide 3-kinase/threonine protein kinase and mitogen-activated protein kinase/extracellular signal-regulated kinase pathways and stimulate astrocyte trophic factor gene expression after anaerobic insult," *Neuroscience*, vol. 136, no. 1, pp. 123–134, 2005.
- [39] M. Chopp, Y. Li, and Z. G. Zhang, "Mechanisms underlying improved recovery of neurological function after stroke in the rodent after treatment with neurorestorative cell-based therapies," *Stroke*, vol. 40, no. 3, supplement, pp. S143–S145, 2009.
- [40] Y. Li, Z. Liu, H. Xin, and M. Chopp, "The role of astrocytes in mediating exogenous cell-based restorative therapy for stroke," *Glia*, vol. 62, no. 1, pp. 1–16, 2014.
- [41] Y. Li, K. McIntosh, J. Chen et al., "Allogeneic bone marrow stromal cells promote glial-axonal remodeling without immunologic sensitization after stroke in rats," *Experimental Neurology*, vol. 198, no. 2, pp. 313–325, 2006.
- [42] L. H. Shen, Y. Li, and M. Chopp, "Astrocytic endogenous glial cell derived neurotrophic factor production is enhanced by bone marrow stromal cell transplantation in the ischemic boundary zone after stroke in adult rats," *Glia*, vol. 58, no. 9, pp. 1074–1081, 2010.
- [43] Y. Li, J. Chen, C. L. Zhang et al., "Gliosis and brain remodeling after treatment of stroke in rats with marrow stromal cells," *Glia*, vol. 49, no. 3, pp. 407–417, 2005.
- [44] H. Ohtaki, J. H. Ylostalo, J. E. Foraker et al., "Stem/progenitor cells from bone marrow decrease neuronal death in global ischemia by modulation of inflammatory/immune responses," *Proceedings of the National Academy of Sciences of the United States of America*, vol. 105, no. 38, pp. 14638–14643, 2008.
- [45] A. M. Sheikh, A. Nagai, K. Wakabayashi et al., "Mesenchymal stem cell transplantation modulates neuroinflammation in focal cerebral ischemia: contribution of fractalkine and IL-5," *Neurobiology of Disease*, vol. 41, no. 3, pp. 717–724, 2011.
- [46] M. Vendrame, C. Gemma, D. de Mesquita et al., "Anti-inflammatory effects of human cord blood cells in a rat model of stroke," *Stem Cells and Development*, vol. 14, no. 5, pp. 595–604, 2005.
- [47] G. Martino and S. Pluchino, "The therapeutic potential of neural stem cells," *Nature Reviews. Neuroscience*, vol. 7, no. 5, pp. 395–406, 2006.
- [48] T. Ben-Hur, "Immunomodulation by neural stem cells," *Journal of the Neurological Sciences*, vol. 265, no. 1–2, pp. 102–104, 2008.
- [49] S.-T. Lee, K. Chu, K.-H. Jung et al., "Anti-inflammatory mechanism of intravascular neural stem cell transplantation in haemorrhagic stroke," *Brain*, vol. 131, no. 3, pp. 616–629, 2008.
- [50] K. Jin, X. Mao, L. Xie et al., "Transplantation of human neural precursor cells in Matrigel scaffolding improves outcome from focal cerebral ischemia after delayed postischemic treatment in rats," *Journal of Cerebral Blood Flow and Metabolism*, vol. 30, no. 3, pp. 534–544, 2010.
- [51] T. Osanai, S. Kuroda, H. Yasuda et al., "Noninvasive transplantation of bone marrow stromal cells for ischemic stroke: preliminary study with a thermoreversible gelation polymer hydrogel," *Neurosurgery*, vol. 66, no. 6, pp. 1140–1147, 2010.
- [52] C.-M. Lin, J.-W. Lin, Y.-C. Chen et al., "Hyaluronic acid inhibits the glial scar formation after brain damage with tissue loss in rats," *Surgical Neurology*, vol. 72, supplement 2, pp. S50–S54, 2009.
- [53] K. L. Schaar, M. M. Brenneman, and S. I. Savitz, "Functional assessments in the rodent stroke model," *Experimental and Translational Stroke Medicine*, vol. 2, article 13, 2010.
- [54] W. Lv, W.-Y. Li, X.-Y. Xu, H. Jiang, and O. Y. Bang, "Bone marrow mesenchymal stem cells transplantation promotes the release of endogenous erythropoietin after ischemic stroke," *Neural Regeneration Research*, vol. 10, no. 8, pp. 1265–1270, 2015.
- [55] D. F. Emerich, E. Silva, O. Ali et al., "Injectable VEGF hydrogels produce near complete neurological and anatomical protection following cerebral ischemia in rats," *Cell Transplantation*, vol. 19, no. 9, pp. 1063–1071, 2010.
- [56] J. Guan, Z. Zhu, R. C. Zhao et al., "Transplantation of human mesenchymal stem cells loaded on collagen scaffolds for the treatment of traumatic brain injury in rats," *Biomaterials*, vol. 34, no. 24, pp. 5937–5946, 2013.
- [57] H. Yu, B. Cao, M. Feng et al., "Combinated transplantation of neural stem cells and collagen type I promote functional recovery after cerebral ischemia in rats," *The Anatomical Record: Advances in Integrative Anatomy and Evolutionary Biology*, vol. 293, no. 5, pp. 911–917, 2010.
- [58] S. Browne and A. Pandit, "Biomaterial-mediated modification of the local inflammatory environment," *Frontiers in Bioengineering and Biotechnology*, vol. 3, article 67, 2015.

- [59] H. Kataoka, H. Kono, Z. Patel, and K. L. Rock, "Evaluation of the contribution of multiple DAMPs and DAMP receptors in cell death-induced sterile inflammatory responses," *PLoS ONE*, vol. 9, no. 8, Article ID e104741, 2014.
- [60] K. L. Rock, J.-J. Lai, and H. Kono, "Innate and adaptive immune responses to cell death," *Immunological Reviews*, vol. 243, no. 1, pp. 191–205, 2011.
- [61] B. Jiang and R. Liao, "The paradoxical role of inflammation in cardiac repair and regeneration," *Journal of Cardiovascular Translational Research*, vol. 3, no. 4, pp. 410–416, 2010.
- [62] C. Bonnans, J. Chou, and Z. Werb, "Remodelling the extracellular matrix in development and disease," *Nature Reviews Molecular Cell Biology*, vol. 15, no. 12, pp. 786–801, 2014.
- [63] W. P. Daley, S. B. Peters, and M. Larsen, "Extracellular matrix dynamics in development and regenerative medicine," *Journal of Cell Science*, vol. 121, no. 3, pp. 255–264, 2008.
- [64] C. Schachtrup, J. K. Ryu, M. J. Helmrick et al., "Fibrinogen triggers astrocyte scar formation by promoting the availability of active TGF-beta after vascular damage," *The Journal of Neuroscience*, vol. 30, no. 17, pp. 5843–5854, 2010.
- [65] M. Pyka, C. Wetzel, A. Aguado, M. Geissler, H. Hatt, and A. Faissner, "Chondroitin sulfate proteoglycans regulate astrocyte-dependent synaptogenesis and modulate synaptic activity in primary embryonic hippocampal neurons," *European Journal of Neuroscience*, vol. 33, no. 12, pp. 2187–2202, 2011.
- [66] A. Klausmeyer, R. Conrad, A. Faissner, and S. Wiese, "Influence of glial-derived matrix molecules, especially chondroitin sulfates, on neurite growth and survival of cultured mouse embryonic motoneurons," *Journal of Neuroscience Research*, vol. 89, no. 2, pp. 127–141, 2011.
- [67] G. J.-R. Delcroix, P. C. Schiller, J.-P. Benoit, and C. N. Montero-Menei, "Adult cell therapy for brain neuronal damages and the role of tissue engineering," *Biomaterials*, vol. 31, no. 8, pp. 2105–2120, 2010.
- [68] M. M. Pakulska, B. G. Ballios, and M. S. Shoichet, "Injectable hydrogels for central nervous system therapy," *Biomedical Materials*, vol. 7, no. 2, Article ID 024101, 2012.
- [69] L. Robert, "Hyaluronan, a truly 'youthful' polysaccharide. Its medical applications," *Pathologie Biologie*, vol. 63, no. 1, pp. 32–34, 2015.
- [70] E. R. Aurand, K. J. Lampe, and K. B. Bjugstad, "Defining and designing polymers and hydrogels for neural tissue engineering," *Neuroscience Research*, vol. 72, no. 3, pp. 199–213, 2012.
- [71] F. Croisier and C. Jérôme, "Chitosan-based biomaterials for tissue engineering," *European Polymer Journal*, vol. 49, no. 4, pp. 780–792, 2013.
- [72] C.-Y. Tsai, L.-C. Woung, J.-C. Yen et al., "Thermosensitive chitosan-based hydrogels for sustained release of ferulic acid on corneal wound healing," *Carbohydrate Polymers*, vol. 135, pp. 308–315, 2016.
- [73] K. Nawrotek, M. Tylman, K. Rudnicka, J. Balcerzak, and K. Kamiński, "Chitosan-based hydrogel implants enriched with calcium ions intended for peripheral nervous tissue regeneration," *Carbohydrate Polymers*, vol. 136, pp. 764–771, 2016.
- [74] L. Mo, Z. Yang, A. Zhang, and X. Li, "The repair of the injured adult rat hippocampus with NT-3-chitosan carriers," *Biomaterials*, vol. 31, no. 8, pp. 2184–2192, 2010.
- [75] S. Lee, C. M. Valmikinathan, J. Byun et al., "Enhanced therapeutic neovascularization by CD31-expressing cells and embryonic stem cell-derived endothelial cells engineered with chitosan hydrogel containing VEGF-releasing microtubes," *Biomaterials*, vol. 63, pp. 158–167, 2015.
- [76] Y. Ding, Y. Qiao, M. Wang et al., "Enhanced neuroprotection of acetyl-11-keto- β -boswellic acid (AKBA)-loaded O-carboxymethyl chitosan nanoparticles through antioxidant and anti-inflammatory pathways," *Molecular Neurobiology*, 2015.
- [77] P. Moshayedi and S. T. Carmichael, "Hyaluronan, neural stem cells and tissue reconstruction after acute ischemic stroke," *Biomatter*, vol. 3, no. 1, 2013.
- [78] P. Gentile, V. Chiono, I. Carmagnola, and P. V. Hatton, "An overview of poly(lactic-co-glycolic) Acid (PLGA)-based biomaterials for bone tissue engineering," *International Journal of Molecular Sciences*, vol. 15, no. 3, pp. 3640–3659, 2014.
- [79] N. B. Skop, F. Calderon, C. H. Cho, C. D. Gandhi, and S. W. Levison, "Improvements in biomaterial matrices for neural precursor cell transplantation," *Molecular and Cellular Therapies*, vol. 2, article 19, 2014.
- [80] Y. Xiong, Y.-S. Zeng, C.-G. Zeng et al., "Synaptic transmission of neural stem cells seeded in 3-dimensional PLGA scaffolds," *Biomaterials*, vol. 30, no. 22, pp. 3711–3722, 2009.
- [81] M. Hazekawa, Y. Sakai, M. Yoshida, T. Haraguchi, and T. Uchida, "Single injection of ONO-1301-loaded PLGA microspheres directly after ischaemia reduces ischaemic damage in rats subjected to middle cerebral artery occlusion," *Journal of Pharmacy and Pharmacology*, vol. 64, no. 3, pp. 353–359, 2012.
- [82] D. Klose, M. Laprais, V. Leroux et al., "Fenofibrate-loaded PLGA microparticles: effects on ischemic stroke," *European Journal of Pharmaceutical Sciences*, vol. 37, no. 1, pp. 43–52, 2009.
- [83] Y. Wang, Y. T. Wei, Z. H. Zu et al., "Combination of hyaluronic acid hydrogel scaffold and PLGA microspheres for supporting survival of neural stem cells," *Pharmaceutical Research*, vol. 28, no. 6, pp. 1406–1414, 2011.
- [84] E. Bible, D. Y. S. Chau, M. R. Alexander, J. Price, K. M. Shakesheff, and M. Modo, "The support of neural stem cells transplanted into stroke-induced brain cavities by PLGA particles," *Biomaterials*, vol. 30, no. 16, pp. 2985–2994, 2009.
- [85] D. Y. Wong, S. J. Hollister, P. H. Krebsbach, and C. Nosrat, "Poly(ϵ -Caprolactone) and poly (L-Lactic-Co-Glycolic Acid) degradable polymer sponges attenuate astrocyte response and lesion growth in acute traumatic brain injury," *Tissue Engineering*, vol. 13, no. 10, pp. 2515–2523, 2007.
- [86] D. W. Hwang, Y. Jin, D. H. Lee et al., "In vivo bioluminescence imaging for prolonged survival of transplanted human neural stem cells using 3D biocompatible scaffold in corticectomized rat model," *PLoS ONE*, vol. 9, no. 9, Article ID e105129, 2014.
- [87] M. Ito, H. Shichinohe, K. Houkin, and S. Kuroda, "Application of cell sheet technology to bone marrow stromal cell transplantation for rat brain infarct," *Journal of Tissue Engineering and Regenerative Medicine*, 2014.
- [88] M. J. Caicco, M. J. Cooke, Y. Wang, A. Tuladhar, C. M. Morshead, and M. S. Shoichet, "A hydrogel composite system for sustained epi-cortical delivery of Cyclosporin A to the brain for treatment of stroke," *Journal of Controlled Release*, vol. 166, no. 3, pp. 197–202, 2013.
- [89] S. N. Tzouanas, A. K. Ekensear, F. K. Kasper, and A. G. Mikos, "Mesenchymal stem cell and gelatin microparticle encapsulation in thermally and chemically gelling injectable hydrogels for tissue engineering," *Journal of Biomedical Materials Research Part A*, vol. 102, no. 5, pp. 1222–1230, 2014.
- [90] A. Banerjee, M. Arha, S. Choudhary et al., "The influence of hydrogel modulus on the proliferation and differentiation of encapsulated neural stem cells," *Biomaterials*, vol. 30, no. 27, pp. 4695–4699, 2009.

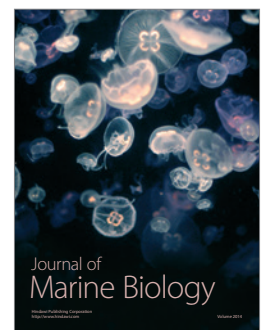
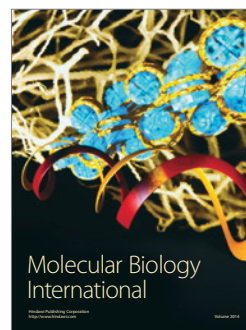
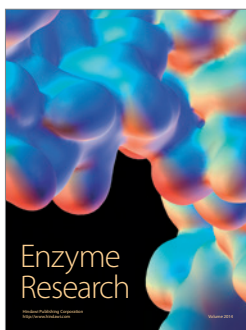
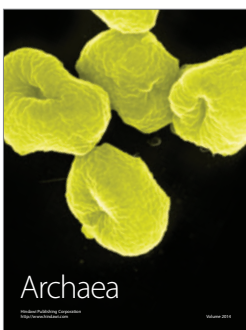
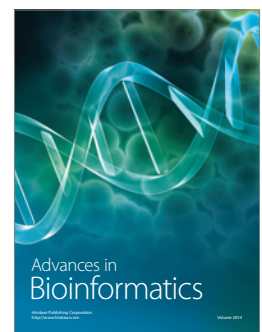
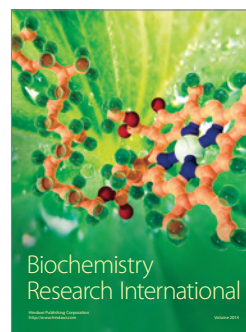
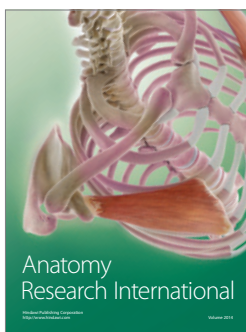
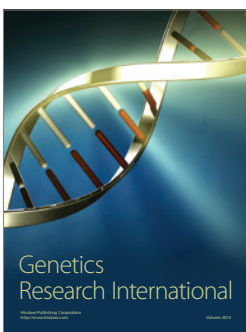
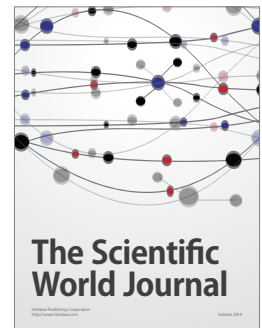
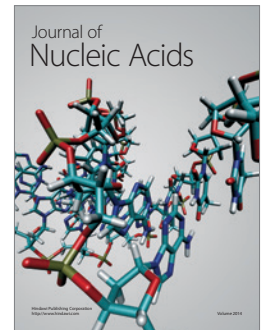
- [91] T. R. Hoare and D. S. Kohane, "Hydrogels in drug delivery: progress and challenges," *Polymer*, vol. 49, no. 8, pp. 1993–2007, 2008.
- [92] D. R. Nisbet, K. E. Crompton, M. K. Horne, D. I. Finkelstein, and J. S. Forsythe, "Neural tissue engineering of the CNS using hydrogels," *Journal of Biomedical Materials Research—Part B Applied Biomaterials*, vol. 87, no. 1, pp. 251–263, 2008.
- [93] J.-C. Yeh, Y.-T. Hsu, C.-M. Su, M.-C. Wang, T.-H. Lee, and S.-L. Lou, "Preparation and characterization of biocompatible and thermoresponsive micelles based on poly(*N*-isopropylacrylamide-co-*N,N*-dimethylacrylamide) grafted on polysuccinimide for drug delivery," *Journal of Biomaterials Applications*, vol. 29, no. 3, pp. 442–453, 2014.
- [94] D. H. Kim, Y. K. Seo, T. Thambi et al., "Enhancing neurogenesis and angiogenesis with target delivery of stromal cell derived factor-1 α using a dual ionic pH-sensitive copolymer," *Biomaterials*, vol. 61, pp. 115–125, 2015.
- [95] J. Lam, W. E. Lowry, S. T. Carmichael, and T. Segura, "Delivery of iPS-NPCs to the stroke cavity within a hyaluronic acid matrix promotes the differentiation of transplanted cells," *Advanced Functional Materials*, vol. 24, no. 44, pp. 7053–7062, 2014.
- [96] K. J. Lampe, R. G. Mooney, K. B. Bjugstad, and M. J. Mahoney, "Effect of macromer weight percent on neural cell growth in 2D and 3D nondegradable PEG hydrogel culture," *Journal of Biomedical Materials Research—Part A*, vol. 94, no. 4, pp. 1162–1171, 2010.
- [97] A. R. Massensini, H. Ghuman, L. T. Saldin et al., "Concentration-dependent rheological properties of ECM hydrogel for intracerebral delivery to a stroke cavity," *Acta Biomaterialia*, vol. 27, pp. 116–130, 2015.
- [98] D. Kai, M. P. Prabhakaran, B. Stahl, M. Eblenkamp, E. Wintermantel, and S. Ramakrishna, "Mechanical properties and *in vitro* behavior of nanofiber-hydrogel composites for tissue engineering applications," *Nanotechnology*, vol. 23, no. 9, Article ID 095705, 2012.
- [99] Y. Wang, M. J. Cooke, N. Sachewsky, C. M. Morshead, and M. S. Shoichet, "Bioengineered sequential growth factor delivery stimulates brain tissue regeneration after stroke," *Journal of Controlled Release*, vol. 172, no. 1, pp. 1–11, 2013.
- [100] K. Nakaguchi, H. Jinnou, N. Kaneko et al., "Growth factors released from gelatin hydrogel microspheres increase new neurons in the adult mouse brain," *Stem Cells International*, vol. 2012, Article ID 915160, 7 pages, 2012.
- [101] N. B. Skop, F. Calderon, S. W. Levison, C. D. Gandhi, and C. H. Cho, "Heparin crosslinked chitosan microspheres for the delivery of neural stem cells and growth factors for central nervous system repair," *Acta Biomaterialia*, vol. 9, no. 6, pp. 6834–6843, 2013.
- [102] L. A. Struzyna, K. Katiyar, and D. K. Cullen, "Living scaffolds for neuroregeneration," *Current Opinion in Solid State and Materials Science*, vol. 18, no. 6, pp. 308–318, 2014.
- [103] L. A. Struzyna, J. A. Wolf, C. J. Mietus et al., "Rebuilding brain circuitry with living micro-tissue engineered neural networks," *Tissue Engineering Part: A*, vol. 21, no. 21-22, pp. 2744–2756, 2015.
- [104] Y. Zhang, F. Rossi, S. Papa et al., "Non-invasive *in vitro* and *in vivo* monitoring of degradation of fluorescently labeled hyaluronan hydrogels for tissue engineering applications," *Acta Biomaterialia*, vol. 30, pp. 188–198, 2016.
- [105] S. K. Hahn, J. K. Park, T. Tomimatsu, and T. Shimoboji, "Synthesis and degradation test of hyaluronic acid hydrogels," *International Journal of Biological Macromolecules*, vol. 40, no. 4, pp. 374–380, 2007.
- [106] A. K. Jha, K. M. Tharp, J. Ye et al., "Enhanced survival and engraftment of transplanted stem cells using growth factor sequestering hydrogels," *Biomaterials*, vol. 47, pp. 1–12, 2015.
- [107] E. Fournier, C. Passirani, C. N. Montero-Menei, and J. P. Benoit, "Biocompatibility of implantable synthetic polymeric drug carriers: focus on brain biocompatibility," *Biomaterials*, vol. 24, no. 19, pp. 3311–3331, 2003.
- [108] J. P. Magnusson, A. O. Saeed, F. Fernández-Trillo, and C. Alexander, "Synthetic polymers for biopharmaceutical delivery," *Polymer Chemistry*, vol. 2, no. 1, pp. 48–59, 2011.
- [109] N. A. Peppas, J. Z. Hilt, A. Khademhosseini, and R. Langer, "Hydrogels in biology and medicine: from molecular principles to bionanotechnology," *Advanced Materials*, vol. 18, no. 11, pp. 1345–1360, 2006.
- [110] E. S. Place, J. H. George, C. K. Williams, and M. M. Stevens, "Synthetic polymer scaffolds for tissue engineering," *Chemical Society Reviews*, vol. 38, no. 4, pp. 1139–1151, 2009.
- [111] E. Duconseille, S. Woerly, C. Kelche, B. Will, and J.-C. Cassel, "Polymeric hydrogels placed into a fimbria-fornix lesion cavity promote fiber (re)growth: a morphological study in the rat," *Restorative Neurology and Neuroscience*, vol. 13, no. 3-4, pp. 193–203, 1998.
- [112] M. K. Nguyen and D. S. Lee, "Injectable biodegradable hydrogels," *Macromolecular Bioscience*, vol. 10, no. 6, pp. 563–579, 2010.
- [113] G. D. Prestwich, "Hyaluronic acid-based clinical biomaterials derived for cell and molecule delivery in regenerative medicine," *Journal of Controlled Release*, vol. 155, no. 2, pp. 193–199, 2011.
- [114] X. Z. Shu, S. Ahmad, Y. Liu, and G. D. Prestwich, "Synthesis and evaluation of injectable, *in situ* crosslinkable synthetic extracellular matrices for tissue engineering," *Journal of Biomedical Materials Research Part A*, vol. 79, no. 4, pp. 902–912, 2006.
- [115] J. M. Anderson, A. Rodriguez, and D. T. Chang, "Foreign body reaction to biomaterials," *Seminars in Immunology*, vol. 20, no. 2, pp. 86–100, 2008.
- [116] J.-Y. Je and S.-K. Kim, "Chitosan derivatives killed bacteria by disrupting the outer and inner membrane," *Journal of Agricultural and Food Chemistry*, vol. 54, no. 18, pp. 6629–6633, 2006.
- [117] P. R. Esser, U. Wölffe, C. Dürr et al., "Contact sensitizers induce skin inflammation via ROS production and hyaluronic acid degradation," *PLoS ONE*, vol. 7, no. 7, Article ID e41340, 2012.
- [118] E. T. Ahrens and J. W. M. Bulte, "Tracking immune cells *in vivo* using magnetic resonance imaging," *Nature Reviews Immunology*, vol. 13, no. 10, pp. 755–763, 2013.
- [119] M. Miyamoto, S. Kuroda, S. Zhao et al., "Bone marrow stromal cell transplantation enhances recovery of local glucose metabolism after cerebral infarction in rats: a serial ¹⁸F-FDG PET study," *Journal of Nuclear Medicine*, vol. 54, no. 1, pp. 145–150, 2013.
- [120] N. Coquery, O. Francois, B. Lemasson et al., "Microvascular MRI and unsupervised clustering yields histology-resembling images in two rat models of glioma," *Journal of Cerebral Blood Flow & Metabolism*, vol. 34, no. 8, pp. 1354–1362, 2014.
- [121] E. Bible, F. Dell'Acqua, B. Solanky et al., "Non-invasive imaging of transplanted human neural stem cells and ECM scaffold remodeling in the stroke-damaged rat brain by 19F- and diffusion-MRI," *Biomaterials*, vol. 33, no. 10, pp. 2858–2871, 2012.

- [122] Y. Jin, I.-Y. Kim, I.-D. Kim et al., “Biodegradable gelatin microspheres enhance the neuroprotective potency of osteopontin via quick and sustained release in the post-ischemic brain,” *Acta Biomaterialia*, vol. 10, no. 7, pp. 3126–3135, 2014.
- [123] E. Bible, O. Qutachi, D. Y. S. Chau, M. R. Alexander, K. M. Shakesheff, and M. Modo, “Neo-vascularization of the stroke cavity by implantation of human neural stem cells on VEGF-releasing PLGA microparticles,” *Biomaterials*, vol. 33, no. 30, pp. 7435–7446, 2012.
- [124] Y.-C. Jin, S.-W. Kim, F. Cheng et al., “The effect of biodegradable gelatin microspheres on the neuroprotective effects of high mobility group box 1 A box in the postischemic brain,” *Biomaterials*, vol. 32, no. 3, pp. 899–908, 2011.
- [125] M. J. Cooke, Y. Wang, C. M. Morshead, and M. S. Shoichet, “Controlled epi-cortical delivery of epidermal growth factor for the stimulation of endogenous neural stem cell proliferation in stroke-injured brain,” *Biomaterials*, vol. 32, no. 24, pp. 5688–5697, 2011.



Hindawi

Submit your manuscripts at
<http://www.hindawi.com>



STUDY 2: Hystem™-HP Hydrogel A Study of In Vivo Biocompatibility

6.1.1 Introduction

Cell therapy provides beneficial effects in pre-clinical studies, but some issues need to be improved to optimize results prior translate to clinics.

When administrated by systemic way (intravenous or intra-arterial), the cell administration results in a whole body distribution of cells with accumulation in other organs such as lung or spleen and a poor homing toward the damage region (Detante et al., 2009).

An alternative is the intracerebral administration, among intracerebral possibilities the lesion cavity seems be ideal due to its proximity to lesion boundary, the site of greatest remodeling after stroke (Carmichael, 2006; Zhong et al., 2010) and by preserving healthy tissue. However when cells are administrated directly inside the lesion cavity an significant cell loss is reported because infarct cavity is a “non hospitable” environment (Baeten and Akassoglou, 2011).

With the aim to provide a solution for this issue, biomaterials have been used as scaffold to transplanted cells (Sarnowska et al., 2013; Struzyna et al., 2014). Recent advances in developing of biomaterials adapted to use in central nervous system has provided a potential alternative for stem cell therapy in many diseases including stroke.

Hydrogels produced from extracellular matrix compounds such as hyaluronic acid provides a three-dimensional environment for stem cells and could be a support for intracerebral engraftment in many CNS diseased such as stroke (Lam et al., 2014; Portalska et al., 2014).

Several biomaterials have been tested *in vitro* and *in vivo* produced from different compounds (*e.g.*: matrix gel, chitosan, hyaluronan...) and with divers mechanical and physical properties (*e.g.*: liquid hydrogel, microspheres, solid scaffolds...) (Lindborg et al., 2015; Thonhoff et al., 2008; Zhong et al., 2010).

Liquid hydrogels which polymerize *in situ* are suitable for intracerebral administration and are easily mixed with cells (Liang et al., 2013; Wang et al., 2010). Hydrogel biocompatibility and degradation rate are variable according to their compounds and physical properties.

In the present study, we tested an injectable hyaluronic based hydrogel HyStem™-HP.

Previous studies have demonstrated the potential of HyStem™-HP *in vitro* and *in vivo* after stroke in mice. Prior to administrate in our model of ischemic stroke co-administrated with mesenchymal stem cells (study 3), we evaluated through a pilot study using healthy rats the potential for long-lasting protect of this hydrogel and their biocompatibility *in vivo*.

For this purpose, we used an *in vivo* follow-up by MRI of HyStem™-HP hydrogel during 28 days and we evaluate the host brain response by immunohistological analysis.

6.1.2 General methodology

Adult male Sprague Dawley rats (Charles River, France), aged of 7-8 weeks (n=7) at the beginning experiment were used in this study. Such as mentioned above (methods section) all procedures were approved by the ethical committee.

Hyaluronic acid hydrogel administration

The biomaterial used in the present study was a hyaluronan–heparin–hydrogel. The HyStem™-HP cell culture scaffold Kit (Sigma-Aldrich, France) is composed by: Hyaluronan (thiol-modified) 99.7% + 0.3% of heparin; Gelin-S™ denatured collagen (thiol-modified) ; Extralink™ polyethylene glycol diacrylate (PEGDA) (cross-linker); Water deionized and degassed.

Hyaluronan is a major constituent of native extracellular matrix. Gelin provides basic cell attachment (Shu et al., 2006), collagen is also a compound of ECM present in extracellular space and basal lamina. PEGDA a crosslinking agent used to induce polymerization.

The three compounds were diluted with degassed water such as indicated by the manufacturer, under aseptic conditions. Solutions of this hydrogel are in a liquid state when separated and form a transparent gel when mixed with the cross-linker PEGDA over a period of 30 min when prepared as follow (1:1:0.5): 4 μ L hyaluronan/heparin sulfate, 4 μ L of gelin and 2 μ L of cross-linker.

Hydrogel administration was performed by stereotaxic intracerebral injection such as described above (methods section). Under anesthesia, 10 μ l of hydrogel was injected on right striatum and 10 μ L of phosphate buffered saline (PBS) was injected in left striatum. The following stereotaxic coordinates were used: *bregma* 0; medial-lateral, \pm 3.5 mm; dorsal-ventral, -5.5mm (Figure 21)

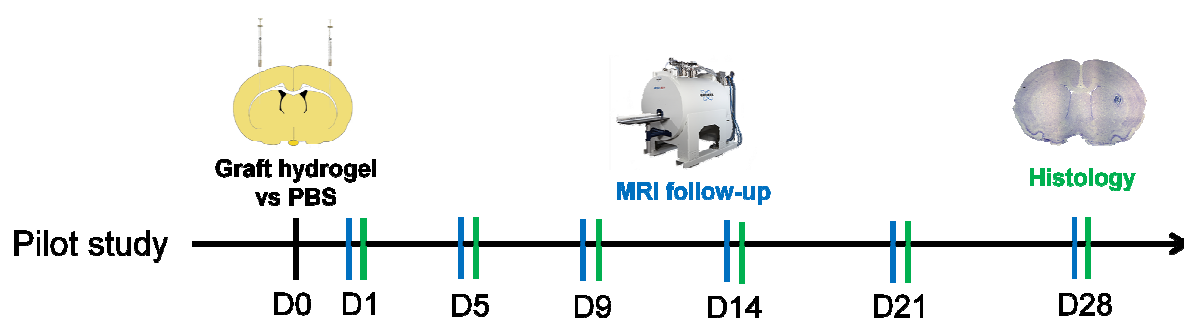


Figure 21: Experimental protocol of experiment biocompatibility. At day 0 rats received an intracerebral injection of hydrogel (right hemisphere) and phosphate buffered saline (PBS in the left hemisphere). MRI evaluations and histological analysis were performed at different time points.

In vivo MRI

MRI was used to detect hydrogel *in vivo*. Anatomical (T_2W) and diffusion images were acquired using a 4.7T magnet (Bruker Biospec®, Germany; MRI facility IRMaGe, Grenoble, France). MRI protocol settings are described in methods section.

The images were acquired at days 1, 5, 9, 14, 21 and 28 and each MRI session had a duration of around 10 minutes.

In the right hemisphere, a zone corresponding to the hydrogel injection site was identified on Apparent Diffusion Coefficient (ADC) map. A region of interest (ROI) Hydrogel was delineated around the voxels with an ADC increase. The volume of ROI Hydrogel was estimated by multiplying the number of voxels in the ROI by the voxel volume (234x234x800 μm). A ROI Contra was delineated on the contralateral hemisphere in the zone of PBS administration (in mirror to ROI Hydrogel). The values of ADC were estimated within each ROI and compared.

Histology and immunostaining

Rats were euthanized after MRI sections (n=1) by time point and brain tissue was processed for histological analysis. Coronal slices (20 μm) were generated per animal around the injection site. Sections of brain containing hydrogel implants were stained with 0.1% cresyl violet (Waldeck GmbH, Munster, Germany) to detect hydrogel.

Brain sections of 20 μm thick section were stained for microglia/macrophage (IBA1), astrocytes (GFAP) detection. Immunohistological images were obtained using an epifluorescence microscope (Nikon Eclipse E600, Tokyo, Japan) and CCD camera (Olympus XC30, Rungis, France); images were acquired in 20x magnification.

Statistical Analysis

Results are presented as the mean values \pm standard deviation (\pm SD). Statistical comparison between ROI hydrogel and ROI Contra were performed using a paired t -test. The statistical significance level was set at $p < 0.05$.

6.1.3 Results

In this pilot study, we use a small cohort of animals (n=7) to observe the brain the HyStemTM-HP hydrogel fate by MRI in healthy brains. One rat died before intracerebral injection of hydrogel.

MRI

Using MRI follow-up of 28 days, we could visually detect the hydrogel until at least day 28 (time point of the last MRI evaluation) after administration. The contralateral PBS injection site was not detectable by MRI. We used two MRI scans to detect hydrogel anatomic T₂W and ADC, hydrogel was most efficiently detected using ADC map. Hydrogel presented a hyperintense signal in ADC map corresponding to a high content of water zone (Figure 22).

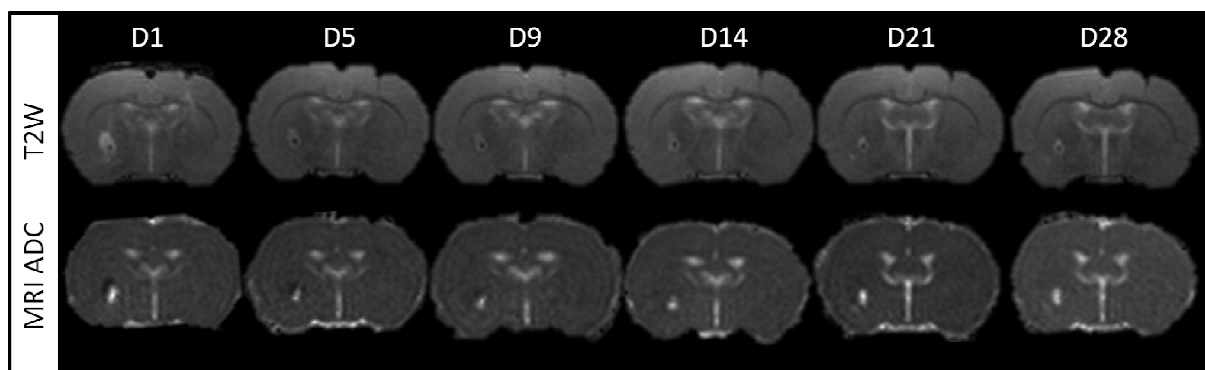


Figure 22: MRI follow-up of hydrogel in healthy brain. Anatomical T₂ Weighted images and apparent diffusion coefficient (ADC) map of a rat in different time points.

Hydrogel volume was apparently held constant across the time, occupying between 2 and 3 slices of ADC map. The mean volume was $1.65 \pm 0.35 \text{mm}^3$ at day 1 (n=6); 1.00 ± 0.46 at day 5 (n=5); 0.96 ± 0.25 at day 9 (n=4); 1.25 ± 0.18 at day 14 (n=3); 1.30 (at day 21) and 1.10 (at day 28).

Comparisons between right (ROI Hydrogel) and left hemisphere (ROI Contra) demonstrated an increase in apparent diffusion coefficient in hydrogel region in all time points. ADC values detected within ROI

Hydrogel and Contra respectively were: (1710 ± 289 vs $845 \pm 37 \mu\text{m}^2/\text{s}$; $p < 0.05$), at day 1 ($n=6$); (1367 ± 425.0 vs $831 \pm 45 \mu\text{m}^2/\text{s}$, $p < 0.05$), at day 5 ($n=5$); (1532 ± 173 vs $818 \pm 22 \mu\text{m}^2/\text{s}$, $p < 0.05$), at day 9 ($n=4$); (1548 ± 106 vs $856 \pm 38 \mu\text{m}^2/\text{s}$, $p < 0.05$), at day 14 ($n=3$), 1639 ± 93 vs $821 \pm 78 \mu\text{m}^2/\text{s}$, at day 21 ($n=2$); and 1831 vs $966 \mu\text{m}^2/\text{s}$ at day 28 ($n=1$).

Statistical analyses were performed only for the four first time points (day 1, 5, 9 and 14) because beyond this point the number of animals was insufficient to perform statistical analysis (Figure 23).

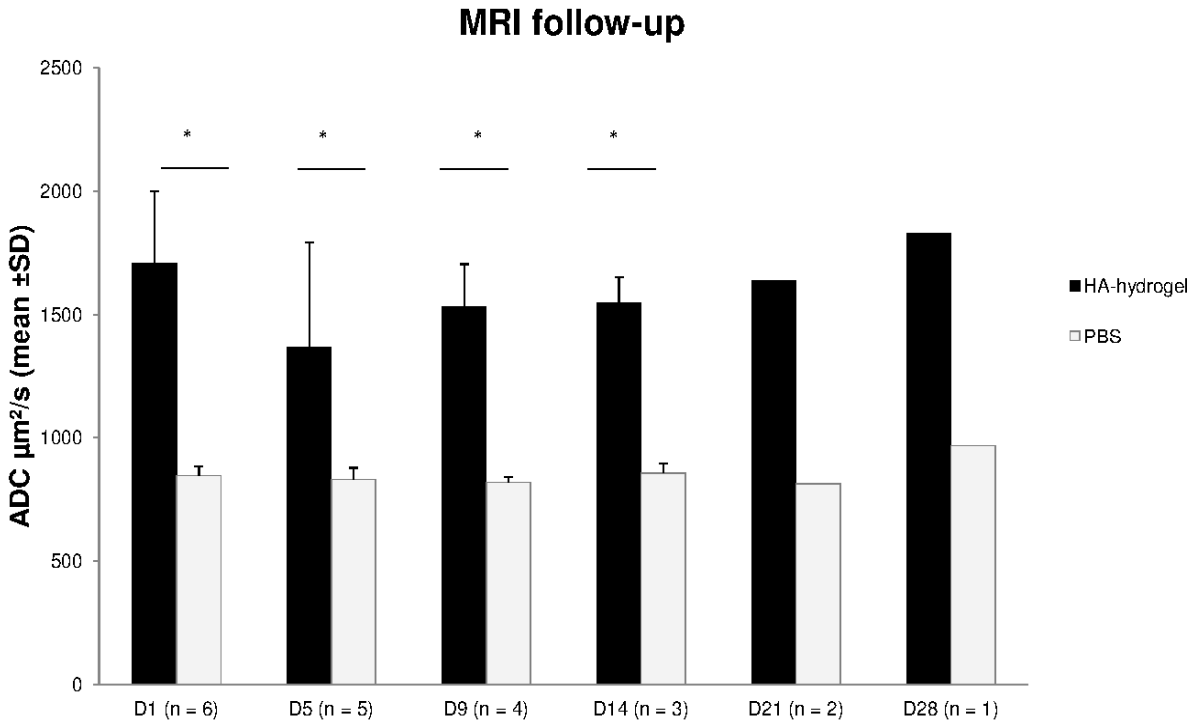


Figure 23: MRI ADC values within the ROI Hydrogel at different time points in comparison to ROI Contra.

Histological analysis

HyStem™-HP hydrogel can be detected with the basic dye cresyl violet. We detect hydrogel in the different time points in the right hemisphere. Based on visual inspection, we observed a retraction of hydrogel border with host tissue after the 9th day.

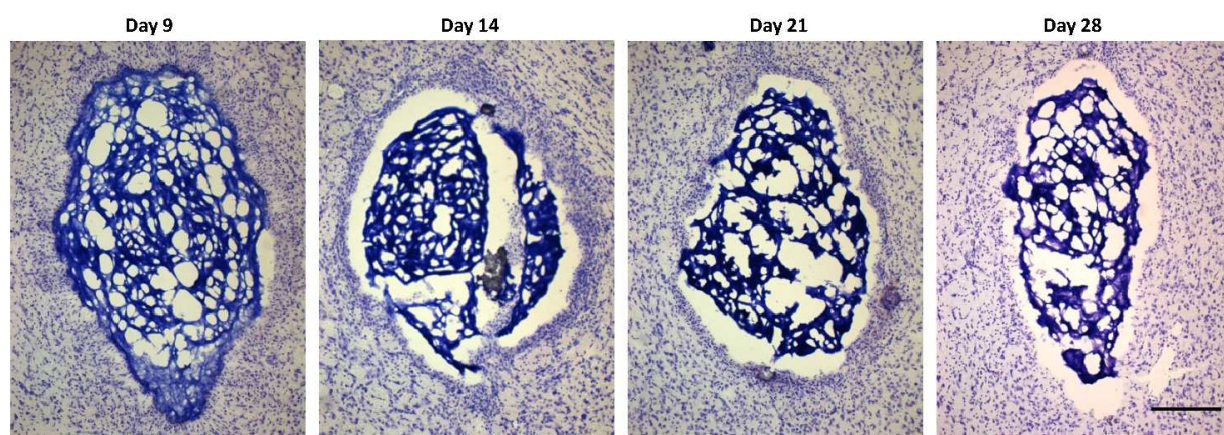


Figure 23: Hydrogel detection by Nissl staining at different time points. Scale bar represents 100 μ m.

Additionally, we detected microglial/macrophage cells (Iba1+) and astrocytes (GFAP+) in the hydrogel edge. No statistical analysis was performed due to the low number of animals by time point. However, an increase of GFAP+ and Iba1+ cells is visually detected in comparison to the contralateral side.

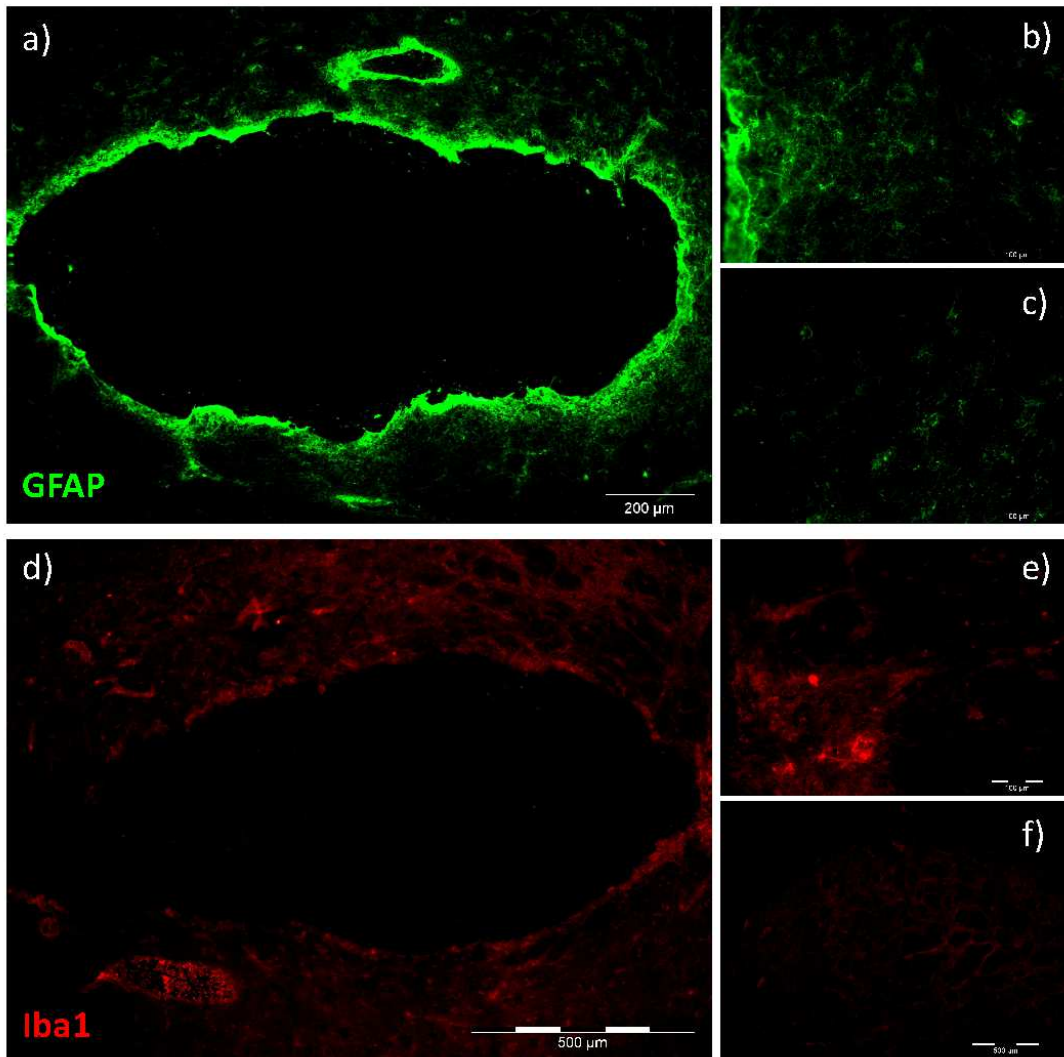


Figure 24: Host response to hydrogel administration. a) Hydrogel administration site (x10 magnification) labeled with glial fibrillary acid protein (GFAP) in green, b) GFAP+ cells in hydrogel border (x40), c) GFAP+ cells in contralateral hemisphere (x40), d) hydrogel administration site (x10 magnification) labeled with microglial/macrophage cells marker Iba1 in red, e) Iba1+ cells in hydrogel border (x40) and f) in the contralateral hemisphere (x40) at day 28.

6.1.4 Discussion

The preliminary results detected in our pilot study put in evidence a long-term stability of HyStemTM-HP hydrogel in rat brain until four weeks after administration. Additionally, the hydrogel is detectable by MRI allowing an *in vivo* follow-up of hydrogel fate. These data are only qualitative due to the low number of animals per time point but are encouraging for the application in stroke model studies.

Hydrogel polymers have a high water content (*i.e.* >90% water) due to their hydrophilic nature. ADC based in diffusion-weighted images use the diffusion of water molecules in the tissue to generate contrast in MR images (Shen et al., 2003). ADC map is a quantitative measure of diffusion process of water molecules on brain tissue. The site of hydrogel injection could be detected by ADC map, we compare this quantitative information with contralateral side (PBS injection) and we observed an increase of more than 50% of ADC mean value on ROI Hydrogel. MRI *in vivo* follow-up can represent an important tool for hydrogels studies to evaluate hydrogel fate. An important thing to be considerate is that in the presence of ischemic stroke, hydrogel fate can be modified by alterations in the local environment and host cells induced by ischemic lesion. Additional studies are required to clarify this question.

Hydrogel studies usually evaluate the stem cell tolerance to hydrogel compounds and concentration *in vitro* and after transfer hydrogel directly to a lesion model *in vivo*. Here we decide to test hydrogel tolerance *in vivo* evaluating the different host cells responses to hydrogel. Although of our limitations (low number of animals) we could observe a good tolerance of host cells to hydrogel transplantation despite the increase of microglia/macrophage (Iba1+) cells activation around hydrogel administration site. HyStemTM-HP hydrogel is a synthetic hyaluronan-based gel. Synthetic hydrogels, are better chemically defined in comparison to natural hydrogels and are biologically inert (Aurand et al., 2012). Although a mild inflammatory response was observed in the lesion border in our pilot study, a previous study using the same hydrogel demonstrated a protective effect induced by the hydrogel promoting a reduction of infiltration of inflammatory cells in hydrogel group (Zhong et al., 2010). Other study using a very similar gel demonstrated a protection of grafted cells mediated by the hydrogel improving stem cell survival

(Liang et al., 2013), one of the principal factors that induce stem cell death after intracerebral graft is the inflammation (modifying the ECM composition).

HyStemTM-HP hydrogel was detected by histological staining (cresyl violet) in an effective way such as demonstrated in a previous study (Liang et al., 2013). We observed a retraction of hydrogel border in relation to host tissue limit since the 14th day. Hydrogels are not permanent implants and are developed to be biodegraded or bioresorbable mediated by enzymatic (i.e by endogenous hyaluronidases) hydrolytic cleavage (Lampe et al., 2010). Hydrogel degradation usually occurs through cleavage of chemical bonds simultaneous at the interior and surface (exterior) of hydrogel (Aurand et al., 2012), and could be an explanation for our observation.

There are many potential biomaterials for application in central nervous system. We choose to test a hyaluronan-based hydrogel material due to its promising results which include improvement in stem cells survival *in vitro* and *in vivo*. We could put in evidence here a long last duration of the hydrogel in rat brain tissue *in vivo* suggesting a potential long-term protection for stem cells.

6.1.5 Conclusion

The preliminary results presented here in our pilot study put in evidence that HyStemTM-HP hydrogel can be detected by MRI, diffusion scans are a good way to detect hydrogel due to the high water content of hydrogel. Additionally, our preliminary results were encouraging concerning long-lasting of the hydrogel in rat brain tissue for until 28 days. An increase of host brain response evidenced by Iba1 and GFAP activation was detected. The hydrogel was detected by cresyl violet staining with a high specificity. Some signals of degradation of hydrogel were detected from 14th day to the end of experiment 28th day. Additional analysis with a high number of rats is required to quantify degradation rate of HyStemTM-HP hydrogel.

STUDY 3 : HYALURONIC ACID HYDROGEL COMBINED WITH MESENCHYMAL STEM CELL THERAPY AFTER ISCHEMIC STROKE

The last study is presented in an article format, additional MRI and histological results should be included and then the paper will be submitted to Biomaterials journal.

Hyaluronic acid hydrogel combined to mesenchymal stem cell therapy after ischemic stroke

Authors: Ligia S. B. BOISSERAND^{a,c}, Jérémie PAPASSIN^{a,b,e}, Tomonobu KODAMA^d, ,
Nora COLLOMB^{a,b}, Anaïck MOISAN^f, Claire ROME^{a,b}, Olivier DETANTE^{a,b,d,e}

- a) Inserm, U1216, BP 170, 38042 Grenoble Cedex 9, France
- b) Grenoble Institut des Neurosciences (GIN), Université Grenoble Alpes, 38000 Grenoble, France
- c) CAPES Foundation, Ministry of Education of Brazil, 70040-020 Brasília, DF, Brazil
- d) Institute for Frontier Medical Sciences, Department of Reparative Materials, Kyoto University, Kyoto 606-8507, Japan
- e) CHU Grenoble Alpes, Stroke Unit, Department of Neurology, CS 10217, 38043 Grenoble, France
- f) Cell Therapy and Engineering Unit, EFS Rhône Alpes, 464 route de Lancey, 38330 Saint-Ismier, France

Corresponding author:

Claire ROME

Grenoble Institut des Neurosciences - GIN

Université Grenoble-Alpes

Inserm U1216

Bâtiment Edmond J. Safra

Chemin Fortuné Ferrini

38700 LA TRONCHE - France

Abstract :

Cell therapy has emerged to regenerate damaged brain in after ischemic stroke. Mesenchymal stem cells (MSC) have shown beneficial effects in post-stroke therapy by reducing cellular death and by potentiating endogenous mechanism of regeneration including neurogenesis and angiogenesis.

With the aim to optimize preclinical results of cell therapy, biomaterials have been engineered to improve engraftment and cell survival, improving brain repair.

We evaluated a hyaluronic acid-based (HA) hydrogel (HyStemTM-HP) combined with 100,000 human MSCs (hMSCs) in a rat model of ischemic stroke. Seven days after stroke, rats were respectively treated by intracerebral injection of 1) HA hydrogel combined with hMSC (n=9); 2) hMSC alone (n=10); or 3) vehicle (n=7). We assessed sensory-motor 3-weeks outcome, lesion size by MRI, hMSC survival, and angiogenesis.

The combination HA-hydrogel+hMSC was able to improve hMSC survival compared to hMSC alone. Angiogenesis was improved by HA-hydrogel+hMSC injection, 3 weeks after administration, compared to the “vehicle” group. No effect was noted on MRI lesion volume. Despite histological effects, behavioral outcome was not improved by HA-hydrogel+hMSC administration. Optimization of biomaterials and their combination with therapeutic cells will be necessary to improve their effects after stroke.

Keywords:

Angiogenesis, Biomaterials, cerebral infarction, stroke, hydrogel, cell therapy, Mesenchymal stem cells.

1. Introduction

Stroke is a major neurological disease remaining one of leading cause of death and long-term disability worldwide (Feigin et al., 2014). Ischemic stroke (80% of stroke cases), results from a dramatic decrease in cerebral blood flow leading a cellular death and compromising brain function.

Currently, the only therapeutic approach approved for acute ischemic stroke is the reperfusion. Vessel reperfusion can be induced by thrombolysis (Kwiatkowski et al., 1999), endovascular thrombectomy or a combination of both (Campbell et al., 2015; Pierot et al., 2015). However, these therapeutic approaches are conditioned to a short therapeutic window (until 6hours after stroke onset) (Wang et al., 2015). After these first hours, there is no effective treatment available besides rehabilitation (Duncan et al., 2005).

Cell-based therapy presents a new hope in the treatment of neurological disorders such as stroke. Stem cells present positive results by improving brain function, reducing lesion size and by inducing recovery in pre-clinical studies (Gutiérrez-Fernández et al., 2015; Moisan et al., 2016; Zhu et al., 2015). Many cell sources (neural and non-neural) and types (multipotent or induced pluripotent) have been used in stroke therapy contributing to brain repair. Mesenchymal stem cells (MSCs) for example, induces neurorestorative effects by improvement of neurogenesis, angiogenesis and inflammatory response by paracrine mechanisms (Castillo-Melendez et al., 2013). Moreover, intracerebral graft of human MSCs (hMSC) is feasible and seems promising in clinics (Steinberg 2016).

Some issues involving cell therapy remains unsolved such as a low number of cells that achieve the lesion site when administrated by intravascular route (intravenous or intra-arterial way) (Detante et al., 2012) and the poor survival of injected cells within the lesion cavity (Hicks et al., 2009).

Recent advances in tissue engineering have developed biomaterials for application in central nervous system. Biomaterials can be produced from a variety of compounds, providing a unique three-dimensional microenvironment similar to the extracellular matrix (ECM) promoting cell survival and engraftment (Aurand et al., 2012). Among them, liquid hydrogels (for *in situ* polymerization) are a promising candidate for cell or trophic factor transplantation, by the advantage to be injected with a minimal invasiveness.

Hyaluronic acid (HA) polysaccharide a major component of ECM, is widely used in clinical applications such as lubricants, wound sealants, or filling agents in esthetic medicine (Pakulska et al., 2012; Robert, 2015). HA-based hydrogels have been used *in vitro* and *in vivo* promoting cell survival, proliferation and differentiation (Liang et al., 2013; Zhong et al., 2010).

In the present study, we assessed a synthetic HA-based hydrogel (HyStemTM-HP), combined with human MSC 7 days after induction of an ischemic stroke. We evaluated the effects of the combination of hydrogel+hMSC on cell survival, brain remodeling, and functional recovery.

2. Methods

2.1 Hyaluronic acid hydrogel gelation time

A hyaluronan–heparin–hydrogel (HyStemTM-HP, Sigma-Aldrich, France) produced from a thiol-modified hyaluronan, heparin, gelin and a cross-linker polyethylene glycol diacrylate (PEGDA) was used. For an optimal administration, we assessed the gelation time of HyStemTM-HP hydrogel when mixed with hMSCs.

As preliminary experiment, Hyaluronan and Gelin were separately dissolved in degassed and deionized water according to manufacturer's instructions. The 3 compounds (hyaluronan, gelin, PEGDA) were mixed in different ratios: 1) hyaluronan: gelin:PEGDA (1:1:0.5) as standard HyStemTM-HP hydrogel; 2) 50 μ L of hyaluronan:gelin: PEGDA (1:1:0.5) mixed

with 10^5 human MSC; 3) hyaluronan:gelin (1:1); 4) gelin:PEGDA (1:0.5); 5) hyaluronan:PEGDA (1:0.5).

At room temperature, in PCR tubes, 50 μ L of each solution were pipetted after 10, 15, 20, 25, 30, 40, and 50min. Complete gelation was considered when pipetting became impossible. Experiments were triplicated.

2.2 Human mesenchymal stem cells culture

Clinical grade hMSCs were isolated from bone marrow aspirate from 4 healthy donors who gave consent. Culture procedures were conducted according to previously described methods (Detante et al., 2012). Native hMSCs were harvested after two passages.

2.3 Animals:

All procedures were conducted according to French guidelines on the use of animals for scientific investigations (permits 2015040716522967 and A3851610008 for the facilities) with ethical committee approval (Grenoble Institute of Neurosciences agreement 004). Fifty-two male Sprague-Dawley rats (Charles River, France), aged of 7 weeks at begins of experiments were initially included in this study: 12 for the histological experiment, and 40 for the behavioral follow-up during 3 weeks after injection.

For all experimental procedures with potential risk of pain or discomfort for the animals, rats were anesthetized. Isoflurane anesthesia was induced by inhalation of a gas mixture of 5% isoflurane (IsoFlo, Abbot Laboratories Ltd, Berkshire, UK) in medical air through a facial mask and maintained between 1.5-2.5% of isoflurane along the surgical procedures. Body temperature was monitored by a rectal probe and maintained at $37^{\circ}\text{C} \pm 0.5^{\circ}\text{C}$ via heating blanket.

2.4 Surgical procedures:

MCAo

Transient focal brain ischemia was induced by middle cerebral artery occlusion (MCAo) using the intraluminal filament model. Incision site was shaved, cleaned and scrubbed with chlorhexidine surgical. Bupivacaine 0.05% (Pfizer, France) was injected subcutaneously (2 mg/kg). Briefly, the right carotid arterial tree was isolated. A monofilament (silicon rubber-coated monofilaments: 0.37 or 0.39mm in diameter, Doccol, Sharon, MA, USA) was advanced through the lumen of the external carotid artery into the internal carotid artery to occlude the right MCA at its origin. After 90min of occlusion, rats were functionally assessed then re-anaesthetized to remove the thread.

Stereotaxic cell transplantation and experimental groups

Using a stereotaxic frame, 10 μ L of HA-hydrogel+hMSC (n=9), hMSC (n=10) or vehicle (PBS, n=7) were administrated in the infarct cavity of MCAo rats seven days after MCAo. The Sham-operated rats underwent the same procedure without MCAo (n=10) and received 10 μ L of PBS.

For the hydrogel-hMSC group, 100,000 hMSCs in 2 μ L were mixed with 3.2 μ L hyaluronan/heparin sulfate, 3.2 μ L gelin and 1.6 μ L cross-linker. The following stereotaxic coordinates were used: *bregma* 0; medial-lateral, \pm 3.5 mm; dorsal-ventral, -5.5mm for a complete cortico-striatal lesion. Stereotaxic coordinates were adapted according to lesion size and localization for only cortical or striatal lesions observed by initial MRI at day 3 (data not shown). Injections were conducted through a 26 G needle in a syringe of 10 μ L (Hamilton, Bonaduz, Switzerland) using an infusion pump with a rate of 2 μ L/min. According to the gelation assessment preliminary results, administration was started 20 minutes after adding

PEGDA cross-linker to others hydrogel compounds and hMSC. The needle was withdrawn 5 min after the end of administration. No immunosuppressant was used.

2.5 Behavioral tests

Rats were subjected to somatosensory tests widely used in stroke models: modified neurological severity score (mNSS) and adhesive removal test (ART). Rats were previously familiarized with the testing environment and trained during 3 days (3 trials) before MCAo. The animals were tested before MCAo (baseline) and functional recovery was tested at day 6 (D6), D14, D21 and D28 post-stroke. The **figure 1.a** describes the complete experimental protocol.

The mNSS is a combination of motor, sensory, balance, and reflex tests graduated from 0 (normal) to 18 (maximal deficit). The ART score is used to assess the asymmetry in dexterity and sensitivity. For this, an adhesive-backed paper dot (1 cm²) was applied on each forepaw. Three trials per rat were performed and the mean time to remove each adhesive was measured with a maximum delay of 180s.

2.6 Magnetic Resonance Imaging (MRI)

Brain lesion was detected and its evolution was evaluated by MRI at different time points (baseline D3, D9, D15, D22, and D29). All MRI data were acquired using a 4.7T magnet (Bruker Biospec®, Germany; MRI facility IRMaGe, Grenoble, France). After a pilot sequence to ensure the correct rat position, anatomical T₂W images were acquired using a spin-echo sequence (repetition time (TR)/echo time (TE) = 7000/50 ms, 31 slices with a voxel size = 234x234x800 μm).

MRI brain images were computed using a program developed in our laboratory within Matlab (MathWorks, Natick, MA, USA). The region of interest (ROI) corresponding to the whole

ischemic lesion was identified as the hyperintense area on T₂W images in the 5 slices (approximately between the coordinates +2.2 and 4.0mm from *bregma*) (ROI Lesion). The volume of ROI Lesion was estimated by multiplying the number of voxels in the ROI by the voxel volume (234x234x800 μm).

2.7 Immunofluorescence

After euthanasia, brains were quickly removed, frozen in -40 °C isopentane, and stored at -80 °C until processing. Coronal cryosections (20 μm thick) were cut along the entire lesion or gel administration site at -20 °C on a cryostat (Leica, Nanterre, France).

For immunofluorescence, parallel series of sections from each animal were incubated with the human nucleus marker (mouse anti-HuNu, 1:200, Millipore), astrocytic marker glial fibrillary astrocytic protein (rabbit anti-GFAP, 1:500, Dako), rat endothelial cell antigen (RECA-1) marker (mouse anti-RECA-1, 1:200, Abcam), mature neurons marker (NeuN) (mouse anti-NeuN, 1:100, Chemicon) basal membrane marker collagen-IV (goat anti-mouse collagen-IV, 1:1000, Southern Biotech) and ionized calcium-binding adaptor molecule 1 (Iba1) as microglia marker (rabbit anti-Iba1, 1:1000, Abcam). Sections were incubated in 3% of the bovine serum albumin and 0.2% PBS-Triton for 30 min prior to overnight incubation with primary antibodies at 4°C. Sections were washed 3 times in PBS-Tween 0.1% (Sigma) followed by incubation with the appropriate secondary antibody (1:500, Alexa488/546/568, Invitrogen) for 2 hours at room temperature. Images were obtained using epifluorescence microscopy (Nikon Eclipse E600, Tokyo, Japan) and a CCD camera (Olympus, Rungis, France).

2.8 Immunofluorescence quantification

The total area occupied by astrocytes (GFAP+), microglia/macrophage cells (Iba1+), blood vessels (RECA1+ and Collagen-IV+), neurons (NeuN+) was determined using Image J (National Institutes of Health, USA). Images containing the ROI Lesion in the boundary of lesion and in contralateral hemisphere ('mirror' to the lesion boundary) were turned into (8-bit) gray scale. A mask of each brain section image was then created using an auto-threshold tool from Image J with the aim to correct background and unequal illumination (shading correction) (Centenaro et al., 2011). The same threshold mask was applied for all animals for each cell type. All lighting conditions and magnifications were held constant. The total percentage (%) area occupied by each cell (including soma and process) was measured.

Immunohistological analyses to detect human cells HuNu+ cells were performed at three time points: at day 7 some hours after injection to be sure of hMSCs viability after administration procedure (n=2 /group), 2 weeks after injection (at D21 post-stroke, n=4 /group) and at D29.

2.9 Statistic Analysis

For repeated measures analyses (lesion volume and behavioral tests), we firstly verify the normality of error (predicted values – residuals). For normal data, we apply repeated measures ANOVA (lesion size) followed by a multiple comparison post-hoc test of Tukey. For non-parametric data, we use a Friedman test followed by a Kruskal-Wallis test (behavioral tests). For the comparison between groups, we use an unpaired T-test (parametric data) or a Mann-Whitney test. The statistical significance level was set at $p < 0.05$. SPSS Statistics (IBM Corp, v20) software was used. Results are presented as mean values \pm standard error of the mean (SEM).

3. Results

Hydrogel gelation assessment

As preliminary results, we observed that gelation of hyaluronan: gelin: PEGDA (1:1:0.5) as standard hydrogel occurred after 15min, and after 30min when it was mixed with hMSC. No gelation was observed for hyaluronan: gelin (1:1) or gelin: PEGDA (1:0.5) mixtures. Complete gelation of Hyaluronan: PEGDA (1:0.5) occurred after 20min. According to these preliminary results, for *in vivo* studies, we started the intracerebral injection of HA-hydrogel-hMSC 20 minutes after hydrogel mixing to obtain an injectable solution followed by a quick intracerebral gelation.

***In vivo* experiment**

Physiological parameters remained within normal limits throughout the procedure and showed no significant differences between groups (data not shown). Four animals were excluded for not presenting an ischemic lesion.

Lesion size after MCAo, measured by MRI does not change after IC administration of HA-hydrogel+hMSC or hMSC (Figure1).

A MRI alteration in anatomic T₂W images compatible with a lesion was detected in our rats submitted to a MCAo. The mean volume for each rat is represented in Table 1 and Figure 1 b,c. Repeated measures analyses of variance put in evidence a reduction of lesion among the difference time points (“time” $F_{(3,26)}=7.123$, $P=0.002$) but not among the different groups (“time*group” $F_{(6,26)}=0.271$, $P=0.947$). Pairwise comparisons detected no difference in the lesion size among the 3 ischemic groups.

Behavioral tests

Rats presented no deficit before MCAo. A significantly reduction of motor deficit across the time was detected by mNSS test in the 3 MCAo groups: HA-hydrogel +hMSC, hMSC and PBS respectively at D6 (4.56 ± 1.19 , $n=9$ vs 4.50 ± 1.04 , $n=10$ vs 5.00 ± 1.49 , $n=7$), D14 (3.33 ± 0.94 , $n=9$ vs 2.70 ± 0.66 , $n=10$ vs 4.43 ± 1.34 , $n=7$); D21 (2.89 ± 0.75 , $n=9$ vs 2.80 ± 0.55 , $n=10$ vs 3.43 ± 0.99 , $n=7$); D28 (2.33 ± 0.50 , $n=9$ vs 2.50 ± 0.45 , $n=10$ vs 2.86 ± 0.93 , $n=7$). Neither HA-hydrogel+hMSC nor hMSC treatment were able to improve functional effects in comparison to PBS control group (Figure 2a). We found a similar result using the sensory-motor ART test, with no difference ($P= 0.091$) among the 3 ischemic groups. The mean time to remove the adhesive in the left (impaired side) for the groups HA-hydrogel+hMSC; hMSC; PBS and Sham respectively was: at pre-MCAo evaluation ($7.1s\pm 0.9$; $12.6s\pm 3.6$; $4.7s\pm 0.6$ and $12.2s\pm 3.2$); at D6 ($71.6s\pm 24.3$; $74.8s\pm 21.7$; $103.2s\pm 24.1$ and $10.1s\pm 3.0$); at D14 ($62.7s\pm 18.2$; $47.8s\pm 11.7$; $50.1s\pm 15.5$ and $19.2s\pm 11.6$); D21 ($49.4s\pm 17.0$; $40.5s\pm 7.6$; $51.0s\pm 22.1$ and $11.5s\pm 4.3$) and at D28 (45.9 ± 19.7 ; 39.9 ± 7.5 ; 51.6 ± 19.1 and 14.7 ± 5.8). Sham group was different from ischemic groups in all time points post MCAo ($P<0.005$) (Figure 2b).

HyStemTM-HP hydrogel improves hMSC survival

Two weeks after administration of hMSC ($n=4$) alone or co-administrated in HystemTM-HP hydrogel ($n=4$), we detected some cells in the lesion zone. In the group hMSC, we detected these cells only in 3 rats while in the group HA-hydrogel+hMSC we detect in the 4 rats. At the end of follow-up study, 21 days after hMSC administration, we detected HuNu positive cells in 6 brain samples in the group HA-hydrogel+hMSC ($n=9$ rats) (66.6%) while, for group hMSC ($n=10$), HuNu positive cells were detected only in 2 rats (20%). (Figure3)

Hydrogel co-administrated with hMSC improves angiogenesis

The combination HA-hydrogel+hMSC promoted an increase in the surface (percentage area %) occupied by vascular markers Collagen-IV (7.44 ± 1.38) when compared to the group PBS (3.77 ± 0.55 , $P=0.03$) but with no difference in comparison to groups hMSC (5.12 ± 0.61) or Sham (4.89 ± 0.66) (Figure 4a). HA-hydrogel+hMSC also increase RECA positive cells (4.56 ± 0.43) when compared to the group Sham (3.06 ± 0.44 , $P=0.02$) with no difference in comparison to the other MCAo groups: hMSC (4.28 ± 0.5), PBS (3.35 ± 0.53) (Figure 4b). We observed, using immunostaining, that Collagen IV and RECA1+ host cells migrate toward the hydrogel zone. This finding suggests a good integration of host cells within hydrogel (Figure 6.a,b).

Astrocytic and microglial response to intracerebral injection

We investigate if hydrogel and hMSC treatment have some effect in host immune response after stroke. We found an increase in the zone occupied by activated astrocytes (GFAP positive cells) including soma and processes in the lesion border for the groups HA-hydrogel+hMSC ($10.7\%\pm 0.9$) hMSC ($12.3\%\pm 1.0$) and PBS ($11.0\%\pm 2.0$) in comparison to the group Sham ($6.2\%\pm 0.8$). No differences were detected among the groups with an ischemic lesion (Figure 5b). No astrocytes GFAP+ were detected within of hydrogel (Figure 6.c).

Similarly, peri-infarct Iba1+ cells were increased in the ischemic groups: HA-hydrogel+hMSC ($5.9\%\pm 1.3$) hMSC ($5.6\%\pm 0.9$) and PBS ($5.0\%1.5$) in comparison to the group Sham ($0.6\%\pm 0.2$) at day 29. No differences were detected among ischemic groups (Figure5,c). Microglia/macrophages cells migrate toward hydrogel, few cells Iba1+ were co-localized with 4',6-diamidino-2-phenylindole (DAPI) a nuclear cell marker (Figure6.d)

Ischemic-induced neuronal loss

An important reduction of the area occupied by neurons NeuN⁺ was detected in MCAo groups: HA-hydrogel+hMSC (3.27%±0.77) hMSC (3.39%±0.79) and PBS (3.20%±0.79) in comparison to group Sham (6.46%±0.73). The ischemic groups were no statistically different each other, indicating no protective effects mediated by hMSCs alone or co-administrated with hydrogel in the lesion boundary at day 29 (Figure 5d).

4. Discussion

The optimization of cell therapeutic effects is a crucial point in post-stroke transplantation. However, a major issue remains in post-stroke intracerebral cell therapy, the substantial loss of transplanted cells (Liang et al., 2013).

The development of tissue engineering emerges such as an alternative to improve this cell engraftment and survival. Several biomaterials have been used with this goal, promoting beneficial effects (Boisserand et al., 2016; Lee et al., 2015).

In the present study, we used a synthetic hydrogel HyStemTM-HP cell culture scaffold co-administrated with hMSCs to evaluate its effects on cell survival, brain remodeling and functional recovery after stroke.

Hydrogel compounds

HyStemTM-HP hydrogel is a synthetic biomaterial used in cell culture application by their properties similar to ECM. Engineered scaffolds are developed to be a three-dimensional structure that promotes cell adhesion, differentiation, minimal immunogenicity and to protect grafted cells from the host immune response (Aurand et al., 2012).

This gel contains hyaluronic acid, one of the main compound of ECM, PEGDA (cross-linker) and Gelin-S (denatured collagen of animal origin). This commercial gel has the advantage to

be liquid after mixing the compounds allowing a homogeneous integration of stem cells. HyStemTM-HP can be injected in a liquid phase and polymerizes *in situ*. This process is not dependent on pH or temperature.

Similar synthetic hyaluronan-based hydrogels were tested *in vitro* and *in vivo* post-stroke promoting differentiation and cell survival (Liang et al., 2013; Mai et al., 2013).

Lesion size

Neither of the treatments, HA-hydrogel+hMSC or hMSC reduced lesion volume significantly with respect to the infarct group at either time point evaluated by MRI.

A reduction of lesion size induced by cell therapy by intravenous (Borlongan et al., 2004) or intracerebral way is reported in pre-clinical studies (Leong et al., 2012; Zhu et al., 2015). Nevertheless, in the present study, we did not detect an effect of the lesion size promoted by HA-hydrogel+hMSC or only hMSCs. This result can be explained by the delay of hMSC administration. We administered the hMSC only one week after stroke, during the subacute phase. Mechanisms implicated on brain protection induced by cell therapy, including reduction of cellular death and inflammation are reported usually when cells are administered during the acute phase, within some hours after stroke onset (Leong et al., 2012; Zhu et al., 2015). Effective improvements after cell therapy, including behavioral improvements are reported despite negative results on lesion size reduction (Gutiérrez-Fernández et al., 2013).

Apparently, 7 days after MCAo lesion size is relatively stable, in this phase cell-based therapies target peri-infarct remodeling (Kelly et al., 2004).

Functional outcome

A spontaneous improvement on sensory-motor behavior was observed in our three ischemic groups. Surprisingly neither of treatments HA-hydrogel+hMSC nor only hMSCs were able to improve the functional recovery in comparison to PBS group (Figure 3a and 3b).

A longer follow-up is maybe required to determine if a synergic effect could be observed. In a recent study from our team, intravenous injection of hMSCs provided functional benefits only 4 to 7 weeks after injection and increased cerebral angiogenesis in the stroke lesion, *via* a release of endogenous angiogenic factors enhancing the stabilization of newborn vessels. They concluded that an enhanced angiogenesis could therefore be a mean to improve functional recovery after stroke (Moisan et al., 2016).

hMSC detection

In the present study human MSCs from bone marrow were used. These cells were detected by immunofluorescence, allowing a visualization and detection of human cells. Human HuNu+ cells were detected at the three time points in both hMSC groups. However, at day 29, HuNu+ cells were detected mainly in brain samples from the HA-hydrogel +hMSC group.

Human MSCs were detected, at day 0 to be sure about intracerebral administration procedure (data not showed, n=2 rats per treated group) and two weeks after administration to evaluate the survival (n=4 per treated group, data not showed). Finally, we detect the hMSC HuNu+ at day 29 (three weeks after administration) in 66% of rats of the group HA-hydrogel+hMSC against 20% in the group hMSC. The increase in cell survival mediated by co-administration with biomaterials is widely reported (Jin et al., 2010; Liang et al., 2013; Sarnowska et al., 2013; Zhong et al., 2010). Zhong et al. for example, demonstrated an increase in neural SC survival using HyStem-HP hydrogel *in vitro*, cells cultured within hydrogel presented an increase in survival rate in conditions of deprivation of trophic factors and nutritional support

(to mimic ischemic conditions) in comparison to the control group (Zhong et al., 2010). Our results confirm stem cell protection mediated by HA-hydrogel in ischemic conditions.

Beneficial responses promoted by MSCs are primarily mediated by paracrine actions (Castillo-Melendez et al., 2013). MSCs secrete trophic factors stimulating brain protection when administered in the acute phase, for example by modulating the inflammatory response to ischemia (Acosta et al., 2015). Trophic factors also improve mechanism implicated in brain repair such as neurogenesis (Salgado et al., 2015) and angiogenesis (Zhu et al., 2015).

HA-hydrogel effectively increased the hMSC survival in the present study.

HA-hydrogel + hMSC hydrogel improves vascular markers

Post-stroke angiogenesis seems to be a major role on brain remodeling (Castillo-Melendez et al., 2013; Taguchi et al., 2004).

Angiogenesis is a biological process involving the growth of new blood vessels from pre-existing vessels. Angiogenesis is quiescent in adult brain in physiological conditions (Carmeliet and Jain, 2000), however, angiogenic process is activated post ischemic stroke.

Recently, studies have shown an increase in vessel density mediated by biomaterial co-administration with stem cells or angiogenic growth factors such as vascular endothelial growth factor (VEGF) (Kim et al., 2015; Portalska et al., 2014). In the present study, an increase in cerebrovascular remodeling markers was also detected. We used two cell markers associated with angiogenesis, RECA-1 (rat endothelial cells) and Collagen type IV (vascular basement membrane) in our study. HA-hydrogel+hMSC group presented the higher percentage (%) of RECA and Collagen-IV (COL-IV) positive cells in lesion boundary, with a significant increase in comparison to PBS group only for COL IV+ cells. Moisan et al. studied the kinetic of angiogenesis after MCAO, showing different time window of endothelial cells proliferation and vessels stability (Moisan et al., 2014). RECA1 increase is

probably associated with the initial phase of endothelial cells proliferation while COL-IV increase is maybe related to stabilization process once that COL-IV⁺ cells are located in vascular basement membrane (Hallmann et al., 2005)

Hydrogel and hMSC treatment on astrocytic and neuronal response

The percentage of astrocytes GFAP⁺ microglia/macrophages cells Iba1⁺ and neurons NeuN⁺ was not altered by HA-hydrogel+hMSC in comparison to the other ischemic groups. Such as expected, in the zone adjacent to lesion border, we detected an astrogliosis, microglia/macrophage activation and a cellular loss, (including neurons NeuN⁺) induced by ischemic lesion. A mild inflammatory response towards the implanted hydrogel similar to synthetic HA-based hydrogel used in our study was observed (Liang et al., 2013). HyStemTM-HP uses a cross-linker (PEGDA) related such as pro-inflammatory.

Nevertheless, the group hydrogel does not presented an increase in the astrogliosis neither in microglia/macrophage activation compared to the other ischemic groups, indicating a good biocompatibility in ischemic conditions.

Conclusion

Biomaterials developed for use in central nervous system such as the hyaluronic-acid-based hydrogel used in the present study, can represent an important step for the improvement of cell therapy.

HyStemTM-HP hydrogel is well-tolerated and effectively improved MSC survival. Post-stroke angiogenesis, one of the main components of post-stroke remodeling was also improved by the combination HA-hydrogel +hMSC. Nevertheless, the improvement of cell survival and vascular density were not able to improve behavioral outcomes. Further optimization of

biomaterials and mixing procedures with cells are warranted to prove a benefit of hydrogel cell therapy in stroke.

References

- Acosta, S.A., Tajiri, N., Hoover, J., Kaneko, Y., and Borlongan, C.V. (2015). Intravenous Bone Marrow Stem Cell Grafts Preferentially Migrate to Spleen and Abrogate Chronic Inflammation in Stroke. *Stroke* 46, 2616–2627.
- Aurand, E.R., Lampe, K.J., and Bjugstad, K.B. (2012). Defining and designing polymers and hydrogels for neural tissue engineering. *Neurosci. Res.* 72, 199–213.
- Boisserand, L.S., Kodama, T., Papassin, J., Auzely, R., Moisan, A., Rome, C., and Detante, O. (2016). Biomaterial Applications in Cell-Based Therapy in Experimental Stroke. *Stem Cells Int.* 2016.
- Borlongan, C.V., Hadman, M., Sanberg, C.D., and Sanberg, P.R. (2004). Central Nervous System Entry of Peripherally Injected Umbilical Cord Blood Cells Is Not Required for Neuroprotection in Stroke. *Stroke* 35, 2385–2389.
- Campbell, B.C.V., Donnan, G.A., Lees, K.R., Hacke, W., Khatri, P., Hill, M.D., Goyal, M., Mitchell, P.J., Saver, J.L., Diener, H.-C., et al. (2015). Endovascular stent thrombectomy: the new standard of care for large vessel ischaemic stroke. *Lancet Neurol.* 14, 846–854.
- Carmeliet, P., and Jain, R.K. (2000). Angiogenesis in cancer and other diseases. *Nature* 407, 249–257.
- Castillo-Melendez, M., Yawno, T., Jenkin, G., and Miller, S.L. (2013). Stem cell therapy to protect and repair the developing brain: a review of mechanisms of action of cord blood and amnion epithelial derived cells. *Neuroendocr. Sci.* 7, 194.
- Centenaro, L.A., Jaeger, M. da C., Ilha, J., de Souza, M.A., Kalil-Gaspar, P.I., Cunha, N.B., Marcuzzo, S., and Achaval, M. (2011). Olfactory and respiratory lamina propria transplantation after spinal cord transection in rats: Effects on functional recovery and axonal regeneration. *Brain Res.* 1426, 54–72.
- Detante, O., Valable, S., de Fraipont, F., Grillon, E., Barbier, E.L., Moisan, A., Arnaud, J., Moriscot, C., Segebarth, C., Hommel, M., et al. (2012). Magnetic resonance imaging and fluorescence labeling of clinical-grade mesenchymal stem cells without impacting their phenotype: study in a rat model of stroke. *Stem Cells Transl. Med.* 1, 333–341.
- Duncan, P.W., Zorowitz, R., Bates, B., Choi, J.Y., Glasberg, J.J., Graham, G.D., Katz, R.C., Lamberty, K., and Reker, D. (2005). Management of Adult Stroke Rehabilitation Care A Clinical Practice Guideline. *Stroke* 36, e100–e143.
- Feigin, V.L., Forouzanfar, M.H., Krishnamurthi, R., Mensah, G.A., Connor, M., Bennett, D.A., Moran, A.E., Sacco, R.L., Anderson, L., Truelsen, T., et al. (2014). Global and regional burden of stroke during 1990–2010: findings from the Global Burden of Disease Study 2010. *Lancet* 383, 245–254.
- Gutiérrez-Fernández, M., Rodríguez-Frutos, B., Ramos-Cejudo, J., Teresa Vallejo-Cremades, M., Fuentes, B., Cerdán, S., and Díez-Tejedor, E. (2013). Effects of intravenous administration of allogenic bone marrow- and adipose tissue-derived mesenchymal stem cells on functional recovery and brain repair markers in experimental ischemic stroke. *Stem Cell Res. Ther.* 4, 11.

Gutiérrez-Fernández, M., Otero-Ortega, L., Ramos-Cejudo, J., Rodríguez-Frutos, B., Fuentes, B., and Díez-Tejedor, E. (2015). Adipose tissue-derived mesenchymal stem cells as a strategy to improve recovery after stroke. *Expert Opin. Biol. Ther.* *15*, 873–881.

Hallmann, R., Horn, N., Selg, M., Wendler, O., Pausch, F., and Sorokin, L.M. (2005). Expression and Function of Laminins in the Embryonic and Mature Vasculature. *Physiol. Rev.* *85*, 979–1000.

Hicks, A.U., Lappalainen, R.S., Narkilahti, S., Suuronen, R., Corbett, D., Sivenius, J., Hovatta, O., and Jolkkonen, J. (2009). Transplantation of human embryonic stem cell-derived neural precursor cells and enriched environment after cortical stroke in rats: cell survival and functional recovery. *Eur. J. Neurosci.* *29*, 562–574.

Jin, K., Mao, X., Xie, L., Galvan, V., Lai, B., Wang, Y., Gorostiza, O., Wang, X., and Greenberg, D.A. (2010). Transplantation of human neural precursor cells in Matrigel scaffolding improves outcome from focal cerebral ischemia after delayed postischemic treatment in rats. *J. Cereb. Blood Flow Metab. Off. J. Int. Soc. Cereb. Blood Flow Metab.* *30*, 534–544.

Kelly, S., Bliss, T.M., Shah, A.K., Sun, G.H., Ma, M., Foo, W.C., Masel, J., Yenari, M.A., Weissman, I.L., Uchida, N., et al. (2004). Transplanted human fetal neural stem cells survive, migrate, and differentiate in ischemic rat cerebral cortex. *Proc. Natl. Acad. Sci. U. S. A.* *101*, 11839–11844.

Kim, D.H., Seo, Y.K., Thambi, T., Moon, G.J., Son, J.P., Li, G., Park, J.H., Lee, J.H., Kim, H.H., Lee, D.S., et al. (2015). Enhancing neurogenesis and angiogenesis with target delivery of stromal cell derived factor-1 α using a dual ionic pH-sensitive copolymer. *Biomaterials* *61*, 115–125.

Kwiatkowski, T.G., Libman, R.B., Frankel, M., Tilley, B.C., Morgenstern, L.B., Lu, M., Broderick, J.P., Lewandowski, C.A., Marler, J.R., Levine, S.R., et al. (1999). Effects of Tissue Plasminogen Activator for Acute Ischemic Stroke at One Year. *N. Engl. J. Med.* *340*, 1781–1787.

Lee, S., Valmikinathan, C.M., Byun, J., Kim, S., Lee, G., Mokarram, N., Pai, S.B., Um, E., Bellamkonda, R.V., and Yoon, Y. (2015). Enhanced therapeutic neovascularization by CD31-expressing cells and embryonic stem cell-derived endothelial cells engineered with chitosan hydrogel containing VEGF-releasing microtubes. *Biomaterials* *63*, 158–167.

Leong, W.K., Henshall, T.L., Arthur, A., Kremer, K.L., Lewis, M.D., Helps, S.C., Field, J., Hamilton-Bruce, M.A., Warming, S., Manavis, J., et al. (2012). Human Adult Dental Pulp Stem Cells Enhance Poststroke Functional Recovery Through Non-Neural Replacement Mechanisms. *Stem Cells Transl. Med.* *1*, 177–187.

Liang, Y., Walczak, P., and Bulte, J.W.M. (2013). The Survival of Engrafted Neural Stem Cells Within Hyaluronic Acid Hydrogels. *Biomaterials* *34*, 5521–5529.

Mai, M., Hempel, U., Hacker, M.C., and Dieter, P. (2013). Effects of HyStemTM-HP Hydrogel Elasticity on Osteogenic Differentiation of Human Mesenchymal Stromal Cells. *Cell. Mol. Bioeng.* *7*, 155–164.

Moisan, A., Favre, I.M., Rome, C., Grillon, E., Naegele, B., Barbieux, M., De Fraipont, F., Richard, M.-J., Barbier, E.L., Rémy, C., et al. (2014). Microvascular Plasticity After Experimental Stroke: A Molecular and MRI Study. *Cerebrovasc. Dis.* 38, 344–353.

Moisan, A., Favre, I., Rome, C., De Fraipont, F., Grillon, E., Coquery, N., Mathieu, H., Mayan, V., Naegele, B., Hommel, M., et al. (2016). Intravenous injection of clinical grade human MSCs after experimental stroke: functional benefit and microvascular effect. *Cell Transplant.*

Pakulska, M.M., Ballios, B.G., and Shoichet, M.S. (2012). Injectable hydrogels for central nervous system therapy. *Biomed. Mater. Bristol Engl.* 7, 24101.

Pierot, L., Soize, S., Benaissa, A., and Wakhloo, A.K. (2015). Techniques for Endovascular Treatment of Acute Ischemic Stroke From Intra-Arterial Fibrinolytics to Stent-Retrievers. *Stroke* 46, 909–914.

Portalska, K.J., Teixeira, L.M., Leijten, J.C.H., Jin, R., van Blitterswijk, C., de Boer, J., and Karperien, M. (2014). Boosting angiogenesis and functional vascularization in injectable dextran-hyaluronic acid hydrogels by endothelial-like mesenchymal stromal cells. *Tissue Eng. Part A* 20, 819–829.

Robert, L. (2015). Hyaluronan, a truly “youthful” polysaccharide. Its medical applications. *Pathol. Biol.* 63, 32–34.

Salgado, A.J., Sousa, J.C., Costa, B.M., Pires, A.O., Mateus-Pinheiro, A., Teixeira, F.G., Pinto, L., and Sousa, N. (2015). Mesenchymal stem cells secretome as a modulator of the neurogenic niche: basic insights and therapeutic opportunities. *Front. Cell. Neurosci.* 249.

Sarnowska, A., Jablonska, A., Jurga, M., Dainiak, M., Strojek, L., Drela, K., Wright, K., Tripathi, A., Kumar, A., Jungvid, H., et al. (2013). Encapsulation of mesenchymal stem cells by bioscaffolds protects cell survival and attenuates neuroinflammatory reaction in injured brain tissue after transplantation. *Cell Transplant.* 22 *Suppl 1*, S67-82.

Taguchi, A., Soma, T., Tanaka, H., Kanda, T., Nishimura, H., Yoshikawa, H., Tsukamoto, Y., Iso, H., Fujimori, Y., Stern, D.M., et al. (2004). Administration of CD34+ cells after stroke enhances neurogenesis via angiogenesis in a mouse model. *J. Clin. Invest.* 114, 330–338.

Wang, H., Chen, M., Wang, F., Dai, L., Fei, A., Liu, J., Li, H., Shen, S., Liu, M., and Pan, S. (2015). Comparison of Therapeutic Effect of Recombinant Tissue Plasminogen Activator by Treatment Time after Onset of Acute Ischemic Stroke. *Sci. Rep.* 5.

Zhong, J., Chan, A., Morad, L., Kornblum, H.I., Fan, G., and Carmichael, S.T. (2010). Hydrogel matrix to support stem cell survival after brain transplantation in stroke. *Neurorehabil. Neural Repair* 24, 636–644.

Zhu, J., Liu, Q., Jiang, Y., Wu, L., Xu, G., and Liu, X. (2015). Enhanced angiogenesis promoted by human umbilical mesenchymal stem cell transplantation in stroked mouse is Notch1 signaling associated. *Neuroscience* 290, 288–299.

Table 1. Estimation of lesion volume using Magnetic Resonance Imaging

Groups	Day 8	Day 15	Day 22	Day29
HA+hMSC	92.3±19.7	87.7±19.7	89.4±19.0	81.5±18.5
hMSC	91.2±16.5	85.9±15.1	86.2±13.5	81.4±13.3
PBS	95.5±23.0	93.5±19.5	93.3±19.5	86.8±17.0
Sham	-	-	-	-

Table1. Lesion volume estimation within the region of interest (ROI) Lesion. No difference was detected by repeated measures analyses of variance (ANOVA) among the different groups. Hyaluronic Acid-based hydrogel (HA) and human Mesenchymal Stem Cells (hMSC) group n=9; hMSC group, n=10; phosphate buffered solution (PBS) group, n=7 and Sham, n=8. Values are presented in mean±standard error of the mean.

Table2.a Modified Neurological severity score test (mNSS)

Groups	Pre	Day 6	Day 14	Day 21	Day28
HA+hMSC	0	4.6±1.2	3.3±0.9	2.9±0.7	2.3±0.5
hMSC	0	4.5±1.0	2.7±0.7	2.8±0.5	2.5±0.4
PBS	0	5.0±1.5	4.4±1.3	3.4±1.0	2.9±0.9
SHAM	0	0	0	0	0

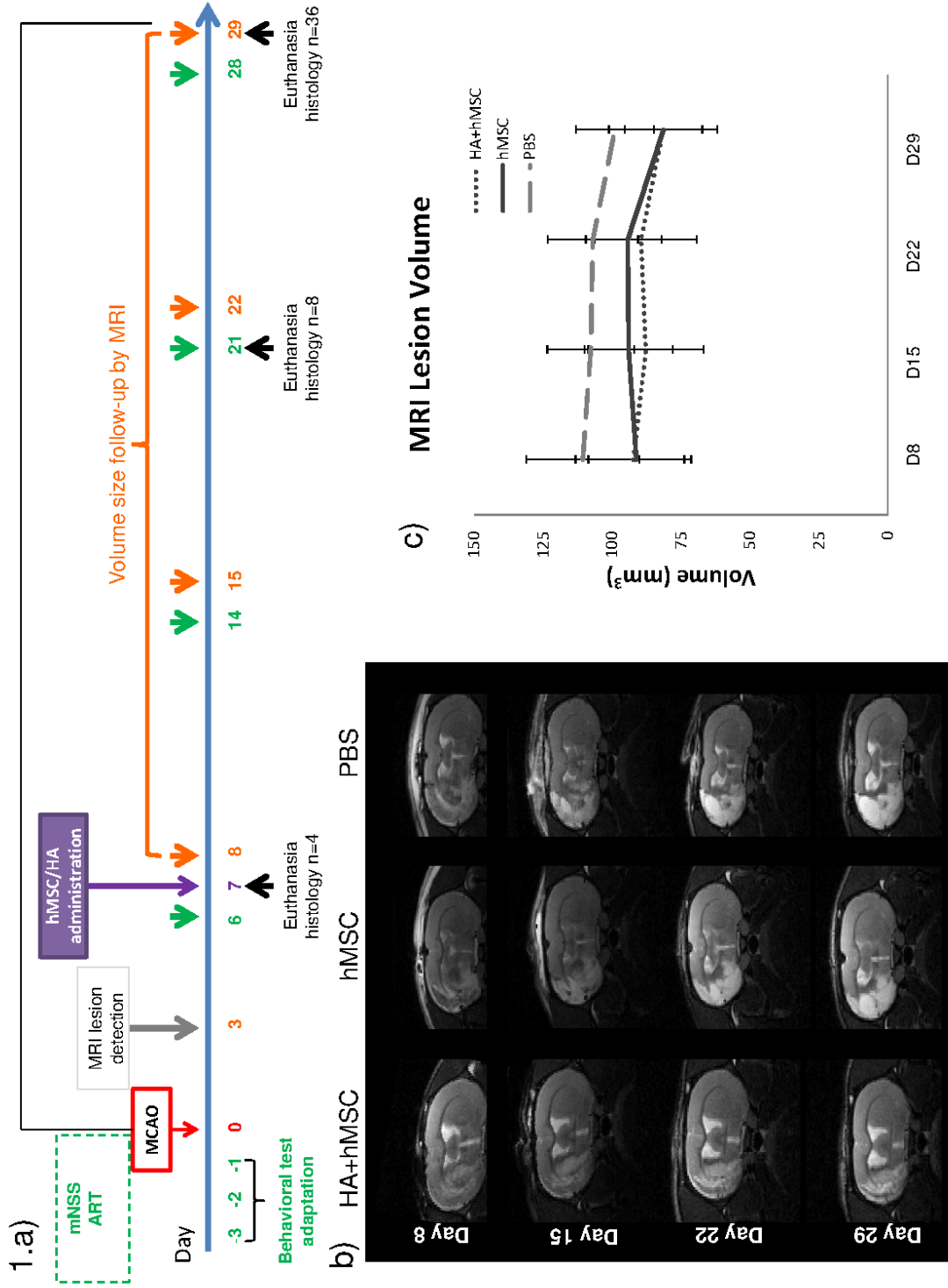
Table 2.b Adhesive removal test (impaired left forepaw)

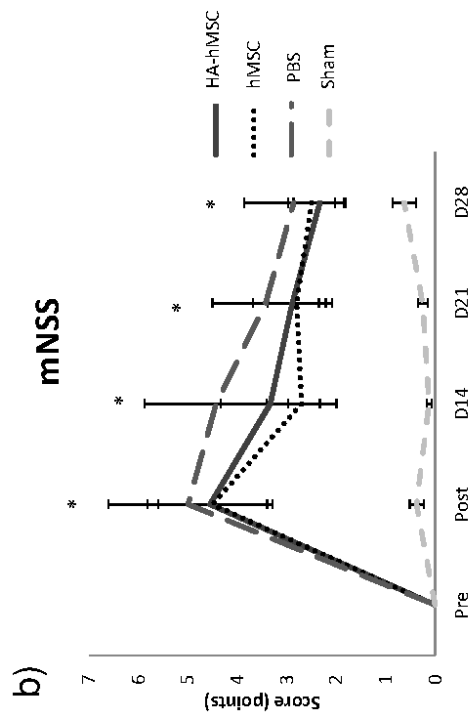
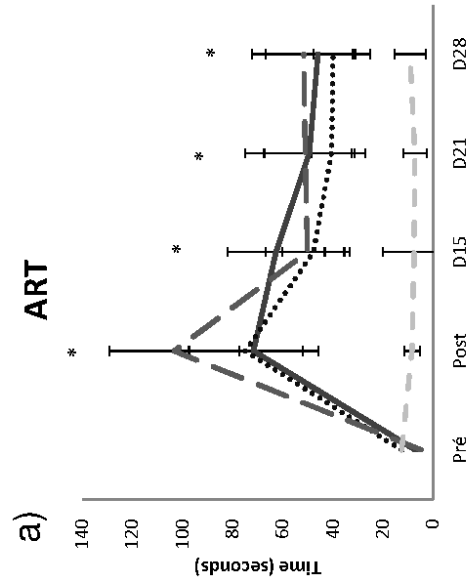
Groups	Pre	Day 6	Day 14	Day 21	Day28
MSC-HA	7.1±0.9	71.63±24.3	62.6±18.2	49.4±17.0	45.9±19.7
hMSC	12.6±3.6	74.80±21.7	47.7±11.7	40.5±7.6	39.9±7.5
PBS	4.7±0.6	103.23±24.1	50.1±15.5	50.9±22.1	51.6±19.1
SHAM	12.2±3.2	10.12±2.9	19.2±11.6	11.5±4.3	14.7±5.8

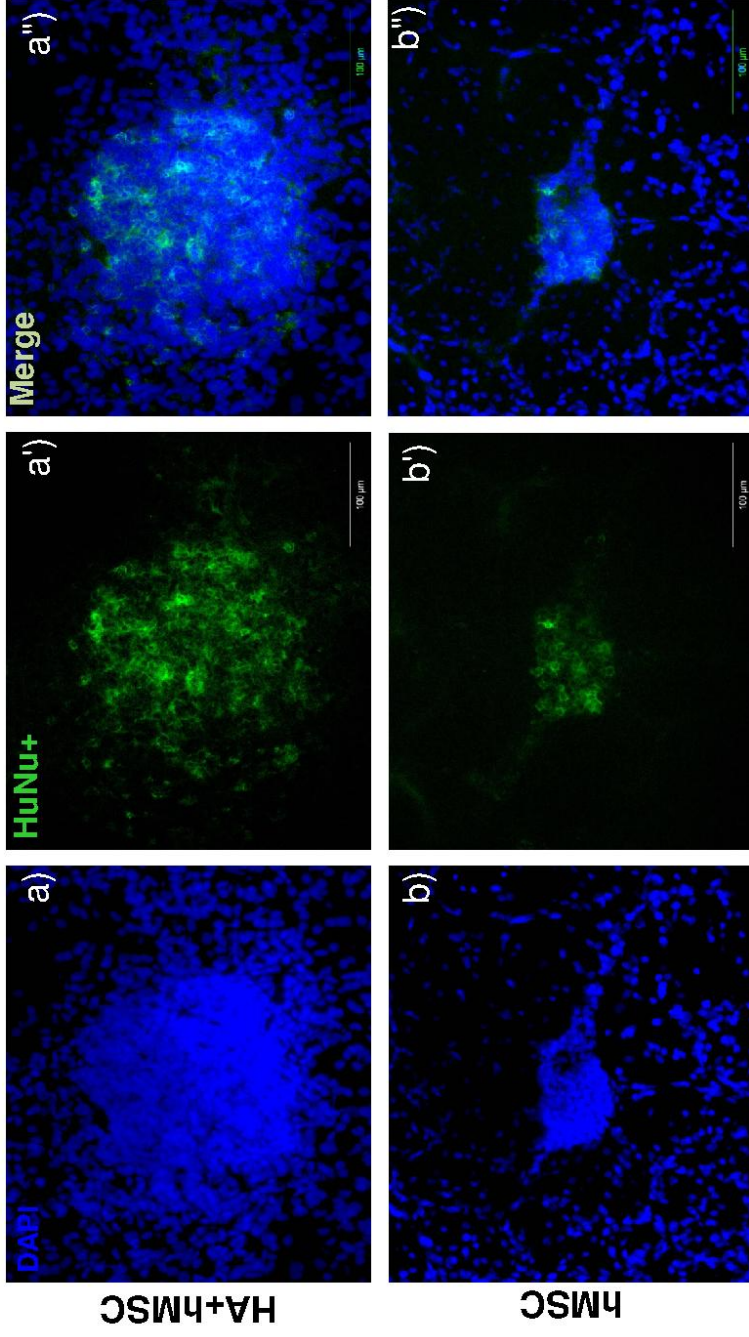
Table 2: Sensory-motor behavioral tests means values by group at different time points.

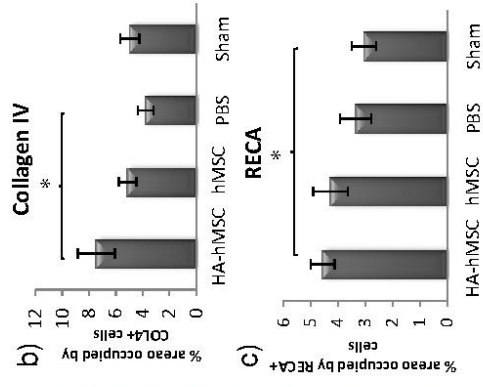
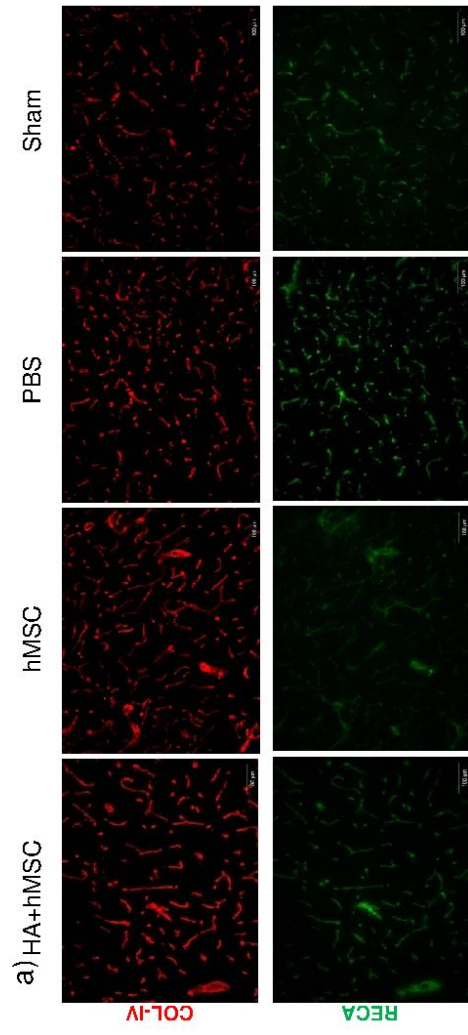
2.a) mNSS test pre middle cerebral artery occlusion (MCAO) induction, no deficits were detected. In bold, values different from pre-MCAO. **2.b)** Mean time in seconds to remove the adhesive from impaired left forepaw at different time points. In bold, values different from pre-MCAO. No differences were detected among ischemic groups after MCAO. Hyaluronic Acid-based hydrogel (HA) and human Mesenchymal Stem Cells (hMSC) group n=9; hMSC group, n=10; phosphate buffered solution (PBS) group, n=7 and Sham, n=8. Values are presented in mean±standard error of mean

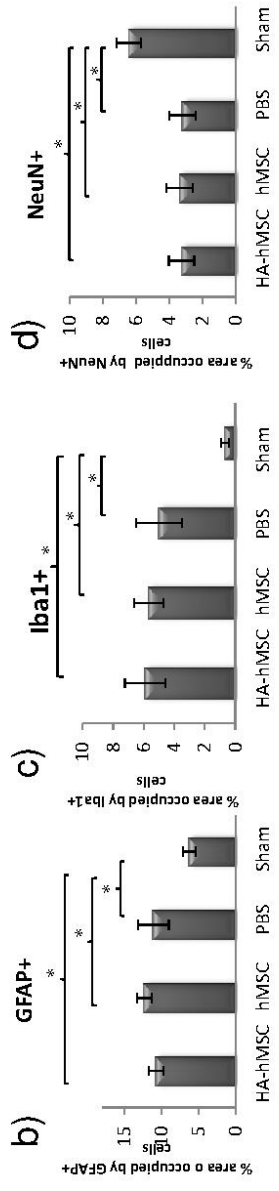
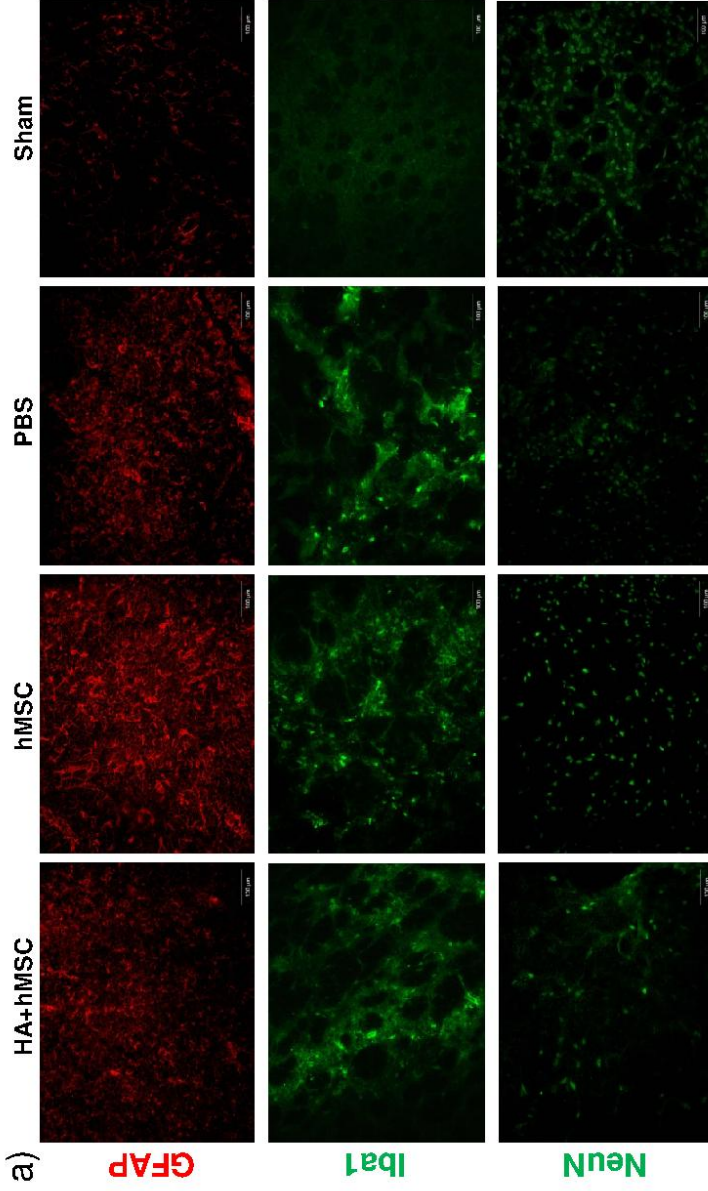
FIGURES











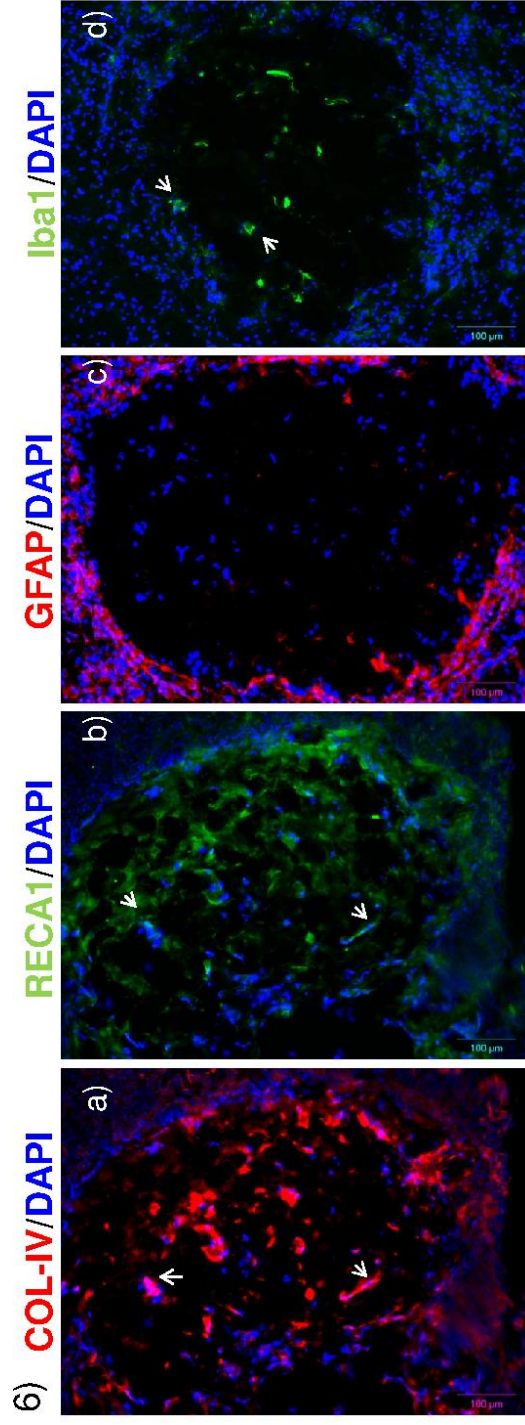


Figure legends:

Figure 1. a) Experimental design. The rats were adapted during three days before surgery in behavioral tests: modified Neurological severity score (mNSS) and adhesive removal test (ART). At day 0 brain ischemia was induced by middle cerebral artery occlusion (MCAO). Brain lesion was detected by magnetic resonance imaging (MRI) and day 3 and animals were reevaluated at days 8, 15, 22 and 29. Treatment using human Mesenchymal Stem Cells (hMSC) associated or not with a hyaluronic acid-based hydrogel (HA) was administrated at day 7. Rats were euthanized at different time points for histological analysis. At day 7, some hours after intracerebral injection (n=2 at group HA-hMSC and 2 at group hMSC); at day 21, two weeks after intracerebral injection (n=4 at group HA-hMSC and 4 at group hMSC) and at the end of experiments at day 29 (n=36 rats). **b)** MRI anatomical images T₂ weighted at different time points for each experimental group. **c)** Lesion volume evaluated by MRI at different time points in the groups that had received a MCAO. No differences were detected among the different groups by a repeated measures evaluation $p > 0.05$. Data are expressed in mean \pm standard error of mean (n=36).

Figure 2. Sensory-motor behavioral tests follow-up. a) Mean time (in seconds) to remove adhesive in adhesive removal test (ART) at different time points. Ninety minutes of middle cerebral artery occlusion (MCAo) produced a sensory deficit evidenced by a difference between ischemic and sham groups (*) $p < 0.05$. Rats treated with HA-hMSC (n=9), hMSC (n=10) were no different from no treatment group PBS (n=7). **b)** Mean of points in modified neurological severity score (mNSS) test, MCAo resulted in a motor deficit evaluated by this composite test when compared to sham group (*) $p < 0.05$. No significant behavioral effects induced by treatments was detected. Data are expressed in mean \pm standard error of mean (n=36).

Figure 3. Human mesenchymal stem cells (hMSC) detection. MSC were detected in the two treated groups HA-hMSC and hMSC using a human nucleus cell marker (HuNu). Representative images of Human cells labeled by the peri-nuclear HuNu antibody (in green) were well co-localized with nuclear DNA marker 4',6-diamidino-2-phenylindole (DAPI) in blue in the group **HA-hMSC: DAPI a**, **HuNu a'**, **merge a''** and **hMSC: DAPI b**, **HuNu b'** and **merge b''** 21 days after administration (at day 29).

Figure 4. Angiogenic markers. a) Image representative of collagen type-IV (in red) and RECA1 (in green) detection in the different experimental groups. b) The percentage of the zone occupied by angiogenic marker collagen type-IV in the group HA-hMSC was increased when compared to the group PBS at day 29 ($p < 0.05$). c) The percentage of the zone occupied by angiogenic marker RECA1 in the group HA-hMSC was increased when compared to the group Sham ($p < 0.05$). Data are expressed in mean \pm standard error of mean ($n=36$).

Figure 5. a) Image representative of glial fibrillary acid protein (GFAP), in red; adult neuronal marker (NeuN) in green, and microglial/macrophage cells (Iba1) in green at different experimental groups. b) The percentage (%) of GFAP+ cells increased in the three ischemic groups when compared to group Sham. c) The % of Iba1+ cells increased in the three ischemic groups when compared to group Sham. Data were considered significant when $p < 0.05$. Data are expressed in mean \pm standard error of mean ($n=36$). d) Brain ischemia induced a neuronal loss in peri-infarct zone when compared to group Sham, evidenced by a reduction of % of zone occupied by cells NeuN+.

Figure 6. Host cells migration toward hydrogel. Some vascular markers, collagen type IV positive (+) cells a); endothelial cells RECA1+ b) were detected within hydrogel and were co-localized with the nuclear DNA cell marker DAPI (indicated by white arrows). Astrocytes glial fibrillary acid (GFAP+) cells were detected essentially at hydrogel boundary c). Microglia/macrophage cells Iba1+ were detected within hydrogel, some cells were co-localized with DAPI.

6.1.6 Additional results

In our second study, we also acquired multiparametric MRI scans to evaluate the lesion evolution and compare the brain recovery mediated by different treatments. The acquisition protocol used is described in the general methodology section. The totality of MRI data was not completely analyzed, additionally, the journal chosen to submit our paper is not a MRI specialized journal. For this reason, results of multiparametric MRI study will be subject of another article which will be prepared after thesis defense.

MRI ADC

Additionally to the lesion volume (results presented in the above article), we evaluated the ADC values within the ROI Lesion. We detected no differences in the mean apparent diffusion coefficient (ADC) at day 29 within the ROI Lesion: HA-hMSC $1775.2 \pm 223.4 \mu\text{m}^2/\text{s}$ (n=9); hMSC $1758.2 \pm 198.8 \mu\text{m}^2/\text{s}$ (n=10); and PBS $1894.0 \pm 235.8 \mu\text{m}^2/\text{s}$ (n= 7). A difference among ischemic and Sham groups ($932,6 \pm 36.8 \mu\text{m}^2/\text{s}$, n=10) was detected by an unpaired T-test ($p < 0.05$) (Figure 25).

MRI perfusion

We detect no difference induced by treatments at day 29 in the global value of CBF within ROI Lesion (HA-hMSC $144.8 \pm 15.5 \text{ mL}/100\text{g}/\text{min}$, n=9; hMSC $151.5 \pm 23.9 \text{ mL}/100\text{g}/\text{min}$, n=10; and PBS $142.2 \pm 26.4 \text{ mL}/100\text{g}/\text{min}$, n= 7). The mean values of CBF presented a high heterogeneity within ROI Lesion (Figure 26) for this reason we did not detect a difference among ischemic and Sham groups ($168.2 \pm 16.3 \text{ mL}/100\text{g}/\text{min}$, n=10).

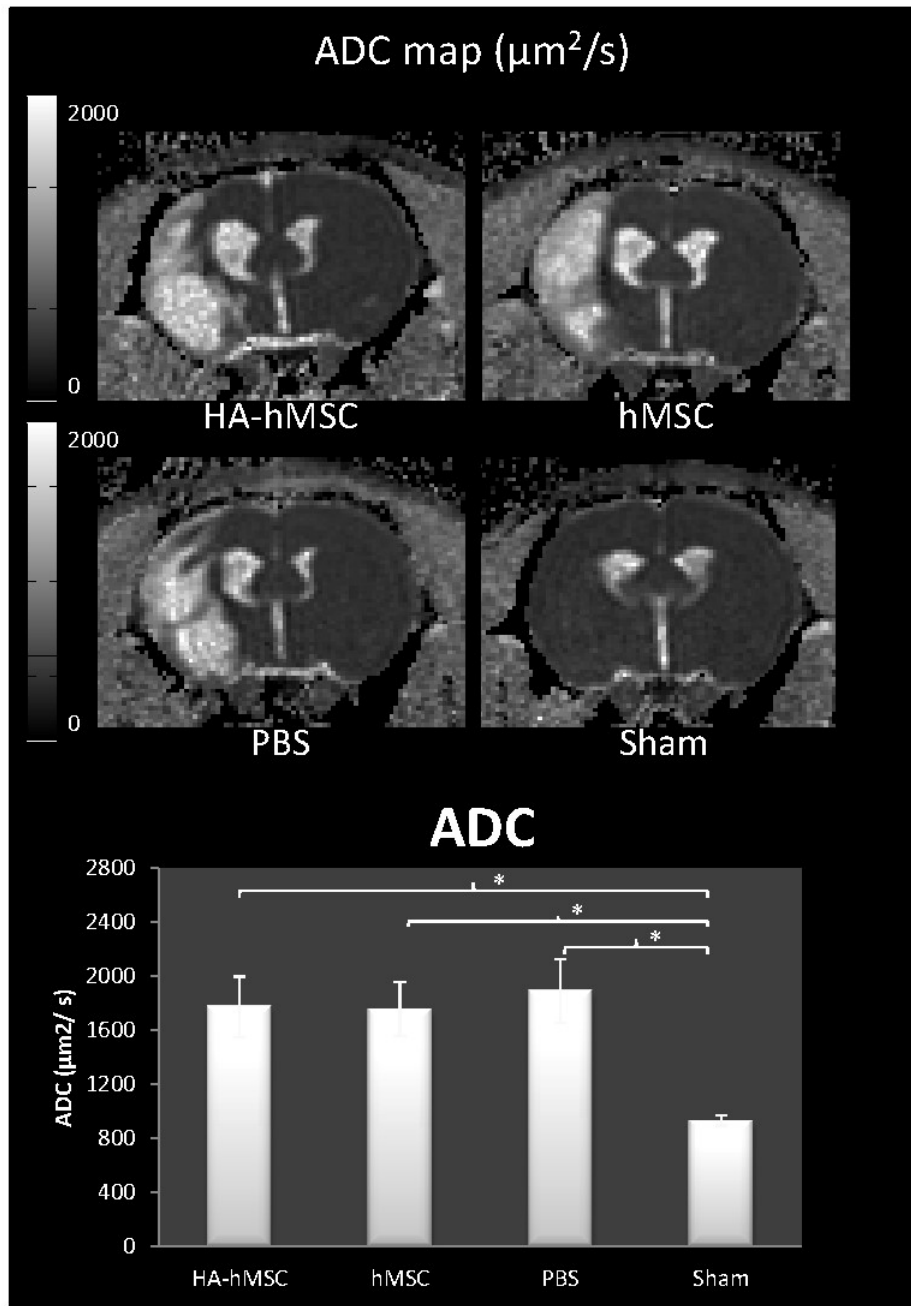


Figure 25: Apparent diffusion coefficient map (ADC). Illustrative images of lesion in ADC 29 days after stroke. Ischemic lesion induced an increase in mean values of ADC within ROI Lesion in the three ischemic groups when compared to group Sham. No differences were detected among ischemic groups. Data were considered significant when $p < 0.05$. Data are expressed in mean \pm standard error of mean (n=36).

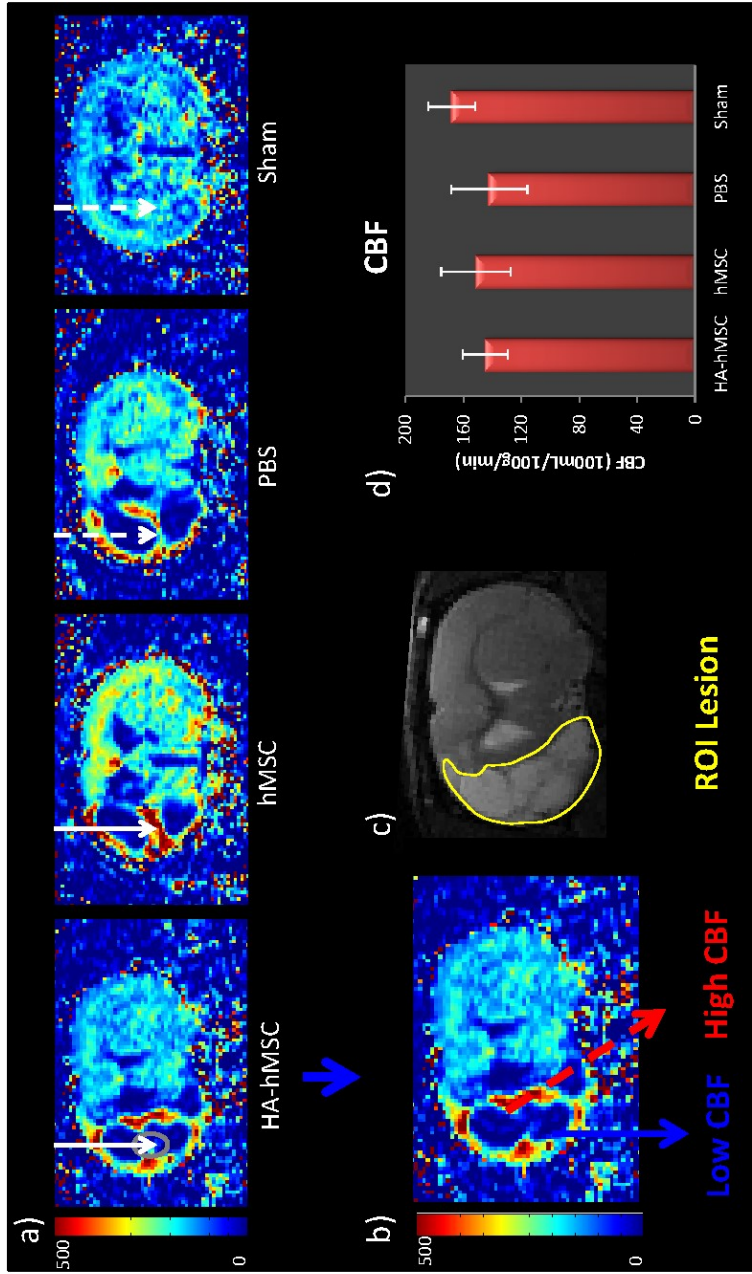


Figure 26: Cerebral blood flow map (CBF). a) Representative images of MRI CBF map at day 29 in the different experimental groups; b) High heterogeneity in the lesion zone evidenced by zones of very high and very low CBF values; white arrows represent the injection site, gray circle represents hydrogel injection site c) Illustrative image of ROI Lesion defined on T₂weighted images, and d) CBF mean values within ROI Lesion and corresponding zone on group sham, due to the high heterogeneity inside this zone, no differences were detected among the experimental groups.

Mortality

Middle cerebral artery occlusion model induced during 90 minutes promoted an important mortality rate, superior to 50%. Rats died principally after reperfusion within the first three days.

Table 3: Mortality rates in the different studies.

	Multiparametric MRI (Study 1)		HA-hMSC follow-up (Study 3)	
	Nbr	%	Nbr	%
Excluded				
Total	22	57%	107	66.8%
Post/during MCAo	10	26.3	25	15.6
Post reperfusion	7	18.4	22	13.7
Within first 3 days	3	7.9	37	23.1
Euthanized	2	5.2	13	8.1
Others *	4	10.5	14	6.2
Included	10	26.3	36+12 (+5exc)	33.1
TOTAL:	38	100	160	100

Others* included rats which died at day 7 during hMSC administration, during MRI session or after the first 3 days. Rats were euthanized due to deteriorating of health. (+5exc) animals excluded by technical issue or lack of lesion/deficit but which survived until the end of the experience.

During first hours, the rats usually died due to brain hemorrhage and/or severe edema such as illustrate in Figure 27. These rats usually presented seizures.

A post operatory special care was performed in an intensive way in the three first days (special care includes providing individually special food, water, and cleaning when the rat could not by itself). The rats that not responded positively to the special care, presenting distress signal, severe weight loss or any problem which could compromise the validity of the results were euthanized in accordance with the humane endpoint established in our the ethical protocol.

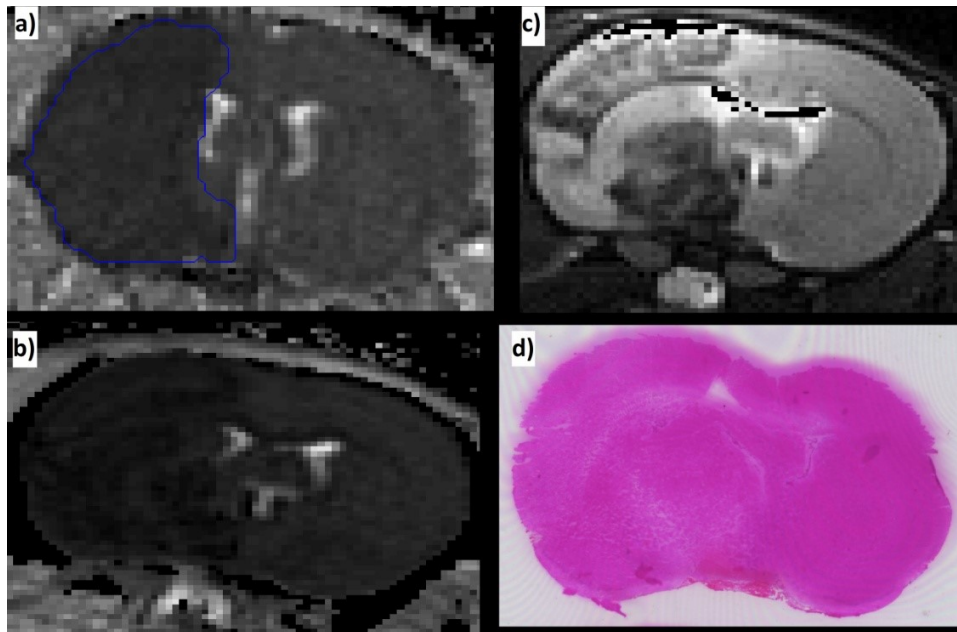


Figure 27: Illustrative MRI and histological images from a rat which died after reperfusion. a) ADC map during occlusion, b) ADC map after death, c) Anatomic T₂W after death, d) corresponding histological slice with Hematoxylin-Erythrosine staining.

6.1.7 Discussion (additional MRI results)

Middle Cerebral Artery occlusion (MCAo) induced by 90 minutes produce an important cortico-striatal lesion for the majority of ischemic animals. Massive lesions usually result in a very important cellular loss and degradation of extracellular matrix, infarct cavity is then fulfilled by extracellular fluid and proteins presenting a hyperintense signal in MRI diffusion. Based on these findings, we were not able to detect hydrogel inside of lesion cavity by MRI after stroke.

Based on a visual inspection and by the incoherence of mean values found within ROI Lesion, we detect a high heterogeneity within ROI Lesion. We detect a very low CBF at the ROI Lesion center and a very high CBF at the lesion boundary. This finding can corroborate our histological findings (an increase of vascular markers) on this region. Moisan *et al.*, in a similar study using hMSC treatment after MCAo demonstrated an increase in angiogenic factors accompanied by an increase in MRI hemodynamic parameters (Moisan et al., 2016)

With the aim to put in evidence the characteristics of lesion and maybe detect some degree of recovery, we decide to create sub-zones of lowest, mean and higher CBF values. These clusters are based on the distribution of contralateral values observed (n=36 rats) such as previously described in other studies in which a high heterogeneity in quantitative MRI perfusion parameters was detected (Ken et al., 2015). Using this classification, we intend to compare the percentage of voxels presenting very low values and very high values in the different groups. This analysis is still in progress.

6.1.8 Conclusions (part II)

In the second part of the present dissertation, we tested the application of biomaterials with the aim to optimize cell therapy effects.

Our pilot study provides evidence that HyStemTM-HP hydrogel has long-lasting duration in brain tissue detected by MRI diffusion and histological detection. HyStemTM-HP hydrogel promoted a host immune response evidenced by the increase of cells GFAP⁺ and Iba1⁺ in the hydrogel border, however, when the hydrogel was administrated in a stroke model, the inflammatory/astrocytic response was not increased in the group hydrogel in comparison with the others ischemic groups.

In the post-stroke follow-up study, HyStemTM-HP hydrogel promoted a protection to hMSC, increasing cell survival. Angiogenesis was improved in HA-hMSC group seven days after induction of ischemic stroke in rats. Unfortunately, despite these effects, neither HA-hydrogel+hMSC nor hMSC treatment resulted in sensory motor recovery.

7 CONCLUSIONS AND PERSPECTIVES

In our experimental studies using a model of ischemic stroke in rats, we are interested in evaluating two important questions: 1) To characterize the alterations in acute phase of stroke detected by multiparametric MRI including diffusion, vascular, hemodynamic and brain tissue oxygenation mapping, and its potential for predicting final necrosis 2) To test a biomaterial hydrogel (HyStemTM-HP) for grafted cells protection within the lesion cavity and its potential for optimizing human mesenchymal stem cells (hMSC) effects. We are able to conclude that:

- Our multiparametric MRI evaluation showed a high heterogeneity at acute phase within the zone of ADC decrease evidenced by significant differences among the regions studied within of the zone of ADC abnormality. This heterogeneity is related to the presence of different degrees of severity into the lesion, this heterogeneity is better detected by voxels-wise approaches such as StO₂ mapping. The region of lesion detected by ADC and StO₂ MRI maps were well correlated to the final necrosis such as demonstrated in our study (Boisserand et al., 2016). However, the lesion volume detected by ADC mapping decreased significantly three weeks after stroke. This could be an indication that salvageable tissue was included within the initial diffusion lesion.

- Our hydrogel *in vivo* biocompatibility study provides evidence that HyStemTM-HP hydrogel has long-lasting duration in brain tissue and could be a good candidate for co-administration with stem cells. HyStemTM-HP hydrogel promoted a host immune response evidenced by the increase of cells GFAP⁺ and Iba1⁺ in the hydrogel edge. Nevertheless, when the hydrogel was administrated in a stroke model, the inflammatory/astrocytic response was not increased by the hydrogel.

- HyStemTM-HP hydrogel promoted cell survival, by protecting hMSC within infarct cavity. Post-stroke angiogenesis was also improved by HA-hMSC treatment seven days after induction of

ischemic stroke in rats. Despite these effects neither HA-hMSC nor hMSC treatment resulted in sensory motor recovery.

Discussion of key findings and perspectives

- Currently, the gold standard in detect viable (penumbra) and non-reversible ischemic areas (ischemic core) is positron emission tomography (PET) $^{15}\text{O}_2$ (Alawneh et al., 2013). Nevertheless, PET scan has a high cost and low availability at hospitals. For this reason, the application of innovating image techniques could be of great interest to the understanding of pathophysiological and recovery process *in vivo*.

Our first study using multiple MRI scans at acute phase allowed to characterize the different zones of ischemia and its heterogeneity during the first minutes (around 100 minutes) of stroke.

Using MRI StO₂ mapping a voxel-wise estimation of tissue oxygen saturation (Christen et al., 2011), we demonstrated that there is salvageable tissue within the zone of ADC decrease, frequently used such as an indicator of irreversible damaged brain. Three weeks after the initial evaluation the volume of infarcted zone presented a good correlation with ADC and StO₂ initial estimations, nevertheless our results confirmed that ADC overestimated the final necrosis.

This first experiment allowed me to acquire some skills required to realize the second experiment (MCAo model, MRI acquisition, and data analysis) which is the principal experiment of my thesis.

These new competences acquired during my thesis are undoubtedly very useful in experimental studies. Multiparametric MRI analysis using hemodynamic and vascular mapping could be an option to evaluate post-stroke remodeling and therapeutic effects such as of cell therapy.

One of our perspectives is to evaluate effects of HA-hydrogel+hMSC treatment through MRI mapping of perfusion (CBF and BVf) and vascular (VSI and density) parameters. These scans were acquired during the follow-up study and the data analysis is ongoing.

- Our pilot study using a biomaterial HyStemTM-HP hydrogel to evaluate the biocompatibility *in vivo* was the first experience with biomaterials in our team. The safety of this hydrogel was previously tested *in vitro* using NSC (Zhong et al., 2010) and was tested using hMSC and the same protocol of preparation that we use (data not shown, experiment done by Dr. Olivier Detante in Kyoto University, Regenerative Medicine Institute IFMS, Japan). An evaluation of hydrogel biocompatibility (host immune response) and degradation was performed. The inflammatory response and astrocytic activation induced by hydrogel in healthy brain did not result in an increase of GFAP/Iba1 in the post-stroke experiment. Additional analysis with a high number of rats is required to quantify degradation rate of HyStemTM-HP hydrogel, a longer follow-up is necessary to demonstrate how long it takes to be completely degraded.

Degradation time is related to cross-linker amount used, a higher concentration of cross-linker results in stronger chemical bonds between polymer compounds and more stability (Aurand et al., 2012). It can increase also hydrogel stiffness which can influence cell survival and differentiation.

The cross-linker used in our experiments (one of the three solutions of HyStemTM-HP kit) was polyethylene glycol diacrylate (PEGDA), the concentration used was the optimal for a gelation at 30min after mixing the compounds with cross-linker. However, PEGDA is associated to increase of inflammatory reaction (Chung et al., 2009).

As a perspective of our experience, we would like to improve technical questions including the biomaterial used to improve the effectiveness of treatment. A new hydrogel produced in our

university by the CERMAV laboratory (Professor Rachel Auzely team) will be tested. This gel is produced by another kind of cross-linking reaction.

-In the context of our follow-up study using a model of MCAo in rats treated with hMSC associated with HyStemTM-HP hydrogel, we demonstrated that hydrogel increased the cell survival evidenced by the higher number of animals with hMSC (HuNu+) at day 29. This protective effect was also demonstrated using neural stem cells in a study of Dr. Carmichael group's (Zhong et al., 2010). The advantage in uses NSC is that in addition to trophic effects, these cells can differentiate into neural or glial (astrocytes) cells when co-administrated with hydrogel hyaluronic acid-based (Moshayedi et al., 2016).

Additionally, hydrogel co-administrated with hMSC increased vascular markers (RECA1 and COL-IV) after three weeks of treatment administration. Angiogenesis is a quiescent process in adult brain which is activated after stroke injury (Carmeliet and Jain, 2011). This mentioned process is a key step in post-stroke brain remodeling because the formation of new vessels is necessary for migration of progenitors cells and trophic factors to the lesion boundary (Castillo-Melendez et al., 2013).

Therapeutic outcomes can be improved also by intracerebral administration of NSC or progenitor cells such as endothelial progenitor cells (EPCs) using hydrogel enriched with trophic factors for a more targeted treatment, for example, to stimulate angiogenesis or differentiation of NSC.

Genetic modification to overexpress trophic factors and hypoxic preconditioning of stem cells can be used for this purpose (Li et al., 2016).

Unfortunately, despite these beneficial effects demonstrated hydrogel co-administrated with hMSC or hMSC alone were not able to improve sensory-motor results. Functional recovery is the principal outcome attempt in experimental stroke studies whereas stroke is a very important cause

of disability. MCAo model promotes reliable deficits and in general way rats present some degree of spontaneous recovery some weeks after stroke.

The Stroke Therapy Academic Industry Roundtable (STAIR) recommend for preclinical tests of novel therapeutics which behavioral outcomes are measured for at last two or three weeks post induction of ischemia (Fisher et al., 2009). This recommendation was applied in our study. Nevertheless, in many studies of cell therapy, behavioral improvements were detected only afterward three weeks (Encarnacion et al., 2011; Moisan et al., 2016; Tornero et al., 2013). Still concerning behavioral tests a very recent study evaluated 16 different behavioral tests commonly used to evaluated MCAo deficits in rats (Trueman et al., 2016). The authors demonstrated that the sample size necessary to detect long-term differences (2 months) between MCAo group *versus* Control is 36 rats for modified neurological severity score (mNSS) and 208 for adhesive removal test (ART) with a power=0.8 and $\alpha=0.05$. For a detection of treatment effect with anticipated 50% in improvement, using the same statistical configurations the number calculated is of 168 rats for mNSS (Trueman et al., 2016). In the mentioned study, the occlusion duration was of 30 minutes, brief MCAo presents higher variability in lesion size requiring a higher sample size (Ström et al., 2013). Fortunately, significant results are reported with small sample sizes, but the homogeneity of lesion size and the choice of most sensitive behavioral tests should be considered to design of future experiments.

The major difficulty of this study was the high mortality rate. A longer time of MCAo promotes a less variable lesion size, but it induces a higher mortality. A study comparing the impact of different experimental stroke methodologies demonstrated that long-time of MCAo (superior to 1 hour) is most lethal than a permanent MCAo (Ström et al., 2013). One important perspective to be considered in future studies is to reduce the MCAo duration to an optimal time which results

in a homogeneous lesion but which reperfusion do not induce to hemorrhage and/or massive brain edema.

Pre-clinical studies are still required to test innovating therapeutic approaches and for the optimization of the current approaches in clinical trials.

8 SCIENTIFIC PRODUCTION

a) Conferences

1) Electronic poster presentation

23rs Annual Meeting of International Society for Magnetic Resonance in Medicine

Title: Quantification of local blood oxygen saturation by MRI to distinguish ischemic core from penumbra in experimental stroke. ISMRM 2015 at Toronto, Canada.

Authors: L. S. B. Boisserand, B. Lemasson, L. Hirschler, V. Hubert, A. Moisan, E. Barbier, C. Rémy, O. Detante.

Prix : *Magna Cum Laude Award*

2) Poster :

Société Française de Résonance Magnétique en Biologie et Médecine at Grenoble, France 2015

Title : Quantification de la saturation locale en O₂ par IRM suite à une ischémie cérébrale

Authors L. S. B. Boisserand, B. Lemasson, L. Hirschler, V. Hubert, A. Moisan, E. Barbier, C. Rémy, O. Detante

23rs Annual Meeting of International Society for Magnetic Resonance in Medicine at Toronto, Canada, 2015

Title: Perfusion/Diffusion mismatch in stroke: what about the hematocrit?

Authors: B. Lemasson, A. Broisat, L. S. B. Boisserand, M. Ahmadi, S. Bacot, A. Soubies, O. Detante, C. Ghezzi, C. Rémy, E. L. Barbier.

46th Annual Meeting of Society for Neurosciences at San Diego, USA, November 2016

Title: Hyaluronic acid hydrogel combined with cell therapy in experimental stroke

Authors: L. S. B. Boisserand, J Papassin, N. Collomb, EL Barbier, C. Rome and O. Detante

b) Publications

Boisserand, Ligia SB, Tomonobu Kodama, Jérémie Papassin, Rachel Auzely, Anaïck Moisan, Claire Rome, and Olivier Detante. “Biomaterial Applications in Cell-Based Therapy in Experimental Stroke.” *Stem Cells International* 2016 (2016).

Ligia Simoes Braga Boisserand; Benjamin Lemasson ; Lydiane Hirschler ; Anaïck Moisan ; Violaine Hubert ; Emmanuel Luc Barbier ; Chantal Rémy ; Olivier Detante “Multiparametric MRI including oxygenation mapping of experimental ischemic stroke” JCBFM. 2016

B. Lemasson, N. Pannetier, N. Coquery, **Ligia S. B. Boisserand**, Nora Collomb, N. Schuff, M. Moseley, G. Zaharchuk, E.L. Barbier*, T. Christen MR Vascular Fingerprinting in Stroke and Brain Tumors Models (Submitted in Scientific Reports)

9 REFERENCES

- Adibhatla, R.M., and Hatcher, J.F. (2009). Lipid Oxidation and Peroxidation in CNS Health and Disease: From Molecular Mechanisms to Therapeutic Opportunities. *Antioxid. Redox Signal.* *12*, 125–169.
- Aguado, B.A., Mulyasmita, W., Su, J., Lampe, K.J., and Heilshorn, S.C. (2012). Improving Viability of Stem Cells During Syringe Needle Flow Through the Design of Hydrogel Cell Carriers. *Tissue Eng. Part A* *18*, 806–815.
- Alawneh, J.A., Moustafa, R.R., Marrapu, S.T., Jensen-Kondering, U., Morris, R.S., Jones, P.S., Aigbirhio, F.I., Fryer, T.D., Carpenter, T.A., Warburton, E.A., et al. (2013). Diffusion and perfusion correlates of the 18F-MISO PET lesion in acute stroke: pilot study. *Eur. J. Nucl. Med. Mol. Imaging* *41*, 736–744.
- Albers, G.W., Caplan, L.R., Easton, J.D., Fayad, P.B., Mohr, J.P., Saver, J.L., and Sherman, D.G. (2002). Transient Ischemic Attack — Proposal for a New Definition. *N. Engl. J. Med.* *347*, 1713–1716.
- Albers, G.W., Thijs, V.N., Wechsler, L., Kemp, S., Schlaug, G., Skalabrin, E., Bammer, R., Kakuda, W., Lansberg, M.G., Shuaib, A., et al. (2006). Magnetic resonance imaging profiles predict clinical response to early reperfusion: The diffusion and perfusion imaging evaluation for understanding stroke evolution (DEFUSE) study. *Ann. Neurol.* *60*, 508–517.
- Allen, C., Thornton, P., Denes, A., McColl, B.W., Pierozynski, A., Monestier, M., Pinteaux, E., Rothwell, N.J., and Allan, S.M. (2012). Neutrophil cerebrovascular transmigration triggers rapid neurotoxicity through release of proteases associated with de-condensed DNA. *J. Immunol. Baltim. Md 1950* *189*, 381–392.
- Alsop, D.C., Detre, J.A., Golay, X., Günther, M., Hendrikse, J., Hernandez-Garcia, L., Lu, H., MacIntosh, B.J., Parkes, L.M., Smits, M., et al. (2015). Recommended implementation of arterial spin-labeled perfusion MRI for clinical applications: A consensus of the ISMRM perfusion study group and the European consortium for ASL in dementia. *Magn. Reson. Med.* *73*, spcone.
- Aoyama, K., Burns, D.M., Suh, S.W., Garnier, P., Matsumori, Y., Shiina, H., and Swanson, R.A. (2005). Acidosis Causes Endoplasmic Reticulum Stress and Caspase-12-Mediated Astrocyte Death. *J. Cereb. Blood Flow Metab.* *25*, 358–370.
- Arvidsson, A., Collin, T., Kirik, D., Kokaia, Z., and Lindvall, O. (2002). Neuronal replacement from endogenous precursors in the adult brain after stroke. *Nat. Med.* *8*, 963–970.
- Attwell, D., Buchan, A.M., Charpak, S., Lauritzen, M., MacVicar, B.A., and Newman, E.A. (2010). Glial and neuronal control of brain blood flow. *Nature* *468*, 232–243.
- Augustin, H.G., Young Koh, G., Thurston, G., and Alitalo, K. (2009). Control of vascular morphogenesis and homeostasis through the angiopoietin–Tie system. *Nat. Rev. Mol. Cell Biol.* *10*, 165–177.
- Aurand, E.R., Lampe, K.J., and Bjugstad, K.B. (2012). Defining and designing polymers and hydrogels for neural tissue engineering. *Neurosci. Res.* *72*, 199–213.

- Baeten, K.M., and Akassoglou, K. (2011). Extracellular matrix and matrix receptors in blood-brain barrier formation and stroke. *Dev. Neurobiol.* *71*, 1018–1039.
- Bain, G., Kitchens, D., Yao, M., Huettner, J.E., and Gottlieb, D.I. (1995). Embryonic Stem Cells Express Neuronal Properties in Vitro. *Dev. Biol.* *168*, 342–357.
- Baird, A.E., Dambrosia, J., Janket, S.-J., Eichbaum, Q., Chaves, C., Silver, B., Barber, P.A., Parsons, M., Darby, D., Davis, S., et al. (2001). A three-item scale for the early prediction of stroke recovery. *The Lancet* *357*, 2095–2099.
- Banerjee, S., Bentley, P., Hamady, M., Marley, S., Davis, J., Shlebak, A., Nicholls, J., Williamson, D.A., Jensen, S.L., Gordon, M., et al. (2014). Intra-Arterial Immunoselected CD34+ Stem Cells for Acute Ischemic Stroke. *Stem Cells Transl. Med.* *3*, 1322–1330.
- Barbier, E.L., Liu, L., Grillon, E., Payen, J.-F., Lebas, J.-F., Segebarth, C., and Rémy, C. (2005). Focal brain ischemia in rat: acute changes in brain tissue T1 reflect acute increase in brain tissue water content. *NMR Biomed.* *18*, 499–506.
- Baron, J.C. (1999). Mapping the ischaemic penumbra with PET: implications for acute stroke treatment. *Cerebrovasc. Dis. Basel Switz.* *9*, 193–201.
- Baron, J.-C., Yamauchi, H., Fujioka, M., and Endres, M. (2014). Selective neuronal loss in ischemic stroke and cerebrovascular disease. *J. Cereb. Blood Flow Metab.* *34*, 2–18.
- Beck, H., and Plate, K.H. (2009). Angiogenesis after cerebral ischemia. *Acta Neuropathol. (Berl.)* *117*, 481–496.
- Bederson, J.B., Connolly, E.S., Batjer, H.H., Dacey, R.G., Dion, J.E., Diringer, M.N., Duldner, J.E., Harbaugh, R.E., Patel, A.B., and Rosenwasser, R.H. (2009). Guidelines for the Management of Aneurysmal Subarachnoid Hemorrhage A Statement for Healthcare Professionals From a Special Writing Group of the Stroke Council, American Heart Association. *Stroke* *40*, 994–1025.
- Berkhemer, O.A., Fransen, P.S.S., Beumer, D., van den Berg, L.A., Lingsma, H.F., Yoo, A.J., Schonewille, W.J., Vos, J.A., Nederkoorn, P.J., Wermer, M.J.H., et al. (2015). A Randomized Trial of Intraarterial Treatment for Acute Ischemic Stroke. *N. Engl. J. Med.* *372*, 11–20.
- Bernard, S.A., Gray, T.W., Buist, M.D., Jones, B.M., Silvester, W., Gutteridge, G., and Smith, K. (2002). Treatment of Comatose Survivors of Out-of-Hospital Cardiac Arrest with Induced Hypothermia. *N. Engl. J. Med.* *346*, 557–563.
- Bhasin, A., Padma Srivastava, M.V., Mohanty, S., Bhatia, R., Kumaran, S.S., and Bose, S. (2013). Stem cell therapy: A clinical trial of stroke. *Clin. Neurol. Neurosurg.* *115*, 1003–1008.
- Boisserand, L.S.B., Lemasson, B., Hirschler, L., Moisan, A., Hubert, V., Barbier, E.L., Rémy, C., and Detante, O. (2016). Multiparametric magnetic resonance imaging including oxygenation mapping of experimental ischaemic stroke. *J. Cereb. Blood Flow Metab.* 0271678X16662044.

Brennan, A.M., Suh, S.W., Won, S.J., Narasimhan, P., Kauppinen, T.M., Lee, H., Edling, Y., Chan, P.H., and Swanson, R.A. (2009). NADPH oxidase is the primary source of superoxide induced by NMDA receptor activation. *Nat. Neurosci.* *12*, 857–863.

Campbell, B.C.V., Mitchell, P.J., Yan, B., Parsons, M.W., Christensen, S., Churilov, L., Dowling, R.J., Dewey, H., Brooks, M., Miteff, F., et al. (2014). A multicenter, randomized, controlled study to investigate EXTending the time for Thrombolysis in Emergency Neurological Deficits with Intra-Arterial therapy (EXTEND-IA). *Int. J. Stroke* *9*, 126–132.

Cao, Y., Sun, Z., Liao, L., Meng, Y., Han, Q., and Zhao, R.C. (2005). Human adipose tissue-derived stem cells differentiate into endothelial cells in vitro and improve postnatal neovascularization in vivo. *Biochem. Biophys. Res. Commun.* *332*, 370–379.

Caplan, A. (2009). Why are MSCs therapeutic? New data: new insight. *J. Pathol.* *217*, 318–324.

Carlén, M., Meletis, K., Göritz, C., Darsalia, V., Evergren, E., Tanigaki, K., Amendola, M., Barnabé-Heider, F., Yeung, M.S.Y., Naldini, L., et al. (2009). Forebrain ependymal cells are Notch-dependent and generate neuroblasts and astrocytes after stroke. *Nat. Neurosci.* *12*, 259–267.

Carmeliet, P., and Jain, R.K. (2000). Angiogenesis in cancer and other diseases. *Nature* *407*, 249–257.

Carmeliet, P., and Jain, R.K. (2011). Molecular mechanisms and clinical applications of angiogenesis. *Nature* *473*, 298–307.

Carmichael, S.T. (2006). Cellular and molecular mechanisms of neural repair after stroke: making waves. *Ann. Neurol.* *59*, 735–742.

Castillo-Melendez, M., Yawno, T., Jenkin, G., and Miller, S.L. (2013). Stem cell therapy to protect and repair the developing brain: a review of mechanisms of action of cord blood and amnion epithelial derived cells. *Neuroendocr. Sci.* *7*, 194.

Centenaro, L.A., Jaeger, M. da C., Ilha, J., de Souza, M.A., Kalil-Gaspar, P.I., Cunha, N.B., Marcuzzo, S., and Achaval, M. (2011). Olfactory and respiratory lamina propria transplantation after spinal cord transection in rats: Effects on functional recovery and axonal regeneration. *Brain Res.* *1426*, 54–72.

Chen, H.H., Chien, C.H., and Liu, H.M. (1994). Correlation between angiogenesis and basic fibroblast growth factor expression in experimental brain infarct. *Stroke* *25*, 1651–1657.

Chen, J., Zhang, Z.G., Li, Y., Wang, Y., Wang, L., Jiang, H., Zhang, C., Lu, M., Katakowski, M., Feldkamp, C.S., et al. (2003). Statins induce angiogenesis, neurogenesis, and synaptogenesis after stroke. *Ann. Neurol.* *53*, 743–751.

Cho, K.J., Cheon, S.Y., and Kim, G.W. (2015). Statins Promote Long-Term Recovery after Ischemic Stroke by Reconnecting Noradrenergic Neuronal Circuitry. *Neural Plast.* *2015*, 585783.

Christen, T., Lemasson, B., Pannetier, N., Farion, R., Segebarth, C., Rémy, C., and Barbier, E.L. (2011). Evaluation of a quantitative blood oxygenation level-dependent (qBOLD) approach to map local blood oxygen saturation. *NMR Biomed.* *24*, 393–403.

Christen, T., Bouzat, P., Pannetier, N., Coquery, N., Moisan, A., Lemasson, B., Thomas, S., Grillon, E., Detante, O., Rémy, C., et al. (2014). Tissue oxygen saturation mapping with magnetic resonance imaging. *J. Cereb. Blood Flow Metab. Off. J. Int. Soc. Cereb. Blood Flow Metab.* *34*, 1550–1557.

Chu, K., Kim, M., Park, K.-I., Jeong, S.-W., Park, H.-K., Jung, K.-H., Lee, S.-T., Kang, L., Lee, K., Park, D.-K., et al. (2004). Human neural stem cells improve sensorimotor deficits in the adult rat brain with experimental focal ischemia. *Brain Res.* *1016*, 145–153.

Chung, A.S., Waldeck, H., Schmidt, D.R., and Kao, W.J. (2009). Monocyte inflammatory and matrix remodeling response modulated by grafted ECM-derived ligand concentration. *J. Biomed. Mater. Res. A* *91*, 742–752.

Chung, A.S., Lee, J., and Ferrara, N. (2010). Targeting the tumour vasculature: insights from physiological angiogenesis. *Nat. Rev. Cancer* *10*, 505–514.

Cross, J.L., Meloni, B.P., Bakker, A.J., Lee, S., and Knuckey, N.W. (2010). Modes of Neuronal Calcium Entry and Homeostasis following Cerebral Ischemia. *Stroke Res. Treat.* *2010*, e316862.

Dalkara, T., and Moskowitz, M.A. (1994). The Complex Role of Nitric Oxide in the Pathophysiology of Focal Cerebral Ischemia. *Brain Pathol.* *4*, 49–57.

Deb, P., Sharma, S., and Hassan, K.M. (2010). Pathophysiologic mechanisms of acute ischemic stroke: An overview with emphasis on therapeutic significance beyond thrombolysis. *Pathophysiology* *17*, 197–218.

Deddens, L.H., Van Tilborg, G.A.F., Mulder, W.J.M., De Vries, H.E., and Dijkhuizen, R.M. (2012). Imaging Neuroinflammation after Stroke: Current Status of Cellular and Molecular MRI Strategies. *Cerebrovasc. Dis.* *33*, 392–402.

Detante, O., Moisan, A., Dimastromatteo, J., Richard, M.-J., Riou, L., Grillon, E., Barbier, E., Desruet, M.-D., De Fraipont, F., Segebarth, C., et al. (2009). Intravenous administration of ^{99m}Tc-HMPAO-labeled human mesenchymal stem cells after stroke: in vivo imaging and biodistribution. *Cell Transplant.* *18*, 1369–1379.

Detante, O., Valable, S., de Fraipont, F., Grillon, E., Barbier, E.L., Moisan, A., Arnaud, J., Moriscot, C., Segebarth, C., Hommel, M., et al. (2012). Magnetic resonance imaging and fluorescence labeling of clinical-grade mesenchymal stem cells without impacting their phenotype: study in a rat model of stroke. *Stem Cells Transl. Med.* *1*, 333–341.

Detante, O., Jaillard, A., Moisan, A., Barbieux, M., Favre, I.M., Garambois, K., Hommel, M., and Remy, C. (2014). Biotherapies in stroke. *Rev. Neurol. (Paris)* *170*, 779–798.

Di Nicola, M. (2002). Human bone marrow stromal cells suppress T-lymphocyte proliferation induced by cellular or nonspecific mitogenic stimuli. *Blood* *99*, 3838–3843.

Díez-Tejedor, E., Gutiérrez-Fernández, M., Martínez-Sánchez, P., Rodríguez-Frutos, B., Ruiz-Ares, G., Lara, M.L., and Gimeno, B.F. (2014). Reparative Therapy for Acute Ischemic Stroke with Allogeneic Mesenchymal Stem Cells from Adipose Tissue: A Safety Assessment: A Phase II Randomized, Double-blind, Placebo-controlled, Single-center, Pilot Clinical Trial. *J. Stroke Cerebrovasc. Dis.* *23*, 2694–2700.

- Dijkhuizen, R.M., and Nicolay, K. (2003). Magnetic Resonance Imaging in Experimental Models of Brain Disorders. *J. Cereb. Blood Flow Metab.* *23*, 1383–1402.
- Dirnagl, U., and Schwab, J.M. (2009). Brain-immune interactions in acute and chronic brain disorders. *Neuroscience* *158*, 969–971.
- Dirnagl, U., Simon, R.P., and Hallenbeck, J.M. (2003). Ischemic tolerance and endogenous neuroprotection. *Trends Neurosci.* *26*, 248–254.
- Drago, D., Cossetti, C., Iraci, N., Gaude, E., Musco, G., Bachi, A., and Pluchino, S. (2013). The stem cell secretome and its role in brain repair. *Biochimie* *95*, 2271–2285.
- Dreier, J.P. (2011). The role of spreading depression, spreading depolarization and spreading ischemia in neurological disease. *Nat. Med.* *17*, 439–447.
- Duchemin, S., Boily, M., Sadekova, N., and Girouard, H. (2012). The complex contribution of NOS interneurons in the physiology of cerebrovascular regulation. *Front. Neural Circuits* *6*, 51.
- Duncan, K., Gonzales-Portillo, G.S., Acosta, S.A., Kaneko, Y., Borlongan, C.V., and Tajiri, N. (2015). Stem cell-paved biobridges facilitate stem transplant and host brain cell interactions for stroke therapy. *Brain Res.* *1623*, 160–165.
- Durukan, A., and Tatlisumak, T. (2007). Acute ischemic stroke: Overview of major experimental rodent models, pathophysiology, and therapy of focal cerebral ischemia. *Pharmacol. Biochem. Behav.* *87*, 179–197.
- Durukan, A., Marinkovic, I., Strbian, D., Pitkonen, M., Pedrono, E., Soenne, L., Abo-Ramadan, U., and Tatlisumak, T. (2009). Post-ischemic blood-brain barrier leakage in rats: One-week follow-up by MRI. *Brain Res.* *1280*, 158–165.
- Encarnacion, A., Horie, N., Keren-Gill, H., Bliss, T.M., Steinberg, G.K., and Shamloo, M. (2011). Long-term behavioral assessment of function in an experimental model for ischemic stroke. *J. Neurosci. Methods* *196*, 247–257.
- Eriksson, P.S., Perfilieva, E., Björk-Eriksson, T., Alborn, A.-M., Nordborg, C., Peterson, D.A., and Gage, F.H. (1998). Neurogenesis in the adult human hippocampus. *Nat. Med.* *4*, 1313–1317.
- Fan, Y.-Y., Shen, Z., He, P., Jiang, L., Hou, W., Shen, Y., Zhang, X.-N., Hu, W.-W., and Chen, Z. (2014). A novel neuroprotective strategy for ischemic stroke: transient mild acidosis treatment by CO₂ inhalation at reperfusion. *J. Cereb. Blood Flow Metab.* *34*, 275–283.
- Feigin, V.L., Forouzanfar, M.H., Krishnamurthi, R., Mensah, G.A., Connor, M., Bennett, D.A., Moran, A.E., Sacco, R.L., Anderson, L., Truelsen, T., et al. (2014). Global and regional burden of stroke during 1990–2010: findings from the Global Burden of Disease Study 2010. *Lancet* *383*, 245–254.
- FENG, N., HAO, G., YANG, F., QU, F., ZHENG, H., LIANG, S., and JIN, Y. (2016). Transplantation of mesenchymal stem cells promotes the functional recovery of the central nervous system following cerebral ischemia by inhibiting myelin-associated inhibitor expression and neural apoptosis. *Exp. Ther. Med.* *11*, 1595–1600.

- Ferro, J.M., and Canhão, P. (2014). Cerebral Venous Sinus Thrombosis: Update on Diagnosis and Management. *Curr. Cardiol. Rep.* 16, 1–10.
- Fisher, M., Feuerstein, G., Howells, D.W., Hurn, P.D., Kent, T.A., Savitz, S.I., and Lo, E.H. (2009). Update of the Stroke Therapy Academic Industry Roundtable Preclinical Recommendations. *Stroke* 40, 2244–2250.
- Gage, F.H. (2000). Mammalian Neural Stem Cells. *Science* 287, 1433–1438.
- Garzón-Muvdi, T., and Quiñones-Hinojosa, A. (2010). Neural Stem Cell Niches and Homing: Recruitment and Integration into Functional Tissues. *ILAR J.* 51, 3–23.
- Gelderblom, M., Leyboldt, F., Steinbach, K., Behrens, D., Choe, C.-U., Siler, D.A., Arumugam, T.V., Orthey, E., Gerloff, C., Tolosa, E., et al. (2009). Temporal and Spatial Dynamics of Cerebral Immune Cell Accumulation in Stroke. *Stroke* 40, 1849–1857.
- George, P.M., and Steinberg, G.K. (2015). Novel Stroke Therapeutics: Unraveling Stroke Pathophysiology and Its Impact on Clinical Treatments. *Neuron* 87, 297–309.
- Giroud, M., Jacquin, A., and Béjot, Y. (2014). The worldwide landscape of stroke in the 21st century. *The Lancet* 383, 195–197.
- Gong, P., Li, C.-S., Hua, R., Zhao, H., Tang, Z.-R., Mei, X., Zhang, M.-Y., and Cui, J. (2012). Mild Hypothermia Attenuates Mitochondrial Oxidative Stress by Protecting Respiratory Enzymes and Upregulating MnSOD in a Pig Model of Cardiac Arrest. *PLOS ONE* 7, e35313.
- Gonzalez, F.F., Larphaveesarp, A., McQuillen, P., Derugin, N., Wendland, M., Spadafora, R., and Ferriero, D.M. (2013). Erythropoietin Increases Neurogenesis and Oligodendroglial Precursor Cells After Neonatal Stroke. *Stroke* 44, 753–758.
- Griese, D.P., Ehsan, A., Melo, L.G., Kong, D., Zhang, L., Mann, M.J., Pratt, R.E., Mulligan, R.C., and Dzau, V.J. (2003). Isolation and Transplantation of Autologous Circulating Endothelial Cells Into Denuded Vessels and Prosthetic Grafts. *Circulation* 108, 2710–2715.
- Gursoy-Ozdemir, Y., Qiu, J., Matsuoka, N., Bolay, H., Bempohl, D., Jin, H., Wang, X., Rosenberg, G.A., Lo, E.H., and Moskowitz, M.A. (2004). Cortical spreading depression activates and upregulates MMP-9. *J. Clin. Invest.* 113, 1447–1455.
- Gutiérrez-Fernández, M., Rodríguez-Frutos, B., Ramos-Cejudo, J., Otero-Ortega, L., Fuentes, B., and Díez-Tejedor, E. (2013). Stem cells for brain repair and recovery after stroke. *Expert Opin. Biol. Ther.* 13, 1479–1483.
- Hacke, W., Kaste, M., Bluhmki, E., Brozman, M., Dávalos, A., Guidetti, D., Larrue, V., Lees, K.R., Medeghri, Z., Machnig, T., et al. (2008). Thrombolysis with Alteplase 3 to 4.5 Hours after Acute Ischemic Stroke. *N. Engl. J. Med.* 359, 1317–1329.
- Hallinan, N., Finn, S., Cuffe, S., Rafee, S., O’Byrne, K., and Gately, K. (2016). Targeting the fibroblast growth factor receptor family in cancer. *Cancer Treat. Rev.* 46, 51–62.

- Hamilton, N.B., Attwell, D., and Hall, C.N. (2010). Pericyte-mediated regulation of capillary diameter: a component of neurovascular coupling in health and disease. *Front. Neuroenergetics* 2, 5.
- Hanisch, U.-K., and Kettenmann, H. (2007). Microglia: active sensor and versatile effector cells in the normal and pathologic brain. *Nat. Neurosci.* 10, 1387–1394.
- Hao, L., Zou, Z., Tian, H., Zhang, Y., Zhou, H., and Liu, L. (2014). Stem Cell-Based Therapies for Ischemic Stroke. *BioMed Res. Int.* 2014, e468748.
- Hara, Y., Tooyama, I., Yasuhara, O., Akiyama, H., McGeer, P.L., Handa, J., and Kimura, H. (1994). Acidic fibroblast growth factor-like immunoreactivity in rat brain following cerebral infarction. *Brain Res.* 664, 101–107.
- Hayashi, T., Noshita, N., Sugawara, T., and Chan, P.H. (2003). Temporal Profile of Angiogenesis and Expression of Related Genes in the Brain after Ischemia. *J. Cereb. Blood Flow Metab.* 23, 166–180.
- Heiss, W.-D. (2012). The ischemic penumbra: how does tissue injury evolve? *Ann. N. Y. Acad. Sci.* 1268, 26–34.
- Hench, L.L., and Polak, J.M. (2002). Third-Generation Biomedical Materials. *Science* 295, 1014–1017.
- Hengartner, M.O. (2000). The biochemistry of apoptosis. *Nature* 407, 770–776.
- Hicklin, D.J., and Ellis, L.M. (2005). Role of the vascular endothelial growth factor pathway in tumor growth and angiogenesis. *J. Clin. Oncol. Off. J. Am. Soc. Clin. Oncol.* 23, 1011–1027.
- Honmou, O., Onodera, R., Sasaki, M., Waxman, S.G., and Kocsis, J.D. (2012). Mesenchymal stem cells: therapeutic outlook for stroke. *Trends Mol. Med.* 18, 292–297.
- Hossmann, K.-A. (2008). Cerebral ischemia: models, methods and outcomes. *Neuropharmacology* 55, 257–270.
- Huang, S., Kim, J.K., Atochin, D.N., Farrar, C.T., Huang, P.L., Suh, J.Y., Kwon, S.J., Shim, W.H., Cho, H., Cho, G., et al. (2013a). Cerebral blood volume affects blood–brain barrier integrity in an acute transient stroke model. *J. Cereb. Blood Flow Metab.* 33, 898–905.
- Huang, S.-H., Wang, L., Chi, F., Wu, C.-H., Cao, H., Zhang, A., and Jong, A. (2013b). Circulating Brain Microvascular Endothelial Cells (cBMECs) as Potential Biomarkers of the Blood–Brain Barrier Disorders Caused by Microbial and Non-Microbial Factors. *PLOS ONE* 8, e62164.
- Huang, W., Lv, B., Zeng, H., Shi, D., Liu, Y., Chen, F., Li, F., Liu, X., Zhu, R., Yu, L., et al. (2015). Paracrine Factors Secreted by MSCs Promote Astrocyte Survival Associated With GFAP Downregulation After Ischemic Stroke via p38 MAPK and JNK. *J. Cell. Physiol.* 230, 2461–2475.
- Iadecola, C. (2004). Neurovascular regulation in the normal brain and in Alzheimer’s disease. *Nat. Rev. Neurosci.* 5, 347–360.
- Iadecola, C., and Anrather, J. (2011). The immunology of stroke: from mechanisms to translation. *Nat. Med.* 17, 796–808.

- Igarashi, H., Tsujita, M., Suzuki, Y., Kwee, I.L., and Nakada, T. (2013). Inhibition of aquaporin-4 significantly increases regional cerebral blood flow: *NeuroReport* 24, 324–328.
- Jablonska, B., Aguirre, A., Raymond, M., Szabo, G., Kitabatake, Y., Sailor, K.A., Ming, G.-L., Song, H., and Gallo, V. (2010). Chordin-induced lineage plasticity of adult SVZ neuroblasts after demyelination. *Nat. Neurosci.* 13, 541–550.
- Jain, R.K. (2003). Molecular regulation of vessel maturation. *Nat. Med.* 9, 685–693.
- Jauch, E.C., Saver, J.L., Adams, H.P., Bruno, A., Connors, J.J. (Buddy), Demaerschalk, B.M., Khatri, P., McMullan, P.W., Qureshi, A.I., Rosenfield, K., et al. (2013). Guidelines for the Early Management of Patients With Acute Ischemic Stroke A Guideline for Healthcare Professionals From the American Heart Association/American Stroke Association. *Stroke* 44, 870–947.
- Je, D., Se, H., Rg, Y., and Ai, C. (1991). Osteogenesis in marrow-derived mesenchymal cell porous ceramic composites transplanted subcutaneously: effect of fibronectin and laminin on cell retention and rate of osteogenic expression. *Cell Transplant.* 1, 23–32.
- Jensen-Kondering, U., and Baron, J.-C. (2012). Oxygen imaging by MRI: can blood oxygen level-dependent imaging depict the ischemic penumbra? *Stroke J. Cereb. Circ.* 43, 2264–2269.
- Jiang, M., Lv, L., Ji, H., Yang, X., Zhu, W., Cai, L., Gu, X., Chai, C., Huang, S., Sun, J., et al. (2011). Induction of pluripotent stem cells transplantation therapy for ischemic stroke. *Mol. Cell. Biochem.* 354, 67–75.
- Jung, S., Gilgen, M., Slotboom, J., El-Koussy, M., Zubler, C., Kiefer, C., Luedi, R., Mono, M.-L., Heldner, M.R., Weck, A., et al. (2013). Factors that determine penumbral tissue loss in acute ischaemic stroke. *Brain* 136, 3554–3560.
- Kamel, H., and Iadecola, C. (2012). Brain-Immune Interactions and Ischemic Stroke. *Arch. Neurol.* 69, 576–581.
- Kempermann, G., Kuhn, H.G., and Gage, F.H. (1997). More hippocampal neurons in adult mice living in an enriched environment. *Nature* 386, 493–495.
- Ken, S., Deviers, A., Filleron, T., Isabelle, C., Jean-Albert, L., Khalifa, J., Lubrano, V., Berry, I., Péran, P., Celsis, P., et al. (2015). Voxel-based evidence of perfusion normalization in glioblastoma patients included in a phase I–II trial of radiotherapy. *J. Neurooncol.* 465–473.
- Kidwell, C.S., Wintermark, M., De Silva, D.A., Schaewe, T.J., Jahan, R., Starkman, S., Jovin, T., Hom, J., Jumaa, M., Schreier, J., et al. (2013). MULTIPARAMETRIC MRI AND CT MODELS OF INFARCT CORE AND FAVORABLE PENUMBRAL IMAGING PATTERNS IN ACUTE ISCHEMIC STROKE. *Stroke J. Cereb. Circ.* 44, 73–79.
- Kim, D.H., Seo, Y.K., Thambi, T., Moon, G.J., Son, J.P., Li, G., Park, J.H., Lee, J.H., Kim, H.H., Lee, D.S., et al. (2015). Enhancing neurogenesis and angiogenesis with target delivery of stromal cell derived factor-1 α using a dual ionic pH-sensitive copolymer. *Biomaterials* 61, 115–125.

- Kis, B., Szabó, C.A., Pataricza, J., Krizbai, I.A., Mezei, Z., Gecse, Á., Telegdy, G., Papp, J.G., and Deli, M.A. (1999). Vasoactive substances produced by cultured rat brain endothelial cells. *Eur. J. Pharmacol.* *368*, 35–42.
- Klehmet, J., Harms, H., Richter, M., Prass, K., Volk, H.D., Dirnagl, U., Meisel, A., and Meisel, C. (2009). Stroke-induced immunodepression and post-stroke infections: Lessons from the preventive antibacterial therapy in stroke trial. *Neuroscience* *158*, 1184–1193.
- Koerner, J., Nestic, D., Romero, J.D., Brehm, W., Mainil-Varlet, P., and Grogan, S.P. (2006). Equine Peripheral Blood-Derived Progenitors in Comparison to Bone Marrow-Derived Mesenchymal Stem Cells. *STEM CELLS* *24*, 1613–1619.
- Koganemaru, S., Sawamoto, N., Aso, T., Sagara, A., Ikkaku, T., Shimada, K., Kanematsu, M., Takahashi, R., Domen, K., Fukuyama, H., et al. (2015). Task-specific brain reorganization in motor recovery induced by a hybrid-rehabilitation combining training with brain stimulation after stroke. *Neurosci. Res.* *92*, 29–38.
- Kovács, Z., Ikezaki, K., Samoto, K., Inamura, T., and Fukui, M. (1996). VEGF and flt Expression Time Kinetics in Rat Brain Infarct. *Stroke* *27*, 1865–1873.
- Kreuzberg, M., Kanov, E., Timofeev, O., Schwaninger, M., Monyer, H., and Khodosevich, K. (2010). Increased subventricular zone-derived cortical neurogenesis after ischemic lesion. *Exp. Neurol.* *226*, 90–99.
- Krupinski, J., Kaluza, J., Kumar, P., Kumar, S., and Wang, J.M. (1994). Role of angiogenesis in patients with cerebral ischemic stroke. *Stroke* *25*, 1794–1798.
- Krupinski, J., Issa, R., Bujny, T., Slevin, M., Kumar, P., Kumar, S., and Kaluza, J. (1997). A Putative Role for Platelet-Derived Growth Factor in Angiogenesis and Neuroprotection After Ischemic Stroke in Humans. *Stroke* *28*, 564–573.
- Kruyt, N.D., Biessels, G.J., DeVries, J.H., and Roos, Y.B. (2010). Hyperglycemia in acute ischemic stroke: pathophysiology and clinical management. *Nat. Rev. Neurol.* *6*, 145–155.
- Kuhn, H.G., Dickinson-Anson, H., and Gage, F.H. (1996). Neurogenesis in the dentate gyrus of the adult rat: age-related decrease of neuronal progenitor proliferation. *J. Neurosci.* *16*, 2027–2033.
- Kurth, C.D., Levy, W.J., and McCann, J. (2002). Near-infrared spectroscopy cerebral oxygen saturation thresholds for hypoxia-ischemia in piglets. *J. Cereb. Blood Flow Metab. Off. J. Int. Soc. Cereb. Blood Flow Metab.* *22*, 335–341.
- Kwakkel, G., and Kollen, B.J. (2013). Predicting activities after stroke: what is clinically relevant? *Int. J. Stroke* *8*, 25–32.
- Lai, C.-H., and Kuo, K.-H. (2005). The critical component to establish in vitro BBB model: Pericyte. *Brain Res. Rev.* *50*, 258–265.
- Lam, J., Lowry, W.E., Carmichael, S.T., and Segura, T. (2014). Delivery of iPS-NPCs to the Stroke Cavity within a Hyaluronic Acid Matrix Promotes the Differentiation of Transplanted Cells. *Adv. Funct. Mater.* *24*, 7053–7062.

Lampe, K.J., Mooney, R.G., Bjugstad, K.B., and Mahoney, M.J. (2010). Effect of macromer weight percent on neural cell growth in 2D and 3D nondegradable PEG hydrogel culture. *J. Biomed. Mater. Res. A* *94A*, 1162–1171.

Lampl, Y., Boaz, M., Gilad, R., Lorberboym, M., Dabby, R., Rapoport, A., Anca-Hershkowitz, M., and Sadeh, M. (2007). Minocycline treatment in acute stroke An open-label, evaluator-blinded study. *Neurology* *69*, 1404–1410.

Lappalainen, R.S., Narkilahti, S., Huhtala, T., Liimatainen, T., Suuronen, T., Närvänen, A., Suuronen, R., Hovatta, O., and Jolkkonen, J. (2008). The SPECT imaging shows the accumulation of neural progenitor cells into internal organs after systemic administration in middle cerebral artery occlusion rats. *Neurosci. Lett.* *440*, 246–250.

Le Blanc, K. (2003). Immunomodulatory effects of fetal and adult mesenchymal stem cells. *Cytherapy* *5*, 485–489.

Lee, S., Hong, Y., Won, J., Lee, M., Hong, Y., Lee, Y., Kang, S.-G., and Chang, K.-T. (2014). Middle cerebral artery occlusion methods in rat versus mouse models of transient focal cerebral ischemic stroke. *Neural Regen. Res.* *9*, 757.

Li, G., Yu, F., Lei, T., Gao, H., Li, P., Sun, Y., Huang, H., and Mu, Q. (2016). Bone marrow mesenchymal stem cell therapy in ischemic stroke: mechanisms of action and treatment optimization strategies. *Neural Regen. Res.* *11*, 0.

Li, Y., Zhang, C., Zhang, X., Zhou, H., and Meng, L. (2014). Effects of mild induced hypothermia on hippocampal connexin 43 and glutamate transporter 1 expression following traumatic brain injury in rats. *Mol. Med. Rep.*

Liang, Y., Walczak, P., and Bulte, J.W.M. (2013). The Survival of Engrafted Neural Stem Cells Within Hyaluronic Acid Hydrogels. *Biomaterials* *34*, 5521–5529.

Liebeskind, D.S., Jahan, R., Nogueira, R.G., Zaidat, O.O., Saver, J.L., and for the SWIFT Investigators (2014). Impact of Collaterals on Successful Revascularization in Solitaire FR With the Intention for Thrombectomy. *Stroke* *45*, 2036–2040.

Lindahl, P., Johansson, B.R., Levéen, P., and Betsholtz, C. (1997). Pericyte Loss and Microaneurysm Formation in PDGF-B-Deficient Mice. *Science* *277*, 242–245.

Lindborg, B.A., Brekke, J.H., Scott, C.M., Chai, Y.W., Ulrich, C., Sandquist, L., Kokkoli, E., and O'Brien, T.D. (2015). A Chitosan-Hyaluronan-Based Hydrogel-Hydrocolloid Supports In Vitro Culture and Differentiation of Human Mesenchymal Stem/Stromal Cells. *Tissue Eng. Part A* *21*, 1952–1962.

Lindvall, O., and Kokaia, Z. (2015). Neurogenesis following Stroke Affecting the Adult Brain. *Cold Spring Harb. Perspect. Biol.* *7*, a019034.

Liu, S., Zhou, J., Zhang, X., Liu, Y., Chen, J., Hu, B., Song, J., and Zhang, Y. (2016). Strategies to Optimize Adult Stem Cell Therapy for Tissue Regeneration. *Int. J. Mol. Sci.* *17*, 982.

- Lois, C., García-Verdugo, J.-M., and Alvarez-Buylla, A. (1996). Chain Migration of Neuronal Precursors. *Science* 271, 978–981.
- Lok, J., Gupta, P., Guo, S., Kim, W.J., Whalen, M.J., Leyen, K. van, and Lo, E.H. (2007). Cell–cell Signaling in the Neurovascular Unit. *Neurochem. Res.* 32, 2032–2045.
- Lok, J., Wang, X.-S., Xing, C.-H., Maki, T.-K., Wu, L.-M., Guo, S.-Z., Noviski, N., Arai, K., Whalen, M.J., Lo, E.H., et al. (2015). Targeting the Neurovascular Unit in Brain Trauma. *CNS Neurosci. Ther.* 21, 304–308.
- Longa, E.Z., Weinstein, P.R., Carlson, S., and Cummins, R. (1989). Reversible middle cerebral artery occlusion without craniectomy in rats. *Stroke J. Cereb. Circ.* 20, 84–91.
- Makino, S., Fukuda, K., Miyoshi, S., Konishi, F., Kodama, H., Pan, J., Sano, M., Takahashi, T., Hori, S., Abe, H., et al. (1999). Cardiomyocytes can be generated from marrow stromal cells in vitro. *J. Clin. Invest.* 103, 697–705.
- Malarkey, E.B., and Parpura, V. (2008). Mechanisms of glutamate release from astrocytes. *Neurochem. Int.* 52, 142–154.
- Malgieri, A., Kantzari, E., Patrizi, M., and Gambardella, S. (2010). Bone marrow and umbilical cord blood human mesenchymal stem cells: state of the art. *Bone marrow and umbilical cord blood human mesenchymal stem cells: state of the art. Int. J. Clin. Exp. Med.* 3, 3, 248, 248–269.
- Marti, H.J.H., Bernaudin, M., Bellail, A., Schoch, H., Euler, M., Petit, E., and Risau, W. (2000). Hypoxia-Induced Vascular Endothelial Growth Factor Expression Precedes Neovascularization after Cerebral Ischemia. *Am. J. Pathol.* 156, 965–976.
- Matsui, T., Tasaki, M., Yoshioka, T., Motoki, Y., Tsuneoka, H., and Nojima, J. (2012). Temperature- and time-dependent changes in TLR2-activated microglial NF- κ B activity and concentrations of inflammatory and anti-inflammatory factors. *Intensive Care Med.* 38, 1392–1399.
- McKinnon, R.D., Matsui, T., Dubois-Dalcq, M., and Aaronson, S.A. (1990). FGF modulates the PDGF-driven pathway of oligodendrocyte development. *Neuron* 5, 603–614.
- Mergenthaler, P., Lindauer, U., Dienel, G.A., and Meisel, A. (2013). Sugar for the brain: the role of glucose in physiological and pathological brain function. *Trends Neurosci.* 36, 587–597.
- Merino, J.J., Gutiérrez-Fernández, M., Rodríguez-Frutos, B., Álvarez-Grech, J., Alcalde, M.E., Vallejo-Cremades, M.T., and Díez-Tejedor, E. (2011). CXCR4/SDF-1 α -chemokine regulates neurogenesis and/or angiogenesis within the vascular niche of ischemic rats; however, does SDF-1 α play a role in repair? *Int. J. Stroke* 6, 466–467.
- Mestriner, R.G., Pagnussat, A.S., Boisserand, L.S.B., Valentim, L., and Netto, C.A. (2011). Skilled reaching training promotes astroglial changes and facilitated sensorimotor recovery after collagenase-induced intracerebral hemorrhage. *Exp. Neurol.* 227, 53–61.
- Ming, G., and Song, H. (2011). Adult Neurogenesis in the Mammalian Brain: Significant Answers and Significant Questions. *Neuron* 70, 687–702.

Miyamoto, N., Pham, L.-D.D., Hayakawa, K., Matsuzaki, T., Seo, J.H., Magnain, C., Ayata, C., Kim, K.-W., Boas, D., Lo, E.H., et al. (2013). Age-Related Decline in Oligodendrogenesis Retards White Matter Repair in Mice. *Stroke* 44, 2573–2578.

Moisan, A., Favre, I.M., Rome, C., Grillon, E., Naegele, B., Barbieux, M., De Fraipont, F., Richard, M.-J., Barbier, E.L., Rémy, C., et al. (2014). Microvascular Plasticity After Experimental Stroke: A Molecular and MRI Study. *Cerebrovasc. Dis.* 38, 344–353.

Moisan, A., Favre, I., Rome, C., De Fraipont, F., Grillon, E., Coquery, N., Mathieu, H., Mayan, V., Naegele, B., Hommel, M., et al. (2016). Intravenous injection of clinical grade human MSCs after experimental stroke: functional benefit and microvascular effect. *Cell Transplant.*

Möller, K., Boltze, J., Pösel, C., Seeger, J., Stahl, T., and Wagner, D.-C. (2014). Sterile inflammation after permanent distal MCA occlusion in hypertensive rats. *J. Cereb. Blood Flow Metab.* 34, 307–315.

Moriscot, C., de Fraipont, F., Richard, M.-J., Marchand, M., Savatier, P., Bosco, D., Favrot, M., and Benhamou, P.-Y. (2005). Human bone marrow mesenchymal stem cells can express insulin and key transcription factors of the endocrine pancreas developmental pathway upon genetic and/or microenvironmental manipulation in vitro. *Stem Cells Dayt. Ohio* 23, 594–603.

Moshayedi, P., Nih, L.R., Llorente, I.L., Berg, A.R., Cinkornpumin, J., Lowry, W.E., Segura, T., and Carmichael, S.T. (2016). Systematic optimization of an engineered hydrogel allows for selective control of human neural stem cell survival and differentiation after transplantation in the stroke brain. *Biomaterials* 105, 145–155.

Moskowitz, M.A., Lo, E.H., and Iadecola, C. (2010). The Science of Stroke: Mechanisms in Search of Treatments. *Neuron* 67, 181–198.

Mostert, J.P., Koch, M.W., Heerings, M., Heersema, D.J., and De Keyser, J. (2008). Therapeutic Potential of Fluoxetine in Neurological Disorders. *CNS Neurosci. Ther.* 14, 153–164.

Muoio, V., Persson, P.B., and Sendeski, M.M. (2014). The neurovascular unit – concept review. *Acta Physiol.* 210, 790–798.

Murphy, T.H., and Corbett, D. (2009). Plasticity during stroke recovery: from synapse to behaviour. *Nat. Rev. Neurosci.* 10, 861–872.

Nayernia, Z., Jaquet, V., and Krause, K.-H. (2014). New Insights on NOX Enzymes in the Central Nervous System. *Antioxid. Redox Signal.* 20, 2815–2837.

Ohtaki, H., Ylostalo, J.H., Foraker, J.E., Robinson, A.P., Reger, R.L., Shioda, S., and Prockop, D.J. (2008). Stem/progenitor cells from bone marrow decrease neuronal death in global ischemia by modulation of inflammatory/immune responses. *Proc. Natl. Acad. Sci.* 105, 14638–14643.

Osman, A.M., Porritt, M.J., Nilsson, M., and Kuhn, H.G. (2011). Long-Term Stimulation of Neural Progenitor Cell Migration After Cortical Ischemia in Mice. *Stroke* 42, 3559–3565.

Parent, J.M., Vexler, Z.S., Gong, C., Derugin, N., and Ferriero, D.M. (2002). Rat forebrain neurogenesis and striatal neuron replacement after focal stroke. *Ann. Neurol.* 52, 802–813.

Park, H.J., Shin, J.Y., Kim, H.N., Oh, S.H., Song, S.K., and Lee, P.H. (2015). Mesenchymal stem cells stabilize the blood–brain barrier through regulation of astrocytes. *Stem Cell Res. Ther.* 6.

Paxinos, G., and Watson, C. (1982). RETRACTED: Plates and Figures. In *The Rat Brain in Stereotaxic Coordinates*, (Academic Press), pp. 13–153.

Petzold, G.C., Haack, S., Halbach, O. von B. und, Priller, J., Lehmann, T.-N., Heinemann, U., Dirnagl, U., and Dreier, J.P. (2008). Nitric Oxide Modulates Spreading Depolarization Threshold in the Human and Rodent Cortex. *Stroke* 39, 1292–1299.

Pierdomenico, L., Bonsi, L., Calvitti, M., Rondelli, D., Arpinati, M., Chirumbolo, G., Becchetti, E., Marchionni, C., Alviano, F., Fossati, V., et al. (2005). Multipotent mesenchymal stem cells with immunosuppressive activity can be easily isolated from dental pulp. *Transplantation* 80, 836–842.

Pizzi, M.A., Alejos, D.A., Siegel, J.L., Kim, B.Y.S., Miller, D.A., and Freeman, W.D. Cerebral Venous Thrombosis Associated with Intracranial Hemorrhage and Timing of Anticoagulation after Hemicraniectomy. *J. Stroke Cerebrovasc. Dis.*

Portalska, K.J., Teixeira, L.M., Leijten, J.C.H., Jin, R., van Blitterswijk, C., de Boer, J., and Karperien, M. (2014). Boosting angiogenesis and functional vascularization in injectable dextran-hyaluronic acid hydrogels by endothelial-like mesenchymal stromal cells. *Tissue Eng. Part A* 20, 819–829.

van Praag, H., Kempermann, G., and Gage, F.H. (1999). Running increases cell proliferation and neurogenesis in the adult mouse dentate gyrus. *Nat. Neurosci.* 2, 266–270.

Prasad, S.S., Russell, M., Nowakowska, M., Williams, A., and Yauk, C. (2012). Gene expression analysis to identify molecular correlates of pre- and post-conditioning derived neuroprotection. *J. Mol. Neurosci.* MN 47, 322–339.

Qian, S.-W., Li, X., Zhang, Y.-Y., Huang, H.-Y., Liu, Y., Sun, X., and Tang, Q.-Q. (2010). Characterization of adipocyte differentiation from human mesenchymal stem cells in bone marrow. *BMC Dev. Biol.* 10, 47.

Qureshi, A.I., Mendelow, A.D., and Hanley, D.F. (2009). Intracerebral haemorrhage. *Lancet* 373, 1632–1644.

Redecker, C., Wang, W., Fritschy, J.-M., and Witte, O.W. (2002). Widespread and Long-Lasting Alterations in GABAA-Receptor Subtypes after Focal Cortical Infarcts in Rats: Mediation by NMDA-Dependent Processes. *J. Cereb. Blood Flow Metab.* 22, 1463–1475.

Reynolds, B.A., and Weiss, S. (1992). Generation of neurons and astrocytes from isolated cells of the adult mammalian central nervous system. *Science* 255, 1707–1710.

Riquelme, P.A., Drapeau, E., and Doetsch, F. (2008). Brain micro-ecologies: neural stem cell niches in the adult mammalian brain. *Philos. Trans. R. Soc. B Biol. Sci.* 363, 123–137.

Risau, W. (1997). Mechanisms of angiogenesis. *Nature* 386, 671–674.

- Robin, A.M., Zhang, Z.G., Wang, L., Zhang, R.L., Katakowski, M., Zhang, L., Wang, Y., Zhang, C., and Chopp, M. (2006). Stromal Cell-Derived Factor 1 α Mediates Neural Progenitor Cell Motility after Focal Cerebral Ischemia. *J. Cereb. Blood Flow Metab.* *26*, 125–134.
- Rosell, A., Cuadrado, E., Ortega-Aznar, A., Hernández-Guillamon, M., Lo, E.H., and Montaner, J. (2008). MMP-9–Positive Neutrophil Infiltration Is Associated to Blood–Brain Barrier Breakdown and Basal Lamina Type IV Collagen Degradation During Hemorrhagic Transformation After Human Ischemic Stroke. *Stroke* *39*, 1121–1126.
- Rossi, D.J., Jamieson, C.H.M., and Weissman, I.L. (2008). Stems Cells and the Pathways to Aging and Cancer. *Cell* *132*, 681–696.
- Rosso, C., Hevia-Montiel, N., Deltour, S., Bardinet, E., Dormont, D., Crozier, S., Baillet, S., and Samson, Y. (2009). Prediction of Infarct Growth Based on Apparent Diffusion Coefficients: Penumbra Assessment without Intravenous Contrast Material. *Radiology* *250*, 184–192.
- Sacco, R.L., Kasner, S.E., Broderick, J.P., Caplan, L.R., Connors, J.J. (Buddy), Culebras, A., Elkind, M.S.V., George, M.G., Hamdan, A.D., Higashida, R.T., et al. (2013). An Updated Definition of Stroke for the 21st Century A Statement for Healthcare Professionals From the American Heart Association/American Stroke Association. *Stroke* *44*, 2064–2089.
- Saharinen, P., Eklund, L., Miettinen, J., Wirkkala, R., Anisimov, A., Winderlich, M., Nottebaum, A., Vestweber, D., Deutsch, U., Koh, G.Y., et al. (2008). Angiopoietins assemble distinct Tie2 signalling complexes in endothelial cell–cell and cell–matrix contacts. *Nat. Cell Biol.* *10*, 527–537.
- Salgado, A.J., Sousa, J.C., Costa, B.M., Pires, A.O., Mateus-Pinheiro, A., Teixeira, F.G., Pinto, L., and Sousa, N. (2015). Mesenchymal stem cells secretome as a modulator of the neurogenic niche: basic insights and therapeutic opportunities. *Front. Cell. Neurosci.* *249*.
- Sarnowska, A., Jablonska, A., Jurga, M., Dainiak, M., Strojek, L., Drela, K., Wright, K., Tripathi, A., Kumar, A., Jungvid, H., et al. (2013). Encapsulation of mesenchymal stem cells by bioscaffolds protects cell survival and attenuates neuroinflammatory reaction in injured brain tissue after transplantation. *Cell Transplant.* *22 Suppl 1*, S67-82.
- Sarraj, A., and Grotta, J.C. (2014). Stroke: new horizons in treatment. *Lancet Neurol.* *13*, 2–3.
- Sasaki, Y., Sasaki, M., Kataoka-Sasaki, Y., Nakazaki, M., Nagahama, H., Suzuki, J., Tateyama, D., Oka, S., Namioka, T., Namioka, A., et al. (2016). Synergic Effects of Rehabilitation and Intravenous Infusion of Mesenchymal Stem Cells After Stroke in Rats. *Phys. Ther.*
- Schwartz-Bloom, R.D., and Sah, R. (2001). γ -Aminobutyric acidA neurotransmission and cerebral ischemia. *J. Neurochem.* *77*, 353–371.
- Seevinck, P.R., Deddens, L.H., and Dijkhuizen, R.M. (2010). Magnetic resonance imaging of brain angiogenesis after stroke. *Angiogenesis* *13*, 101–111.
- Semenza, G.L. (1998). Hypoxia-inducible factor 1: master regulator of O₂ homeostasis. *Curr. Opin. Genet. Dev.* *8*, 588–594.

- Seo, J.H., and Cho, S.-R. (2012). Neurorestoration Induced by Mesenchymal Stem Cells: Potential Therapeutic Mechanisms for Clinical Trials. *Yonsei Med. J.* 53, 1059.
- Shen, Q., Meng, X., Fisher, M., Sotak, C.H., and Duong, T.Q. (2003). Pixel-by-Pixel Spatiotemporal Progression of Focal Ischemia Derived Using Quantitative Perfusion and Diffusion Imaging. *J. Cereb. Blood Flow Metab.* 23, 1479–1488.
- Shu, X.Z., Ahmad, S., Liu, Y., and Prestwich, G.D. (2006). Synthesis and evaluation of injectable, in situ crosslinkable synthetic extracellular matrices for tissue engineering. *J. Biomed. Mater. Res. A* 79, 902–912.
- Sinden, J.D., and Muir, K.W. (2012). Stem cells in stroke treatment: the promise and the challenges. *Int. J. Stroke* 7, 426–434.
- Slevin, M., Kumar, P., Gaffney, J., Kumar, S., and Krupinski, J. (2006). Can angiogenesis be exploited to improve stroke outcome? Mechanisms and therapeutic potential. *Clin. Sci.* 111, 171–183.
- Sofroniew, M.V., and Vinters, H.V. (2009). Astrocytes: biology and pathology. *Acta Neuropathol. (Berl.)* 119, 7–35.
- Solchaga, L.A., Penick, K.J., and Welter, J.F. (2011). Chondrogenic Differentiation of Bone Marrow-Derived Mesenchymal Stem Cells: Tips and Tricks. In *Mesenchymal Stem Cell Assays and Applications*, M. Vemuri, L.G. Chase, and M.S. Rao, eds. (Totowa, NJ: Humana Press), pp. 253–278.
- Stanimirovic, D.B., and Friedman, A. (2012). Pathophysiology of the Neurovascular Unit: Disease Cause or Consequence? *J. Cereb. Blood Flow Metab.* 32, 1207–1221.
- Steinberg, G.K., Kondziolka, D., Wechsler, L.R., Lunsford, L.D., Coburn, M.L., Billigen, J.B., Kim, A.S., Johnson, J.N., Bates, D., King, B., et al. (2016). Clinical Outcomes of Transplanted Modified Bone Marrow-Derived Mesenchymal Stem Cells in Stroke: A Phase 1/2a Study. *Stroke J. Cereb. Circ.*
- Strazielle, N., and Ghersi-Egea, J.F. (2013). Physiology of Blood–Brain Interfaces in Relation to Brain Disposition of Small Compounds and Macromolecules. *Mol. Pharm.* 10, 1473–1491.
- Strbian, D., Durukan, A., Pitkonen, M., Marinkovic, I., Tatlisumak, E., Pedrono, E., Abo-Ramadan, U., and Tatlisumak, T. (2008). The blood–brain barrier is continuously open for several weeks following transient focal cerebral ischemia. *Neuroscience* 153, 175–181.
- Ström, J.O., Ingberg, E., Theodorsson, A., and Theodorsson, E. (2013). Method parameters' impact on mortality and variability in rat stroke experiments: a meta-analysis. *BMC Neurosci.* 14, 41.
- Strong, A.J., Anderson, P.J., Watts, H.R., Virley, D.J., Lloyd, A., Irving, E.A., Nagafuji, T., Ninomiya, M., Nakamura, H., Dunn, A.K., et al. (2007). Peri-infarct depolarizations lead to loss of perfusion in ischaemic gyrencephalic cerebral cortex. *Brain* 130, 995–1008.
- Struzyna, L.A., Katiyar, K., and Cullen, D.K. (2014). Living scaffolds for neuroregeneration. *Curr. Opin. Solid State Mater. Sci.* 18, 308–318.

- Sullivan, R., Duncan, K., Dailey, T., Kaneko, Y., Tajiri, N., and Borlongan, C.V. (2015). A possible new focus for stroke treatment – migrating stem cells. *Expert Opin. Biol. Ther.* *15*, 949–958.
- Sun, X., Zhang, Q.-W., Xu, M., Guo, J.-J., Shen, S.-W., Wang, Y.-Q., and Sun, F.-Y. (2012). New striatal neurons form projections to substantia nigra in adult rat brain after stroke. *Neurobiol. Dis.* *45*, 601–609.
- Sun, X., Sun, X., Liu, T., Zhao, M., Zhao, S., Xiao, T., Jolkkonen, J., and Zhao, C. (2015). Fluoxetine enhanced neurogenesis is not translated to functional outcome in stroke rats. *Neurosci. Lett.* *603*, 31–36.
- Tae-Hoon, L., and Yoon-Seok, L. (2012). Transplantation of mouse embryonic stem cell after middle cerebral artery occlusion. *Acta Cir. Bras.* *27*, 333–339.
- Taguchi, A., Sakai, C., Soma, T., Kasahara, Y., Stern, D.M., Kajimoto, K., Ihara, M., Daimon, T., Yamahara, K., Doi, K., et al. (2015). Intravenous Autologous Bone Marrow Mononuclear Cell Transplantation for Stroke: Phase1/2a Clinical Trial in a Homogeneous Group of Stroke Patients. *Stem Cells Dev.* *24*, 2207–2218.
- Tajiri, N., Kaneko, Y., Shinozuka, K., Ishikawa, H., Yankee, E., McGrogan, M., Case, C., and Borlongan, C.V. (2013). Stem Cell Recruitment of Newly Formed Host Cells via a Successful Seduction? Filling the Gap between Neurogenic Niche and Injured Brain Site. *PLOS ONE* *8*, e74857.
- Takahashi, K., and Yamanaka, S. (2006). Induction of Pluripotent Stem Cells from Mouse Embryonic and Adult Fibroblast Cultures by Defined Factors. *Cell* *126*, 663–676.
- Takeda, Y.S., and Xu, Q. (2015). Neuronal Differentiation of Human Mesenchymal Stem Cells Using Exosomes Derived from Differentiating Neuronal Cells. *PLOS ONE* *10*, e0135111.
- Tang, Y.-H., Ma, Y.-Y., Zhang, Z.-J., Wang, Y.-T., and Yang, G.-Y. (2015). Opportunities and Challenges: Stem Cell-Based Therapy for the Treatment of Ischemic Stroke. *CNS Neurosci. Ther.* *21*, 337–347.
- Taupin, P., and Gage, F.H. (2002). Adult neurogenesis and neural stem cells of the central nervous system in mammals. *J. Neurosci. Res.* *69*, 745–749.
- Thiel, A., and Vahdat, S. (2015). Structural and Resting-State Brain Connectivity of Motor Networks After Stroke. *Stroke* *46*, 296–301.
- Thomson, J.A., Itskovitz-Eldor, J., Shapiro, S.S., Waknitz, M.A., Swiergiel, J.J., Marshall, V.S., and Jones, J.M. (1998). Embryonic Stem Cell Lines Derived from Human Blastocysts. *Science* *282*, 1145–1147.
- Thonhoff, J.R., Lou, D.I., Jordan, P.M., Zhao, X., and Wu, P. (2008). Compatibility of human fetal neural stem cells with hydrogel biomaterials in vitro. *Brain Res.* *1187*, 42–51.
- Thored, P., Arvidsson, A., Cacci, E., Ahlenius, H., Kallur, T., Darsalia, V., Ekdahl, C.T., Kokaia, Z., and Lindvall, O. (2006). Persistent Production of Neurons from Adult Brain Stem Cells During Recovery after Stroke. *STEM CELLS* *24*, 739–747.
- Thored, P., Wood, J., Arvidsson, A., Cammenga, J., Kokaia, Z., and Lindvall, O. (2007). Long-Term Neuroblast Migration Along Blood Vessels in an Area With Transient Angiogenesis and Increased Vascularization After Stroke. *Stroke* *38*, 3032–3039.

- Thored, P., Heldmann, U., Gomes-Leal, W., Gisler, R., Darsalia, V., Taneera, J., Nygren, J.M., Jacobsen, S.-E.W., Ekdahl, C.T., Kokaia, Z., et al. (2009). Long-term accumulation of microglia with proneurogenic phenotype concomitant with persistent neurogenesis in adult subventricular zone after stroke. *Glia* 57, 835–849.
- Tornero, D., Wattananit, S., Grønning Madsen, M., Koch, P., Wood, J., Tatarishvili, J., Mine, Y., Ge, R., Monni, E., Devaraju, K., et al. (2013). Human induced pluripotent stem cell-derived cortical neurons integrate in stroke-injured cortex and improve functional recovery. *Brain J. Neurol.* 136, 3561–3577.
- Troprès, I., Grimault, S., Vaeth, A., Grillon, E., Julien, C., Payen, J.F., Lamalle, L., and Décorps, M. (2001). Vessel size imaging. *Magn. Reson. Med. Off. J. Soc. Magn. Reson. Med. Soc. Magn. Reson. Med.* 45, 397–408.
- Troprès, I., Lamalle, L., Farion, R., Segebarth, C., and Rémy, C. (2004). Vessel size imaging using low intravascular contrast agent concentrations. *Magn. Reson. Mater. Phys. Biol. Med.* 17, 313–316.
- Troprès, I., Pannetier, N., Grand, S., Lemasson, B., Moisan, A., Péoc'h, M., Rémy, C., and Barbier, E.L. (2015). Imaging the microvessel caliber and density: Principles and applications of microvascular MRI. *Magn. Reson. Med.* 73, 325–341.
- Trueman, R.C., Diaz, C., Farr, T.D., Harrison, D.J., Fuller, A., Tokarczuk, P.F., Stewart, A.J., Paisey, S.J., and Dunnett, S.B. (2016). Systematic and detailed analysis of behavioural tests in the rat middle cerebral artery occlusion model of stroke: Tests for long-term assessment. *J. Cereb. Blood Flow Metab.* 0271678X16654921.
- Ueno, Y., Chopp, M., Zhang, L., Buller, B., Liu, Z., Lehman, N.L., Liu, X.S., Zhang, Y., Roberts, C., and Zhang, Z.G. (2012). Axonal Outgrowth and Dendritic Plasticity in the Cortical Peri-Infarct Area After Experimental Stroke. *Stroke* 43, 2221–2228.
- Velayudhan, V., Ferretti, J., Pawha, P., Chen, Y.-H., and Tenenbaum, L. (2016). Stroke Imaging: Overview, Computed Tomography, Magnetic Resonance Imaging.
- Veltkamp, R., and Gill, D. (2016). Clinical Trials of Immunomodulation in Ischemic Stroke. *Neurotherapeutics* 1–10.
- Verdegem, D., Moens, S., Stapor, P., and Carmeliet, P. (2014). Endothelial cell metabolism: parallels and divergences with cancer cell metabolism. *Cancer Metab.* 2, 19.
- Vu, Q., Xie, K., Eckert, M., Zhao, W., and Cramer, S.C. (2014). Meta-analysis of preclinical studies of mesenchymal stromal cells for ischemic stroke. *Neurology* 82, 1277–1286.
- Wang, H., Chen, M., Wang, F., Dai, L., Fei, A., Liu, J., Li, H., Shen, S., Liu, M., and Pan, S. (2015). Comparison of Therapeutic Effect of Recombinant Tissue Plasminogen Activator by Treatment Time after Onset of Acute Ischemic Stroke. *Sci. Rep.* 5.
- Wang, L., Chopp, M., Zhang, R.L., Zhang, L., LeTourneau, Y., Feng, Y.F., Jiang, A., Morris, D.C., and Zhang, Z.G. (2009). The Notch pathway mediates expansion of a progenitor pool and neuronal differentiation in adult neural progenitor cells after stroke. *Neuroscience* 158, 1356–1363.

- Wang, L.-S., Chung, J.E., Chan, P.P.-Y., and Kurisawa, M. (2010). Injectable biodegradable hydrogels with tunable mechanical properties for the stimulation of neurogenic differentiation of human mesenchymal stem cells in 3D culture. *Biomaterials* *31*, 1148–1157.
- Wang-Fischer, Y., Divani, A., Prado, R., and Koetzner, L. (2009). Surgical Model of Stroke Induced by Intraluminal Filament Implantation. In *Annual of Stroke Model in Rats*, p.
- Wexler, S.A., Donaldson, C., Denning-Kendall, P., Rice, C., Bradley, B., and Hows, J.M. (2003). Adult bone marrow is a rich source of human mesenchymal “stem” cells but umbilical cord and mobilized adult blood are not. *Br. J. Haematol.* *121*, 368–374.
- Winship, I.R., and Murphy, T.H. (2009). Remapping the Somatosensory Cortex after Stroke: Insight from Imaging the Synapse to Network. *The Neuroscientist* *15*, 507–524.
- Woitzik, J., Hecht, N., Pinczolits, A., Sandow, N., Major, S., Winkler, M.K.L., Weber-Carstens, S., Dohmen, C., Graf, R., Strong, A.J., et al. (2013). Propagation of cortical spreading depolarization in the human cortex after malignant stroke. *Neurology* *80*, 1095–1102.
- Won, S.J., Tang, X.N., Suh, S.W., Yenari, M.A., and Swanson, R.A. (2011). Hyperglycemia promotes tPA-induced hemorrhage by promoting superoxide production. *Ann. Neurol.* *70*, 583–590.
- Wong, C.H.Y., Jenne, C.N., Lee, W.-Y., Léger, C., and Kubes, P. (2011). Functional Innervation of Hepatic iNKT Cells Is Immunosuppressive Following Stroke. *Science* *334*, 101–105.
- Xing, C., Arai, K., Lo, E.H., and Hommel, M. (2012). Pathophysiologic cascades in ischemic stroke. *Int. J. Stroke Off. J. Int. Stroke Soc.* *7*, 378–385.
- Yamashita, T., Ninomiya, M., Acosta, P.H., García-Verdugo, J.M., Sunabori, T., Sakaguchi, M., Adachi, K., Kojima, T., Hirota, Y., Kawase, T., et al. (2006). Subventricular Zone-Derived Neuroblasts Migrate and Differentiate into Mature Neurons in the Post-Stroke Adult Striatum. *J. Neurosci.* *26*, 6627–6636.
- Yamashita, T., Kawai, H., Tian, F., Ohta, Y., and Abe, K. (2011). Tumorigenic Development of Induced Pluripotent Stem Cells in Ischemic Mouse Brain. *Cell Transplant.* *20*, 883–891.
- Yemisci, M., Gursoy-Ozdemir, Y., Vural, A., Can, A., Topalkara, K., and Dalkara, T. (2009). Pericyte contraction induced by oxidative-nitrative stress impairs capillary reflow despite successful opening of an occluded cerebral artery. *Nat. Med.* *15*, 1031–1037.
- Yin, K.-J., Hamblin, M., and Chen, Y.E. (2015). Angiogenesis-regulating microRNAs and ischemic stroke. *Curr. Vasc. Pharmacol.* *13*, 352–365.
- Zappia, E., Casazza, S., Pedemonte, E., Benvenuto, F., Bonanni, I., Gerdoni, E., Giunti, D., Ceravolo, A., Cazzanti, F., Frassoni, F., et al. (2005). Mesenchymal stem cells ameliorate experimental autoimmune encephalomyelitis inducing T-cell anergy. *Blood* *106*, 1755–1761.
- Zhang, P., Lei, X., Sun, Y., Zhang, H., Chang, L., Li, C., Liu, D., Bhatta, N., Zhang, Z., and Jiang, C. (2016). Regenerative repair of Pifithrin- α in cerebral ischemia via VEGF dependent manner. *Sci. Rep.* *6*.

Zhang, R., Xue, Y.-Y., Lu, S.-D., Wang, Y., Zhang, L.-M., Huang, Y.-L., Signore, A.P., Chen, J., and Sun, F.-Y. (2006a). Bcl-2 enhances neurogenesis and inhibits apoptosis of newborn neurons in adult rat brain following a transient middle cerebral artery occlusion. *Neurobiol. Dis.* 24, 345–356.

Zhang, R.L., Zhang, Z.G., Lu, M., Wang, Y., Yang, J.J., and Chopp, M. (2006b). Reduction of the Cell Cycle Length by Decreasing G1 Phase and Cell Cycle Reentry Expand Neuronal Progenitor Cells in the Subventricular Zone of Adult Rat after Stroke. *J. Cereb. Blood Flow Metab.* 26, 857–863.

Zhang, R.L., Zhang, Z.G., Wang, Y., LeTourneau, Y., Liu, X.S., Zhang, X., Gregg, S.R., Wang, L., and Chopp, M. (2007). Stroke Induces Ependymal Cell Transformation into Radial Glia in the Subventricular Zone of the Adult Rodent Brain. *J. Cereb. Blood Flow Metab.* 27, 1201–1212.

Zhao, H., Steinberg, G.K., and Sapolsky, R.M. (2007). General versus Specific Actions of Mild-Moderate Hypothermia in Attenuating Cerebral Ischemic Damage. *J. Cereb. Blood Flow Metab.* 27, 1879–1894.

Zhao, T., Zhang, Z.-N., Rong, Z., and Xu, Y. (2011). Immunogenicity of induced pluripotent stem cells. *Nature* 474, 212–215.

Zhong, J., Chan, A., Morad, L., Kornblum, H.I., Fan, G., and Carmichael, S.T. (2010). Hydrogel matrix to support stem cell survival after brain transplantation in stroke. *Neurorehabil. Neural Repair* 24, 636–644.

Ziv, Y., Ron, N., Butovsky, O., Landa, G., Sudai, E., Greenberg, N., Cohen, H., Kipnis, J., and Schwartz, M. (2006). Immune cells contribute to the maintenance of neurogenesis and spatial learning abilities in adulthood. *Nat. Neurosci.* 9, 268–275.

Zlokovic, B.V. (2008). The Blood-Brain Barrier in Health and Chronic Neurodegenerative Disorders. *Neuron* 57, 178–201.

del Zoppo, G.J. (2010). The neurovascular unit in the setting of stroke. *J. Intern. Med.* 267, 156–171.

Zuk, P.A. (2002). Human Adipose Tissue Is a Source of Multipotent Stem Cells. *Mol. Biol. Cell* 13, 4279–4295.

10 APPENDIX



Research internship report (November 2014-February 2015)

Master 1 Ingénieries pour la Santé et le Médicament

Université Joseph Fourier

“Do early Apparent Diffusion Coefficient maps have a prognostic value in the Middle Cerebral Artery occlusion stroke model?”

Ninon Rouchossé

Medicine Student DFASM 2

Internship supervisors: Dr Olivier DETANTE,

Ligia SIMOES BRAGA BOISSERAND.

Grenoble Institut des Neurosciences

Team 5: "Functional NeuroImaging and Brain Perfusion"

Sommaire

❖	<i>ABSTRACT</i>	3
❖	<i>RÉSUMÉ</i>	4
❖	<i>INTRODUCTION</i>	5
❖	<i>MATERIALS AND METHODS</i>	7
	General anesthesia and surgery	7
	MRI procedure.....	8
	Image analysis	8
	Histology	9
	Statistics.....	9
❖	<i>RESULTS</i>	10
	Volume of ROI “Edema”	10
	ADCr of ROI “Edema”	10
	Automatic clusters	10
❖	<i>DISCUSSION</i>	13
❖	<i>CONCLUSION</i>	16
❖	<i>REFERENCES</i>	17
❖	<i>ANNEXES</i>	20

Remerciements à Olivier Detante, Emmanuel Barbier, Chantal Remy, Ligia Simoes Braga Boisserand et Benjamin Lemasson pour leur aide et leurs conseils avisés.

❖ ABSTRACT

Introduction. Cerebral ischemia represents 80% of strokes, which are the second leading cause of death worldwide. The essential issue in the clinical setting is to urgently define the size of the final infarct (necrosis) and estimate the prognosis of the patient in order to avoid futile treatment (thrombolysis and/or thrombectomy) when its benefit would not be sufficient. We aimed to explore the prognostic value of early Apparent Diffusion Coefficient (ADC) maps, an MRI sequence, in rats that endured a model of acute stroke. *Material:* 23 Sprague-Dawley male rats underwent middle cerebral artery occlusion (MCAo) during 90 minutes, during which two ADC maps were computed around 30 (T30) and 60 minutes (T60) after MCAo. Two groups were constituted based on the survival of the rats in the following 24 hours. We delineated in the three central brain slices the Region Of Interest (ROI) “Contra” in the healthy hemisphere and “Edema” as the region of decreased ADC. We calculated ADC ratio (ADC “Edema”/ADC “Contra”) and the volume of ROI “Edema”. *Results:* The rats that did not survive the MCAo (Group D, n=13) had a bigger lesion at T30 (median = 238.1 mm³; interquartile range (IR) = 172.1) - and at T60 (median = 236.6 mm³ (IR = 142.6) than rats that survived (Group S, n=10) - respectively 29.6 mm³ (IR = 111.1) and 38.7mm³(IR = 120.1). The ADCr was not different at T30 and T60 between the two groups but group D showed a significant decrease of ADCr between T30 (mean = 0.765, SD=0.034) and T60 (mean = 0.729, SD = 0.033), unlike group S (0.763 (SD = 0.062) and 0.757 (SD = 0.068)). *Conclusion:* The rats that died soon after cerebral ischemia had bigger lesions than the survivors, with significant ADC decrease within the first hour following the stroke. However individual analysis of these two features allows no reliable survival prediction. Nevertheless, the use of diffusion MRI in acute stroke models can help to identify early biomarkers of prognosis in ischemic stroke.

❖ RÉSUMÉ

Introduction: Les accidents vasculaires cérébraux (AVC) sont la seconde cause de décès dans le monde et sont dus dans 80% des cas à une ischémie cérébrale. Estimer rapidement la taille de l'infarctus final et le pronostic du patient est essentiel pour éviter un traitement risqué (thrombolyse et/ou thrombectomie) quand le bénéfice attendu n'est pas suffisant. Nous avons évalué la valeur pronostique précoce d'une séquence IRM : les cartes de coefficient apparent de diffusion (ADC) chez des rats ayant subi un modèle d'AVC. *Matériels:* 23 rats mâle Sprague Dawley ont subi une occlusion de l'artère cérébrale moyenne (oACM) pendant 90 minutes, durant lesquelles deux cartes ADC ont été acquises, à 30 (T30) et 60 minutes (T60). Deux groupes ont été constitués selon la survie des rats dans les 24 heures suivantes. Nous avons délimité sur les trois coupes centrales du cerveau les régions d'intérêt (ROI) « Contra » dans l'hémisphère sain, et « Edema » dans la région d'ADC abaissée. Nous avons calculé le ratio d'ADC (ADC « Edema » / ADC « Contra ») et le volume de la ROI « Edema ». *Résultats:* Les rats qui n'ont pas survécu à l'oACM (Groupe D, n=13) avaient une plus grande lésion à T30- (médiane= 238,1 mm³ (interquartile range (IR) = 172.1)- et T60 (médiane de 236,6 mm³ ; IR = 142.65) que les rats ayant survécu (Groupe S, n=10)- respectivement 29,6 mm³ (111,1) et 38,7 mm³ (120,1). L'ADCr n'était pas significativement différent à T30 et T60 entre les deux groupes mais le groupe D a présenté une diminution significative de l'ADC entre 30 minutes (moyenne = 0,765 ; SD = 0.034) et 60 minutes (moyenne = 0,729 ; SD = 0.033) contrairement au groupe S (respectivement, 0,763 (0.062) et 0,757 (0,068)). *Conclusion:* Les rats décédés peu après l'ischémie avaient une lésion plus grande que les survivants, avec une diminution significative de l'ADC dans l'heure suivant l'oACM. Cependant, l'analyse individuelle de ces deux critères ne permet pas de prédire la survie. Ainsi, l'utilisation de l'IRM de diffusion dans les modèles expérimentaux d'AVC peut permettre d'identifier des bio-marqueurs pronostiques précoces de l'AVC ischémique.

❖ INTRODUCTION

Strokes are the second leading cause of death in the world with 6.7 million deaths in 2012¹, and a major cause of acquired disability in developed countries².

Cerebral ischemia represents 80% of strokes. An ischemic stroke is defined as a sudden perfusion decrease below the cerebral blood flow auto-regulation threshold. The supply in oxygen and energy is reduced and consequently the cerebral tissue suffers: an anoxic depolarization appears, followed by the death of the cells if the flow is still disrupted. It is usually caused by proximal artery or cardiac emboli³. Intravenous thrombolysis by Alteplase or thrombectomy are the only treatments of ischemic strokes which have proven their efficacy so far. Their aim is to re-establish the blood flow in the affected region as soon as possible so that the part of the tissue which has not yet gone into necrosis can be saved. However, the therapeutic window extends only until 4.5 hours (or 6 hours for bridging thrombectomy) after the stroke onset⁴, which means that an important part of patients cannot benefit from it⁵.

Thus, the essential issue in the clinical setting is to urgently identify the salvageable tissue and to predict the size of the final infarct corresponding to the functional outcome of the patient.

Predicting the size of the final infarction is closely linked to the identification of the tissue-at-risk of infarction, also called the penumbra⁶. It is defined as the tissue functionally impaired by the diminution of local blood flow. It becomes electro-physiologically silent and participates in the clinical deficit. However the tissue is not irreversibly damaged: membranes are preserved and the cells could still survive if the re-oxygenation occurred early enough. If no reperfusion occurs, the tissue-at-risk will gradually go into necrosis and thus, the infarct core will irreversibly grow³.

The gold standard for the identification of tissue-at-risk remains the positron emission tomography (PET) scan, which has led to the metabolic definition of penumbra: it is characterized by a regional cerebral blood flow (rCBF) between 12 and 22 ml/100g/min, a regional cerebral metabolic rate of O₂ (rCMRO₂) above 65 μ mol/100g/min and an increased oxygen extraction fraction (OEF) (50 to 90%), in comparison with the ischemic core, where the rCBF is lower than 12 ml/100g/min, the rCMRO₂ lower than 65 μ mol/100g/min and the OEF collapsed. On the other hand, the oligemic tissue is characterized by a mild decrease of rCBF, between 50 and 22 ml/100g/min, and it is not at risk of infarction⁷.

Because of the irradiation caused by PET, its high cost and limited availability in the clinical setting, other techniques have been promoted. Above all, MRI is from now on used in some clinical settings to assess the penumbra: it can actually be approximated by the mismatch between the Diffusion weighted Imaging (DWI) and the Perfusion Weighted Imaging (PWI)⁸. Indeed, the DWI aims to assess the diffusion of H₂O molecules and it is used to identify the ischemic core where the water diffusion is significantly impaired because of water entry into cells, causing cell edema, whereas the PWI should approximate the region of impaired perfusion, constituted of the ischemic core and the penumbra. However this method has shown some limitations: it appeared that the diffusion lesion seems to overestimate the ischemic core and the final lesion⁹, while the PWI lesion could contain some oligemic tissue because of the lack of established thresholds to assess perfusion.¹⁰

Thus, other MRI methods are being developed, such as BOLD (Blood oxygen level dependent) imaging, which aims to better discriminate the core from the penumbra.^{11,12}

Other teams focused on the maps of apparent diffusion coefficient (ADC): By combining T2-weighted imaging and DWI in 3 different direction planes, an apparent diffusion coefficient (ADC)-cartography is

obtained. This allows a quantitative assessment of tissue diffusion¹³. It appeared that a mild decrease in ADC can be observed in the tissue at risk of infarction in experimental models¹⁴ and human studies¹⁵. Based on these findings, algorithms and models based on acute imaging have been designed in order to predict the final infarcted lesion^{16,17}.

Regarding prognosis, it makes sense to hypothesize that the outcome would worsen with the size of the stroke and the clinical state at admission. Thus, it has been shown that the size of the DWI lesion is correlated with the outcome¹⁸ and even better when combined with clinical state at admission¹⁹. Furthermore, the predicted infarct core, predicted ischemic penumbra and predicted final infarct through ADC-based method were found to be correlated with clinical outcome²⁰. ADC measurements also appeared to improve the correlation with the clinical outcome when combined with DWI volume²¹.

In rat stroke experiments, a high mortality and outcome variability have been observed. Moreover, the mortality rate is often not even reported in literature. This variability has been considered as a possible reason for the discrepancy between treatment effectiveness in preclinical studies and its failure on clinical ones²².

Indeed, the exclusion of dead rats from data analysis may bias the estimation of stroke outcome whereas taking into account these data may give some information about the prognosis factors in strokes.

Objectives: Based on these findings, we analyzed in a retrospective way the ADC imaging features obtained in two groups of rats who endured a model of stroke: the first group included rats who survived the stroke, the second one included rats who did not survive the first 24 hours after the stroke. Our primary endpoints were the normalized ADC value of the stroke lesion and its volume at 30 minutes and 60 minutes after Middle Cerebral Artery occlusion (MCAo).

We hypothesized that rats that died would have deeper diffusion abnormalities and bigger lesions on early ADC maps.

❖ MATERIALS AND METHODS

Thirty-nine Sprague-Dawley male rats weighing 300g underwent the procedure before my participation in the study.

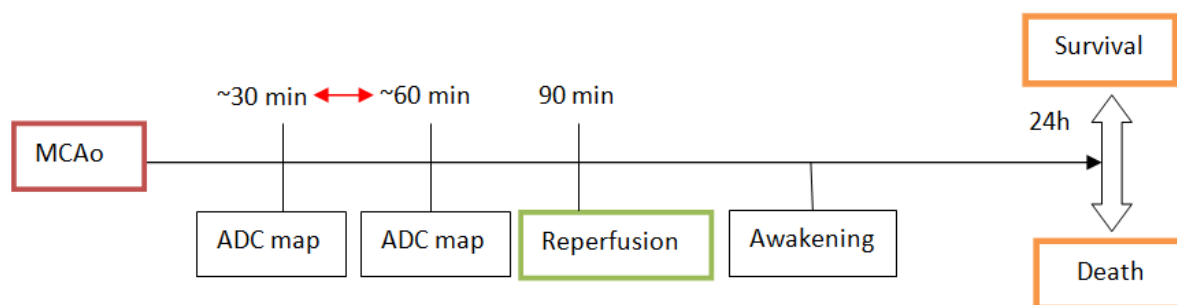


Figure 1: Experimental Procedure

Animal procedures conformed to the French guidelines (A3851610008 for animal care facilities).

General anesthesia and surgery

Anesthesia was induced by 5% isoflurane (Forène, Abbott Laboratory) in air. Anesthesia was maintained throughout the procedure by 1.5-2.5% Isoflurane with 30% of oxygen through a facial mask. Rectal temperature was maintained at $37.0 \pm 0.5^\circ\text{C}$ with an electrical heating blanket (water blanket for MRI) connected to a rectal probe. An external oxymeter was used to check blood saturation of oxygen.

Transient focal brain ischemia was realized by intraluminal occlusion of the right middle cerebral artery (MCA) during 90 minutes (cf *Annex n°1*). This produces extensive infarcts in the cortex and the striatum within MCA territory.

First, the right carotid bifurcation was exposed and isolated. The external carotid artery, the internal carotid artery (ICA) and the common carotid artery (CCA) were clamped. The ascending pharyngeal and occipital branches of the external carotid artery were electro-coagulated and transected. The external carotid artery was transected, creating a stump. After the removal of the ICA ligature, a cylinder of melted adhesive (length = 2mm, diameter = 0.37mm) attached to a nylon thread (diameter = 0.22mm) was pushed from the lumen of the right external carotid artery into the ICA. It was advanced through the right ICA toward the right anterior cerebral artery (ACA) to occlude the right MCA at its origin. Finally the CCA flow was reestablished. Local sub-cutaneous anesthesia by bupivacaine was added. The thread was removed after 90 minutes of ischemia, allowing reperfusion.

The flow chart is represented in *Annex n°2*. Three rats were immediately excluded because of the absence of reliable or available data.

After 24 hours, 21 rats had died and 15 had survived. Among rats that did not survive the first 24 hours after ischemia, 8 had no reliable imaging data. Finally, the Group D including rats that died was composed of 13 rats.

Rats that survived were followed up until day 21; 3 had no lesion at Day 21 and 2 were euthanized for ethical reasons. Finally, the Group S including rats that survived the stroke was composed of 10 rats.

MRI procedure

Between the MCAo and the reperfusion, the rats underwent multimodal MRI in a 4.7 Tesla magnet linked to a Bruker® console. The acquisition of the sequences lasted 56 minutes (*Annex n°3*). The rat head was maintained motionless by teeth and ears fixations. The rat pulse oxymetry, rectal temperature, and abdominal breath movements were evaluated.

A catheter was introduced in the vein of the tail to allow contrast agent injection.

Apparent diffusion coefficient

Two sets of Diffusion weighted imaging were computed, one around 30 minutes after surgery and the second around 60 minutes after.

Apparent Diffusion Coefficient (ADC) maps are obtained by computing the mean of the diffusion weighted images observed in 3 directions of space, with two different diffusion-weighting degrees (expressed by the factor b , $b=0$ and $b=1000 \text{ s.mm}^{-2}$). Thus, ADC maps give quantitative information of water molecules diffusion in $\text{mm}^2.\text{s}^{-1}$. A hypo-signal in the ADC map means restricted diffusion of water molecules.

In the acute phase of ischemia, failure of the ionic pumps in the ischemic core leads to cell edema. Consequently, the extracellular water diffusion is restricted and the region of ischemia appears as a zone of decreased ADC on ADC map.

Image analysis

Regions of interest (ROI) (cf Annex n°4)

We used the program *Images Analyses*, developed in our team, to analyze the MRI sequences.

The ROI “Edema” was created by manual delineation of visually decreased ADC region in the right hemisphere. The ROI “Contra” was manually delineated in the contralateral hemisphere as a “mirror” of ROI “Edema”. It represents a region of healthy tissue.

The ROI “Hemisphere” was created by manual delineation of the ipsilateral hemisphere, excluding the ventricles.

Volume

To obtain an approximation of the ischemic lesion volume, we delineated the ROI Edema on the 9 slices of the ADC sequence. It covers a third of the whole brain (from the olfactory bulb to the cerebellum) and almost the totality of the MCA territory.

The sequence has a matrix of $128*128$ voxels, a field of view of $30*30 \text{ (mm}^2\text{)}$, and the distance between the slices is 0.8 mm.

As a result:

- Voxel size: $(30/128)^2 \text{ (mm}^2\text{)}$
- ROI size (mm^2) = amount of voxels in ROI * voxel size
- ROI volume (mm^3) = amount of voxels in ROI * voxel size * 0.8

ADC ratio

To obtain the ADC ratio, we used the three central slices of the brain.

For each slice, we calculated the ADCr by dividing the ADC value of the ROI “Edema” by the ADC value of the ROI “Contra”. Then, we calculated the mean ADCr of the three slices for each rat.

Indeed, ADCr appeared to be a better criterion of ADC decrease than absolute ADC value because of the variation of ADC seen in the ROI “Contra” between rats and slices.

Automatic clusters in ROI “Edema” (cf Annex n°5)

In order to analyze the ADC and its time course more accurately in the ROI, we used an automatic process available on our data analysis software *Images Analysis*. We split the original manually delineated ROI “Edema” into three ROIs defined by the degree of ADC decrease.

We created the ROI “Mild edema” as a cluster including voxels with an ADCr between 0.9 and 0.8. It was calculated using the mean ADC value of the ROI “Contra” of the group.

ex : in group (D): mean ADC value in ROI « Contra » = 800

*ROI « Mild edema » = voxels with ADC among $[800*0.8= 640; 800*0.9=720]$ in Edema ROI*

The software automatically generated a cluster including all the voxels in the chosen interval of ADC value $[640; 720]$ within the original ROI “Edema”.

We also created the ROI “Severe edema” as the cluster including the voxels with an ADCr between 0.8 and 0.6, and the ROI “Very severe edema” as the cluster including the voxels with an ADCr below 0.6.

For each cluster, we calculated the proportion it represented within the ROI “Edema” by dividing the total number of voxels in the cluster by the total number of voxels in the ROI “Edema”. Thus, each cluster is described as a percentage of the global ROI “Edema”.

Histology

The study was built in a retrospective way, using the data of another study that excluded the dead rats. As a result, no histology was done on the rats of the group D except one (“Stroke 38”, Annex n°6), whereas rats of the group S were euthanized after 21 days and their brains were used to do histology tests.

Statistics

We used the software SPSS 20.0 (IBM®) for statistical analysis. The results are expressed in “Mean (Standard Deviation)” if the data was normal, and in “Median (Interquartile range)” if not. We tested the normality of the data distribution using the Shapiro-Wilk test.

To compare data between our two time points within a group, we used a paired samples t-test if the distribution was normal, or a Related-Samples Wilcoxon Signed rank test if not.

To compare data between the two groups, we used an independent samples t-test if the distribution was normal and the variances homogenous (tested by Levene’s test), or an Independent samples Mann-Whitney U Test if one or both conditions were not verified.

We used a significance level of 5%.

❖ RESULTS

Volume of ROI “Edema” (cf Figure n°2)

The distribution was not normal in the samples. The results will be expressed as: *Median (interquartile range)*

In the group including rats that survived the stroke, the median of edema volume at T30 was 29.6 mm³ (111.1) and 38.7 mm³ (120.1) at T60. The volume at T60 was significantly bigger than the volume at T30 (p=0.005).

In the group including rats that didn't survive stroke, the median of edema volume at T30 was 238.1 mm³ (172.2) and 236.6 mm³ (142.6) at T60. The volumes at T30 and T60 were not significantly different (p=0.345).

The edema volumes at T30 and T60 were significantly bigger in group D than in Group S (respectively p=0.001 and p=0.003).

Individual values are represented in *Annex n°7*.

The volumes of the ROI ‘Hemisphere’ in group (S) were 378.1 mm³ (22.2) at T30 and 383.8 mm³ (23.5) at T60 and in group (D) 390.6 mm³ (45.2) at T30 and 385.2 mm³ (33.3) at T60. No difference was found between the groups and the time points.

ADCr of ROI “Edema” (cf Figure n°3)

The distribution was normal in the samples. The results will be expressed as *Mean (Standard deviation)*.

In group S, the mean ADCr at T30 was 0.763 (0.062) and 0.757 (0.068) at T60. There was no significant difference between ADCr at T30 and T60 in group S (p=0.673).

In group D, the mean ADCr at T30 was 0.765 (0.034) and 0.729 (0.033) at T60. ADCr at T60 was significantly lower than ADCr at T30 in group D (p=0.000).

No significant differences were found in terms of ADCr between the two groups at T30 (p=0.879) and at T60 (p=0.166).

Individual values are represented in *Annex n°8*.

Automatic clusters (represented in *Figure n°4* with means)

Proportion of voxels with ADCr higher than 0.9 in ROI “Edema”

The distribution was not normal. Results will be expressed as *Median (Interquartile Range)*

In group S, the proportion of voxels with ADCr above 0.9 at T30 was 9.5% (25) and 17% (19) at T60 with no significant difference between the two values (p=0.385).

In group D, 12% (13) of voxels had an ADCr above 0.9 at T30 and 7% (6) at T60. It was significantly lower at T60 (p=0.009).

The proportion of voxels with very slightly decreased ADCr was not significantly different between the two groups at T30 whereas it was significantly lower in Group D at T60.

Proportion of “Mild edema” in ROI “Edema”

The distribution was normal in the samples. The results will be expressed as *Mean (Standard deviation)*.

In group S, the mean proportion of “Mild edema” at T30 was 21.1% (11.3) and 20.2% (8.1) at T60. It was not significantly different between T30 and T60 (p= 0.654).

In group D, the mean proportion of “Mild edema” at T30 was 21.3% (9.6) and 15.6% (6.6) at T60. It was significantly lower at T60 than at T30 ($p=0.048$).

The proportion of “Mild edema” was not significantly different between the two groups at T30 ($p=0.966$) and at T60 ($p=0.149$).

Proportion of “Severe edema” in ROI “Edema”

The distribution was normal in the samples. The results will be expressed as *Mean (Standard deviation)*.

In group S, the mean proportion of “Severe edema” at T30 was 53.8% (17.8) and 46.6% (9.2) at T60. It was not significantly different between T30 and T60 ($p=0.061$).

In group D, the mean proportion of “Severe edema” at T30 was 59.7% (15.0) and 64.6% (10.4) at T60. It was not significantly different between T30 and T60 ($p=0.226$).

The proportion of “Severe edema” was not significantly different at T30 between the two groups, whereas it was significantly bigger in Group D than in Group S at T60 ($p<0.001$).

Proportion of “Very severe edema” in ROI “Edema”

The distribution was not normal. Results will be expressed as *Median (Interquartile range)*.

In group S, the median proportion of “Very severe edema” at T30 was 8.4% (11) and 11.3% (17) at T60. It was not significantly different between T30 and T60 ($p=0.059$).

In group D, the median proportion of “Very severe edema” at T30 was 3.3% (6) and 11.9% (11) at T60. It was significantly bigger at T60 than at T30 ($p=0.005$).

The proportion of “Very severe edema” was not significantly different at T30 ($p=0.166$) and T60 (0.522) between the two groups.

The distribution of cluster for each rat is represented as volumes (Ex: Volume « mild edema » = % « mild edema » * edema volume) in *Annex n°9*.

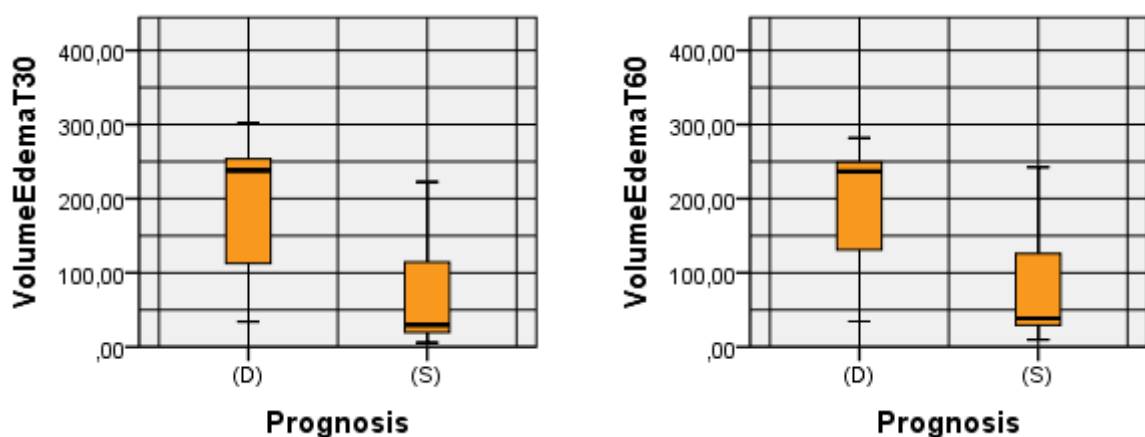


Figure n°2: Box plots representing Volume of ROI “Edema” (mm³) in Group D (D) and Group S (S) at T30 and T60

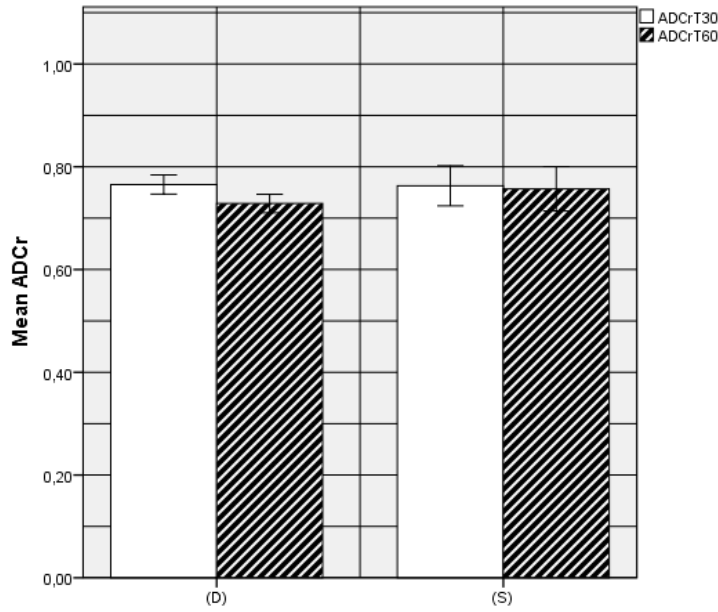


Figure n°3: Histogram representing Mean ADCr at T30 (white) and T60 (hatched) in Group D (D) and Group S (S). (Errors bars: +/- 2 Standard Error)

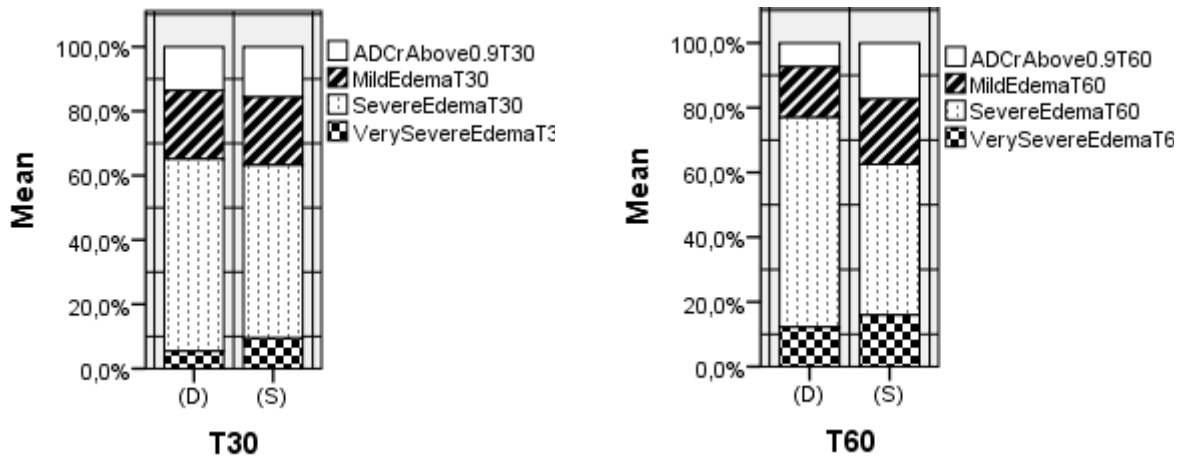


Figure n°4: Histograms representing the distribution of clusters in ROI “Edema” in groups D and S at T30 and T60. (We used means to allow comparisons between clusters.)

To resume, early after the stroke, rats that died later on showed a bigger edema volume than rats that survived. They also showed a decrease of ADCr between 30 and 60 minutes after stroke (unlike rats that survived), supported by a decrease of « Mild edema » and an increase of « Very severe edema ».

It suggests that the mean **rate of early ADC decrease** and the **lesion size** are different between the two groups.

However, on a graph representing ΔADCr ($[\text{ADCr T60} - \text{ADCr T30}] / \text{ADCr T30}$) depending on edema volume at T60 (*Annex n°10*), we are not able to identify two different patterns based on ADCr decrease rate and lesion volume between the two groups.

❖ DISCUSSION

Infarct size correlated with outcome

We found that the infarct volume was significantly higher at 30 minutes and 60 minutes after the stroke in group D than in group S. We can consider that survival is the main prognosis parameter on rats; it is rather different in humans, because of the difference in health care quality which fortunately allows much better survival in humans. Thus, the outcome in humans can be assessed by different criteria.

Engelter ST & al²³ found that the infarct volume on ADC maps of stroke patients at 41 hours after stroke onset correlated significantly with the length of hospitalization and the functional outcome after 6 months.

Schwamm & al²⁴ described a positive correlation between follow-up National Institutes of Health Stroke Scale (NIHSS) score, which assesses the degree of neurological deficiency, and the initial DWI lesion volume in stroke patients. Beaulieu & al²⁵ found the same correlation.

Oppenheim²¹ reported a significantly larger DWI volume at time of admission in the group including patients that will develop malignant middle cerebral artery infarction.

Despite the significant difference in lesion volume between the two groups, we observed an important variation of volume within groups (cf *Annex n°7*). This has been described in the literature concerning MCAo model. Ström²² reported an infarct size coefficient of variation average of $28.9 \pm 21.3\%$, with a range from 1.7 to 148.

Infarct growth in rats that survived

We observed that the lesion grew from 30 minutes to 60 minutes after stroke onset in group S.

Hoehn-Berlage & al²⁶ found that, in MCA-occluded rats, a large territory of reduced ADC appeared within minutes after the stroke and that this region grew continuously during the 2 hours of observation; Minematsu & al²⁷ also reported a slight increase of the DWI lesion in MCA-occluded rats between 30 minutes and 3 hours after ischemia onset. However, the data in these studies are not split depending on rat survival. Yet, we could not highlight the infarct growth on rats that died later on. It can either be explained by a lack of power; or maybe the lesion in group D, which was significantly bigger than in group S, increased severely before our first imaging time point, and then remained big but quite stable; whereas lesions in group S increased more slowly, allowing us to see their growth between our two time points.

Early decrease of ADC value in rats that died

It is known that ADC value is significantly decreased in the territory of the occluded artery in the early stages of stroke^{28,29}. As a consequence, in the clinical setting, a DWI hyper-intensity (corresponding to an ADC decrease) in the first hours after stroke onset allows physicians to diagnose the ischemic stroke. Our issue was to demonstrate whether the early evolution of the ADC decrease is different depending on the severity of the stroke and then the prognosis.

We found that normalized ADC value (ADC edema /ADC contralateral) decreased significantly at very early stages of stroke, between 30 minutes and 60 minutes after stroke, in group D.

Again, it is very difficult to find animal experiments that separate very early imaging data based on survival, most of all because the animals are often sacrificed early after the imaging process in order to analyze the histological status. Thus, the outcome of the subjects, had they lived on, is unknown. Minematsu & al²⁷ found an

increased DWI-signal intensity (i.e. decrease of ADC) in the MCA-territory at 30 minutes of MCAO in rats, which increased further at 3 hours of MCAO. Moreover Hossmann & al³⁰ showed an ADC decline of 68% of control (i.e. ADCr 68%) after 10 minutes of ischemia which reached 63% after 50 minutes of ischemia on cats submitted to complete cerebro-circulatory arrest. We did not find a significant early decrease of ADC in rats that survived. We can assume that the ADC in Group S also showed a decrease but slower than in Group D so that it could not be seen at 30 and 60 minutes after stroke.

Heterogeneity of the ADC reduced region

To explore this discrepancy in ADC evolution from 30 minutes to 60 minutes after stroke onset between group D and group S, we analyzed the profile of ADC decrease by splitting the lesion into three : cluster ADCr = 0.9-0.8 (mild edema), cluster ADCr = 0.8-0.6 (severe edema), and cluster ADC <0.6 (very severe edema). These thresholds were chosen based on literature ADCr values. Oppenheim and Grandin⁶ showed that the best ADCr threshold to discriminate voxels destined for final infarct from those that are part of oligemic tissue was 0.91. Another ADCr threshold of 0.8 appeared to be the limit between tissue potentially reversible and tissue irreversibly damaged¹⁴.

It appeared that the region of “severe edema” constitutes the major part of the lesion in both groups and both time points. It was significantly bigger at 60 minutes after stroke in group D than in group S even if we couldn’t show a significant difference in global ADC value between S and D.

Then, in group D, the proportion of “mild edema” decreased from 30 minutes to 60 minutes while the proportion of “very severe edema” increased.

To summarize, we found that the early rate of ADC decrease, more than the ADC value, was linked with the survival of rats that underwent ischemic stroke.

Helpern³¹ showed that DWI in MCAo model could demonstrate a statistically significant change in three regions defined by histology as severe irreversible damage, relatively mild, and apparent reversible damage. Hoehn-Berlage & al²⁶ showed in MCAo rats that an ADCr of 77 +/- 3 % corresponded to a region of energy depletion located in the core of the lesion and an ADCr below 90 +/- 4 % was associated with tissue acidosis. If we extrapolate with caution these findings to our study, we could say that the region defined as severe and very severe edema would be a region of tissue acidosis and energy depletion, whereas the region with ADC between 0.9 and 0.8, defined as mild edema, would represent a region of tissue acidosis with preserved energy balance. It could be considered as a region of penumbra.

Hasegawa³² showed by a 45 minute MCAo rat model that more than 70% of the ROI with slight ADC decline before reperfusion exhibited no infarction. (The method of ADC measures allows no comparison with our values). Sakoh & al¹⁴ displayed on a model of MCAo in pigs that the infarction coincided with a threshold CMRO₂ (measured by positron emission tomography) of 50% of the contralateral value and a threshold ADCr of 75% (which is closed to the global ADCr values we obtained). He showed that ADCr values above 80% are potentially reversible until 6 hours of MCAo whereas lesions with ADCr below 75% are irreversible as early as 2 hours after MCAo. Fiehler³³ investigated ADC normalization in stroke patients after thrombolytic therapy and found that tissue with more severe initial decrease in ADC was less likely to demonstrate normalization.

These studies agree to assume that the decrease of ADC is correlated with the degree of tissue damage. Therefore, in group D, the bigger proportion of “severe edema” along with the growth of “very severe edema”

and shrinking of “mild edema” from 30 to 60 minutes can be interpreted as a quicker process of irreversible tissue damage in rats that died later on than in rats who survived stroke.

However, it cannot explain why we could not find a significant difference between ADCr at T60 between S and D. Yet, Schwamm & al²⁴ found a negative correlation between the initial mean ADCr and the follow-up NIHSS score at 7.4 hours after stroke onset in humans. Wardlaw³⁴ demonstrated that ADCr in stroke patients was associated with functional outcome because it was associated with the stroke severity; It was not found as an independent outcome predictor. Oppenheim & al²¹ reported lower ADC values in a group of patients that developed malignant infarcts later on. Maybe we would have been able to show a significant difference of ADCr depending on survival at later time points.

Limitations

Our ROI Edema was created by manual outlining of the visually-decreased ADC region. It is an operator-dependent procedure that can create a bias between groups. However it is considered as the reference standard for the measurement of stroke volume and it is often used as a first step for further automatic measurements⁶¹⁷. An automatic method with threshold-derived ADC volumes without previous manual editing can strongly over- or underestimate the lesion³⁶.

The automatic method we used to analyze the ROI “Edema” showed that it contained 7 to 17% of voxels with an ADCr above 0.9. However, the global ADCr value of the lesion was consistent with the literature¹⁴²⁶. The presence of voxels with very slightly decreased ADCr within the global ADC-decreased lesion could be explained by the heterogeneity of the stroke lesion. A new model has indeed been proposed, suggesting that in the early minutes and hours after ischemia onset, the core contains pockets of injury like ‘mini-cores’, surrounded by ‘mini-penumbras’⁷.

Because of the retrospective way the study was built, we could not assess the size of final infarct, which would have given us a definitive evaluation of infarct size in both groups. However, early DWI lesion was found to be correlated with final infarct in rats²⁷ and in humans²⁵.

For the same reasons, no post-mortem examination was done. As a result, we have been unable to exclude the potential confusing causes of death such as subarachnoid hemorrhage, which has been reported in approximate 12% of MCAo procedures³⁵. At least, no hemorrhage had been identified on early cerebral imaging.

We did not assess the presence of hypothalamic lesion. Hypothalamic ischemia occurs in MCAO occlusion of 60 minutes or greater, leading to hyperthermia, while it is rarely seen in human stroke. Hyperthermia exacerbates cell death³⁵. We did not find a significant difference of temperature after ischemia between the two groups (T° in Group S: 37.65°C, SD 0.88; T° in Group D: 37.63°C, SD : 1.03; p=0.952) but it could be an important confusion factor in individual analysis.

❖ CONCLUSION

We observed that the group comprising rats that will die later on (D) had a bigger stroke volume (defined as the ADC-decreased region) than the group including rats that survived the 90minute MCA occlusion (S). Group D also displayed a decrease in ADCr at very early stages of stroke that was not seen in Group S. However, the individual analysis allows no survival prediction based on these two features. Other features could be needed for an individual survival prediction, such as the location of ischemia (hypothalamic lesion), the body temperature or the presence of complications like subarachnoid hemorrhage. The use of diffusion MRI in acute stroke models can help to identify early biomarkers of prognosis in ischemic stroke.

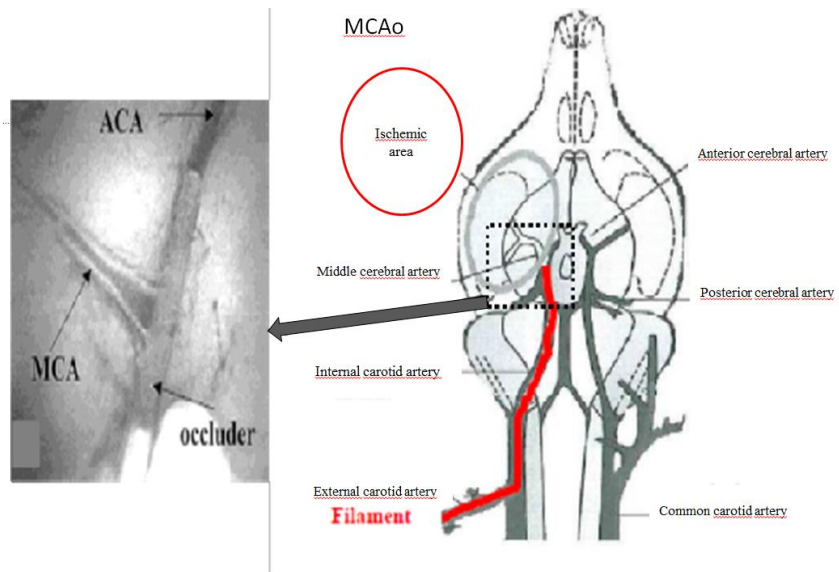
❖ REFERENCES

1. WHO | The top 10 causes of death [Internet]. [cited 2015 Jan 15]; Available from: <http://www.who.int/mediacentre/factsheets/fs310/en/>
2. Les chiffres clés de l'AVC - Ministère des Affaires sociales, de la Santé et des Droits des femmes - www.sante.gouv.fr [Internet]. [cited 2015 Jan 15]; Available from: <http://www.sante.gouv.fr/les-chiffres-clés-de-l-avc.html>
3. Detante L, PhysioPathologie ischémie cérébrale EMC v1 longue.pdf.
4. Wey H-Y, Desai VR, Duong TQ. A review of current imaging methods used in stroke research. *Neurol. Res.* 2013;35:1092–1102.
5. Kleindorfer D, Lindsell CJ, Brass L, Koroshetz W, Broderick JP. National US estimates of recombinant tissue plasminogen activator use: ICD-9 codes substantially underestimate. *Stroke J. Cereb. Circ.* 2008;39:924–928.
6. Oppenheim C, Grandin C, Samson Y, Smith A, Duprez T, Marsault C, Cosnard G. Is there an apparent diffusion coefficient threshold in predicting tissue viability in hyperacute stroke? *Stroke J. Cereb. Circ.* 2001;32:2486–2491.
7. Del Zoppo GJ, Sharp FR, Heiss W-D, Albers GW. Heterogeneity in the penumbra. *J. Cereb. Blood Flow Metab. Off. J. Int. Soc. Cereb. Blood Flow Metab.* 2011;31:1836–1851.
8. Schlaug G, Benfield A, Baird AE, Siewert B, Lövblad KO, Parker RA, Edelman RR, Warach S. The ischemic penumbra: operationally defined by diffusion and perfusion MRI. *Neurology.* 1999;53:1528–1537.
9. Heiss W-D, Sobesky J, Hesselmann V. Identifying thresholds for penumbra and irreversible tissue damage. *Stroke J. Cereb. Circ.* 2004;35:2671–2674.
10. Fisher M, Bastan B. Identifying and utilizing the ischemic penumbra. *Neurology.* 2012;79:S79–85.
11. Christen T, Lemasson B, Pannetier N, Farion R, Segebarth C, Rémy C, Barbier EL. Evaluation of a quantitative blood oxygenation level-dependent (qBOLD) approach to map local blood oxygen saturation. *NMR Biomed.* 2011;24:393–403.
12. Jensen-Kondering U, Baron J-C. Oxygen imaging by MRI: can blood oxygen level-dependent imaging depict the ischemic penumbra? *Stroke J. Cereb. Circ.* 2012;43:2264–2269.
13. Hoa D. L'IRM pas à pas. Campus medica. Sauramps medical; 2008.
14. Sakoh M, Ohnishi T, Ostergaard L, Gjedde A. Prediction of tissue survival after stroke based on changes in the apparent diffusion of water (cytotoxic edema). *Acta Neurochir. Suppl.* 2003;86:137–140.
15. Schaefer PW, Ozsunar Y, He J, Hamberg LM, Hunter GJ, Sorensen AG, Koroshetz WJ, Gonzalez RG. Assessing tissue viability with MR diffusion and perfusion imaging. *AJNR Am. J. Neuroradiol.* 2003;24:436–443.
16. Drier A, Tourdias T, Attal Y, Sibon I, Mutlu G, Lehericy S, Samson Y, Chiras J, Dormont D, Orgogozo J-M, Dousset V, Rosso C. Prediction of subacute infarct size in acute middle cerebral artery stroke: comparison of perfusion-weighted imaging and apparent diffusion coefficient maps. *Radiology.* 2012;265:511–517.
17. Rosso C, Hevia-Montiel N, Deltour S, Bardinet E, Dormont D, Crozier S, Baillet S, Samson Y. Prediction of infarct growth based on apparent diffusion coefficients: penumbral assessment without intravenous contrast material. *Radiology.* 2009;250:184–192.

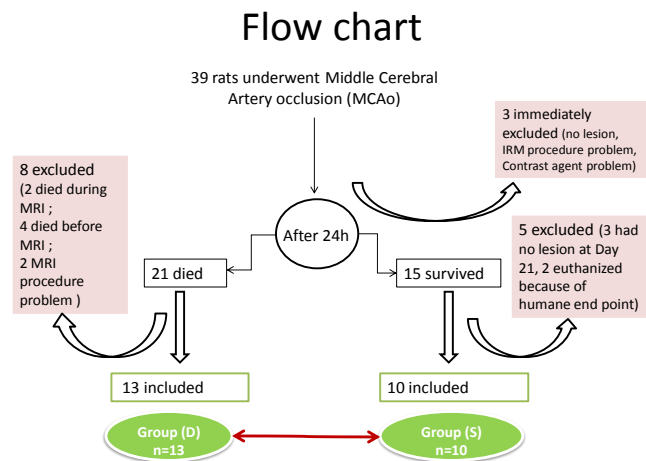
18. Lövblad KO, Baird AE, Schlaug G, Benfield A, Siewert B, Voetsch B, Connor A, Burzynski C, Edelman RR, Warach S. Ischemic lesion volumes in acute stroke by diffusion-weighted magnetic resonance imaging correlate with clinical outcome. *Ann. Neurol.* 1997;42:164–170.
19. Baird AE, Dambrosia J, Janket S, Eichbaum Q, Chaves C, Silver B, Barber PA, Parsons M, Darby D, Davis S, Caplan LR, Edelman RE, Warach S. A three-item scale for the early prediction of stroke recovery. *Lancet.* 2001;357:2095–2099.
20. Ma L, Gao P, Hu Q, Lin Y, Jing L, Xue J, Chen Z, Wang Y, Liu M, Cai Y. Effect of baseline magnetic resonance imaging (MRI) apparent diffusion coefficient lesion volume on functional outcome in ischemic stroke. *Neurol. Res.* 2011;33:494–502.
21. Oppenheim C, Samson Y, Manai R, Lalam T, Vandamme X, Crozier S, Srour A, Cornu P, Dormont D, Rancurel G, Marsault C. Prediction of malignant middle cerebral artery infarction by diffusion-weighted imaging. *Stroke J. Cereb. Circ.* 2000;31:2175–2181.
22. Ström JO, Ingberg E, Theodorsson A, Theodorsson E. Method parameters' impact on mortality and variability in rat stroke experiments: a meta-analysis. *BMC Neurosci.* 2013;14:41.
23. Engelter ST, Provenzale JM, Petrella JR, DeLong DM, Alberts MJ. Infarct volume on apparent diffusion coefficient maps correlates with length of stay and outcome after middle cerebral artery stroke. *Cerebrovasc. Dis. Basel Switz.* 2003;15:188–191.
24. Schwamm LH, Koroshetz WJ, Sorensen AG, Wang B, Copen WA, Budzik R, Rordorf G, Buonanno FS, Schaefer PW, Gonzalez RG. Time course of lesion development in patients with acute stroke: serial diffusion- and hemodynamic-weighted magnetic resonance imaging. *Stroke J. Cereb. Circ.* 1998;29:2268–2276.
25. Beaulieu C, de Crespigny A, Tong DC, Moseley ME, Albers GW, Marks MP. Longitudinal magnetic resonance imaging study of perfusion and diffusion in stroke: evolution of lesion volume and correlation with clinical outcome. *Ann. Neurol.* 1999;46:568–578.
26. Hoehn-Berlage M, Norris DG, Kohno K, Mies G, Leibfritz D, Hossmann KA. Evolution of regional changes in apparent diffusion coefficient during focal ischemia of rat brain: the relationship of quantitative diffusion NMR imaging to reduction in cerebral blood flow and metabolic disturbances. *J. Cereb. Blood Flow Metab. Off. J. Int. Soc. Cereb. Blood Flow Metab.* 1995;15:1002–1011.
27. Minematsu K, Li L, Fisher M, Sotak CH, Davis MA, Fiandaca MS. Diffusion-weighted magnetic resonance imaging: rapid and quantitative detection of focal brain ischemia. *Neurology.* 1992;42:235–240.
28. Schlaug G, Siewert B, Benfield A, Edelman RR, Warach S. Time course of the apparent diffusion coefficient (ADC) abnormality in human stroke. *Neurology.* 1997;49:113–119.
29. Warach S, Chien D, Li W, Ronthal M, Edelman RR. Fast magnetic resonance diffusion-weighted imaging of acute human stroke. *Neurology.* 1992;42:1717–1723.
30. Hossmann KA, Fischer M, Bockhorst K, Hoehn-Berlage M. NMR imaging of the apparent diffusion coefficient (ADC) for the evaluation of metabolic suppression and recovery after prolonged cerebral ischemia. *J. Cereb. Blood Flow Metab. Off. J. Int. Soc. Cereb. Blood Flow Metab.* 1994;14:723–731.
31. Helpert JA, Dereski MO, Knight RA, Ordidge RJ, Chopp M, Qing ZX. Histopathological correlations of nuclear magnetic resonance imaging parameters in experimental cerebral ischemia. *Magn. Reson. Imaging.* 1993;11:241–246.
32. Hasegawa Y, Fisher M, Latour LL, Dardzinski BJ, Sotak CH. MRI diffusion mapping of reversible and irreversible ischemic injury in focal brain ischemia. *Neurology.* 1994;44:1484–1490.
33. Fiehler J, Knudsen K, Kucinski T, Kidwell CS, Alger JR, Thomalla G, Eckert B, Wittkugel O, Weiller C, Zeumer H, Röther J. Predictors of apparent diffusion coefficient normalization in stroke patients. *Stroke J. Cereb. Circ.* 2004;35:514–519.

34. Wardlaw JM, Keir SL, Bastin ME, Armitage PA, Rana AK. Is diffusion imaging appearance an independent predictor of outcome after ischemic stroke? *Neurology*. 2002;59:1381–1387.
35. Carmichael ST. Rodent models of focal stroke: size, mechanism, and purpose. *NeuroRx J. Am. Soc. Exp. Neurother*. 2005;2:396–409.
36. Thomas RGR, Lymer GK, Armitage PA, Chappell FM, Carpenter T, Karaszewski B, Dennis MS, Wardlaw JM. Apparent diffusion coefficient thresholds and diffusion lesion volume in acute stroke. *J. Stroke Cerebrovasc. Dis. Off. J. Natl. Stroke Assoc*. 2013;22:906–909.

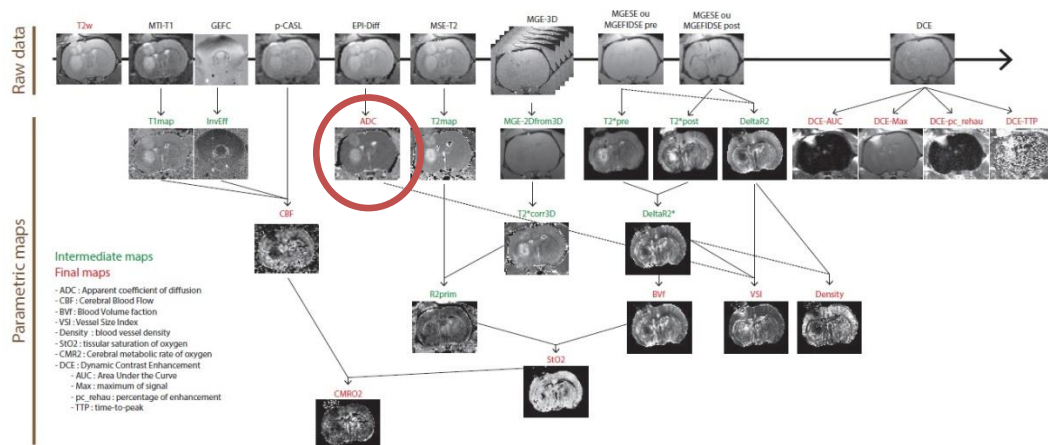
❖ ANNEXES



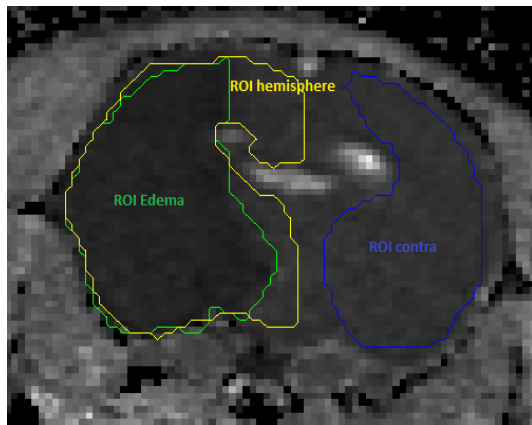
Annex n°1: Middle cerebral artery occlusion model (Moisan et al)



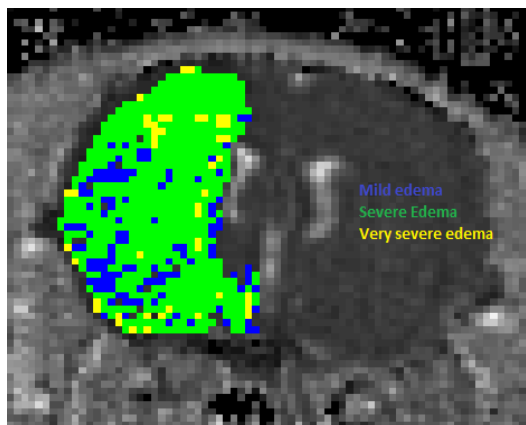
Annex n°2: Flow chart



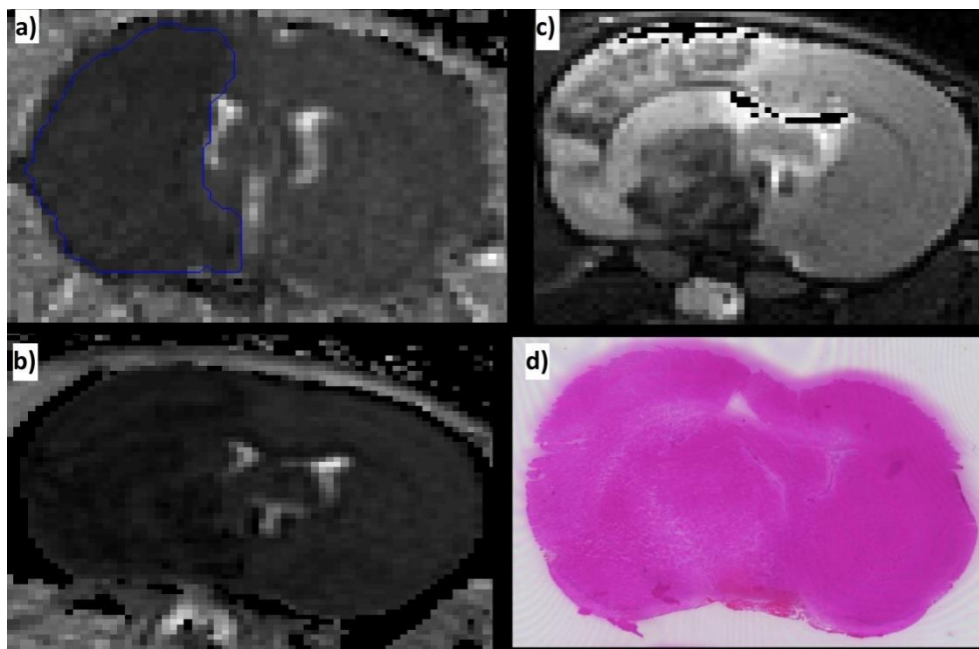
Annex n°3: Computing the MRI parametric maps



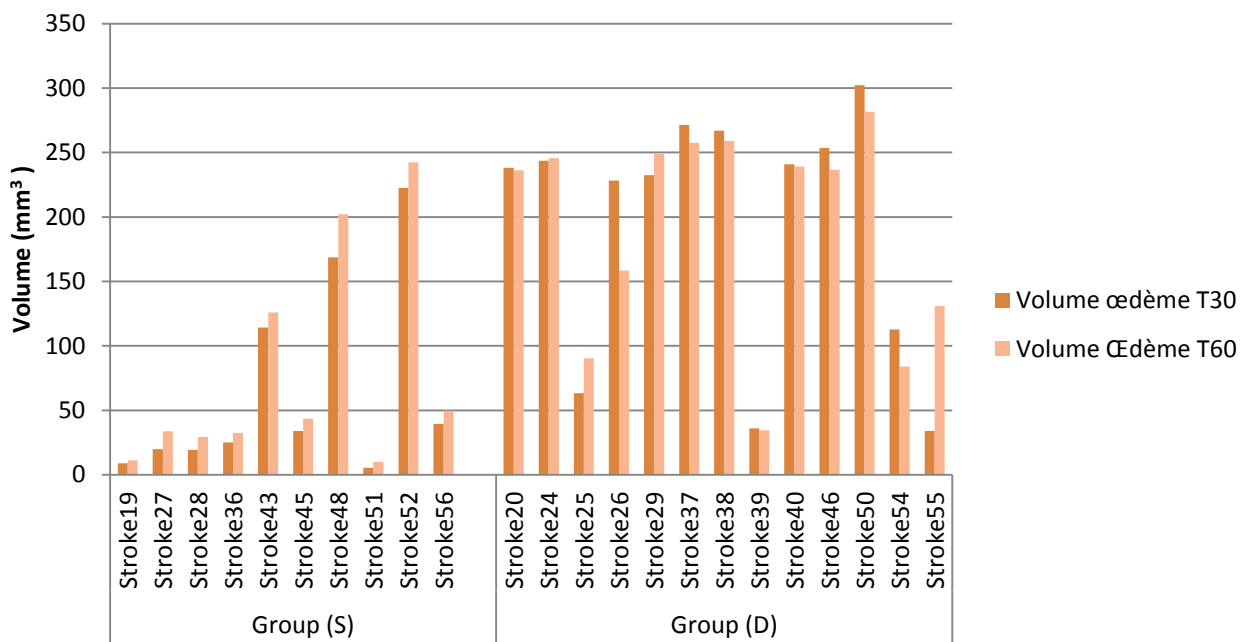
Annex n°4: Manual delineation of ROI



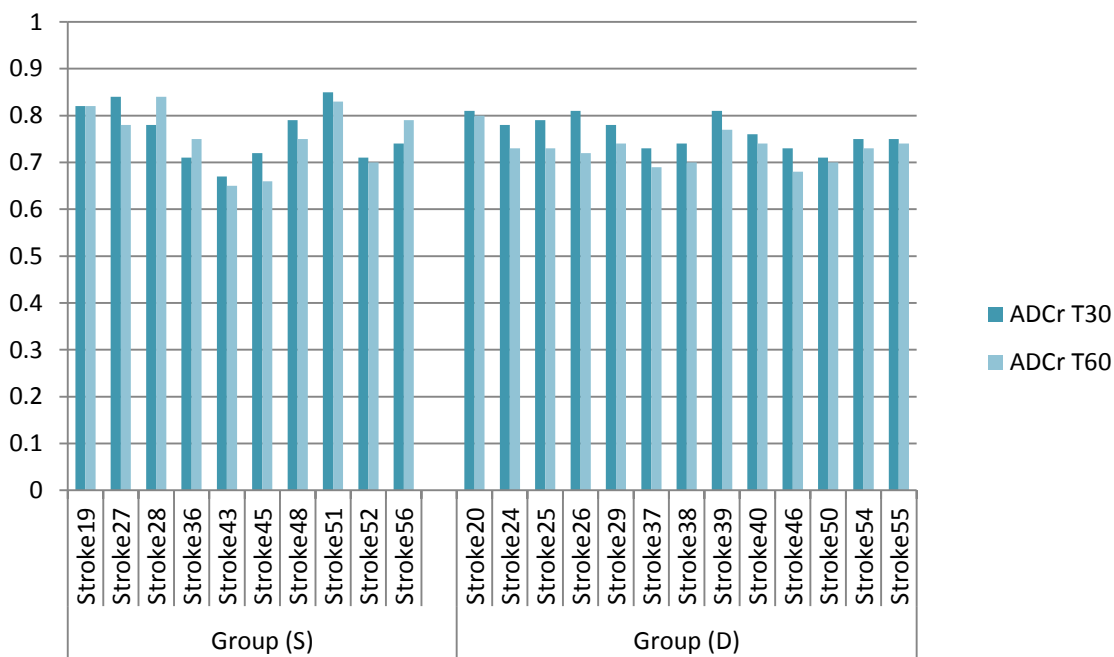
Annex n°5: Automatic clusters in ROI "Edema"



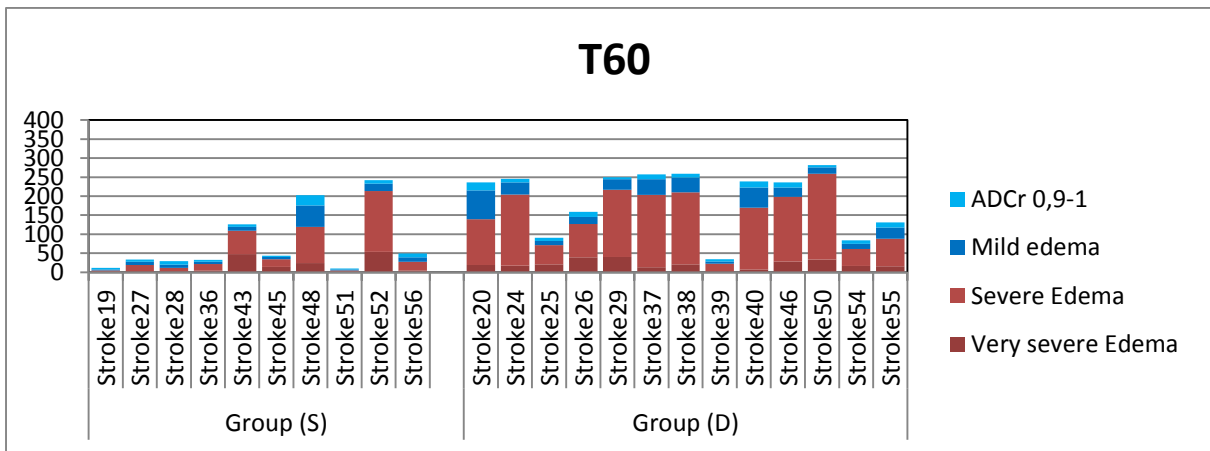
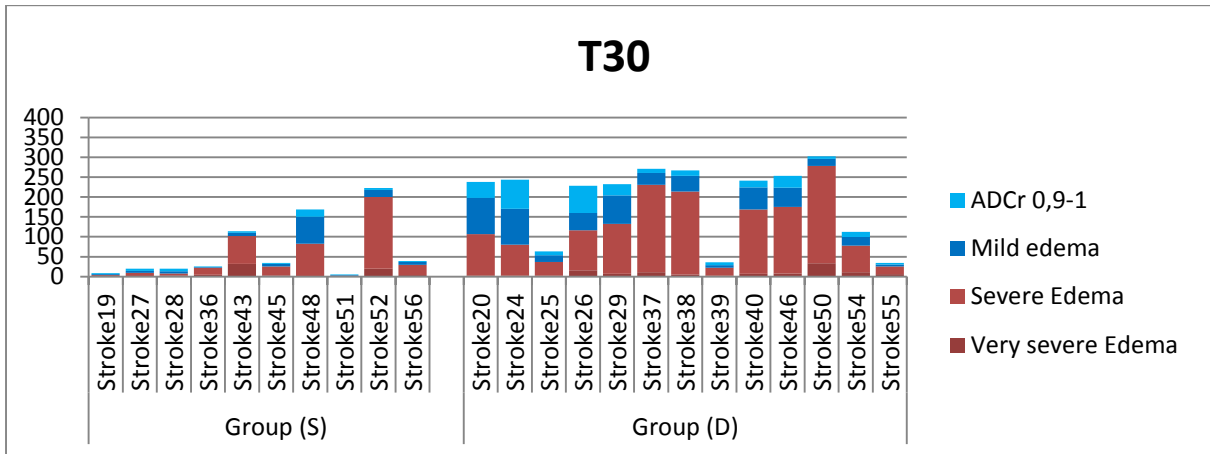
Annex n°6: Stroke 38, Group D: a) ADC map T60, b) ADC map after death, c) T2 after death, d) corresponding histological slice with Hematoxylin-Eosin staining.



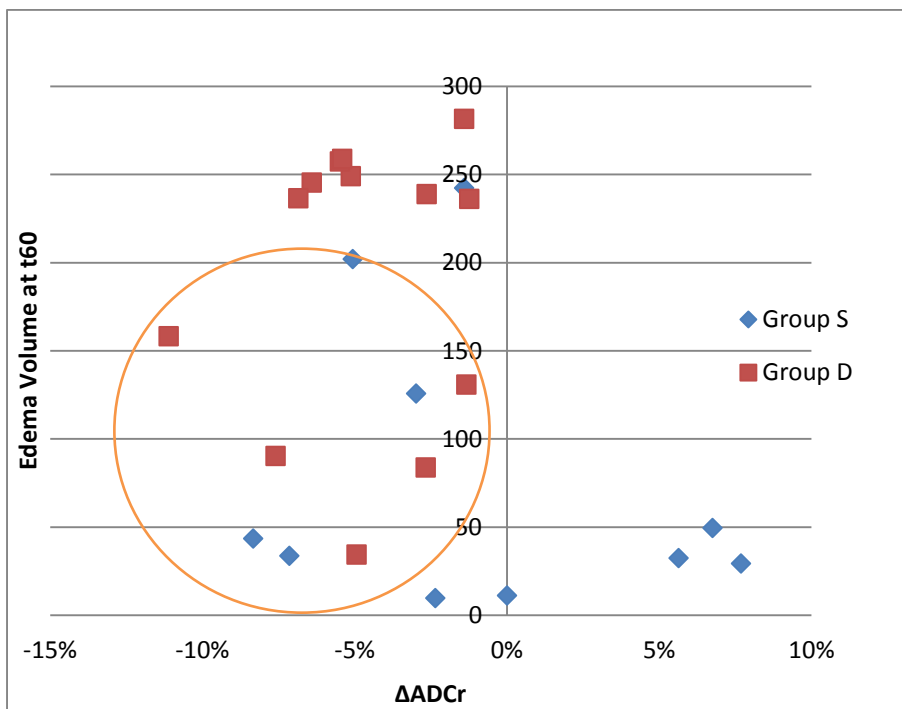
Annex n°7: Histogram representing individual edema volumes at T30 and T60.



Annex n°8: Histogram representing individual ADCr values at T30 and T60



Annex n°9: Volume of automatic clusters, individual values (mm3) at T30 and T60.



Annex n°10: Delta ADCr and Edema Volume at T60. $\Delta ADCr = (ADCr T60 - ADCr T30) / ADCr T30$. The orange circle aims to point out that subjects of both groups have similar position on the graph.